BIOLOGICAL ADHESION IN WET ENVIRONMENTS: ADAPTATIONS AND MECHANISMS

KI WOONG KANG

CHURCHILL COLLEGE

Supervised by Dr. Walter Federle

This dissertation is submitted for the degree of Doctor of Philosophy

University of Cambridge, July 2020

DECLARATION

This thesis is the result of my own work and includes nothing which is the outcome of work done in collaboration except as declared in the acknowledgements and specified in the text. It is not substantially the same as any that I have submitted, or, is being concurrently submitted for a degree of diploma or other qualification at the University of Cambridge or any other University or similar institution except as declared in the acknowledgments and specified in the text. I further state that no substantial part of my dissertation has already been submitted, or, is being concurrently submitted for any such degree, diploma or other qualification at the University of Cambridge or any other University or similar institution except as declared in the Preface and specified in the text. This thesis does not exceed the prescribed word limit of 60,000 words.

Cambridge, July 2020

Signed: Ki Woong Kang

SUMMARY

BIOLOGICAL ADHESION IN WET ENVIRONMENTS: ADAPTATIONS AND MECHANISMS

KI WOONG KANG

Physiochemical conditions in water are fundamentally different to those in air; hence, organisms require special adaptations to adhere in wet environments. In my thesis, I have investigated three study systems to elucidate mechanisms for adhesion under wet conditions.

In Chapters 2 and 3, I explore an aquatic insect (Diptera: Blephariceridae) that uses suction organs to attach to rocks in raging alpine torrents. Suction-based attachment is driven by physical processes requiring a pressure difference and a seal to maintain it. Through my investigations, I have identified several key principles for biological suction attachments to wet and rough surfaces. Using three-dimensional reconstructions of blephariceridsuction organs and *in vivo* visualisation of the adhesive contact zone, I found several internal and external morphological adaptations that are important for strong adhesion under water. Moreover, I characterised a mechanism for rapid detachment which is the first detailed account of an actively controlled detachment system in biological suction organs.

In Chapter 4, I investigate the contribution of physical and chemical mechanisms to the powerful attachment of common limpets (*Patella vulgata*) to rocks in the intertidal zone. I demonstrate that suction is not the primary contributor to their attachment forces; rather, it is their adhesive pedal mucus that is responsible. This adhesive mucus comprises of a complex mixture of glycans and proteins, many of which share homology with adhesive secretions from other marine invertebrates, such as sea stars, sea anemones, and flatworms.

In Chapters 5 and 6, I study the physical and chemical properties of sticky secretions from carnivorous pitcher plants (*Nepenthes*) that help to capture, retain, and digest insects. I show that the viscoelastic pitcher fluid readily adheres to but not easily dewets from insect cuticle, and forms stable filaments as the insect attempts to escape that require significant work to overcome. In addition, the surface tension is reduced in pitcher fluid compared

to water, making insects sink more easily into the former and facilitating further wetting of the cuticle. Chemical characterisation of the pitcher fluid revealed that its sticky filamentous property is caused by a polysaccharide with a glucurono-mannan backbone structure, which is chemically stable and contains carboxylic groups for strong interactions. Glucurono-mannan are an understudied group of plant polysaccharides that are present in mucilaginous secretions from across the plant kingdom, including sticky capture fluids from other carnivorous plants. My findings show that pitcher plant fluid can be used as a study system for future investigations into the origins and functional role of glucurono-mannan in carnivorous plants.

In summary, my thesis has identified novel adaptations and principles for biological adhesion under wet conditions using three selected study systems, hence expanding our understanding of the underlying physical and chemical mechanisms and providing inspiration for biomimetic adhesives with improved performance in wet environments.

ACKNOWLEDGEMENTS

I would like to begin by thanking my supervisor, Walter Federle. Time and again I have heard how important it is to have a good relationship with your PhD supervisor, and I am extremely fortunate to have worked with Walter, who is supportive, patient, and kind.

I also had the privilege of collaborating with Patrick Flammang (University of Mons, Belgium) and Paul Dupree (University of Cambridge), who have both been extremely welcoming and supportive. I would like to say a special thank you to Birgit Lengerer, who supervised me in Patrick's group and taught me many new skills in molecular biology, and Rita Marques and Theodora Tryfona, for helping me get started in Paul's lab and for always offering to help.

I would like to thank my thesis advisors David Aldridge and Marta Zlatic for their valuable feedback on my intermediate reports. I especially want to express my gratitude to David, who has always provided insightful comments and uplifting encouragements in his advisor reports.

I am fortunate to have been part of the friendly and supportive Insect Biomechanics Group, and I thank everyone who has helped me over the years. I believe almost every single member who have passed through the lab over the last four years has helped me collect or maintain my study animals, so I express my sincere gratitude to you all: Simon Chen, Patrick Brechka, Simon Reichel, Freddie Püffel, Marie-Yon Strücker, Manasse Pinsuwan, Jorn Jager, Markus Unruh, Eva Schulenberg, Jack Smith, Jake Stone, and Caroline Grannemann. I hope that you all enjoyed the fish and chips in Sheringham or the beautiful scenery in Switzerland. I am especially thankful to Simon Chen for his remarkable ability to build custom equipment, his willingness to help at a moment's notice, and for his infectious curiosity of all insects.

I would like to thank Kristie Ho and Hauke Isermann, for their patience in having a novice supervisor and for helping me grow as a mentor and a researcher.

I have had access to several cutting-edge imaging equipment for my studies, and I am deeply indebted to everyone who provided training and guidance: Richard Johnston (Swansea University) and Thomas van de Kamp (Karlsruhe Institute of Technology,

Germany) for computed microtomography; Karin Muller and Jeremy Skepper for scanning electron microscopy; and Matt Wayland for confocal microscopy. Using these new techniques to visualise my study animals from a completely new perspective has been an eye-opening experience.

I am grateful to have pursued my PhD as a member of the BioSmartTrainee Innovative Training Network. I am fortunate to have received training and feedback from renowned scientists during the programme. I am also incredibly thankful to my dear friends from BioSmartTrainees for their unwavering support and for making this journey so fun and memorable: Marco Dompé, Mehdi Vahdati, Francisco Cedano, Justine Tavera, Maria Villiou, Aurélie Féat, Ugo Sidoli, Dimitris Mintis, and Vaishali Chopra. I would also like to thank Sandra Martinka and Alla Synytska for their superb administration of the multinational network.

This thesis would not have been possible without the financial support from EU Horizon 2020. I also received funding for various research and conference trips, for which I would like to thank: The Company of Biologists, the Royal Entomological Society, Churchill College, the Santander Mobility Grants, ENBA COST action, the Malacological Society of London, and the Cambridge Philosophical Society.

A heart-felt thank you to the many people who have made my time in Cambridge so special. It has not been easy settling into a new environment far from home, but I am incredibly lucky to have had the love and support from my Churchill College friends Karen Duffy, Jocelino Rodrigues, Tom Winder, Hannah Wauchope, and Jacques Serizay. Thank you for making sure my birthdays were full of laughter over the last four years.

I would like finish by thanking my parents Herbert and Maria, and my sister Hai Sue, for letting me keep all sorts of creatures as a child and for encouraging me to pursue my passions, even if it meant being on the opposite side of the world. And to Diana: thank you for brightening my days since the day we met.

PUBLICATIONS AND COLLABORATIONS

Chapters two to six presented in this thesis were prepared as manuscripts and have been either published or are about to be submitted. As a result, there may be some repetition between chapters when introducing key topics and techniques. Since all chapters involved collaborations, I use the pronoun 'we' instead of 'I' throughout. Their specific contributions for each chapter are stated below.

Chapter 2

This chapter has been published in an open access journal: **Kang, V.**, Johnston, R., van de Kamp, T., Faragó, T., & Federle, W. (2019). Morphology of powerful suction organs from blephariceridlarvae living in raging torrents. *BMC Zoology*, *4*, 10. I have lightly revised it to keep the formatting coherent within the thesis.

Richard Johnston scanned samples using the computed microtomography (micro-CT) scanner at Swansea University, Wales, and reconstructed the scans. Thomas van de Kamp and Tomáš Faragó helped me scan samples at the X-ray synchrotron at Karlsruhe Institute of Technology, Germany and reconstructed the scans. Walter Federle assisted with field collection trips and contributed to the experimental design. I conceived the project, coordinated field collection trips, conducted the experiments, analysed the data, and wrote the first draft. All co-authors gave feedback on the manuscript. In addition, Karin Muller at the Cambridge Advanced Imaging Institute and Matthew Wayland at the Zoology Imaging Facility assisted me with scanning electron microscopy and laser confocal scanning microscopy, respectively.

Chapter 3

Robin White at Carl Zeiss Research Microscopy Solutions scanned samples for me using their nano-CT scanner and reconstructed the scans. Simon Chen built the experimental set-ups (centrifuge and flow-chamber) and helped with field collection. Michael Sutcliffe and I gathered the surface profilometry data. Walter Federle helped conceive the project and contributed to the experimental design. I conceived the project, conducted the experiments, analysed the data, and wrote the manuscript.

Chapter 4

This chapter has been published in an open access journal: **Kang, V.**, Lengerer, B., Wattiez, R., & Flammang, P. (2020). Molecular insights into the powerful mucus-based adhesion of limpets (*Patella vulgata* L.). *Open Biology, 10*, 200019. I have lightly revised it to keep the formatting coherent within the thesis.

Patrick Flammang, Birgit Lengerer, and I conceived the project and designed the experiments. Birgit helped me with the RNA extraction for transcriptome sequencing and taught me how to do the *in situ* hybridisation and lectin staining assays. Ruddy Wattiez collected the protein mass spectrometry data and compiled the proteome. RNA sequencing and *de novo* transcriptome assembly were carried out by BGI Genomics, China. In addition to the molecular biology experiments, I conducted the pressure measurement trials, carried out analysis of the proteomics data, and wrote the first draft of the manuscript. All co-authors gave feedback on the manuscript.

Chapter 5

Walter and I conceived the project. Hauke Isermann helped conduct a portion of the force experiments and the initial analysis under my supervision. Saksham Sharma measured the surface tension using pendant drop tensiometry and analysed the data. I conducted additional force experiments, analysed and interpreted the data, conducted statistical analysis, and wrote the manuscript. Walter gave feedback on the manuscript.

Chapter 6

Paul Dupree, Walter Federle, and I conceived the project. Rita Marques taught me how to conduct various plant biochemistry protocols. Theodora Tryfona helped me with the mass spectrometry experiments. I conducted the experiments, analysed the data, and wrote the manuscript. Walter provided supervision and feedback on the manuscript.

I have also contributed to the following publications that are not included in the thesis:

Wang, Y., **Kang, V.**, Arzt, E., Federle, W., & Hensel, R. (2019). Strong Wet and Dry Adhesion by Cupped Microstructures. *ACS Applied Materials & Interfaces, 11*, 26483–26490.

Wang, Y., **Kang, V.**, Arzt, E., Federle, W., & Hensel, R. (Submitted). Switchable underwater adhesion by deformable cupped microstructures. *Small.*

Abstract: Switchable underwater adhesion can be useful for numerous applications but is extremely challenging due to the presence of water at the contact interface. Here, we report on deformable cupped microstructures (diameters typically 100 μm) that can switch between high (~1 MPa) and low (<0.2 MPa) adhesion strength by adjusting the retraction velocity from 100 to 0.1 μm/s. The velocity at which the switch occurs is determined by specific design parameters of the cupped microstructure, such as the cup width and angle. The results are compared with theoretical predictions by calculating the water penetration into the contact zone and the expansion of the cup during retraction. Our work paves the way for controlling wet adhesion on demand and may inspire further applications in smart adhesives.

Kang V., Federle, W. (In preparation for *Biological Reviews*). Learning from biological suction organs: strategies for bio-inspired suction devices.

Abstract: In this review, we propose a clear set of definitions for suction attachment that is based on the underlying physical mechanisms. We outline the different approaches for quantifying biological suction performance and examine the most common methods to distinguish studies whose results can be reliably compared. In addition, we extract fundamental principles that are shared between the diverse types of suction organs and present strategies that can be useful for future bio-inspired suction devices. Finally, we assess the latest bio-inspired suction devices and use the definitions and principles that we herein propose to better understand which strategies were applied, why they were used, and how well they performed. We hope that this review will provide clarity for researchers studying suction attachments and inspire others to develop the next generation of attachment devices with improved functionalities.

CONTENTS

1 INTRODUCTION 1
1.1 NET-WINGED MIDGE LARVAE 2
1.2 LIMPETS 5
1.3 PITCHER PLANTS 9
2 MORPHOLOGY OF POWERFUL SUCTION ORGANS FROM BLEPHARICERID LARVAE LIVING IN RAGING TORRENTS 12
2.1 SUMMARY 12
2.2 INTRODUCTION 12
2.3 METHODS 15
2.4 RESULTS 19
2.5 DISCUSSION 29
2.6 CONCLUSION 34
3 EXTREME SUCTION PERFORMANCE FROM A SPECIALISED AQUATIC INSECT (DIPTERA: BLEPHARICERIDAE) 36
3.1 SUMMARY 36
3.2 INTRODUCTION 36
3.3 METHODS 39
3.4 RESULTS 45
3.5 DISCUSSION 59
3.6 CONCLUSION 64
4 MOLECULAR INSIGHTS INTO THE POWERFUL MUCUS-BASED ADHESION OF LIMPETS (*PATELLA VULGATA* L.) 65
4.1 SUMMARY 65
4.2 INTRODUCTION 65
4.3 MATERIALS AND METHODS 69
4.4 RESULTS 77
4.5 DISCUSSION 90
4.6 CONCLUSION 98
5 HOW A STICKY FLUID FACILITATES PREY RETENTION IN A CARNIVOROUS PITCHER PLANT (*NEPENTHES RAFFLESIANA*) 100
5.1 SUMMARY 100
5.2 INTRODUCTION 100
5.3 MATERIALS AND METHODS 104

5.4 RESULTS 111
5.5 DISCUSSION 122
5.6 CONCLUSION 128
6 PITCHER PLANTS (GENUS *NEPENTHES*) HAVE CO-OPTED THE WIDE-SPREAD POLYSACCHARIDE GLUCURONO-MANNAN TO PRODUCE STICKY INSECT CAPTURE FLUID 130
6.1 SUMMARY 130
6.2 INTRODUCTION 130
6.3 ABBREVIATIONS 132
6.4 METHODS 133
6.5 RESULTS 136
6.6 DISCUSSION 142
6.7 CONCLUSION 150
7 CONCLUDING REMARKS 151
8 APPENDIX 156
8.1 SUPPLEMENTARY MATERIAL FOR CHAPTER 2 156
8.2 SUPPLEMENTARY MATERIAL FOR CHAPTER 3 158
8.3 SUPPLEMENTARY MATERIAL FOR CHAPTER 4 159
8.4 SUPPLEMENTARY MATERIAL FOR CHAPTER 5 172
8.5 SUPPLEMENTARY MATERIAL FOR CHAPTER 6 176
9 BIBLIOGRAPHY 179

LIST OF FIGURES

FIGURE 1.1. LARVAE OF NET-WINGED MIDGES SURVIVE IN TORRENTIAL ALPINE RIVERS. .. 3
FIGURE 1.2. LIMPETS ATTACH POWERFULLY TO ROCKS IN THE INTERTIDAL ZONE. 6
FIGURE 1.3. PITCHER PLANTS ARE CARNIVOROUS PLANTS THAT USE THEIR HIGHLY MODIFIED LEAVES AS PITFALL TRAPS TO CATCH INSECT PREY..... 11
FIGURE 2.1. HABITAT AND CRAWLING LOCOMOTION OF *LIPONEURA CINERASCENS* LARVAE. 13
FIGURE 2.2. SUCTION ATTACHMENT ORGAN FROM *LIPONEURA CORDATA*..... 20
FIGURE 2.3. MICROSTRUCTURES ON THE SUCTION DISCS OF TWO *LIPONEURA* SPECIES. ... 22
FIGURE 2.4. SUCTION DISC OF *L. CINERASCENS* LARVA IN CONTACT WITH A GLASS SURFACE, VISUALISED USING *IN VIVO* INTERFERENCE REFLECTION MICROSCOPY..... 23
FIGURE 2.5. MICROTRICHIA ON THE VENTRAL SURFACE OF A 4TH INSTAR *LIPONEURA CORDATA* SUCTION DISC..... 26
FIGURE 2.6. THE V-NOTCH SYSTEM AND ITS MOVEMENT IN A SUCTION ORGAN FROM *LIPONEURA CINERASCENS*. 27
FIGURE 2.7. THE V-NOTCH APODEME EXTENDS POSTERIORLY INTO THE BODY TO ATTACH TO A DEDICATED MUSCLE..... 27
FIGURE 2.8. DETAILED VIEWS OF THE V-NOTCH VALVE-LIKE STRUCTURES FROM *LIPONEURA CORDATA*, RECONSTRUCTED FROM MICRO-CT DATA. 28
FIGURE 2.9. MICROTRICHIA FROM *LIPONEURA CINERASCENS*. 32
FIGURE 3.1. OVERVIEW OF THE SUCTION ATTACHMENT ORGANS OF *HAPALOTHRIX LUGUBRIS*. 47
FIGURE 3.2. MICRO-CT RENDERING OF *H. LUGUBRIS* SUCTION ORGAN HIGHLIGHTS ITS INTERNAL ORGANISATION IN 3D. 48
FIGURE 3.3. ULTRASTRUCTURE OF THE SUCTION DISC. 49
FIGURE 3.4. ATTACHMENT PERFORMANCE OF THREE SPECIES OF BLEPHARICERID LARVAE (*HAPALOTHRIX LUGUBRIS, LIPONEURA CORDATA, L. CINERASCENS*) ON SMOOTH HORIZONTAL SURFACE. 51
FIGURE 3.5. ATTACHMENT PERFORMANCE OF *H. LUGUBRIS* COLL1 LARVAE ON SURFACES OF VARYING ROUGHNESS. 52
FIGURE 3.6. PEAK SHEAR ATTACHMENT OF *H. LUGUBRIS* COLL2 ON SOFT (POLYMER-BASED) VERSUS HARD (GLASS) SUBSTRATES. 53
FIGURE 3.7. CONSERVATIVE ESTIMATES FOR THE SHEAR ATTACHMENT STRENGTH OF *H. LUGUBRIS* AND *L. CORDATA* ON SMOOTH SURFACE. 54

FIGURE 3.8. COMPARISON OF SHEAR ATTACHMENT PERFORMANCE OF *H. LUGUBRIS* COLL1 LARVAE VERSUS STICK INSECTS (*CARAUSIUS MOROSUS*) ON SMOOTH AND ROUGH SURFACES. 56
FIGURE 3.9. *IN VIVO* VISUALISATION OF *H. LUGUBRIS* SUCTION DISC CONTACT ON DIFFERENT SUBSTRATES. 58
FIGURE 4.1. LIMPETS (*PATELLA VULGATA*) HAVE EVOLVED POWERFUL ATTACHMENTS TO WITHSTAND CRASHING TIDAL WAVES AND PREDATORY ATTACKS. 67
FIGURE 4.2. THREE TYPES OF PEDAL MUCUS WERE SAMPLED FROM INDIVIDUAL *P. VULGATA* LIMPETS. 72
FIGURE 4.3. REPRESENTATIVE *IN VIVO* SUB-PEDAL PRESSURE VALUES FROM *P. VULGATA* WITH SCHEMATICS SHOWING THE DIFFERENT TRIAL CONDITIONS. 78
FIGURE 4.4. OVERVIEW OF *P. VULGATA* FOOT TISSUE AND THE CHEMISTRY OF GLANDULAR SECRETIONS. 82
FIGURE 4.5. CONSERVED PROTEIN DOMAINS PRESENT IN A SUBSET OF LIMPET PEDAL MUCUS PROTEINS. 85
FIGURE 4.6. COMPARISON BETWEEN *P-VULGATA_3* AND SCO-SPONDIN FROM *GALLUS GALLUS*. 86
FIGURE 4.7. *IN SITU* HYBRIDISATION (ISH) OF FIVE PROTEIN SEQUENCES CONFIRMS THE PRESENCE AND LOCALITY OF THE TARGET MRNA WITHIN *P. VULGATA* FOOT. 88
FIGURE 5.1. ANT RETENTION TESTS IN WATER AND *NEPENTHES RAFFLESIANA* PITCHER FLUID (PF). 112
FIGURE 5.2. A REPRESENTATIVE FORCE-TIME PLOT FROM FORCE MEASUREMENT TRIALS OF ANT GASTERS DIPPED INTO WATER COMPARED TO *N. RAFFLESIANA* PF. 113
FIGURE 5.3. EFFECT OF *N. RAFFLESIANA* PF ON THE PEAK ATTRACTIVE FORCE AND WORK OF RETRACTION FOR AN ANT GASTER. 115
FIGURE 5.4. USING ANT ANTENNAE TO PROBE THE SURFACE TENSION OF WATER VERSUS PITCHER FLUID. 117
FIGURE 5.5. SURFACE TENSION VALUES OF *NEPENTHES RAFFLESIANA* AND *N. INERMIS* PF COMPARED TO KNOWN FLUIDS AS MEASURED BY PENDANT DROP TENSIOMETRY. 118
FIGURE 5.6. SCANNING ELECTRON MICROSCOPY (SEM) IMAGES OF ANT GASTERS AFTER TESTING IN WATER (BLUE FRAME) AND *N. RAFFLESIANA* PF (GREEN FRAME). 120
FIGURE 5.7. DYNAMIC DEWETTING BEHAVIOUR OF *N. RAFFLESIANA* PF (GREEN BACKGROUND) AND WATER (BLUE BACKGROUND) ON DIFFERENT SURFACES VISUALISED VIA INTERFERENCE REFLECTION MICROSCOPY. 121

FIGURE 6.1: PROTOCOL DEVELOPMENT TO OBTAIN GLCA-MAN OLIGOMERS FROM RAW *NEPENTHES RAFFLESIANA* PITCHER FLUID VIA PARTIAL ACID HYDROLYSIS AND ETHANOL WASHES..... 137
FIGURE 6.2: PACE AND MALDI-TOF-MS ANALYSES REVEAL THE REPETITIVE NATURE OF THE BACKBONE OF THE PURIFIED *N. RAFFLESIANA* PITCHER FLUID POLYSACCHARIDE. 138
FIGURE 6.3: MONOSACCHARIDE IDENTIFICATION THROUGH EXTENDED ACID HYDROLYSIS. 140
FIGURE 6.4: POLYSACCHARIDES ISOLATED FROM *N. PERVILLEI* AND *N. RAFFLESIANA* PITCHER FLUID HAVE THE SAME BACKBONE STRUCTURE. 142
FIGURE 6.5: OVERVIEW OF VASCULAR PLANT PHYLOGENY WITH AN EMPHASIS ON PLANT ORDERS FROM WHICH POLYSACCHARIDES WITH GLUCURONO-MANNAN BACKBONES HAVE BEEN CHARACTERISED 147

LIST OF TABLES

TABLE 1.1. SUMMARY OF STUDIES ON LIMPET ATTACHMENT MECHANISM. 7

TABLE 2.1. SUMMARY OF MEASUREMENTS OF RELEVANT STRUCTURES FROM *LIPONEURA CORDATA* SUCTION ORGANS. 25

TABLE 3.1. SURFACE PROFILOMETRY OF TEST SUBSTRATES USED TO ASSESS ATTACHMENT PERFORMANCE 42

TABLE 3.2. SHEAR STRENGTH ESTIMATES FOR SUCTION-BASED ATTACHMENTS OF *HAPALOTHRIX LUGUBRIS* AND *LIPONEURA CORDATA*. 54

TABLE 4.1. LIST OF LECTIN-BASED STAINS USED TO INVESTIGATE SUGAR RESIDUES PRESENT IN THE LIMPET PEDAL SOLE. 81

TABLE 4.2. SUMMARY OF PUTATIVE ADHESIVE PROTEINS AND THEIR CHARACTERISTICS. 89

TABLE 6.1. STUDIES THAT HAVE ISOLATED AND CHARACTERISED ACIDIC POLYSACCHARIDES WITH GLUCURONO-MANNAN (GLCA-MAN) BACKBONE ARCHITECTURE. 148

1 INTRODUCTION

'It has long been an axiom of mine that **the little things** are infinitely the most important.'- *The Adventures of Sherlock Holmes* (1891), Sir Arthur Conan Doyle.

As scientists, we often rely on study systems to test our hypotheses. These systems can range from atoms to planets and everything in between. The study system must behave in a such a manner that invokes curiosity and interest from others, and also help us investigate our ideas. Those of us in the field of adhesion science have a number of systems to choose from, including those that are synthetic (e.g., polymers or artificial substrates) or biological (e.g., geckos, mussels, or insects). While synthetic systems allow for very specific experimental manipulations, the allure of biological systems is their complexity and diversity - all the bewildering adaptations that have been selected during evolution. And yet, from these complex organisms, with some luck and persistence, it is possible to decipher mechanisms that are impactful far beyond the original organism and are relevant across disciplines and systems. In the field of adhesion, this is exemplified by paradigm-shifting research on geckos, mussels, and climbing insects, to name but a few.

Biological adhesive systems are especially helpful for studying adhesion as many of them work in challenging conditions wherein conventional adhesives fail. For example, gecko feet can attach and detach extremely rapidly and resist contamination despite numerous applications on natural surfaces (Autumn, Niewiarowski, & Puthoff, 2014; Federle & Labonte, 2019). There are also many natural systems that adhere well underwater, a feat that is particularly challenging for synthetic adhesives as "water and adhesive are in conflict," according to the late K. W. Allen (Waite, 1987). Many of our current adhesive technologies perform poorly underwater due to the drastic reduction or total loss of adhesive forces otherwise available on land (e.g., van der Waals interactions, capillary forces, and electrostatic interactions), as well as lubrication from a thin water layer or biofilm (Ditsche & Summers, 2014; Stewart, Ransom, & Hlady, 2011; Waite, 1987). Yet, for numerous organisms, adhesion under such conditions is a way of life: they can adhere to substrates with slippery biofilms or with varying levels of roughness, often against

strong hydrodynamic forces. Hence, exploring these biological systems and understanding the underlying mechanisms can reveal novel insights into adhesion under wet conditions and may also be useful for future biomimetic adhesives.

For my thesis I have chosen to study three biological adhesive systems to address different questions related to adhesion under wet conditions:

1. Blephariceridae larvae (Diptera: Blephariceridae): Using this system, I investigate how suction organs can be used for dynamic underwater adhesion and how they can cope with wet and rough substrates.
2. Limpets (*Patella vulgata*): With this species, I explore the role of suction and glue-like secretions as mechanisms for adhesion in the intertidal zone, a challenging marine habitat with crashing waves and cyclic exposure to predators.
3. Pitcher plants (*Nepenthes rafflesiana*): I use this system to investigate how sticky fluids secreted by these carnivorous plants adhere to insects that have fallen into the fluid-filled pitfall traps and help retain the prey.

1.1 Net-winged midge larvae

The net-winged midges belong to a monophyletic family of dipteran insects (Blephariceridae) consisting of around 320 species, and is present on all continents except Antarctica (Gil-Azevedo & Santos, 2016; Zwick, 2004). Their developmental stages are aquatic, where they attach to surfaces in fast-flowing freshwater streams and cascades with water velocities exceeding 3 m/s (Figure 1.1a) (Craig, 1966; Frutiger & Buergisser, 2002). Since the identification of the Blephariceridae in the 19th century, entomologists have been fascinated by how the larvae stay attached in such harsh environments (Craig, 1969; Kellogg, 1900; Loew, 1844; Osten Sacken, 1895). Although attachment mechanisms in other animals are often debated long after the initial description of the species (see below for limpets), with blephariceridae larvae the main attachment mechanism was undisputed: each larva has six distinctive suction organs for attaching to wet and biofilm-covered rocks (Figure 1.1b). These “technically perfect suckers” (Zwick, 2004) are hallmarks of the blephariceridae larvae and allow them to inhabit extreme habitats where few competitors or predators are present (Hora, 1930). As remarked by Komárek in 1922:

‘These suckers are surelly the best air-pump which we know in the whole animal King-dom and their princip and mode of use are the same as in the air-pump apparat constructed by man.’ p.65, (Komárek & Wimmer, 1922).

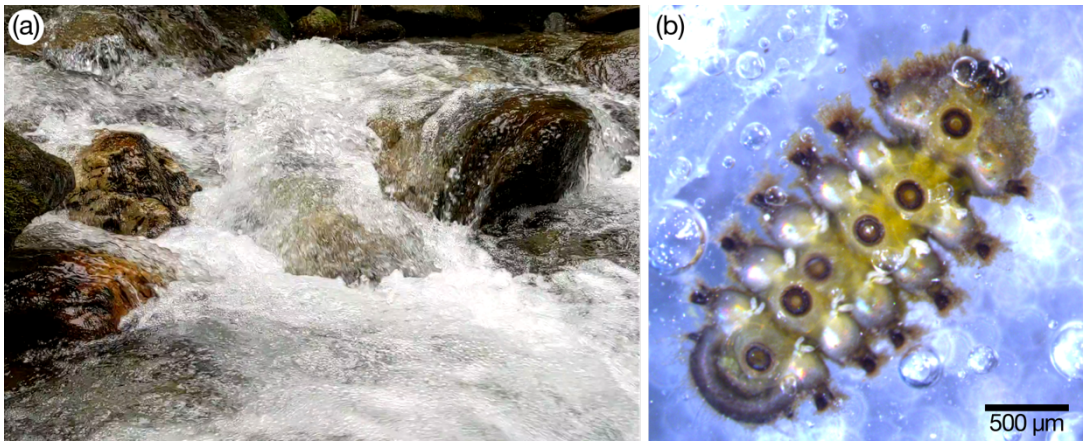

Figure 1.1. Larvae of net-winged midges survive in torrential alpine rivers. (a) Typical habitat for blephariceridae larvae. They are found on rocks beneath the frothing region. (b) *Hapalothrix lugubris* larva with six ventromedian suction organs. The larvae are able to crawl using the organs (note the blurred fourth organ).

Early morphological studies on the blephariceridae suction organ outlined structures thought to be important in creating and maintaining a powerful attachment: a suction disc, which contacts the substratum, a perimeter of hairs around the outside of the disc for sealing (likely incorrect, see Chapters 2 & 3), a central piston and associated muscles for manipulating the pressure, and a distinct cut into the disc called a V-notch for detachment (Komárek, 1914; Mannheims, 1935; Rietschel, 1961). Although researchers first identified these components in 1914 (Komárek, 1914) and elaborated on them through subsequent studies until 1961 (Bischoff, 1928; J. W. Campbell, 1920; Hofeneder, 1927; Mannheims, 1935; Rietschel, 1961), their observations were limited by the resolution of light microscopy and restricted to two-dimensional sections of fixed specimens. Moreover, as the field of biological adhesion had yet to develop, researchers lacked crucial mechanistic insights needed to evaluate the function of these organs. Due to these reasons, while the morphology of the blephariceridae suction organs was seemingly well-understood, the mechanisms underlying their powerful adhesion remain unresolved.

It is also both interesting and perplexing that, despite the enormous diversity of insects and the multitude of attachment devices found in them (S. N. Gorb, 2002), suction organs are rare in this group. Although male diving beetles (Dytiscidae) have circular discs for

holding onto females during courtship and copulation, these suction cups are simple structures that lack muscular control and work best on smooth surfaces (Karlsson Green, Kovalev, Svensson, & Gorb, 2013). In contrast, there is an impressive diversity in the morphology of suction attachment organs found in animals besides insects that represent at least seven different taxa, including octopuses, squids, limpets, leeches, parasitic worms, gastromyzophorous tadpoles (Aguayo, Lavilla, Vera Candioti, & Camacho, 2009; Aiken & Khan, 1992; Arita, 1967; Fukushima et al., 2017; Hora, 1930; Kampowski, Eberhard, Gallenmüller, Speck, & Poppinga, 2016; Kier & Smith, 1990, 2002; Nixon & Dilly, 1977; A. M. Smith, 1991b, 1996; Vera Candioti, Haas, Altig, & Peixoto, 2017), and many fish species, such as remora fish, clingfish, lumpsucker, catfish, and lampreys, to name a few (for remora fish, clingfish, and lumpsuckers, see (Arita, 1967; Davenport & Thorsteinsson, 1990; Fulcher & Motta, 2006); for a detailed summary of rheophilic freshwater fish species with specialised adhesive structures, see (Lujan & Conway, 2015)). Almost all of these animals are aquatic and have to overcome the challenges of adhering to different surfaces in wet conditions. It is likely that suction attachments are favoured in wet environments (and less efficient in air) for the following reasons:

1. Mucous secretions can help with sealing: an effective seal between the organ and the environment is crucial for suction attachments. Aquatic animals, including all fishes, gastropods, and cephalopods, possess a mucous outer layer (Ditsche, Wainwright, & Summers, 2014; Kier & Smith, 2002; Prezant, 1985; A. M. Smith, 1992). Mucus can help seal the suction organ on rough surfaces and minimise leakage. In addition, it can also contribute to overall attachment through viscous adhesion. While it is unknown if blephariceridlarvae also secrete mucus, surfaces in water are inevitably coated in biofilm that produce extracellular polymeric substances (EPS) which may result in a similar function (Ditsche, Michels, Kovalev, Koop, & Gorb, 2014; Prezant, 1985).
2. High attachment strengths with small movements: due to the incompressibility of water, a small reduction in volume inside a water-filled organ will result in a much higher stress pressure difference than if air-filled (Kier & Smith, 1990). Moreover, as water can sustain negative pressures (subject to cavitation), even at sea-level a suction organ can achieve a higher theoretical maximum strength when filled with water than with air (Cochard, 2006; A. M. Smith, 1996).
3. Hydrostatic pressure increases with depth in favour of higher adhesive strength: suction attachment strengths depend on the surrounding pressure and the

cavitation threshold of the water. Since hydrostatic pressure increases by 0.1 MPa for every 10 m depth in water, suction organs can reach higher stresses in deeper waters (Ditsche & Summers, 2014).

Given the abundance of independently evolved suction organs and the advantages they provide, it is clear that they are an effective strategy for underwater attachment. Yet, despite the expansive literature on suction organ morphology, mechanistic studies are scarce and only exist for a handful of species, such as the remora fish, clingfish, diving beetles, and octopuses (Beckert, Flammang, & Nadler, 2015; Chen, Shih, Wu, Yang, & Chi, 2014; Ditsche, Wainwright, et al., 2014; Fulcher & Motta, 2006; Karlsson Green et al., 2013; Kier & Smith, 1990, 2002; Tramacere, Beccai, et al., 2013; Tramacere, Kovalev, Kleinteich, Gorb, & Mazzolai, 2013; Wainwright, Kleinteich, Kleinteich, Gorb, & Summers, 2013). Moreover, many of the previous investigations primarily focussed on measuring peak attachment forces and did not probe the underlying mechanisms of adhesion. Thus, basic questions on the function of suction organs remain unsolved; in particular, it is unclear how specialised structures within the organs interact with rough substrates, and how suction attachments can be dynamic for locomotion.

In Chapters 2 and 3, I examine the morphology and ultrastructure of blephariceridsuction organs using advanced imaging techniques (computed microtomography, confocal microscopy, *in vivo* interference reflection microscopy, and various scanning electron microscopy methods), paying close attention to structures that can facilitate adhesion and friction in high-drag environments. I evaluate the attachment performance of blephariceridlarvae on various defined substrates to investigate the functional roles of a selection of these structures. Moreover, I identified a novel system (the V-notch apodeme and muscles) that is dedicated to rapid active detachments of the organ, which plays a key role in the rapid locomotion of the larvae.

1.2 Limpets

Limpets (the Patellogastropoda clade) are an ancient group of marine gastropods, thought to be the most primitive extant taxa of Gastropoda (Nakano & Ozawa, 2007). The oldest limpet fossils date as far back as the Middle Ordovician (ca. 450 million years ago) (Nakano & Ozawa, 2007). Limpets have spread around the world and can be found in habitats ranging from rocky seashores to deep-sea thermal vents. The common limpet,

Patella vulgata (Patellidae), is widespread in Europe, while lottiid limpets such as the owl limpet (*Lottia gigantea*) can be found along the coast of the Pacific Northwest (Nakano & Ozawa, 2007). Limpets that inhabit the upper intertidal zone have evolved powerful attachments to survive in this challenging environment, where they are exposed to strong hydrodynamic forces from crashing waves with velocities of 10 m/s and repeated predatorial attacks (Figure 1.2a) (Denny, 1988; Denny & Blanchette, 2000; Grenon & Walker, 1981; Hahn & Denny, 1989; Pound, Miller, King, & Burnaford, 2020).

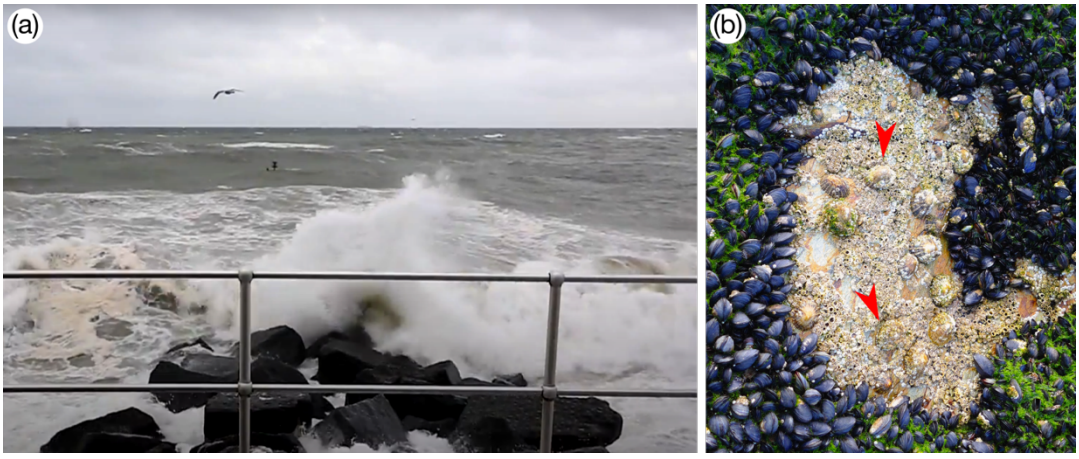

Figure 1.2. Limpets attach powerfully to rocks in the intertidal zone. (a) Crashing waves at Sheringham, UK, where limpets were collected for this thesis. Image copyright: Chris Taylor. (b) Limpets (red arrowheads) inhabit the same niche as barnacles and mussels, except limpets move around to feed. Image from pxfuel.

Limpet attachment strengths range from 0.1 to 1.1 MPa (Branch & Marsh, 1978; Coleman, Browne, & Theobalds, 2004; Denny, Daniel, & Koehl, 1985; Grenon & Walker, 1981; A. M. Smith, 1991b). To put this in context, the attachment strengths of marine mussels and barnacles that are permanently adhered to slate are between 0.56 to 0.93 MPa (Waite, 2002; A. B. Yule & Walker, 1984). Since adult barnacles and mussels secrete glues to survive in the intertidal zone and attach with comparable strengths to limpets, one could hypothesise that a similar mechanism is used by limpets (Figure 1.2b). Unlike their sessile neighbours, however, limpets are mobile grazers, and some species are known to travel considerable distances (relative to body size) to feed on biofilm and detritus (Branch & Marsh, 1978; Burgos-Rubio, De la Rosa, Altamirano, & Espinosa, 2015). This adds another layer of complexity when trying to understand limpet adhesion: how do they attach strongly to natural rock surfaces (and stop moving) when exposed, yet transition into weaker locomotive adhesion for feeding?

Table 1.1. Summary of studies on limpet attachment mechanism. Adapted from (Grenon & Walker, 1980).

Authors	Species	Proposed mechanism of adhesion
Réaumur, 1711	*P. vulgata*	Secretion of an adhesive substance
Woodward, 1875	*P. vulgata*	Suction
Davis, 1895	*P. vulgata*	Secretion of an adhesive substance
Piéron, 1909	*P. vulgata*	Suction and interlocking of foot
Menke, 1911	*Patella sp.*	Secretion of an adhesive substance
Parker, 1911	*Patella sp.*	Suction
Loppens, 1922	*P. vulgata*	Suction
Abe, 1931	*L. dorsuosa* (syn. *Acmaea dorsuosa*)	Suction & secretion of an adhesive substance
Thomas, 1948	*Cellana tramoserica*	Secretion of an adhesive substance
Crisp, 1973	*Patella sp.*	Secretion of an adhesive substance & Stefan adhesion
Branch & Marsh, 1978	Various patellid species	Mucous cohesion and surface tension; foot rigidity
Grenon & Walker, 1981	*P. vulgata*	Secretion of an adhesive substance and foot rigidity
Smith, 1991	Various lottiid species	Suction (also mentions adhesive secretions)
Smith, 1992	Various lottiid species	Alternating between suction and adhesive secretions
Smith, 1999	*L. limatula*	Adhesive secretions (differences between trail and adhesive mucus)

Unlike blephariceridlarvae, where there was a consensus on the main mode of attachment from the beginning, researchers have debated the adhesion mechanism of limpets for centuries (Table 1.1). As one can infer from the number of different mechanisms proposed over the years, limpet attachment is a complex phenomenon. Indeed, attachment strengths appear to depend on a plethora of variables, including when the limpet last moved (Denny et al., 1985; A. M. Smith, 1991b, 1992), surface properties such as roughness and surface energy (Grenon & Walker, 1981), species (Branch & Marsh, 1978; Grenon & Walker, 1981), and it varies even between individuals within an aggregation (A. M. Smith, 1991b). Nevertheless, the two main hypothesized mechanisms are suction and glue-like adhesion. The last detailed mechanistic studies on lottiid limpet attachment concluded that these limpets alternate between suction-based attachments when active during high tide and high strength attachments using glue-like mucus when stationary and exposed at low tide (A. M. Smith, 1991b, 1992; A. M. Smith, Kier, & Johnsen, 1993). Initial biochemical characterisation of *L. limatula* pedal mucus showed it consisted largely of

water (~93%), with the rest comprising proteins, sugar, and inorganic matter (A. M. Smith, Quick, & St. Peter, 1999). Gel electrophoresis of solubilised mucus confirmed that proteins of several different sizes were present, and analysis of their amino acid compositions revealed a preponderance of charged and polar residues. Crucially, Smith *et al.* demonstrated that there were specific differences between the molecular composition mucus secreted during stationary adhesion and locomotion, suggesting that limpets can manipulate their pedal mucus for adhesion (A. M. Smith et al., 1999).

Although an initial investigation of the molecular composition of *P. vulgata* pedal mucus also found proteins with a higher proportion of charged or polar amino acids, the researchers did not collect different types of pedal mucus for comparison (Grenon & Walker, 1980). Moreover, several studies argued against suction being the mechanism of adhesion in *Patella* limpets, although they did not use direct pressure measurements (Branch & Marsh, 1978; Grenon & Walker, 1980, 1981). Hence, a mechanistic study into patellid limpet adhesion is necessary to determine if the dual mechanism of suction and adhesive mucus as seen in lottiid limpets also applies to *P. vulgata*. In addition, while we know that proteins are an important component of both patellid and lottiid pedal mucus, none of them have been sequenced thus far. This represents a significant gap in our knowledge on limpet adhesion and of marine invertebrate adhesion overall, considering the amount of available information on bio-adhesives of other marine invertebrates, such as barnacles, mussels, sea stars, sea urchins, marine flatworms, and sandcastle worms (Hennebert, Flammang, Demeuldre, Hennebert, & Santos, 2016; Hennebert, Maldonado, Ladurner, & Flammang, 2015; Lengerer & Ladurner, 2018; Stewart et al., 2011). Characterising the molecular composition of marine bio-adhesives is a key first step in identifying the interactions that can promote adhesion and cohesion. This approach has yielded valuable insights into the role of various functional groups (e.g., *L*-dopamine, sulphation and phosphorylation) and processes (e.g., ligand binding / cross-linking, complex coacervation) that are important for underwater adhesives (Petrone, 2013; Stewart et al., 2011; Waite, 2017). A deeper investigation into the molecular composition of limpet pedal mucus, therefore, can help us understand if and how it can function as an adhesive.

In Chapter 4, I explore the powerful attachment of *P. vulgata* to elucidate the contribution of suction and to characterise the pedal adhesive secretions. I investigate whether patellid

limpets can generate pressure differences on par with those measured in lottiid limpets in previous studies. Furthermore, I develop a systematic approach to isolate different types of pedal mucus, and consequently characterise the constituent proteins and glycans. In doing so, I provide a detailed characterisation of the molecular composition of limpet pedal adhesive mucus and offer considerable new insight into patellid limpet adhesion.

1.3 Pitcher plants

Animals, however, are not the only biological systems to secrete adhesive substances. Plants use adhesive secretions to fulfil various functions, such as to climb up surfaces in the case of ivy plants (*Hedera* genus) (Zhang, Liu, Prest, & Fischer, 2008) or to catch insects, as seen in sundew plants (*Drosera* genus) (A. Ellison & Adamec, 2018). While the ivy uses its adhesive to anchor itself to surfaces (Yujian Huang et al., 2016), sundew plants rely on sticky mucilage to catch insect prey (Adlassnig, Lendl, Peroutka, & Lang, 2010). Sticky traps are one of the main capture strategies of carnivorous plants, which often inhabit low-quality soils and have evolved to catch and digest animals (usually insects) to supplement their nutritional intake (Adlassnig et al., 2010; A. Ellison & Adamec, 2018). This capture mechanism is traditionally associated with carnivorous plants that produce droplets of the sticky mucilage through glandular hairs (trichomes) on their leaves, as seen in *Drosera, Triphyophyllum, Drosophyllum, Byblis,* and *Pinguicula* (Adlassnig et al., 2010). These leaves resemble sticky flytrap paper in their function, where the adhesive readily adheres to insects lured to the plant and prevents them from escaping (Adlassnig et al., 2010; Kokubun, 2017). It turns out, however, that other carnivorous plants also secrete sticky fluids to facilitate prey capture.

Nepenthes pitcher plants are well-known examples of carnivorous plants that use a pitfall trap strategy to catch prey (Płachno & Muravnik, 2018; Thorogood, Bauer, & Hiscock, 2018). These pitchers are highly modified leaves that have evolved several different structural adaptations that promote insect capture, including a slippery peristome around the rim of the pitcher and a waxy inner wall that hinders the prey from climbing out (Figure 1.3a) (Bauer, Grafe, & Federle, 2011; Bohn & Federle, 2004; Bonhomme et al., 2011; Płachno & Muravnik, 2018). Once the prey falls inside, it lands in a pool of pitcher fluid that can be watery or sticky, depending on the species (Bonhomme et al., 2011). Of the ~160 to 180 extant species of *Nepenthes*, at least 17 (~10%) produce sticky pitcher

fluid that forms filaments when stretched (Figure 1.3b) (Bonhomme et al., 2011; Płachno & Muravnik, 2018). Researchers have used *Nepenthes rafflesiana* as a study system to show that viscoelastic pitcher fluid, which exhibits both solid-like and liquid-like behaviour in a time-dependent manner, is more effective at retaining insects than water, and the benefit afforded by the viscoelasticity persists in spite of significant dilution by water (Bauer et al., 2011; Gaume & Forterre, 2007). Moreover, a sticky pitcher fluid may offer an advantage for capturing flying insects that may otherwise evade the pitcher's slippery walls (Bazile, Moguédec, Marshall, & Gaume, 2015; Bonhomme et al., 2011).

While previous researchers have proposed the viscoelastic behaviour of the fluid is an important mechanism of prey capture (Gaume & Forterre, 2007), they did not explore in detail a crucial element of the fluid-prey interaction: pitcher fluid adhesion to insect cuticle. To prevent escape, pitcher fluid first needs to adhere to insect cuticle and then resist detachment caused by the struggling insect. Therefore, it needs to readily wet and strongly resist dewetting from the cuticular surface to function effectively as an adhesive trap. The fluid also has to remain sticky for several weeks while the pitcher is open and catching prey in the face of constant risk of microbial degradation.

In Chapter 5, I investigate how viscoelastic pitcher fluid adheres to insect cuticle and impedes escape using *N. rafflesiana* as the study system. I quantify the peak adhesive force and the work needed to retract ant abdomens (gasters) from pitcher fluid to understand its effect on fallen prey. In addition, I examine the role of surface tension in insect capture by pitcher fluid. I also visualise the wetting and dewetting behaviour of pitcher fluid on various surfaces to understand how a wet adhesive like pitcher fluid resists dewetting and hence detachment. After examining the mechanisms responsible for the adhesive property of *N. rafflesiana* pitcher fluid, in Chapter 6 I focus on identifying the molecules that give rise to the fluid's behaviour. Consequently, I propose that *N. rafflesiana* pitcher fluid can be a useful system for exploring the origin of these molecules and their functions not just in the sticky fluids of carnivorous plants but for plants in general.

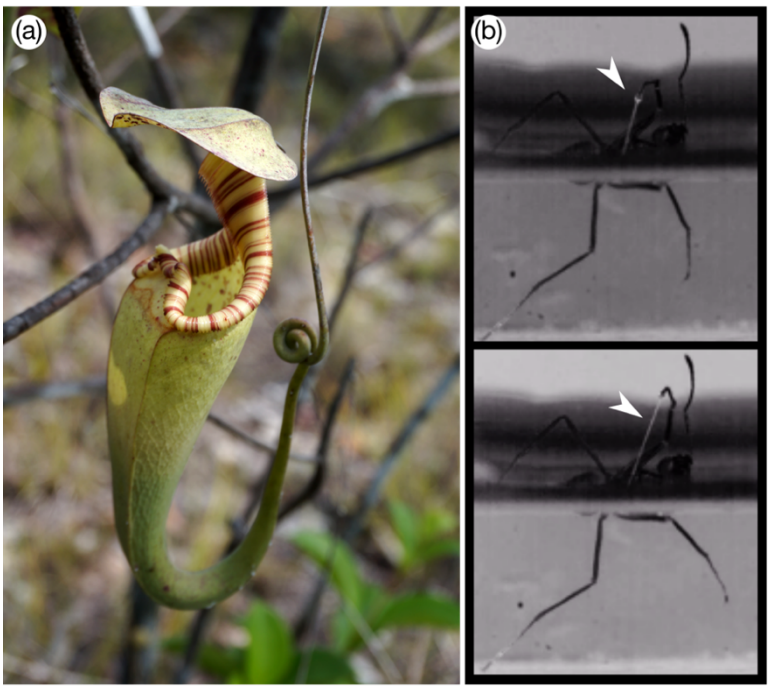

Figure 1.3. Pitcher plants are carnivorous plants that use their highly modified leaves as pitfall traps to catch insect prey. (a) *Nepenthes rafflesiana* pitcher plant has a slippery peristome (banded rim) that causes insects to fall inside. (b) Inside the pitcher, *N. rafflesiana* secretes a sticky viscoelastic fluid that adheres to insects and prevents escape. Here, an ant is struggling in sticky pitcher fluid, pulling out long fluid filaments (white arrowhead).

Adhesion in wet environments is a fundamental process for many living systems. Understanding how different plants and animals achieve this requires an interdisciplinary approach that considers both the physical and chemical interactions at the molecular and whole-organism levels. Hence, I investigate the mechanisms of adhesion in my chosen study systems through the combined perspectives of biomechanics, molecular biology, and biochemistry.

2 MORPHOLOGY OF POWERFUL SUCTION ORGANS FROM BLEPHARICERID LARVAE LIVING IN RAGING TORRENTS

2.1 Summary

Suction organs provide powerful yet rapid attachments for many aquatic animals, including octopuses, squids, remora fish, and clingfish. While the functional morphology of suction organs from some cephalopods and fishes has been investigated in detail, there are only a few studies on such attachment devices in insects. In this study, we characterised the morphology and ultrastructure of the suction attachment organs of aquatic net-winged midge larvae (genus *Liponeura*). The larvae use these suction organs to generate powerful attachments to rocks in rapid alpine waterways where flow-rates can be up to 3 m/s. We identified structural adaptations important for the function of the suction attachment organs in *L. cinerascens* and *L. cordata*. First, a dense array of spine-like microtrichia covering each suction disc comes into contact with the substrate upon attachment. Hairy structures have also been found on the contact zones of suction organs from octopus, clingfish, and remora fish. These spine-like microtrichia may contribute to the seal and provide increased shear force resistance in high-drag environments. Second, specialised rim microtrichia at the suction disc periphery were found to form a continuous ring in close contact and may serve as a seal on a variety of surfaces. Third, a V-shaped cut on the suction disc (the V-notch) is actively peeled open via two cuticular apodemes inserting on its flanks. The apodemes are attached to dedicated V-notch opening muscles, thereby providing a unique detachment mechanism. The complex cuticular design of the suction organs, along with specialised muscles that attach to them, allows blephariceridlarvae to generate powerful attachments which can withstand strong hydrodynamic forces and quickly detach for locomotion. Structural adaptations from these suction organs could translate into future bioinspired attachment systems that perform well on a wide range of surfaces.

2.2 Introduction

Firmly attached to rocks in rapid alpine streams, rivers, and bases of waterfalls, the aquatic larvae of net-winged midges (Diptera: Blephariceridae) have fascinated

entomologists for over a century due to their powerful adhesion and complex attachment organs (Kellogg, 1900, 1903; Komárek, 1914; Loew, 1844). In these challenging environments, where the water velocity can reach up to 3 m s^{-1} (Frutiger & Buergisser, 2002), the midge larvae spend most of their development cycle on underwater rock surfaces, where they move around and graze on diatoms (Figure 2.1; Supplementary Video SV1). The larvae are capable of forward and reverse crawling, as well as rapid side-ways movement in response to threats (Frutiger, 1998). For all these locomotion types, the larvae need to quickly detach and firmly re-attach individual suction organs to avoid dislodgment from the fast water flow. Such tumultuous conditions are favourable for these larvae as few other insects can withstand the large hydrodynamic forces, thereby decreasing competition and predation (Frutiger, 1998; Hermann, Mullen, & Wallace, 1975; Hora, 1930). Some blephariceridlarvae attach so strongly that forces greater than 600 times their body weight are needed to detach them perpendicularly from the rocks (based on force and weight measurements from *Hapalothrix lugubris* (Frutiger, 2002)), surpassing all recorded values of insect attachment strengths (Federle, Rohrseitz, & Hölldobler, 2000; S. N. Gorb, Gorb, & Kastner, 2001).

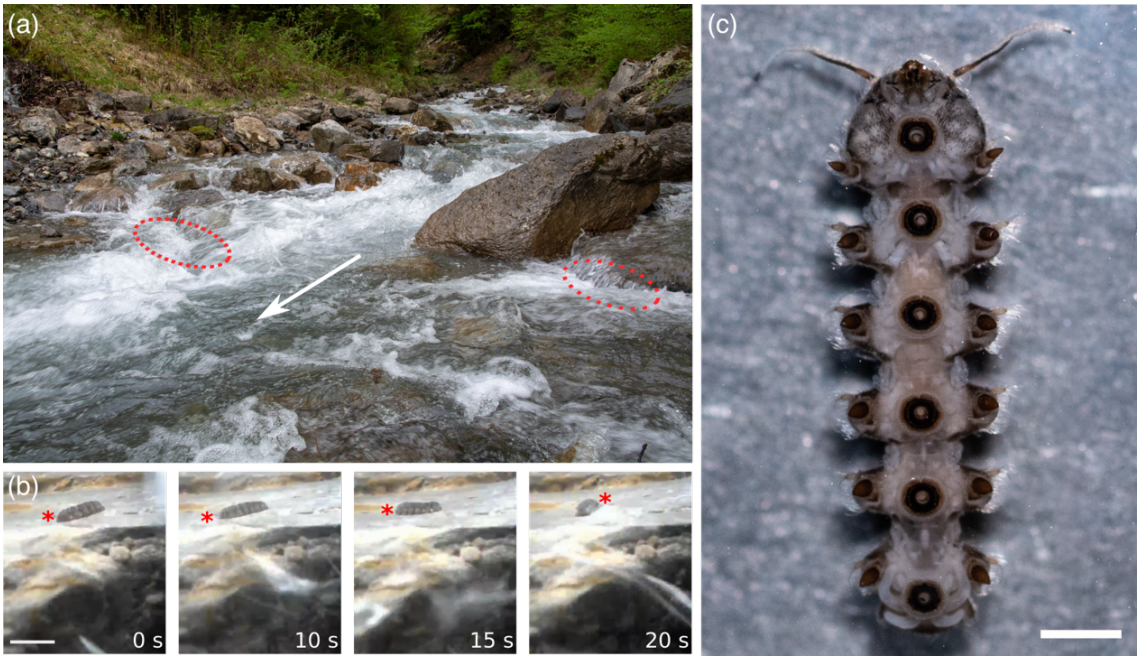

Figure 2.1. Habitat and crawling locomotion of *Liponeura cinerascens* larvae. (a) Fast-flowing alpine river (Oltschibach, Switzerland), one of the collection sites for *L. cinerascens*. Encircled areas indicate sampling locations. (b) Selected frames from in situ underwater video recording of *L. cinerascens*, showing the larva (head marked with an asterisk) performing a clockwise turn to crawl against the flow (arrowhead points downstream). See Supplementary Video SV1 for full video. Scale bar 10 mm. (c) Ventral view of 4th instar *L. cinerascens* larva collected from the study site shown in (a). Scale bar 1 mm.

Previous studies have investigated how blephariceridlarvae manage to attach, forage, and grow in their natural habitats (Bischoff, 1928; J. W. Campbell, 1920; Craig, 1966; Frutiger, 1998; Frutiger & Buergisser, 2002; Frutiger & Gammeter, 1998; Frutiger & Jolidon, 2000; Kellogg, 1903; Komárek, 1914; Mannheims, 1935; Rietschel, 1961; Tonnoir, 1930). The functional morphology and development of blephariceridlarvae was reviewed and studied in detail by Rietschel over 50 years ago (Rietschel, 1961). The larvae have streamlined flat bodies to minimise drag and, unlike most other rheophilic invertebrates that use hooks and claws to attach to biofilm-covered rocks (Ditsche, Michels, et al., 2014; Ditsche & Summers, 2014), they rely primarily on suction: each larva has six ventromedian suckers with central pistons that are controlled by strong muscles, similar to stalked suckers in some decapods (A. M. Smith, 1996). The cavity that houses the piston (called "Manschette" (cuff) by Rietschel and "Chitinsäckchen" (cuticle sac) by other authors (Hofeneder, 1927; Komárek, 1914), translated from German) has a thick sclerotised wall, presumably to withstand the low pressures generated when the piston is raised for suction attachment (Rietschel, 1961). Note that numerous German publications on blephariceridmorphology (e.g. (Komárek, 1914),(Mannheims, 1935), (Hofeneder, 1927)) appear to use the term "chitin" interchangeably with "cuticle" without experimental evidence that the material is specifically chitin. We adopt the term "cuff" to avoid any erroneous characterization of the underlying material.

The suction disc, which is the ventralmost component of the suction organ, comes into contact with the surface and serves as the main point of attachment. A seal (closure of the suction chamber to minimise leakage of water into the contact zone) is required for suction-based attachments, biological or synthetic. Therefore, it has been suggested that in net-winged midge larvae, the seal is provided by the fringe layer, a thin flexible membrane with hairy projections around the perimeter of the disc, which moulds to the surface contours upon contact (Frutiger, 2002; Rietschel, 1961). Rietschel also hypothesised that in order to increase shear resistance against the strong hydrodynamic drag forces in fast-flowing waters, the larva uses small cuticular hair-like structures (called "microtrichia" by Rietschel) as "anchors" to penetrate into the biofilm layer (Rietschel, 1961). This idea, however, has yet to be tested experimentally.

A conspicuous V-shaped opening at the anterior side of the suction disc, called a V-notch, has led to different interpretations in previous studies. Rietschel proposed that water within the suction organ is expelled through this V-notch when the disc forms a new attachment to the surface (Rietschel, 1961), while Frutiger believed that the structure serves both as a water outlet and the initiation point for detachment (Frutiger, 2002). While Hora also thought that the V-notch served as an outlet, he went further to propose that the membranes around the V-notch could function like a backwater valve or a heart valve where fluid is pushed out but prevented from flowing back into the contact zone (Hora, 1930). There was, however, no detailed characterisation of the V-notch structure or the surrounding membranes to support this claim; hence, it is still unclear how the larva controls the V-notch to open the seal.

Despite the wealth of knowledge from these earlier light microscopy studies on the blephariceridsuction organs, many questions remain unexplored until now. The advancement of imaging technologies and biomechanical methods has enabled us to probe deeper into how these organs generate effective attachments. Furthermore, there is a growing interest from the engineering and applied sciences to adopt principles from biological suction organs to create synthetic suction devices that can out-perform existing technologies (Baik et al., 2017; Bandyopadhyay, Hrubes, & Leinhos, 2008; Bing-Shan et al., 2009; Sareh et al., 2017; Tramacere, Follador, Pugno, & Mazzolai, 2015; Yueping Wang et al., 2017). Most of the engineering inspiration to date has been drawn from two well-studied animals which use suction – the octopus and the remora suckerfish. In this study, we present an updated morphology of the suction organs in blephariceridlarvae (using two species – *Liponeura cinerascens* and *Liponeura cordata*) based on evidence from confocal laser scanning microscopy (CLSM), X-ray computed microtomography (micro-CT), and scanning electron microscopy (SEM). Furthermore, we present for the first time *in vivo* observations of the contact zone of suction organs using interference reflection microscopy (IRM).

2.3 Methods

2.3.1 Sample collection and maintenance

Specimens were collected from alpine streams in Austria (near Völs, Innsbruck) and Switzerland (near Interlaken). Some of the specimens were immediately fixed in 70% ethanol, while the rest were brought back to the laboratory in Cambridge and maintained

in a climate-controlled aquarium tank at 5°C. Rocks collected from the sampling sites provided diatoms and other biofilm as a source of food, and a timer-controlled LED light promoted biofilm growth. Collected larvae were identified to species and developmental stage based on identification keys from Frutiger (Frutiger & Jolidon, 2000) and Zwick (Zwick, 1980). Due to the difficulty in maintaining the larvae in laboratory conditions, all experiments were conducted within five days of collection.

2.3.2 *In vivo* imaging using interference reflection microscopy (IRM)

We imaged the surface contact of live blephariceridlarvae with Interference Reflection Microscopy (IRM). The application of IRM to characterize adhesive systems has been described in previous studies on insects and tree frogs (Dirks, Li, Kabla, & Federle, 2012; Federle, Barnes, Baumgartner, Drechsler, & Smith, 2006). Briefly, an individual larva was placed on a glass coverslip with a small droplet of aquarium water. Excess water was wicked away (a small amount was left to prevent desiccation), and the attached suction organs were observed under green light (546 nm wavelength) using either a 20x or 100x Leica oil immersion objective. Images and videos were recorded using a CMOS USB3 camera (DMK 23UP1300, The Imaging Source Europe GmbH, Bremen, Germany) and their proprietary software (IC Capture v2.4.642.2631). Analysis of video recordings and images were carried out using FIJI (Schindelin et al., 2012) (https://imagej.net/Fiji).

2.3.3 Scanning electron microscopy (SEM) of suction organs

Two types of SEM were used to characterise the morphology of the suction organ: a field emission SEM (FEI Verios 460) at the Cambridge Advanced Imaging Centre (CAIC), and a cryo-SEM (Zeiss EVO HD15 with Quorum PP3010T preparation system) at Sainsbury Laboratory Cambridge University. For field emission SEM (FESEM), samples were prepared as follows: Specimens in 70% ethanol were plunge-frozen in liquid ethane then freeze-dried overnight (Quorum Emitech K775X). To visualise internal structures and cross-sectional slices of the suction organs, the samples were plunge-frozen as described, mounted on a custom-designed aluminium block cooled with liquid nitrogen, then fractured using a double-edged razor blade. All samples were mounted on aluminium SEM stubs using double-sided carbon tapes and conductive silver paint to minimise charging. Samples were consequently sputter-coated using 16 to 32 nm of iridium depending on the amount of expected charging. For cryo-SEM, samples were removed

from 70% ethanol, mounted on stubs using colloidal carbon glue, then plunged into a pre-cooled Quorum PP3010T preparation system. Frozen fully hydrated samples were coated with 5 nm platinum immediately prior to imaging.

2.3.4 X-ray microtomography (micro-CT) of dissected suction organs

A single suction organ from a *Liponeura cordata* fourth instar larva (fixed in 70% ethanol) was dissected and stained in Lugol's iodine (PRO.LAB Diagnostics, UK) for 4 days. The stained sample was rinsed in 70% ethanol, transferred in ethanol to a specimen holder made from a micropipette tip attached to a needle holder, and sealed with hot-melt adhesive to avoid evaporation. The sample was analysed via X-ray Microscopy (XRM) using a lab-based Zeiss Xradia Versa 520 (Carl Zeiss XRM, Pleasanton, CA, USA) X-ray Microscope, using a CCD detector system with scintillator-coupled visible light optics, and tungsten transmission target. Multiple scans at varying resolution and field-of-view were carried out to give both an overall visualization, and to reveal regions of interest at higher resolution. For the overall scan an X-ray tube voltage of 70 kV, and a tube current of 85 µA were used, with an exposure of between 7000 - 10000 ms, and a total of 3201 projections. An objective lens giving an optical magnification of 20x was selected with binning set to 2, producing isotropic voxel (3-D pixel) sizes of between 0.5402 – 0.7111 µm. The tomograms were reconstructed from 2-D projections using a Zeiss commercial software package (XMReconstructor, Carl Zeiss), a cone-beam reconstruction algorithm based on filtered back-projection. XMReconstructor was also used to produce 2-D grey scale slices for subsequent analysis. 3D volume rendering and segmentations were carried out using Dragonfly v3.6 (Object Research Systems Inc, Montreal, Canada) and Drishti v2.6.4 (Limaye, 2012).

2.3.5 Synchrotron X-ray micro-tomography of dissected suction organs

Microtomographic scans of a single unstained and ethanol-fixed suction organ was performed at the UFO imaging station of the KIT light source. A parallel polychromatic X-ray beam produced by a 1.5 T bending magnet was spectrally filtered by 0.5 mm Al at a peak at about 15 keV, and a full-width at half maximum bandwidth of about 10 keV. A fast indirect detector system consisting of a 12 µm LSO:Tb scintillator (Cecilia et al., 2011), diffraction limited optical microscope (Optique Peter) and 12bit pco.dimax high speed camera with 2016 x 2016 pixels resolution (dos Santos Rolo, Ershov, van de Kamp,

& Baumbach, 2014) was employed for taking 3,000 projections at 70 fps and an optical magnification of 10X (1.22 μm effective pixel size). The control system concert (Vogelgesang et al., 2016) was used for automated data acquisition. Tomographic reconstruction was performed with a GPU-accelerated filtered back projection algorithm implemented in the UFO software framework40. 3D volume rendering of tomographic data was done using Drishti v2.6.4 (Limaye, 2012).

2.3.6 Confocal laser scanning microscopy (CLSM) of dissected suction organs

In order to prepare samples of optimal thickness, each suction organ was dissected from samples fixed in 70% ethanol. For ventral views of the suction disc, excess tissue was further excised to leave only the disc material for imaging. Dissected samples were rehydrated to 1x phosphate buffered solution (PBS) by being placed inside 50% ethanol-50% PBS, 25% ethanol-75% PBS, and 100% 1x PBS for 5 minutes at each concentration. Two different stains were used: Calcofluor white (Fluorescent Brightener 28, Sigma F3543), a non-specific fluorochrome that binds to chitin, cellulose, and other β-1-3 and β-1-4 polysaccharides (Harrington, Hageage, & Abmm, 2003), and Congo Red (Sigma C6277), also a non-specific fluorochrome that has been used to successfully stain small arthropods for CLSM (Michels, 2010).

Calcofluor white (CFW) stock solution (1% w/v) was prepared by dissolving the powder in 1x PBS in a water bath set to 65°C for 15 – 20 minutes. Samples were stained in 0.1% CFW for 4 hours, washed 3 times in 1xPBS, then mounted on glass slides using the method described by Michels (Michels, 2010) in Fluoromount (Sigma F4680).

Congo Red was prepared as described previously (Michels, 2010), with slight modifications: The solution was gently heated in a water bath at 65°C to fully dissolve the powder, and the stock solution was shielded from light using aluminium foil and kept in a dark cupboard. Samples were stained for 24 hours, removed from stain, rinsed 3 times in PBS at 10 minutes per rinse, then mounted as described above.

CLSM images were acquired using Olympus Fluoview FV3000 (Olympus Corp., Tokyo, Japan) using 405 nm excitation wavelength for CFW and 561 nm for Congo Red. Detection wavelengths were 412 – 512 nm and 580 - 680 nm for CFW and Congo Red

respectively. Since Congo Red is sensitive to bleaching, image acquisition settings were adjusted accordingly, and stained samples were imaged within 8 hours of mounting. Mounted CFW samples were sufficiently stable and could be imaged over 3-4 days if kept in the fridge. Image contrast, brightness, and false-colouring were adjusted using Fiji (Schindelin et al., 2012) (https://imagej.net/Fiji).

2.4 Results

The attachment organs of blephariceridlarvae resemble in shape the suction organs from octopus and squid (Figure 2.2a). The blephariceridsuction organ consists of the suction disc (Figure 2.2b, c), which contacts the surface and has a central opening that connects to the suction chamber. The suction chamber is stabilised by a ring-shaped cuticular cuff and can be evacuated by a central piston, which has a rounded cone-shaped cap. The cuff is surrounded by a circular cuticular fold (Figure 2.2a), with muscles attaching near the base of the fold via apodemes (Figure 2.2b, c). The muscles likely help to move or position the entire suction organ.

2.4.1 Suction disc

The suction disc is the ventralmost part of the suction organ and is therefore the structure that contacts the surface (Figure 2.2c). Suction disc diameters for fourth instar larvae of *L. cinerascens* and *L. cordata* were 426 ± 11 µm (n = 3 larvae; mean ± SD hereafter) and 377 ± 9 µm (n = 2 larvae), respectively. Morphometrics of suction disc diameters and larval body lengths of several species of blephariceridshave been reported elsewhere (Frutiger, 2002) and are in good agreement with our values. The disc appears darkly pigmented (Figure 2.1c) and is stabilised by sclerotised internal radial rays (Rietschel, 1961). We identified various functionally-important structural adaptations of the suction organ, which are described in detail in the following sections.

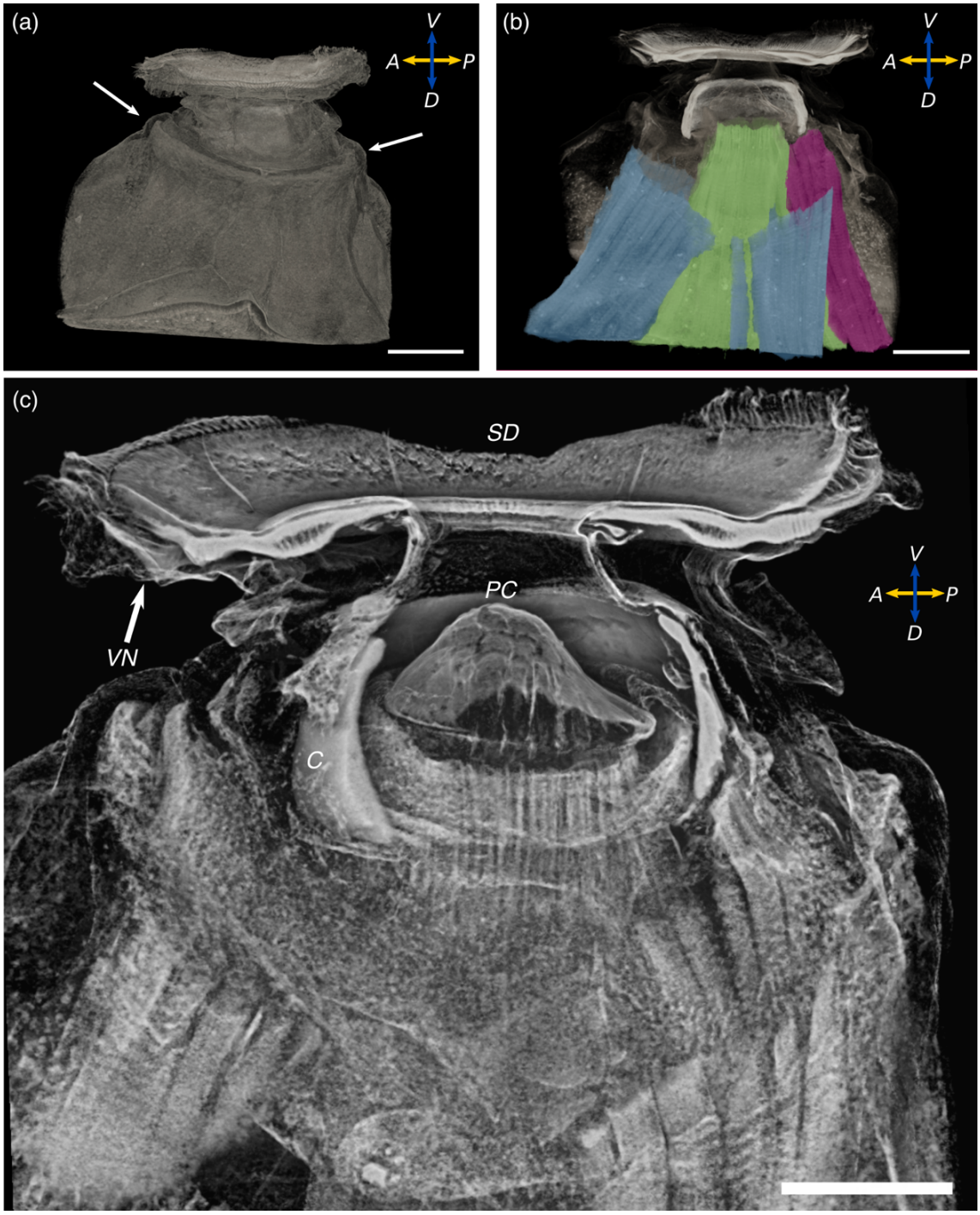

Figure 2.2. Suction attachment organ from *Liponeura cordata*; 3D reconstruction from micro-CT data. (a) External morphology of the organ (arrows point to the cuticular fold). (b) Sagittal plane showing three muscle groups inserting into the suction organ (green: piston muscles, magenta: cuff muscles, blue: cuticular fold muscles). (c) Sagittal plane highlighting the suction disc (SD), V-notch (VN), piston cone (PC), and the cuff (C). Major muscle groups are also visible (for labels refer to b). A: anterior, P: posterior, V: ventral, D: dorsal. Scale bars 100 µm.

2.4.1.1 Microstructures on the suction disc

In vivo observations of larvae attaching to a glass coverslip using IRM and SEM images of the surface of suction organs showed various microstructures on the disc (Figure 2.3). Beginning with the most peripheral structures in *L. cordata*, two rings of hairs called the "fringe" by previous authors form the outer margin of the suction disc (Frutiger, 2002; Rietschel, 1961). Some fringe hairs came into close contact with the surface, but these did not form a continuous sealing rim around the circumference. Instead, we observed a region just proximal to the fringe forming an almost continuous ring of close contact with the surface (as evident from the dark zero-order interference; Figure 2.3a). It is likely that this zone is important for sealing the suction chamber to allow the suction organ to generate and maintain sub-ambient pressures. Based on the *in vivo* IRM images, the width of the zone in close contact was 1.89 ± 0.02 µm (n = 2 larvae; see Table 2.1 and Figure 2.3a). SEM images of this region showed a pronounced cuticular rim of the same width (1.86 ± 0.07 µm, n = 2 larvae) at this location, formed by short flat cuticular projections joined side-by-side in an uninterrupted regular series (Figure 2.3b, c). Each structure, referred to as a rim microtrichium, was 0.64 ± 0.12 µm wide (n = 4 larvae; see Table 2.1) and oriented radially and approximately parallel to the surface (Figure 2.3c). These rim microtrichia repeated all the way around the perimeter of the disc, forming a continuous region of close contact around the attachment organ. In contrast, we did not observe such rim microtrichia around the disc rim perimeter in *L. cinerascens* (Figure 2.3d). Instead, SEM images of the suction discs showed a dense array of short and upright microtrichia at the same location as the rim microtrichia in *L. cordata* (Figure 2.3e, f).

The suction disc rim was not the only region of the suction disc that came into close contact with the substrate during attachment. *In vivo* IRM recordings showed a dense array of microstructures immediately proximal to the rim (towards the central opening) also coming into contact (Figure 2.4; Supplementary Video SV2). Individual microstructures formed small, roughly circular contact areas on glass coverslips (0.07 ± 0.02 µm^2, n = 2 *L. cinerascens* larvae), indicating that the tips made close contact. Video recordings showed a pulsing movement of the microstructures, which may be caused by the flow of water into and out of the contact zone (Supplementary Video SV3). SEM images of the suction disc show that these microstructures are spine-like microtrichia (Figure 2.3b-c, e-f). These microtrichia were present in both *Liponeura* species and were limited to an outer zone that covers approximately 30% of the total suction disc area

(Figure 2.5a). They are longer than the rim microtrichia and are curved, tapered in shape, and have distinct bulbous bases (Figure 2.5b). There is a gradual transition from the flat rim microtrichia to the longer spine-like microtrichia. While the morphology of the short rim microtrichia differs between the two *Liponeura* species, the spine-like microtrichia structure is highly conserved (Supplementary Figure 1). Additional characteristics of the spine-like microtrichia, including their dimensions, density, and pitch (relative to the suction disc plane) are summarised in Table 2.1.

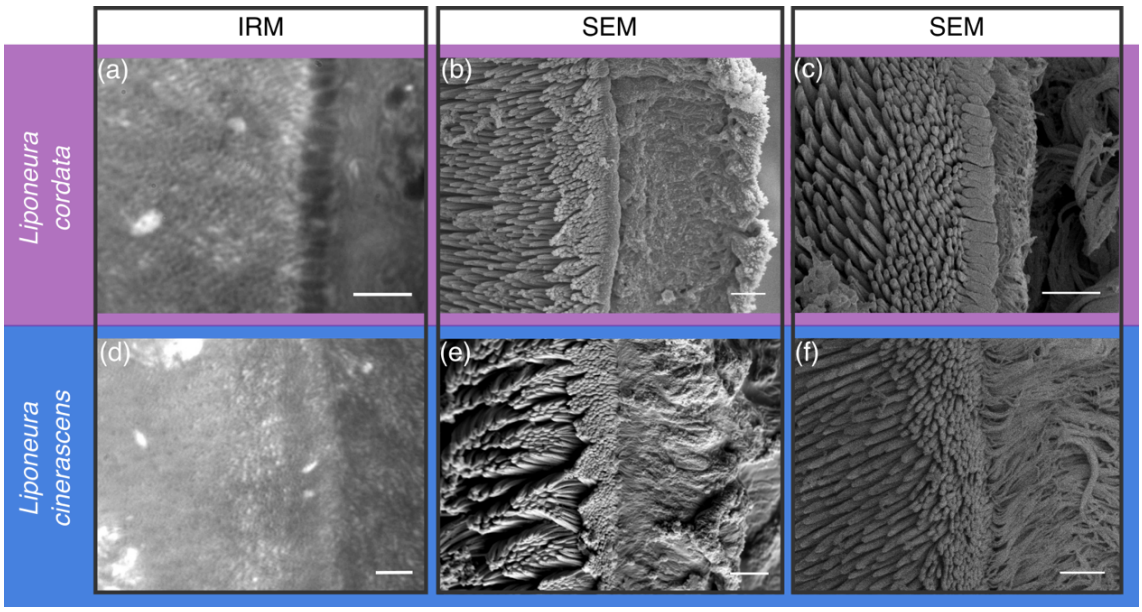

Figure 2.3. Microstructures on the suction discs of two *Liponeura* species. In *L. cordata.* (*a* – *c*), there is a well-defined contiguous ring of rim microtrichia. (*a*) *in vivo* image of a suction disc in contact with glass using IRM shows a row of rim microtrichia in close contact with the surface (black). (*b*, *c*) SEM images of the rim highlight the distinct flattened large microtrichia present in *L. cordata* in (*c*). *(d)* In comparison, the rim zone is less distinct in *L. cinerascens*. (*e*, *f*) SEM images highlight that in *L. cinerascens*, a rim is formed by a region of short, upright microtrichia. Note the fringe layer to the right of the rim. Scale bars (*a*) & (*d*): 3 µm, (*b*) & (*e*): 5 µm, (*c*) & (*f*): 3 µm.

In addition to the rim and spine-like microtrichia, we observed fine structures near the central opening also making contact (Figure 2.4). These fine central microtrichia are much shorter than the spine-like microtrichia, and lack the pitch and curvature (Figure 2.5b). We observed that when the piston was retracted (lowering the internal pressure), the central area was brought closer to the surface and a larger area of the central microtrichia zone came into contact (Supplementary Video SV4).

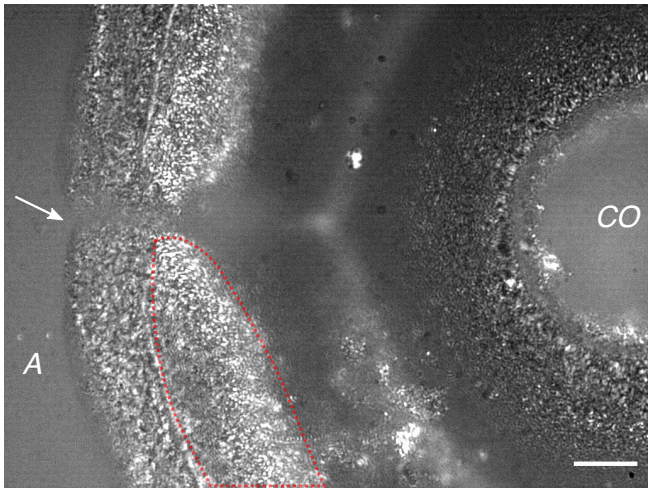

Figure 2.4. Suction disc of *L. cinerascens* larva in contact with a glass surface, visualised using *in vivo* interference reflection microscopy (IRM). Small, roughly circular black dots represent microtrichia in close contact to the surface (see region encircled in red). White regions are slightly further away, and grey regions even further from the surface. Arrow points to the V-notch (see text for details). *A*: anterior; *CO*: central opening. Scale bar: 15 µm.

2.4.1.2 V-notch

At the anterior side of each suction disc, the V-notch sharply disrupts the circular outline of the disc in both *Liponeura* species (Figure 2.5a and Figure 2.6). When the V-notch is shut, the sealing rim is almost continuous (Figure 2.4), but when fully opened, the V-notch gap is 2.6 ± 0.3% (n = 3, *L. cinerascens*) of the perimeter of the disc (i.e., for a fourth instar larva with 440 µm disc diameter, the V-notch is around 36 µm wide). The V-notch extended from the edge until the inner margin of the spine-like microtrichia zone (33.3 ± 2.7% of the suction disc radius, from n = 3, *L. cinerascens*) and the area surrounding the base of the V-notch lacked spine-like microtrichia. Through *in vivo* IRM recordings, we clearly observed local, active movements of the V-notch: when the suction disc was firmly attached to a surface, the V-notch was closed, but prior to detachment during locomotion, the two lateral flanks of the V-notch were peeled open (starting from the outer ends), thereby breaking the seal and rapidly equalising the pressure (Figure 2.6a, and Supplementary Video SV5). We also observed frequent rapid twitching of the flanks of the V-notch, which resulted in quick opening and closing without full detachment. From CLSM images of *L. cinerascens*, we found two long tendon-like cuticular apodemes attached to the flanks of the V-notch that wrapped around the cuff (but within the outer wall of the suction disc) and projected to muscles in the lateral-posterior direction (Figure 2.6b). Although the ends of the apodemes were beyond the scanning depth of CLSM, we

successfully traced the entire length of the structures using 3D renderings from X-ray synchrotron scan data of *L. cinerascens* (Figure 2.7). We discovered that each apodeme extends deep into the body, beyond the base of the cuticular fold, where it attaches to a dedicated muscle (Figure 2.7b). The apodeme was estimated to be 500 - 600 µm long (n=1 larva based on the synchrotron-based data) and 3.1 ± 0.8 µm in diameter (n = 2 *L. cinerascens* larva based on CLSM). The sarcomere length of the V-notch muscle was 7.1 µm (n = 1 larva). The V-notch apodemes did not appear to be attached to the cuff wall or to any surface as they circumvented around the cuff and into the body. The cross-sectional area of the V-notch muscles was smaller than that of other muscle groups associated with the suction organ (piston, cuff, and cuticle fold muscles; see Table 2.1).

In addition to the apodemes and muscles of the V-notch, a second novel feature of the V-notch was identified: in a sagittal view rendering from micro-CT data, it can be seen that the V-notch is shaped like a cupped hand and distinctly juts out further dorsally than the posterior side of the suction disc that has no V-notch (Figure 2.8). This membranous structure may have a valve-like function, as it could be seen widening and fluttering as the piston was lowered and water expelled through the valve, but when the piston was raised and the internal pressure lowered, this "valve" stopped moving (Supplementary Video SV6). It is likely that this structure and the associated movements serve to seal the V-notch, as proposed previously without direct evidence (Hora, 1930).

Table 2.1. Summary of measurements of relevant structures from *Liponeura cordata* suction organs.

	Liponeura cordata		***Liponeura cinerascens***	
Structural characteristics	**Mean ± SD**	**Number of individuals**	**Mean ± SD**	**Number of individuals**
Spine-like microtrichia				
Length (μm)	5.39 ± 0.05	2	7.6 ± 1.9	4
Diameter* (μm)	1.17 ± 0.02	2	1.5 ± 0.1	3
Pitch (° rel. to horizontal)	40.8 ± 0.5	2	38.4 ± 5.8	3
Density (μm^{-2})	0.44 ± 0.04	2	0.44 ± 0.1	6
Sealing rim width (µm)				
From SEM images	1.86 ± 0.07	3	--	--
From *in vivo* IRM images	1.89 ± 0.02	2	--	--
Rim microtrichia width (µm)	0.64 ± 0.12	4	--	--
Spine-like microtrichia zone coverage (% of total suction disc area)	30%	1	27%	3
Sarcomere lengths (µm)				
Cuticular fold muscle	8.2 ± 0.0	2	6.6 ± 0.2	2
Cuff muscle	7.6 ± 0.5	2	4.8	1
Piston muscle	5.6	1	6.7 ± 0.4	2
V-notch muscle	--	--	7.1	1
Cross-sectional muscle area (μm^2)				
Cuticular fold muscle‡	12,000	1	--	--
Cuff muscle‡	4,800	1	--	--
Piston muscle‡	13,000	1	--	--
V-notch muscleØ	--	--	950	1

Note: Standard deviation measures deviation between individuals where available. --: structures not fully accessible or visible for measurements. * Diameters of spine-like microtrichia were measured just above the bulbous base. ‡ Cross-sectional areas were estimated by taking orthogonal slice through the muscle before attachment using *L. cordata* micro-CT data. Ø Cross-sectional area of the V-notch muscle was estimated using *L. cinerascens* synchrotron-based CT data.

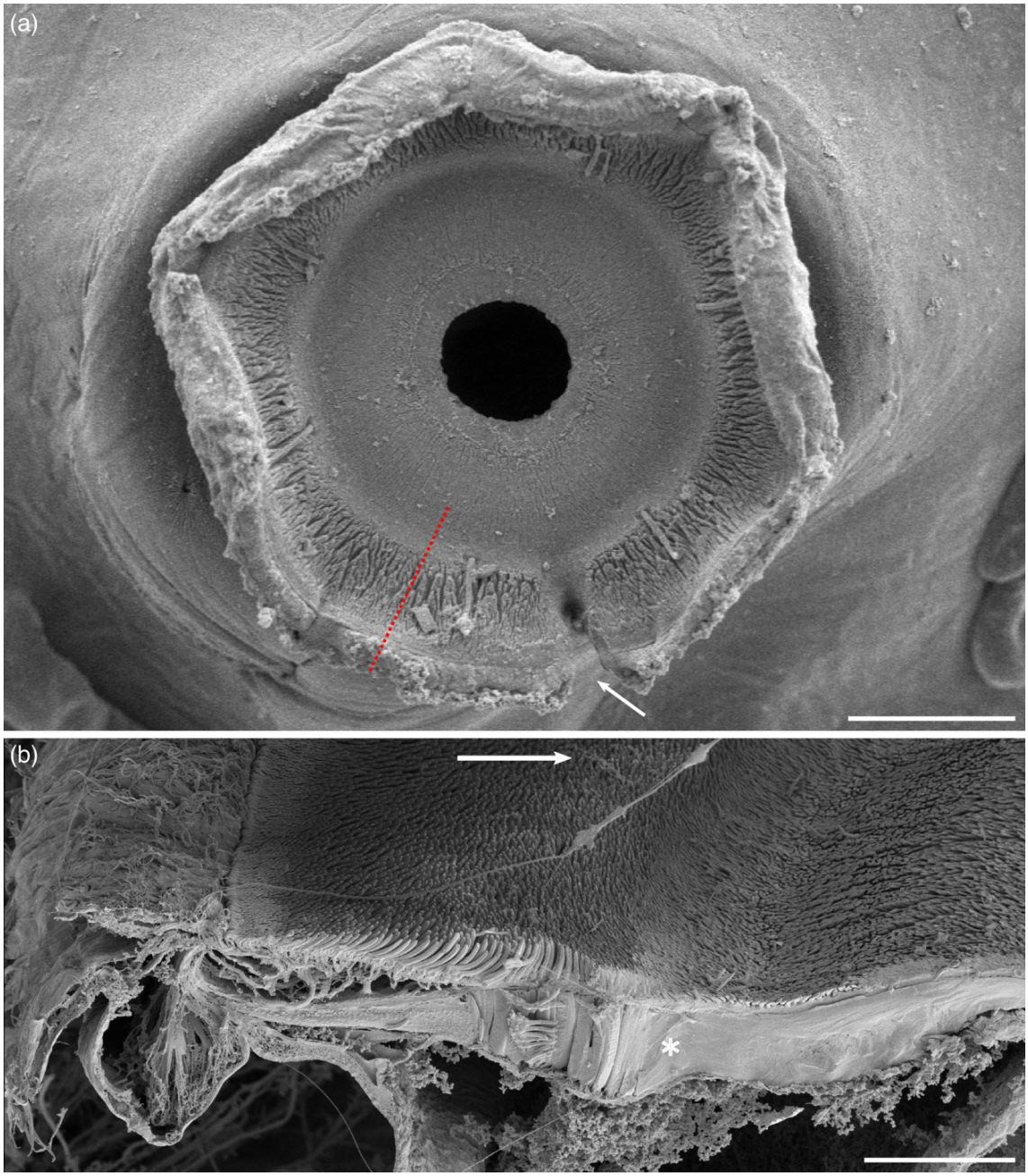

Figure 2.5. Microtrichia on the ventral surface of a 4th instar *Liponeura cordata* suction disc. (a) Cryo-SEM showing the location of the microtrichia region. Note the V-notch is in the open state (see arrow). The red dotted line indicates the approximate length and location of the freeze-fracture represented in *b.* Scale bar 100 µm. (b) Freeze-fracture SEM highlighting the different types of microtrichia found on the suction disc. The rim microtrichia are flat and short, while the spine-like microtrichia immediately proximal are long, curved, and oriented towards the centre. The central zone with short and approximately perpendicular microtrichia begins inward from the palisade layer (marked with an asterisk). Arrow points towards the centre of the suction disc. Scale bar 20 µm.

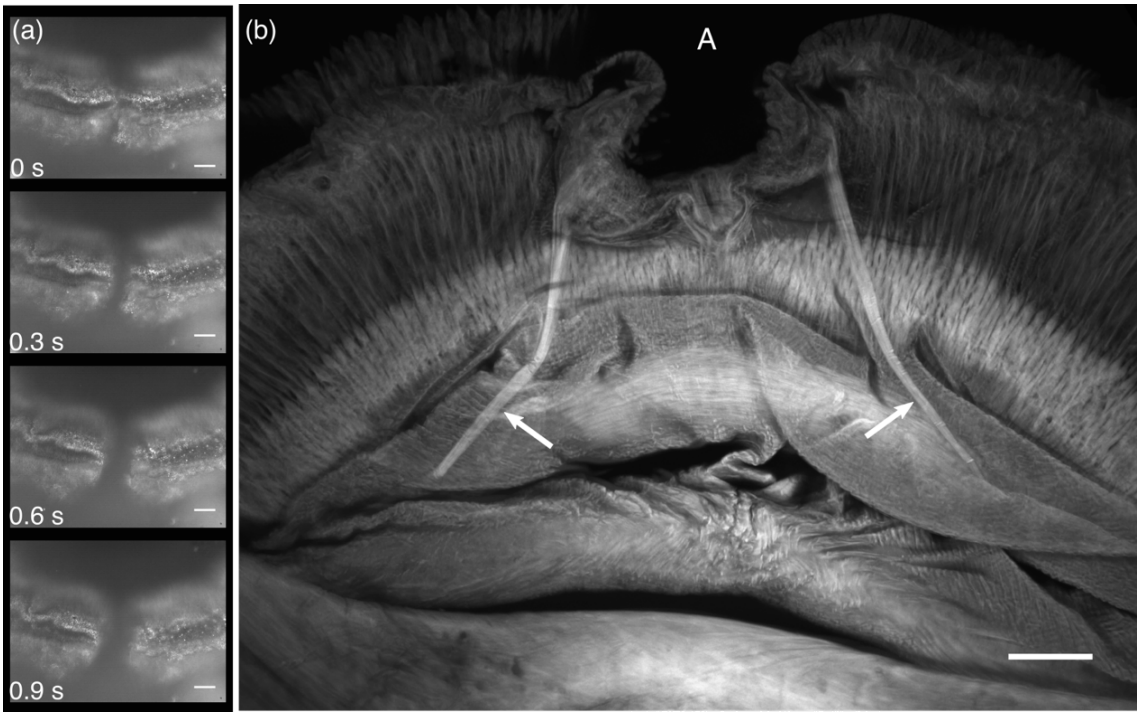

Figure 2.6. The V-notch system and its movement in a suction organ from *Liponeura cinerascens*. (a) Selected frames from *in vivo* IRM recording showing the V-notch being pulled open from the flanks (see Supplementary Video SV5 for the full video). (b) Confocal microscopy image of a Congo Red-stained suction organ reveals the two apodemes attaching to the V-notch flanks (see arrows) that mediate active muscular control of the V-notch. Scale bars 30 µm. *A*: anterior.

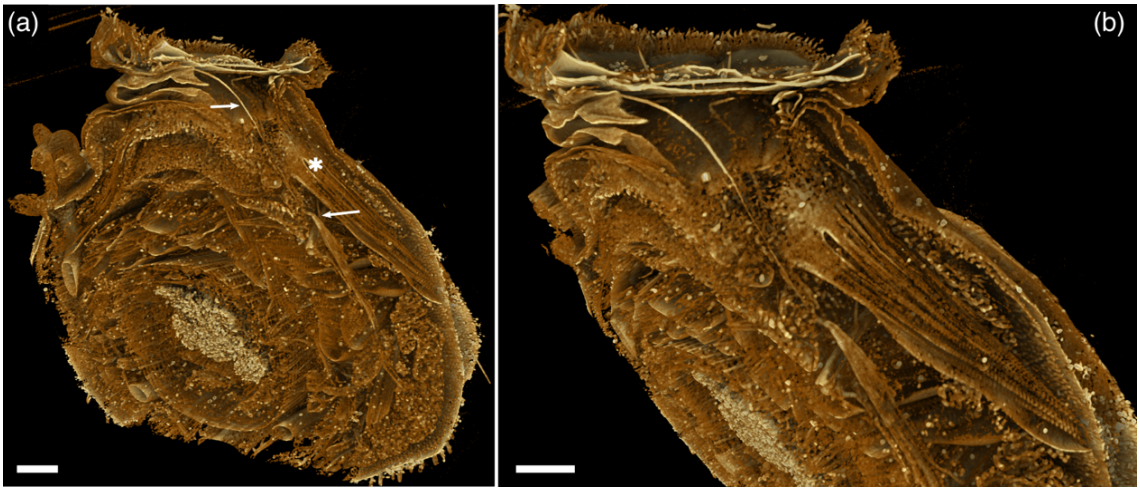

Figure 2.7. The V-notch apodeme extends posteriorly into the body to attach to a dedicated muscle. 3D reconstruction using X-ray synchrotron data of *Liponeura cinerascens*. (a) Overview of the suction organ digitally dissected to reveal the apodeme and the V-notch muscle (arrows). The muscle attaches to the inner dorsal wall. Note the cuff muscles next to the V-notch muscles (marked by an asterisk). (b) Lateral view of the apodeme and V-notch muscle. The curvature of the apodeme is clearly visible. Scale bars 100 µm.

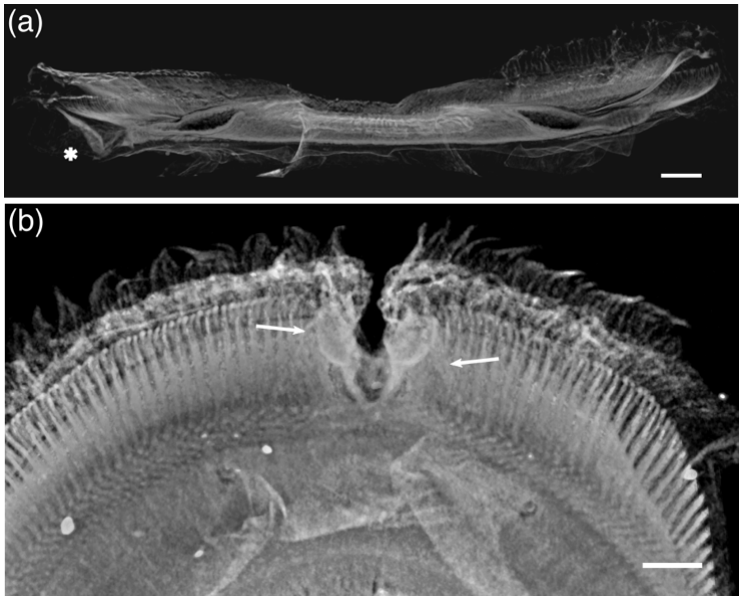

Figure 2.8. Detailed views of the V-notch valve-like structures from *Liponeura cordata*, reconstructed from micro-CT data. (a) Sagittal view of a suction disc rendered to reveal internal structures. The V-notch flap juts out dorsally from the suction disc (marked with an asterisk) compared to the opposite (posterior) side of the disc and could function as a backwater valve to prevent influx of water during piston contraction (see Supplementary Video SV6). (b) Dorsal view of the V-notch valves showing their flap-like morphology. Note that the V-notch apodemes attach to the flanks of the flaps (arrows). Scale bars 30 µm.

2.4.2 Piston and cuff

The blepharicerid larva uses a central piston to lower the pressure within the contact zone, similar to the stalked suckers of decapods (A. M. Smith, 1996). The rounded conical cap of the piston is comprised of dark sclerotised cuticle. This rounded cone is surrounded by the cuff, which has similar characteristics and is connected to the rounded cone via a thin flexible membrane. A reservoir of water is always kept within the volume enclosed by the cuff, which is important when generating pressure differentials as water is an incompressible fluid, so that small volume changes from piston movements can lead to large reductions in internal pressure. A pair of large muscles called the piston muscles (Rietschel, 1961) extend from the left and right sides of the dorsal cuticle and attach to the piston cone via multiple thread-like intracellular attachments, referred to as tonofibrils by Rietschel (Rietschel, 1961) (Figure 2.2c and Supplementary Figure 2). The muscles are positioned such that contraction leads to a movement in the dorsal direction. Sarcomere lengths from the piston muscles of fourth instar *L. cinerascens* were on average 6.7 ± 0.4 µm (n = 2 larvae) and 5.6 µm for fourth instar *L. cordata* (n = 1 larva).

Besides piston muscles, there is a pair of large muscles that extend from the inner dorsal wall and attach to the base of the membrane surrounding the cuff wall (Figure 2.2b, magenta). These cuff muscles are found only at the posterior end of the cuff, hence unlike the piston muscles, contraction of cuff muscles leads to an asymmetric directional pull on the organ. Cuff muscle sarcomere lengths from *L. cinerascens* were 4.8 µm (n = 1 larva) and 7.6 ± 0.5 µm *L. cordata* (n = 2).

2.4.3 Cuticular fold

The cuticular fold is formed by generous folding of the outer cuticle (Figure 2.2a) and partly encapsulates the piston apparatus (Figure 2.2b, blue). Near the cuticular fold, to the left and right sides of the suction organ, we observed two pairs of large muscles called cuticular fold muscles that could help to manoeuvre the suction organ. This is in agreement with previous studies that illustrated the muscles attaching to the organ such that contraction would lead to a force acting on the entire organ (Komárek, 1914; Rietschel, 1961). Note that the cuticular fold muscles attach to the suction organ and not the fold itself so that a contraction would retract the organ into the body of the larva. In *L. cinerascens*, the sarcomeres from the cuticular fold muscles were on average 6.6 ± 0.2 µm in length, whereas in *L. cordata* they were 8.2 ± 0.0 µm (n = 2 for each species). As both muscle pairs are located on the lateral sides of the organ, contraction is likely to produce movements in either vertical or lateral directions and limited movements in forward or reverse.

2.5 Discussion

2.5.1 Increasing shear resistance in suction attachments

The blepharicid larvae have evolved highly complex suction organs with unique structural adaptations for powerful and effective attachment on various surfaces. One such feature is the dense array of microtrichia within the suction disc. Rietschel proposed that these cuticular projections, which he compared to the gecko's adhesive setae, help the larva resist lateral forces by penetrating into biofilm layers and anchoring the animal (Rietschel, 1961). While the suction organs of male diving beetles (Chen et al., 2014; Karlsson Green et al., 2013) and medicinal leeches (Kampowski et al., 2016) have smooth surfaces, the surfaces of suckers from octopus, remora fish, and clingfish have similar small projections or spine-like structures (Bing-Shan et al., 2009; Ditsche, Wainwright, et al.,

2014; Fulcher & Motta, 2006; Kier & Smith, 1990; Wainwright et al., 2013). The proposed primary function of these structures is to come into contact with the surface and increase resistance to shear forces. In the remora fish, stiff mineralised conical structures called spinules are found at the tip of lamellae and can be actively rotated erect or flat using muscles attached to the lamellae (Beckert et al., 2015; Fulcher & Motta, 2006; Yueping Wang et al., 2017). The remora spinules have an aspect ratio of approximately 2:1 (average length and width of roughly 500 μm and 270 μm, respectively) and can interlock with surface asperities using pointed tips angled at 34° relative to the horizontal (Yueping Wang et al., 2017). They are arranged in consecutive rows and their tips face the posterior end of the fish. While the blephariceridmicrotrichia are different to the remora spinules in that they are thinner and longer (aspect ratio of around 5:1), more numerous (tens of thousands per individual compared to around a thousand in remora) and arranged as arrays covering the suction disc (compared to row arrangement in remora), they have similar shapes, tips, and pitch (Figure 2.9). Since remora spinules and blephariceridmicrotrichia are both found on suction attachment organs that need to withstand strong drag forces, the main function of these structures could be similar - to increase friction force on rough substrates and thereby improving attachment performance. Peak attachment force measurements on live remora fish on smooth versus rough (shark-skin) surfaces showed that higher shear forces were needed to detach them from rough surfaces (Fulcher & Motta, 2006), suggesting that the spinules are important in increasing the friction force between the suction organ and rough surfaces; subsequent quantitative studies confirmed that remora spinule tip contact significantly enhances friction by interlocking with asperities (Beckert et al., 2015; Yueping Wang et al., 2017). Even on smooth surfaces, small fibres could increase friction by making tip or side contact (Labonte, Williams, & Federle, 2014; D. H. Lee, Kim, Fearing, & Maboudian, 2011; Majidi, Groff, & Fearing, 2005), but typically, adhesion-based shear forces are strongly reduced underwater. Overall, these findings support the idea that microtrichia from blephariceridsuction discs increase the resistance to shear forces, which may be critical for animals living in high-drag aquatic environments. Further studies are needed to quantify the friction forces from the microtrichia zone to better understand the function of this characteristic morphology.

2.5.2 Sealing in suction organs

A seal is required for suction-based attachment, where a sustained pressure difference is critical for maintaining adhesive strength. In the case of the octopus and remora fish, it is assumed that a soft fleshy rim moulds to the surface roughness to provide an efficient seal (Fulcher & Motta, 2006; Kier & Smith, 1990). With abalones and clingfish, it has been proposed that a dense network of micrometre-sized fibrous structures - cilia in abalones (incorrectly labelled as "nanofibrils" in (Lin, Brunner, Chen, Talke, & Meyers, 2009)) and "microvilli" in clingfish - helps the adhesive organ mould extremely well to any surface roughness and thereby generate an effective seal (Lin et al., 2009; Wainwright et al., 2013). If such fibres are able to displace the water film and form dry adhesive contacts with the surface, they could contribute significantly to both normal and shear detachment forces (Lin et al., 2009; Wainwright et al., 2013). The dense array of microtrichia on the surface of blephariceridsuction discs could serve similar functions as the fibrils in clingfish and abalones. It is noteworthy that we found two different rim morphologies: flat rim microtrichia in *L. cordata* (Figure 2.3c), as opposed to a densely packed array of short rim microtrichia in *L. cinerascens* (Figure 2.3f). Even without a continuous rim contact as seen in *L. cordata*, it is possible that the dense array of rim microtrichia in *L. cinerascens* can reduce the flow of water into the suction chamber by decreasing the gaps between individual elements to extremely small sizes. As the flow-rate through a narrow slit is proportional to the cube of its width, gap size has a dramatic effect on flow rate. Reduction in flow rate may also apply to the spine-like microtrichia zone, albeit to a lesser degree due to the wider gaps between each fibre. The hierarchy of extremely dense rim microtrichia to dense spine-like microtrichia, however, may help the blephariceridsuction organ generate a good seal even on natural substrates with a wide range of surface roughness length scales.

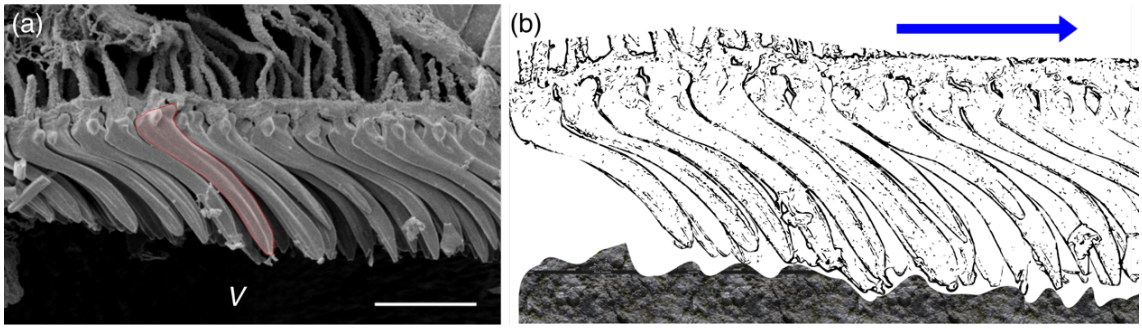

Figure 2.9. Microtrichia from *Liponeura cinerascens*. (*a*) Freeze-fracture SEM of a suction disc showing a single microtrichium (shaded in red) to highlight the curvature and pitch angle (see Table 2.1 for measurements). *V*: ventral. Scale bar 5 µm. (*b*) Schematic depiction of microtrichia making tip contact with a hypothetical rough rock surface. Arrow points towards the centre of the suction disc.

2.5.3 Generating large pressure differences using specialised piston and musculature

The attachment strength of the blepharicerid suction organ is directly related to the pressure difference between the organ and the external environment. Upon contraction, the piston muscles pull the piston away from the surface, thereby significantly lowering the internal pressure relative to the surroundings (assuming there is close to zero leakage), and leading to a powerful suction force. As water is nearly incompressible, the pull will increase the internal volume only minimally but may elastically deform the walls of the chamber, and the cuff in particular. The piston muscles must be capable of generating large forces to maximise the potential attachment strengths. Gronenberg *et al.* found that muscle fibres in ant mandibles with long sarcomeres (approximately 5 µm in length) were characteristic of slow and forceful muscles, while short sarcomeres (approximately 2 µm) were typically attributes of fast muscles (Gronenberg, Paul, Just, & Hölldobler, 1997). Since the average sarcomere lengths of piston muscle fibres were 5.6 and 6.7 µm in *L. cordata* and *L. cinerascens,* respectively, the piston muscles may also be adapted for high force as opposed to speed. Furthermore, we found that the cross-sectional area of the piston muscles was the largest out of the muscle groups within the suction organ. As a stronger piston pull leads to a larger pressure difference, and as muscle force scales with the cross-sectional area, the piston muscles are designed to generate strong forces for powerful attachments. Maie *et al.* presented a similar argument as a possible explanation for the positive allometry of suction-based pressure and adhesive forces found in climbing gobiid fishes (Maie, Schoenfuss, & Blob, 2012). These fishes use ventral suction organs to travel upstream and sometimes to scale waterfalls, and the increase in the cross-

sectional area of the sucker retractor muscles could be a factor in the positively allometric scaling.

2.5.4 Mechanism for rapid detachment of a suction organ

The V-notch appears to be a unique feature of the blephariceridsuction discs as no such structures have been reported from other well-studied suction organ systems. Previous researchers proposed that the V-notch provides a detachment mechanism for the suction organ (Frutiger, 2002; Hora, 1930; Komárek, 1914; Rietschel, 1961). Since these larvae are able to locomote using the suckers (up to 0.96 mm s^{-1} in rapid evasive movement, or approximately 0.1 body lengths per second (Frutiger, 1998)), they need to repeatedly and rapidly release the powerful suction attachment and detach the suction discs. From video footage of moving larvae on a glass aquarium surface, Frutiger suggested that the detachment begins at the V-notch and spreads radially to create an opening for sudden depressurisation of the organ (Frutiger, 2002), but the exact sequence of this process was still unclear (Figure 5 in (Frutiger, 2002)). When the piston muscle was contracted and the suction organ was fully engaged, the V-notch remained closed so that the surface contact of the rim of the suction disc was continuous (Supplementary Video SV6). As the larva prepared for detachment, the V-notch apodemes were pulled, peeling the V-notch flanks away from the surface. Subsequent influx of water through this opening equalised the pressure within the suction chamber so that the suction disc could be lifted from the substrate, presumably using the strong cuticular fold muscles. Our *in vivo* recordings highlighted fine control of the V-notch, including independent movements of each V-notch flank, and twitching of the flanks; on several occasions, one flank was pulled just a few micrometres before relaxing and closing the gap. Such movements are unlikely to be passive (i.e., caused by external flow, or displacements from larger-scale muscle-driven body movements) given the independent control of each V-notch flank and the speed of the twitching. Indeed, we discovered that the apodemes extend into the body to connect directly to a pair of dedicated V-notch muscles. The larva, therefore, has specific motor control of the V-notch, allowing them to open it independently at a range of speeds. This V-notch system is, to our knowledge, the first description of a mechanism specifically dedicated to detachment of a biological suction organ. It would be fascinating to explore the development of such a long apodeme running extensively through intracuticular space, and how these structures and the entire suction organ are re-built between each moult.

While the V-notch muscles open the V-notch, it is not clear how the V-notch can be closed and sealed. Previous researchers have used the term "valvular gateway" to describe the V-notch structure (J. W. Campbell, 1920; Hora, 1930), and Hora further proposed that the membranous flaps of the V-notch are arranged to allow water expulsion but not influx. Our *in vivo* observations provide additional support for this idea, as the membranous flaps could be seen to widen and vibrate from water being expelled as the piston was lowered, while the valves narrowed and ceased to move when the piston was raised and the internal pressure lowered. The valves could be closed passively by the pressure differential during suction cup attachment. Hence, the V-notch valves could function similar to heart valves, which rely on pressure differentials to open and close during heart contractions to prevent backflow between the atrium and the ventricle (Sacks, Merryman, & Schmidt, 2009). Interestingly, the mitral heart valves also have chord-like attachments called the chordae tendineae that resemble the V-notch and its apodemes (Lam, Ranganathan, Wigle, & Silver, 1970). The chordae tendineae primarily act to prevent valvular prolapse by tethering them to the papillary muscles of the inner ventricular wall when the pressure rises from ventricular contraction. The V-notch tendons, in addition to actively peeling open the structure, could also serve as a tether to prevent the V-notch valves from folding into the contact zone when the organ is engaged; we never observed this in our *in vivo* studies.

2.6 Conclusion

The larvae of Blephariceridae need to withstand powerful hydrodynamic forces in their habitats. They rely on six complex suction organs with several unique adaptations to generate strong attachment yet rapid detachment. Firstly, a continuous sealing rim may minimise leakage; it consisted of flat rim microtrichia in *Liponeura cordata*, and a dense array of short microtrichia in *Liponeura cinerascens.* Secondly, a dense region of spine-like microtrichia probably increases shear resistance on rough surfaces, similar to structures in the suction pad of remora fish helping them to attach onto rough shark skins. Lastly, the V-notch on the anterior side of the suction disc can be actively pulled open via two apodemes attached to its flanks, independently controlled by dedicated V-notch muscles. Despite these new insights into the functional morphology of the blephariceride suction system, many questions remain open for future investigations. For example, while we have identified four muscle groups, the V-notch, piston, cuff, and cuticular fold

muscles, their individual role in manoeuvring the organ and generating the suction pressure still needs to be clarified. Further work is also needed to elucidate the contribution of microtrichia to shear force resistance. A better understanding of these specialised natural suction systems could lead to new bio-inspired strategies to attach strongly to smooth and rough surfaces in both wet and dry conditions.

3 EXTREME SUCTION PERFORMANCE FROM A SPECIALISED AQUATIC INSECT (DIPTERA: BLEPHARICERIDAE)

3.1 Summary

Suction is widely used by animals for strong and controllable underwater adhesion but is less well understood than adhesion of terrestrial climbing animals. Here we investigate the attachment performance of net-winged midge larvae (*Hapalothrix lugubris*, *Liponeura cordata* and *L. cinerascens*, Blephariceridae), which attach underwater to rocks in torrential streams. We measured their attachment forces on various well-defined rough substrates and found that the blephariceridae larvae attach with extreme strength to smooth substrates and are drastically less affected by micro-rough substrates than terrestrial climbing insects. Through *in vivo* visualisation of the suction organ in contact with transparent microstructured substrates, we demonstrated that it can accommodate large asperities and mould around them to form a seal. Moreover, we show that specialised spine-like microtrichia can interact with the surface by making contact with their tips. The suction organs slipped less on soft substrates, suggesting penetration of the substrate by the spine-like microtrichia. Our results illustrate the performance and versatility of blephariceridae suction organs and introduce an insect model system for investigating biological suction attachments.

3.2 Introduction

The ability to readily attach and detach from surfaces is found among many animals, both on land and in water. It allows animals to explore new habitats, to develop new reproductive strategies, to find food, and to escape predation (Fulcher & Motta, 2006; Karlsson Green et al., 2013; Maie et al., 2012). Notwithstanding the growing interest in aquatic invertebrates that secrete glue-like substances for adhesion, mechanistic studies on biological adhesion have mainly focussed on terrestrial climbing animals, such as geckos, tree-frogs, insects, and spiders (Federle & Labonte, 2019; Lengerer & Ladurner, 2018). The fundamental principles derived from these model systems have greatly expanded our knowledge on how climbing animals achieve and control adhesion.

Climbing animals use specialised adhesive organs to scale surfaces at speed; they are typically comprised of claws (used to interlock with surface asperities) and adhesive pads (for adhering to smoother surfaces) (Bullock & Federle, 2011; Dai, Gorb, & Schwarz, 2002). There are two distinct types of adhesive pads: hairy pads, made up of dense arrays of fine hairs, and smooth pads, which are soft sac-like structures with a relatively smooth surface (Federle, 2006). Both hairy and smooth pads are highly compliant to help them mould to the surface and increase the contact area for stronger adhesion. Moreover, smooth and hairy systems of climbing insects are covered in a fluid secretion that increases the effective contact area on rough surfaces and also gives rise to capillary and viscous forces to further enhance adhesion (Dirks & Federle, 2011; Persson, 2002). In comparison, geckos rely on dry adhesion: the extremely fine hairs on their toepads make close contact with the surface and engage in van der Waals interactions (Autumn et al., 2002). For climbing animals, regardless of the type of adhesion or adhesive pad structure, it is crucial to have control over their adhesion for rapid locomotion (Federle & Labonte, 2019). Many animals, therefore, rely on direction-dependent adhesion, where a pull towards the body increases adhesion while a push decreases it (Autumn, 2006; Autumn et al., 2014; Federle & Labonte, 2019). This elegant mechanism for strong yet controllable adhesion has inspired researchers to develop biomimetic adhesives mostly for applications in air (Hensel, Moh, & Arzt, 2018).

While terrestrial climbing animals have received much attention from researchers investigating controllable biological adhesion, the ability to dynamically attach to surfaces is also vital for diverse aquatic animals. Since capillary and van der Waals forces are ineffective underwater (i.e., fully immersed and wetted contact zones), aquatic animals rely on different mechanisms for adhesion, such as glue-like secretions (bio-adhesives) and suction (Ditsche & Summers, 2014). Interlocking by claws and hooks is also common, and these structures function similarly to those in terrestrial animals. Glue-like bio-adhesives, used by a variety of animals (e.g., barnacles, mussels, echinoderms, flatworms, and limpets), are complex mixtures of proteins and polysaccharides that can form chemical interactions with the surface (Hennebert et al., 2016; Kamino, 2008; Lengerer & Ladurner, 2018; A. M. Smith, 2016b). In contrast, animals that use suction organs achieve adhesion by actively reducing the pressure under the suction organ and resisting shear forces on various surfaces (Beckert et al., 2015; Kier & Smith, 1990;

Chapter 2). However, while the morphology of suction organs has been described in a variety of animals, few studies have measured their performance and investigated their mechanisms of adhesion. Some of the better-understood examples are suction organs from octopuses and squids, remora fish, clingfish, and leeches (Arita, 1967; Beckert et al., 2015; Fulcher & Motta, 2006; Gradwell, 1972; Kampowski et al., 2016; Kier & Smith, 1990; A. M. Smith, 1991a, 1996; Wainwright et al., 2013). In these study animals, researchers have identified several adaptations and proposed functions for them, such as radial grooves in octopuses for transmitting low pressure throughout the sealed contact zone, spinules in remora fish for interlocking with rough surfaces to increase shear resistance, and dense arrays of microvilli in clingfish for increasing shear resistance. These findings have led to a number of bio-inspired suction devices with improved performance over conventional synthetic suction cups, which often fail to attach to rough and biofilm-covered surfaces (Ditsche & Summers, 2019; Ditsche, Wainwright, et al., 2014; Yueping Wang et al., 2017).

It is important to note that as suction organs of different species likely adapted to the specific physical demands of their surroundings, there is an immense diversity in structure and function yet to be discovered and studied. This is perhaps best exemplified by the larvae of net-winged midges (Diptera: Blephariceridae). These aquatic insects use suction organs to attach to underwater rock surfaces beneath torrential alpine streams and near waterfalls (Hora, 1930; Chapter 2). Only two studies to date have measured their attachment performance: in the first study, Frutiger *et al.* detached larvae (*Hapalothrix lugubris, Liponeura cinerascens minor,* and *L. cordata*) from natural rock surfaces and obtained average peak normal forces ranging from 33 to 83 mN, depending on the species (Frutiger, 2002). These values were not normalised by contact area or body-weight, and the test surfaces (natural rock) were not characterised in terms of their roughness and the presence of biofilm. In the second study, Liu *et al.* studied attachment of *Blepharicera* sp. larvae to substrates of different roughness and wettability (Liu, Chang, Chuang, Lin, & Chen, 2020) and reported that larvae attached less well on rougher surfaces, but did not provide any quantitative information on attachment forces. Hence, despite these investigations, several aspects of the blephariceride suction attachment remain poorly understood, such as the interactions between the microtrichia, surface asperities, and surface compliance, the ability of the suction disc to attach to well-defined rough surfaces, and performance in terms of adhesive and shear stresses. Thus, a more mechanistic

investigation is necessary to understand how the blephariceridsuction organs attach to various surfaces in wet conditions.

In this study, we investigated the structure and function of suction organs using larvae of *Hapalothrix lugubris* (Blephariceridae). We conducted a detailed morphological characterisation to provide novel insights into structures that likely have a functional role in blephariceridsuction attachment. To understand how well the larvae attach to different surfaces, we quantified their performance on smooth, micro-rough, and coarse-rough surfaces, as well as on hard and soft smooth substrates. We examined the function of microtrichia through *in vivo* visualisation of the contact zone during suction attachments to smooth and microstructured substrates. Furthermore, we directly compared attachment performances of blephariceridsuction organs and smooth adhesive pads of stick insects (*Carausius morosus*) to understand how two fundamentally different adhesive systems cope with rough surfaces. The ability to make such comparisons within the same taxa highlights a key advantage of using blephariceridlarvae as a model system for studying biological suction attachments.

3.3 Methods

3.3.1 Sample collection and maintenance

Liponeura cinerascens larvae were collected from fast-flowing alpine rivers near Meiringen, Switzerland (GPS location 46° 44' 05.6" N, 8° 06' 55.4" E, in May 2018), and close to Grinzens, Tirol, Austria (47° 12' 41.4" N, 11° 15' 28.1" E in September 2018). At the latter site, *Liponeura cordata* and *Hapalothrix lugubris* were also collected. *H. lugubris* was collected again in October 2019, and due to the larger weights of these individuals (9.3 ± 3.4 mg compared to 2.1 ± 0.6 mg), the two collections were kept separate during analysis and referred to as Collection 1 and 2 (Coll1/2) throughout. For all the species, we collected third and fourth instar larvae that were large enough to be handled for experiments. Wearing fishing waders and diving gloves, we removed rocks from the most turbulent areas of the river and brought them to the riverbank for specimen collection. Although it was previously noted that the larvae can attach so firmly that they are torn upon detachment (Komárek, 1914), we found that a gentle nudge using soft-touch tweezers can elicit an evasive response from them, whereupon they could be easily picked up using tweezers and placed in specially prepared 50 mL Falcon tubes. These tubes were

first rinsed with stream water, flicked dry to remove most but not all of the water, then a small patch of wet moss was added to the bottom to retain moisture before being sealed with the screw-top cap. All larvae were kept in these tubes in an ice-box during collection and transport. Rocks were returned to their approximate locations after collection.

For long-term maintenance of the larvae, an aquarium tank was set up with water and small rocks from the collection site. A filter unit with two outlets for a small water cascade was used to filter the water and to simulate the natural environment. Multiple air-pumps were also placed close to the aquarium walls to provide ample oxygenation and additional regions with turbulent flow. To promote algal growth, an over-tank LED light was set on a 12h day-night cycle. The aquarium was kept in a 4°C climate room (mean temperature of 3.2 ± 0.9°C; mean ± SD) to replicate alpine stream temperatures.

3.3.2 Scanning electron microscopy of *Hapalothrix lugubris* suction organs

Scanning electron microscopy (SEM) was used to image fourth instar *H. lugubris* larvae (Coll1) as described previously (Chapter 2). In brief, samples fixed in 70% ethanol (v/v) were flash-frozen in liquid ethane cooled with liquid nitrogen and freeze-fractured immediately afterwards with a double-edged razor blade on a cooled aluminium block to obtain longitudinal views. Samples were freeze-dried overnight then carefully mounted on SEM aluminium stubs using carbon tape and silver paint. They were then sputter-coated with 15 nm of iridium and imaged using a field emission SEM (FEI Verios 460).

3.3.3 X-ray microtomography (micro-CT) of blephariceridsuction organ

One *H. lugubris* Coll1 fourth instar larva was fixed in 2% paraformaldehyde and 2% glutaraldehyde (v/v) in 0.05 M sodium cacodylate buffer (pH 7.4) for 7 days at 4°C. The larva was then dissected into six pieces - each containing one suction organ - and fixed for an additional day. The samples were then rinsed multiple times in 0.05 M sodium cacodylate buffer followed by deionised water (DIW) before dehydration through a graded ethanol series: 50%, 75%, 95%, 100% (v/v) and 100% dry ethanol. The dehydrated samples were then critical-point dried using 4 flushes of liquid CO_2 on a Quorum E3100 critical-point drier.

One critical-point dried suction organ was used for imaging via X-ray microtomography (micro-CT). The sample was mounted on a standard dressmaker's pin using UV-curable glue then imaged using a lab-based Zeiss Xradia Versa 520 (Carl Zeiss XRM, Pleasanton, CA, USA) X-ray Microscope. The sample was scanned at 0.325 µm/pixel with accelerating X-ray tube voltage of 50 kV and a tube current of 90 µA. A total of 2401 projections collected at 20 sec exposure intervals were used to perform reconstruction using a Zeiss commercial software package (XMReconstructor, Carl Zeiss), utilizing a cone-beam reconstruction algorithm based on filtered back-projection. Subsequent 3D volume rendering and segmentations were carried out using Dragonfly v4.0 (Object Research Systems Inc, Montreal, Canada) and Drishti v2.6.4 (Limaye, 2012).

3.3.4 Measuring attachment performance of blephariceridlarvae using a centrifuge

Insect attachment forces were measured using a custom centrifuge set-up described previously (Federle et al., 2000). The centrifuge operated on the following principle: a platform with the test substrates and the insect was driven by a brushless motor, and a light barrier sensor was triggered per rotation. This signal was used synchronise image acquisition from a CMOS USB camera (DMK 23UP1300, The Imaging Source Europe GmbH, Bremen, Germany), and image frames and their corresponding times were recorded using StreamPix4 software (NorPix Inc., Montreal, Canada). For safety reasons, the maximum centrifugation speed was limited to approximately 75 rotations per second (rps). The centrifuge was used to measure attachment performances of blephariceridlarvae (*L. cinerascens*, *L. cordata*, and *H. lugubris* Coll1), as well as *Carausius morosus* stick insects (see below for details). A MATLAB script was used to analyse the video recordings of the centrifuge trials, allowing digitisation of the insect's position immediately prior to detachment to obtain the peak centripetal acceleration.

Effect of surface roughness on the peak shear force of blephariceridlarvae was measured using the following substrates: smooth (clean polyester film), micro-rough (polishing film with nominal asperity size of 0.05 µm; Ultra Tec, CA, US), and coarse-rough (30 µm polishing film, Ultra Tec). The same substrate types were used for the adhesion tests, but a polished polymethyl methacrylate (PMMA) surface was used as the smooth substrate. Surface characteristics (average roughness (mean height deviation) R_a, root-mean-squared roughness R_q, and maximum peak-to-valley height (PV)) of the micro-rough film

were obtained using white-light interferometry with a scan area of 0.14 × 0.10 mm (Zygo NewView 200, Zygo Corporation, CT, USA; see Supplementary Materials for more details). Since the coarse-rough film could not be captured with this method, we used a Z-stack image focal-depth analysis technique as described elsewhere with a scan area of 0.44 × 0.58 mm (Sarmiento-Ponce, Sutcliffe, & Hedwig, 2018). For both surfaces, three regions were selected at random and imaged. Interferometry images were analysed using MetroPro software (Zygo), and a custom MATLAB script was used to reconstruct the surface profile from the Z-stack images (The MathWorks, Inc., MA, United States). Surface profiles of the different test substrates are shown in Table 3.1.

Table 3.1. Surface profilometry of test substrates used to assess attachment performance. R_a: average roughness (mean height deviation), R_q: root-mean-squared roughness, PV: maximum peak-to-valley height. NA: Not applicable.

	Surface characteristics (mean ± SD)		
Test surfaces	**Ra (µm)**	**Rq (µm)**	**PV (µm)**
Rough surfaces			
Micro-rough (0.05 µm grain size)	0.32 ± 0.01	0.40 ± 0.01	4.56 ± 0.22
Coarse-rough (30 µm grain size)	7.97 ± 0.06	10.37 ± 0.08	78.82 ± 1.38
Microtextured substrates			
10×10 µm	NA	NA	2.04 ± 0.18
3×3 µm	NA	NA	4.48 ± 0.08
3×3 µm	NA	NA	1.69 ± 0.03

Since *L. cinerascens* and *L. cordata* were difficult to maintain in laboratory conditions, these two species were tested only on smooth horizontal surfaces (n = 43 and n = 10, respectively). The full range of tests (adhesion and friction on smooth, micro-rough, coarse-rough surfaces) were conducted for *H. lugubris* Coll1 (n = 9 to 15 for shear tests; n = 10 for all adhesion tests). Prior to the experiments, individuals were selected from the laboratory aquarium and placed inside 50 mL Falcon tubes packed with moss (as described above). This tube was kept on ice for the duration of the experiment. For each run, a larva was carefully removed from the tube and placed on the test surface. A droplet of water (taken from the aquarium) was used to wash excess debris from the insect, and lab tissue paper was used to wick away excess water without removing all moisture from the larva. These steps were necessary to prime the larvae for the centrifugation trials as

they often displayed defensive behaviour from being handled. The larvae adhered and remained still once primed, and between two to four repetitions were performed for each larva. Note that centrifuge trials were conducted within seven days of collection.

To study the effect of surface stiffness on the contact of suction disc, shear forces of *H. lugubris Coll2* larvae were measured on smooth plastic (same as above; n = 11), smooth glass (clean coverslips; n = 12), and a smooth plastic made from a soft polymer (commercial non-slip kitchen mat; n = 11). SEM images of the soft polymer surface confirmed that it was smooth (data not shown). For this set of force measurements, an improved model of the centrifuge was used that allowed maximum speeds of 120 rps, and therefore even the highest attachment forces of H. lugubris could be measured reliably. Due to the damaging effects of the high speeds necessary to detach individuals, each H. lugubris Coll2 specimen was tested once on this centrifuge.

After the trials, all the larvae were blot-dried on filter paper and weighed using an analytical balance (1712 MP8, Sartorius GmbH, Göttingen, Germany). Statistical analyses were conducted on log10-transformed force data using R v3.6.2 run in RStudio v 1.2.5033 (R Core Team, 2019; RStudio Team, 2019).

3.3.5 Calculating peak stress values on smooth horizontal plastic surface

Adhesive stress and shear stress (defined as the peak attachment force divided by the contact area) were calculated using suction disc areas measured for *L. cordata* and *H. lugubris* larvae. Larvae were placed on microscope slides so that the suction organs fully contacted the glass and imaged with a stereomicroscope. Every tested *L. cordata* and *H. lugubris* Coll1 specimen was imaged, while a subset of the individuals from *H. lugubris* Coll2 were measured (n = 6). A representative organ was selected from each *L. cordata* and *H. lugubris* Coll1 larva, and the contact area calculated by fitting a circle inclusive of the outer fringe layer using FIJI (Schindelin et al., 2012) (https://imagej.net/Fiji). The peak attachment force was then divided by this contact area to determine the peak stress for each larva. For *H. lugubris* Coll2 larvae, the mean contact area of the six individuals was set as the reference to determine the adhesive and shear stress of each larva.

3.3.6 Measuring peak shear and normal attachment forces of stick insects

Stick insects (*Carausius morosus*) were used as a model for terrestrial insect adhesion, and their attachment on surfaces with varying roughness was measured to compare against blephariceridlarval attachment. Second-instar nymphs with undamaged legs and tarsi were selected for centrifuge adhesion and shear experiments using smooth, micro-rough, and coarse-rough surfaces (n = 10 per surface). No adhesion forces could be measured on the micro-rough surface as stick insects failed to hold their body weight during preliminary tests. Before each trial, we checked that the specimen was in contact with the surface using all six legs and that the surface was uncontaminated. Stick insects were oriented with the head facing out, and each individual was tested twice and weighed afterwards. The higher attachment force per individual was used as the peak attachment force.

3.3.7 *In vivo* observation of suction organs attaching to smooth and micro-patterned substrates

In order to examine blephariceridlarvae locomoting for extended periods of time, a custom flow-chamber was built to imitate the fast-flow conditions of their natural environments (Supplementary Figure 1). Two aluminium plates (approximately 60×100 mm in height×width) each with a rectangular window were used to sandwich an inner chamber made out of polydimethylsiloxane (PDMS; Sylgard 184, Dow Corning, MI, USA). This inner chamber had a lemon-shaped chamber to serve as the observation arena, and an inlet and an outlet for water circulation. Two microscope coverslips (0.16-0.19 mm thickness, Agar Scientific, Stansted, UK) were used to encase the inner chamber. Two to five larvae were placed on the bottom coverslip, and once the top coverslip was placed over the arena, four clamps were used to squeeze the aluminium plates and coverslips against the PDMS. The soft PDMS moulded closely to the plates and created a water-tight seal. Aquarium water (kept cool in an ice bath) was pumped via a micro-pump (M200S-V, TCS Micropumps Ltd, UK), and the input voltage was controlled by a microprocessor. Using this flow-chamber, we recorded *H. lugubris* midge larvae locomotion and the attachment/detachment of suction organs on smooth glass surfaces via interference reflection microscopy (IRM). IRM has been used previously to investigate the contact between animal adhesive organs and the substrate (Federle et al., 2006; Federle, Riehle, Curtis, & Full, 2002). Videos were recorded using a USB3 CMOS

camera (DMK 23UP1300, see above) and IC Capture software (v2.4.642.2631, The Imaging Source GmbH) at 30 frames per second (FPS).

To observe how suction organs respond to surface roughness, we used transparent micro-structured surfaces with well-defined micro-ridges and grooves fabricated by photolithography and nanoimprinting (Y. Zhou, Robinson, Steiner, & Federle, 2014). In brief, a master was first produced using photolithography, and a PDMS mould of this master was then used to cast the final surface out of epoxy. Three micro-ridge geometries were used in our experiments: (1) 3×3×2 µm (ridge width × groove width × ridge height); (2) 3×3×4 µm; and (3) 10×10×2 µm. As ridge height is only approximately controlled through the spin-coating of photoresist when producing the master, we measured it from the epoxy replicas using white-light interferometry (see above and Supplementary Materials). Since these surfaces could not be used in combination with the flow-chamber, a *H. lugubris* larva was placed on the substrate, gently motivated with soft-touch forceps, and recorded as they moved around for a short period of time on the surface. A well-performing individual was used for both the 3×3×2 µm and 10×10×2 µm substrates, while a different larva was used on the 3×3×4 µm surface.

3.4 Results

3.4.1 Morphology of *Hapalothrix lugubris* suction attachment organ

The general morphology of *H. lugubris* suction organs was highly similar to our previous findings for the genus *Liponeura* (Chapter 2). *H. lugubris* larvae have six ventromedian suction organs (Figure 3.1a & b) with each organ comprising a suction disc covered in a dense array of microtrichia, a central opening and a piston, a suction chamber surrounded by a cuticular cuff, and a V-notch (Figures 3.1 & 3.2). The suction disc contacts the surface for attachment, and the piston and underlying piston muscles (Figures 3.1c & 3.2a) actively lower the pressure inside the suction chamber (Chapter 2). As seen in *Liponeura* species, there are also two apodemes attaching to the V-notch in *H. lugubris*, which mediate its muscle-controlled opening for rapid detachment of the suction organ (Figure 3.2b; see also Chapter 2). Note that we observed no claw-like structures in blephariceridlarvae.

The ventral disc surface of *H. lugubris* is covered in a dense array of microtrichia, much like *L. cordata* and *L. cinerascens* (Figures 3.1c & 3.3). The suction disc sealing rim, which seals the disc for suction attachment, closely resembles that of *L. cinerascens* and comprises a small dense array of upright and short rim microtrichia (Figure 3.1c). This is different to *L. cordata*, which has a distinct rim made up of a single row of flat rim microtrichia (Chapter 2). Going from the rim to the centre of the disc, the short rim microtrichia transition into the longer spine-like microtrichia (6.7 ± 0.7 µm in length; mean of means ± standard deviation of the mean; n = 2 individuals), then to small central microtrichia.

3.4.2 Spine-like microtrichia and fan-fibres

We gained additional insights into the ultrastructure and internal organisation of the spine-like microtrichia through multiple imaging modalities (freeze-fracture SEM, 3D models from micro-CT data, and *in vivo* transmitted light microscopy; Figure 3.3). While Rietschel has previously described internal fan-fibre networks in a space on the dorsal side of the outer region of the suction disc (Rietschel, 1961) (Figure 3.3a), we discovered that each internal fibre leads to a single microtrichium (Figure 3.3b). Moreover, all the microtrichia that were fractured during sample preparation appeared to be solid (in-filled) cuticular structures (Figure 3.3c). The small internal fibres leading into the microtrichia branch out from thicker trunks originating from the ventral side of the outer radial beams (Figure 3.3b & d). The radial beams themselves alternate between a wide and a narrow beam and are also solid cuticular structures (Figure 3.3d). The radial beams originate from the palisade layer (Figure 3.3a; contiguous columnar structures that roughly coincide with the beginning of the spine-like microtrichia zone) based on *in vivo* transmitted light microscopy images and micro-CT data (Figure 3.3e & f). Using the micro-CT data, we counted 72 beams in a 90° segment of the disc, corresponding to 288 beams per disc (assuming no interruption from the V-notch) and a centre-to-centre spacing of around 4 µm or 1.3°.

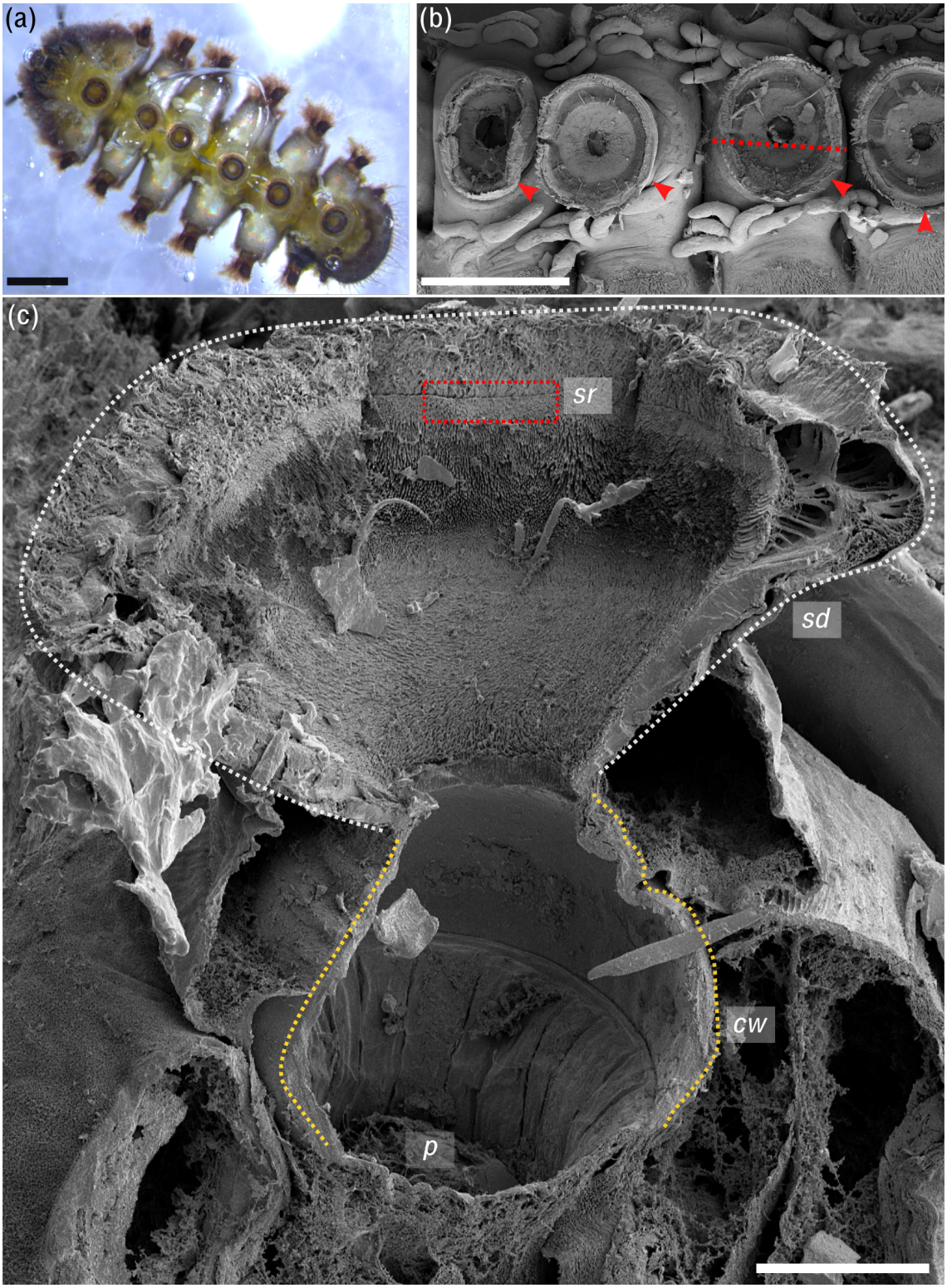

Figure 3.1. Overview of the suction attachment organs of *Hapalothrix lugubris*. (a) Six ventromedian suction organs of a third instar *H. lugubris*. Scale bar 500 µm. (b) Scanning electron micrograph of a flash-frozen and freeze-dried *H. lugubris* larva. Red arrows point to suction organs. Tracheal gills are visible on both sides of the organ. Scale bar 500 µm. Dotted line shows approximate location of fracture line for (c). (c) Freeze-fracture reveals components important for attachment: suction disc (outlined in white dotted line, sd), sealing rim (red box, sr), cuff wall (yellow dotted line, cw), and the piston (p). The ventral surface of the suction disc is covered by a dense array of microtrichia (see Figure 3.3 for details). Scale bar 50 µm.

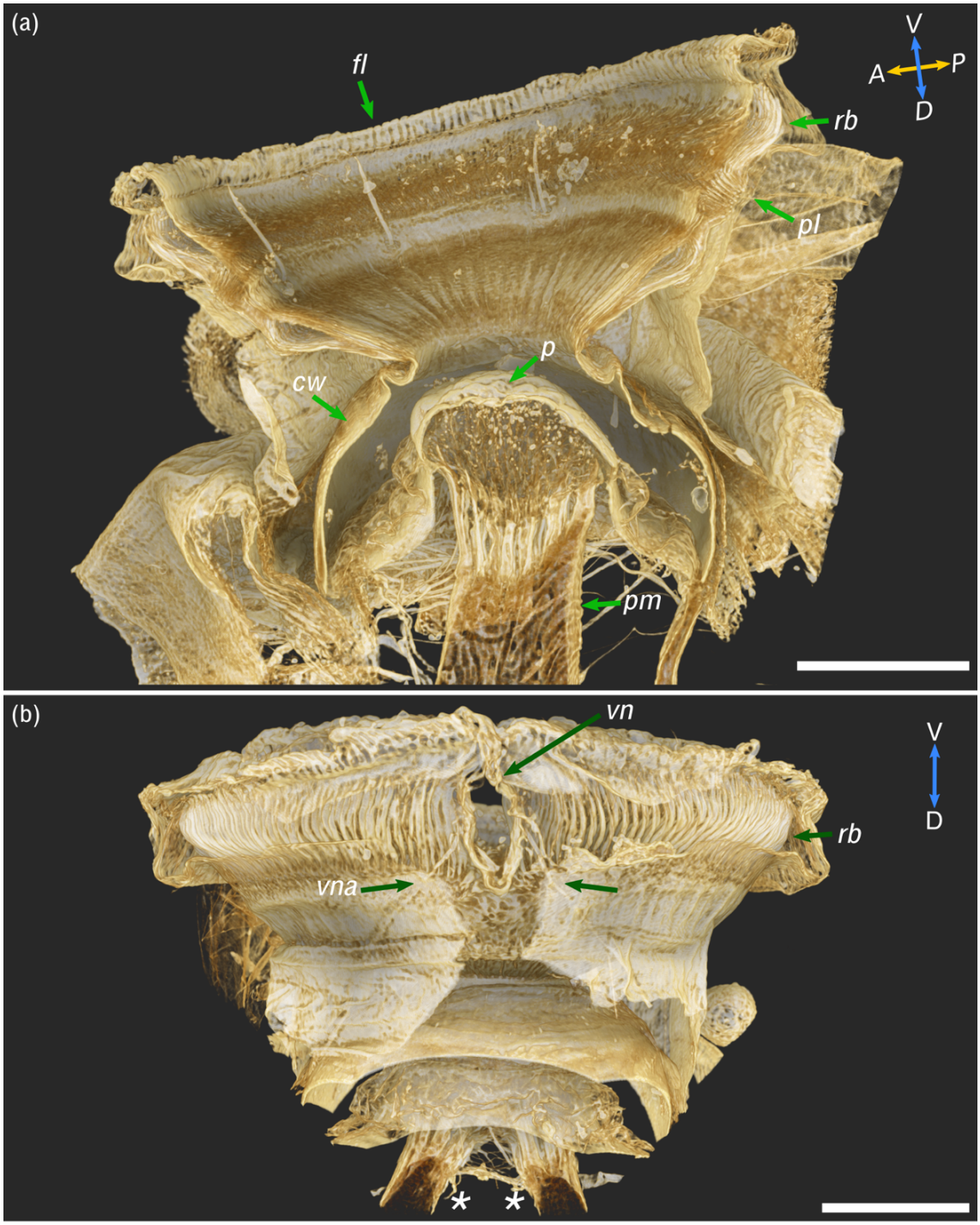

Figure 3.2. Micro-CT rendering of *H. lugubris* suction organ highlights its internal organisation in 3D. (a) Sagittal view, showing the following structures: outer radial beams (rb), palisade cell layer (pl), piston cone (p), and piston muscles (pm). The cuff wall (cw) encircles the suction cavity, and the outer fringe layer (fl) encircles the disc. A: anterior, P: posterior, D: dorsal, V: ventral. (b) View from anterior side, showing the V-notch (vn) and its pair of apodemes (vna) extending dorsally into the body. Outer cuticle has been digitally dissected to reveal the radial beams (rb). Note the pair of piston muscles extending dorsally (*). Scale bars 100 µm.

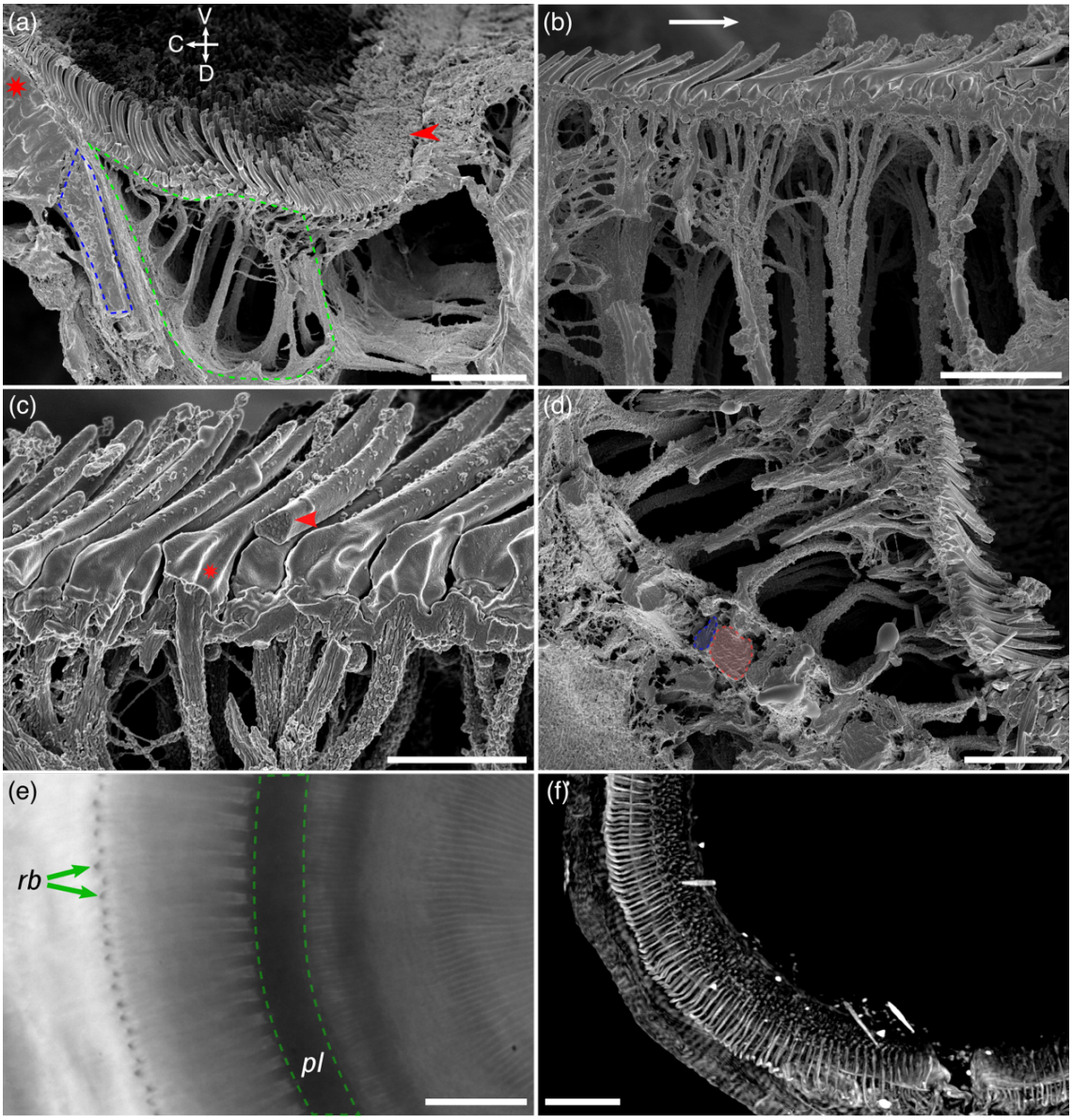

Figure 3.3. Ultrastructure of the suction disc. (a-d) Scanning electron micrographs of freeze-fractured suction organ cuticle (radial fracture plane). (a) Outer region of suction disc. The sealing rim and its short rim microtrichia are marked by a red arrowhead. Internal radial beams (highlighted in blue) originate from the palisade layer (red *). The fan-fibre space is highlighted in green. Note the spine-like microtrichia point towards the disc centre. V: ventral, D: dorsal, C: disc centre. Scale bar 10 µm. (b-d) Details of microtrichia in region of fan-fibre space. (b) Each microtrichium connects to an internal fibre; these fine fibres represent the endings of thicker branched fibres originating from the radial beams. Arrow points towards centre. Scale bar 5 µm. (c) Microtrichia are largely solid cuticular structures (arrowhead), each connected to a fan-fibre (*). Scale bar 2 µm. (d) Fan-fibres extend to the radial beams, which alternate between thin (blue) and wide beams (red). Scale bar 6 µm. (e) *In vivo* light microscopy emphasises the radial beam (rb) and the palisade layer (pl). Scale bar 20 µm. (f) Micro-CT image confirms that radial beams originate from the palisade layer. Centre-to-centre spacing of the beams is around 4 µm or 1.3°. Scale bar 40 µm.

3.4.3 Attachment performance of blepharicerid larvae on different substrates

3.4.3.1 Blepharicerid larvae performance on smooth surfaces

We measured peak shear forces of three blepharicerid species on smooth surfaces (Figure 3.4). The peak shear force per body-weight was 585 ± 330 for *L. cordata* (mean ± SD), 320 ± 142 for *L. cinerascens*, and 1,120 ± 282 for *H. lugubris* Coll1 (Figure 3.4a). Note that a few individuals could not be detached using the centrifuge even at 75 rps; for these individuals we used the maximum centrifugal acceleration from a successful detachment on the same test substrate as a conservative estimate of their attachment performance. For *H. lugubris* Coll2, however, we were able to test the larvae on an improved model of the centrifuge that reached sufficient speeds to detach all individuals. The peak shear attachment force per body-weight for *H. lugubris* Coll2 was 1,170 ± 475 (mean ± SD), not significantly different from *H. lugubris* Coll1 (Wilcoxon ranked sum test; W = 79, $p = 0.88$). There was, however, a significant difference in peak shear force due to the heavier mass of Coll2 individuals, with 18.8 ± 5.0 mN vs. 91.6 ± 38.2 mN for Coll1 and Coll2, respectively (mean ± SD; Figure 3.4b; Welch's *t*-test; $t_{13.9} = 9.84$, $p < 0.001$). The best shear attachment performance out of all the blepharicerid trials was obtained from *H. lugubris* Coll2, with a maximum shear force per body weight of 1,970 and 173 mN in peak shear force (note: values from two different individuals).

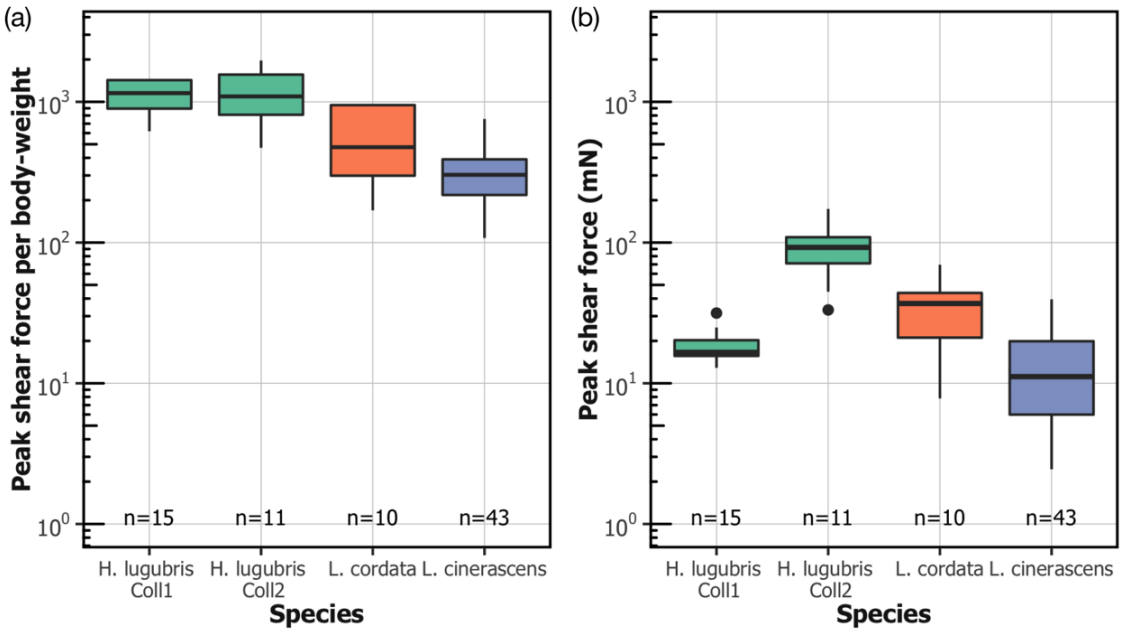

Figure 3.4. Attachment performance of three species of blephariceridlarvae (*Hapalothrix lugubris, Liponeura cordata, L. cinerascens*) on smooth horizontal surface. Data for *H. lugubris* represent two field collections (Coll1 & 2) which were analysed separately because of differing body weights (see text for details). (a) Peak shear force per body-weight. (b) Peak shear force. Centre lines, boxes, whiskers, and filled dots represent the median, the inter-quartile range (IQR), 1.5-times IQR, and outliers, respectively.

3.4.3.2 Effect of surface roughness and compliance on the attachment performance of blephariceridlarvae

Peak shear and adhesion force per body-weight for *H. lugubris* larvae Coll1 were measured on smooth, micro-rough, and coarse-rough surfaces (Figure 3.5). The type of tested substrate had a significant effect on peak shear force, with the larvae attaching best on smooth, followed by micro-rough, then coarse-rough substrates (one-way ANOVA, $F_{2,31}$= 99.7; $p < 0.001$ for all multiple pair-wise comparisons using Tukey's post hoc test).The same effect was observed for peak adhesion force per body-weight (one-way ANOVA, $F_{2,27}$ = 71.81; $p < 0.001$ for all multiple pair-wise comparisons using Tukey's post hoc test).

To assess whether substrate compliance had an effect on shear attachment forces, we compared the attachment of *H. lugubris* larvae Coll2 between clean glass slides and a smooth soft polymer. We found no significant differences between the shear force per body-weight on the glass surface and the soft plastic surface (Figure 3.6a; independent *t*-test, t_{21}= 1.36, p = 0.19). However, the attachment of the larvae on the two substrates

differed in a visible way: while almost all the larvae slid on the hard glass surface prior to detachment, this happened less often on the smooth soft polymer substrate (Figure 3.6b; 11 out of 12 on glass versus 3 out of 11 on soft polymer; Fisher's exact test: $p < 0.01$).

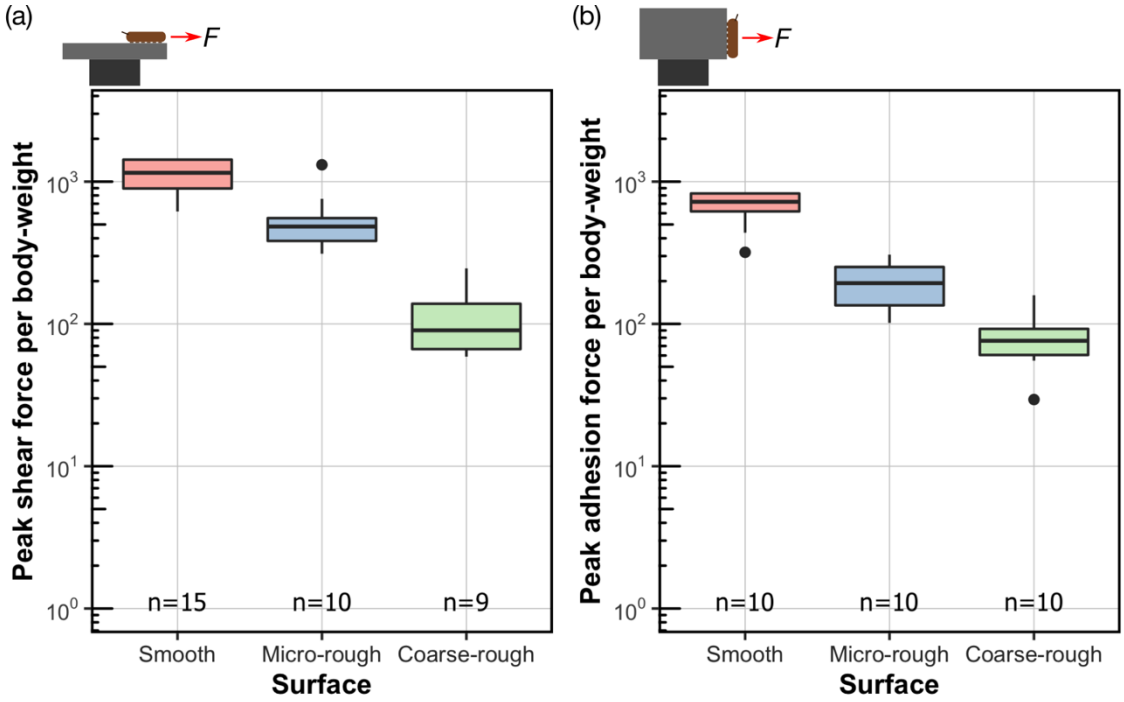

Figure 3.5. Attachment performance of *H. lugubris* Coll1 larvae on surfaces of varying roughness. (a) Peak shear force per body-weight. (b) Peak adhesion force per body-weight. Centre lines, boxes, and filled dots represent the median, the inter-quartile range, and outliers, respectively.

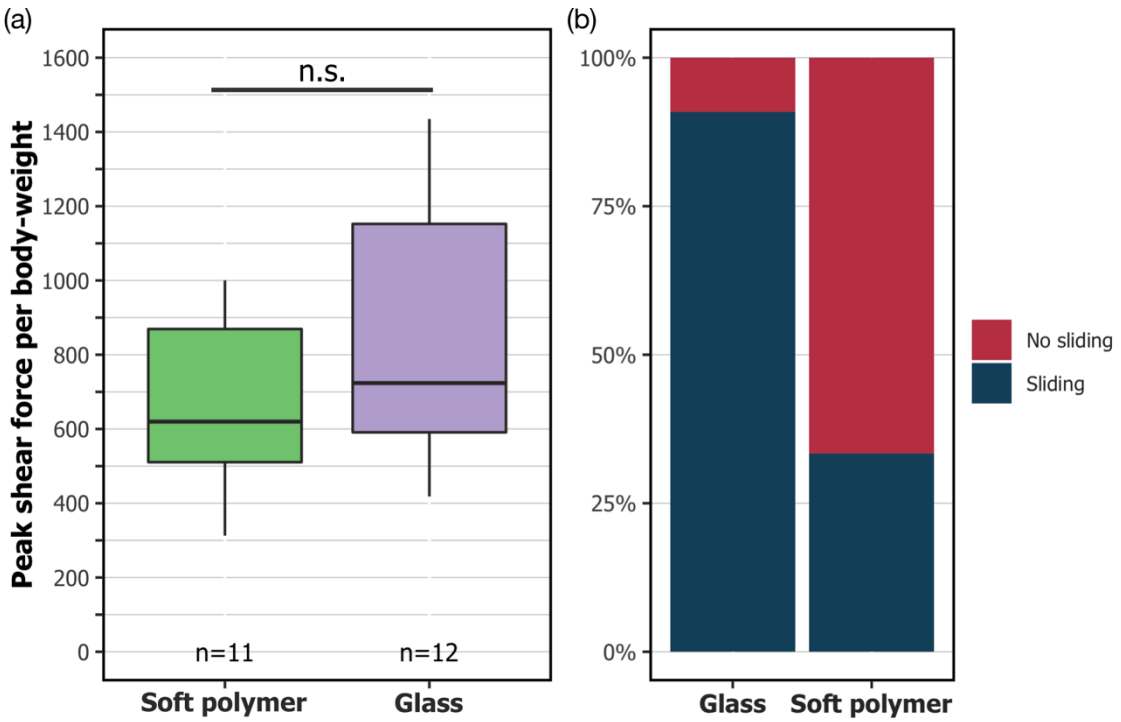

Figure 3.6. Peak shear attachment of *H. lugubris* Coll2 on soft (polymer-based) versus hard (glass) substrates. (a) *H. lugubris* attached well to both soft and hard substrates (n.s.: not significant). (b) Although there was no difference in attachment performance, *H. lugubris* was significantly more likely to slide on hard glass than soft polymer.

3.4.3.3 Estimates of peak shear stress on smooth surfaces

Suction disc areas measured for *L. cordata* and *H. lugubris* (Coll 1 and 2) were used to estimate the peak shear stress. Shear stresses of 43.4 ± 25.9 kPa, 39.3 ± 10.6 kPa, and 48.6 ± 20.3 kPa (mean ± SD) were found for *L. cordata*, *H. lugubris* Coll1, and *H. lugubris* Coll2, respectively (Table 3.2 and Figure 3.7). These values, however, are conservative estimates because: (1) the contact area measurements included the outer fringe which lies outside the suction disc seal, and (2) we assumed that all six suction organs were in contact immediately before detachment. We thus derived more realistic estimates of the shear stresses by first taking into account that the outer fringe layer amounted for 33% to the total imaged contact area (n = 18 suction discs from 6 individuals) and applying this correction factor to the conservative shear stress values; second, since we often observed the larvae attaching with fewer than their six suction organs immediately prior to detachment (also noted by Frutiger in (Frutiger, 2002)), we assumed that three organs were in contact and responsible for the peak shear force. When these assumptions were considered, the shear stresses were 111.5 ± 57.5 kPa, 116.6 ± 31.4 kPa, and 144.2 ± 60.2 kPa (mean ± SD) for *L. cordata*, *H. lugubris* Coll1, and *H.*

lugubris Coll2, respectively (Table 3.2). Shear stress values for *H. lugubris* Coll1 tested on different rough surfaces followed the same trend as the shear attachment performances, wherein the values decreased on rough surfaces (data not shown).

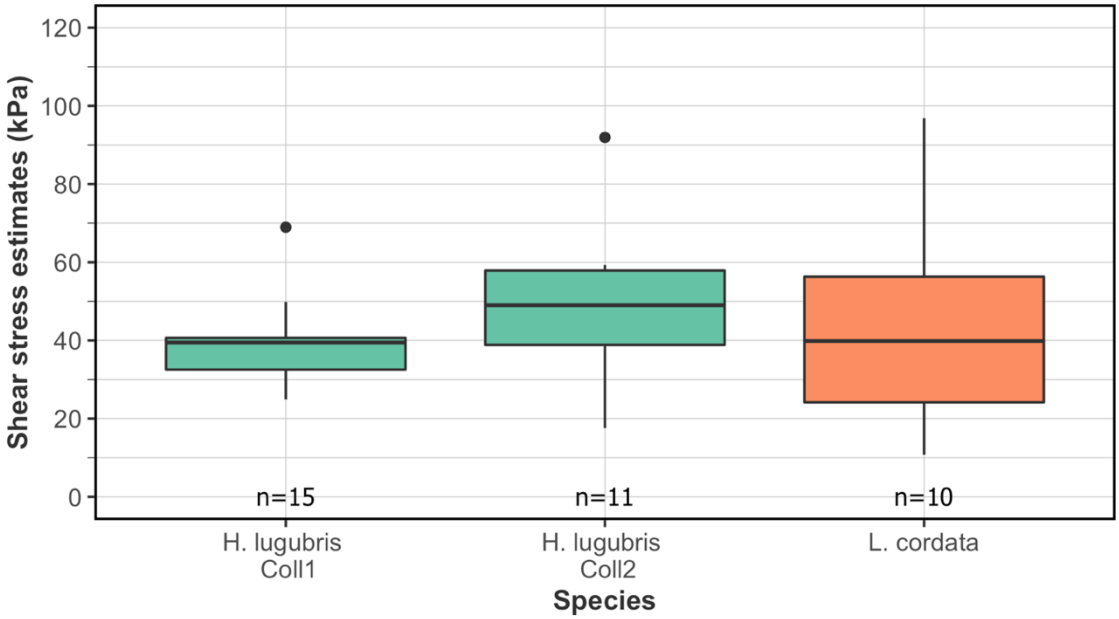

Figure 3.7. Conservative estimates for the shear attachment strength of *H. lugubris* and *L. cordata* on smooth surface. Calculations based on the total contact area of all six suction organs inclusive of the outer fringe layer.

Table 3.2. Shear strength estimates for suction-based attachments of *Hapalothrix lugubris* and *Liponeura cordata*.

		Conservative* (kPa)		**RealisticΔ (kPa)**	
Species	**n**	**Mean**	**SD**	**Mean**	**SD**
Liponeura cordata	10	43.4	25.9	111.5	57.5
Hapalothrix lugubris Coll1	15	39.3	10.6	116.6	31.4
Hapalothrix lugubris Coll2	11	48.6	20.3	144.2	60.2

*Conservative: contact area based on suction disc inclusive of outer fringe layer; all six organs in contact prior to detachment.

ΔRealistic: based on three organs in contact immediately prior to detachment and contact areas excluding the outer fringe layer.

3.4.4 Attachment performance of suction organs to rough substrates compared to smooth adhesive pads

While blephariceridattachment performance decreased with increasing roughness, we observed a different pattern with stick insects (Figure 3.8). Stick insects rely on a combination of their smooth adhesive pads and claws for attachment, where the former facilitates strong adhesion on smooth surfaces and the latter provides adhesion to coarse-rough substrates. Thus, we found that stick insects adhered equally well to smooth and coarse-rough surfaces (one-way ANOVA, $F_{2,27}$= 77.0; p = 0.97 using Tukey's post hoc test). On micro-rough surfaces, however, where neither the smooth pad nor the claws proved effective, their shear force per body-weight decreased 16-fold (based on the mean of back-transformed values) compared to the smooth surface (same ANOVA as above; p < 0.001 using Tukey's post hoc test). Attachment performance of *H. lugubris* Coll1 larvae was also affected by micro-roughness, but to a much lesser degree than in stick insects, with a two-fold decrease (based on the mean of back-transformed values) in shear force per body-weight (same ANOVA as Figure 3.5a; p < 0.001 using Tukey's post hoc test).

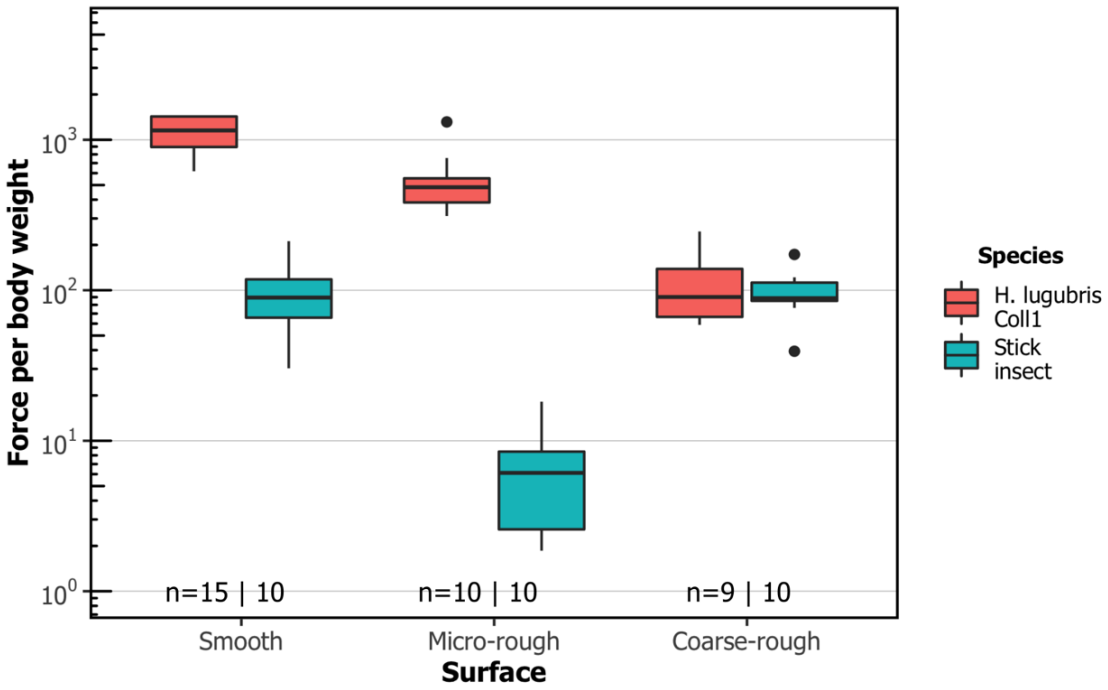

Figure 3.8. Comparison of shear attachment performance of *H. lugubris* Coll1 larvae versus stick insects (*Carausius morosus*) on smooth and rough surfaces. Sample sizes shown with *H. lugubris* Coll1 on the left and stick insects on the right. *H. lugubris* larvae use suction organs for adhesion in wet conditions, whereas stick insects rely on smooth adhesive pads and claws. Using their suction organs, *H. lugubris* larvae can attach well on all tested surfaces, although there is a decrease in performance with increased roughness. Stick insects, however, attach well on smooth and coarse-rough surfaces but poorly on micro-rough surfaces. Centre lines, boxes, whiskers, and filled dots represent the median, the inter-quartile range (IQR), 1.5-times IQR, and outliers, respectively.

3.4.5 *In vivo* visualisation of suction organs attaching to glass and microstructured substrates

Using IRM, we observed the contact zone of *H. lugubris* suction discs *in vivo*. The attachment-detachment behaviour on smooth glass substrates closely resembled that of the related *Liponeura* species (Frutiger, 2002; Chapter 2): the suction disc came into close contact with the surface at the outer fringe layer, disc rim, microtrichia zone, and around the central opening (Figure 3.9a; Supplementary Video 1). When the piston was raised away from the surface, the contact area of the disc centre increased as a result of the reduced hydrostatic pressure. When the organ was attached, the microtrichia consistently made tip contact with the surface; no side contact was observed even when the piston was raised, reducing the internal pressure and pulling the disc closer towards the surface. Detachment of the suction organ and forward movement was often preceded by an active opening of the V-notch (Supplementary Video 2). While we did not observe a distinct

sealing rim in *H. lugubris* as seen in *Liponeura cordata* (Chapter 2), dense rim microtrichia came into close contact with the smooth glass surface during attachment, which closely resembled the sealing behaviour of *L. cinerascens*.

While the outer fringe layer and the microtrichia made close contact on smooth substrates, we observed different outcomes on transparent microstructured substrates. On the 10×10×2 µm substrate, the microtrichia made contact on both the ridges and the grooves, as evidenced by black dots in the IRM recordings (Figure 3.9b). Similar to our observations on smooth glass surfaces, only the tips of the microtrichia made contact on the ridges and inside the grooves. The outer fringe layer also made contact, although not uniformly. With the 3×3×2 µm substrate, we again observed microtrichia tips and outer fringe layer coming into close contact on both the ridges and in the grooves (Figure 3.9c & d). In contrast, on the 3×3×4 µm substrate, the microtrichia and the outer fringe layer made contact only on the ridges but not inside the grooves (Figure 3.9e & f). Moreover, we observed microbial organisms freely floating and moving within the grooves (confirming the lack of close contact) but not on the ridges where the microtrichia and fringe layer were close to the surface. Consistently, no particles or bacteria floating in the channels were observed during the trials with the other two microstructured surfaces (3×3×2 µm and 10×10×2 µm).

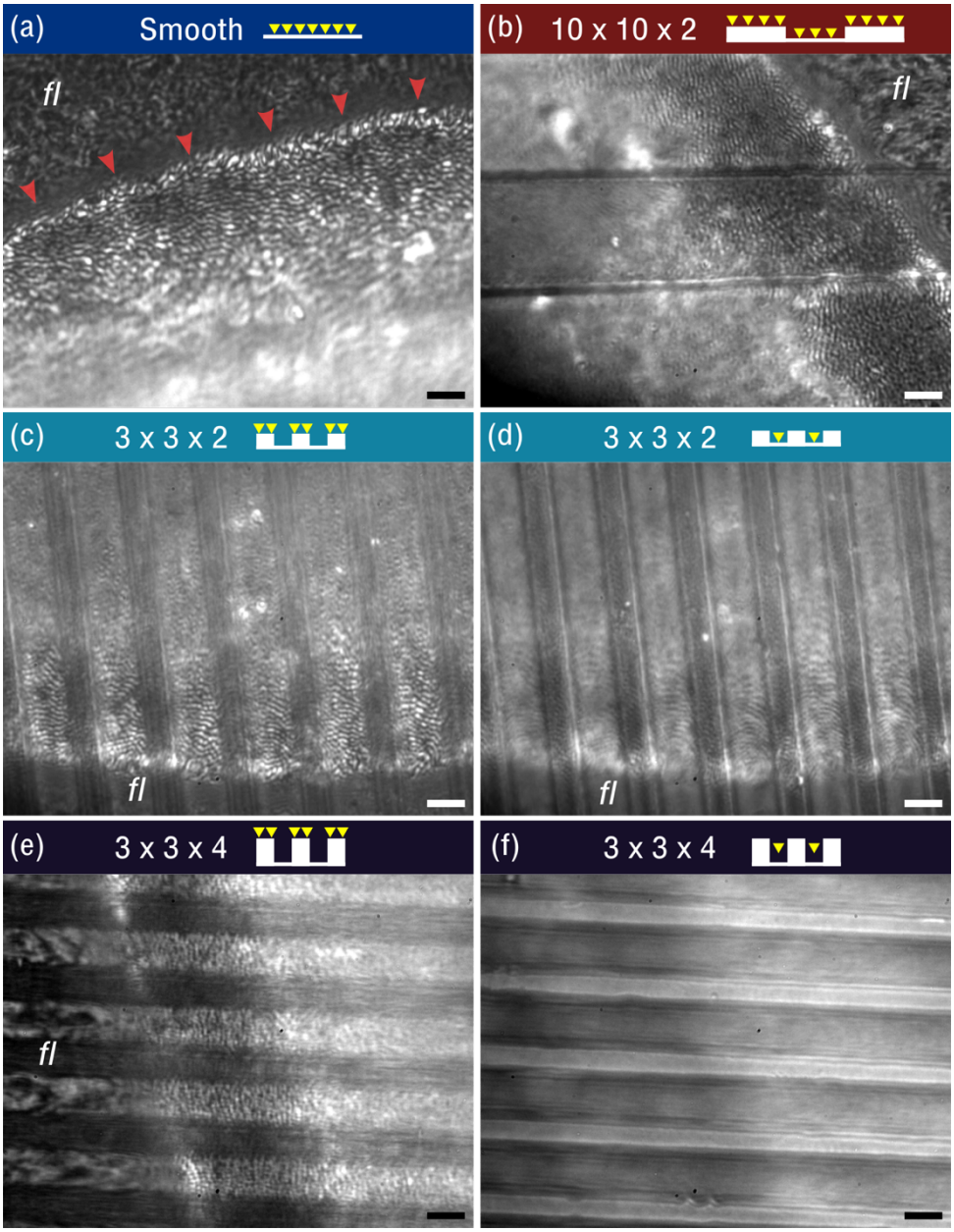

Figure 3.9. *In vivo* visualisation of *H. lugubris* suction disc contact on different substrates. (a) On smooth glass, microtrichia make tip contact (black dots). Note the outer fringe layer (fl) outside the seal (red arrowheads). Schematic of the contacts shown with yellow arrowheads representing microtrichia. (b) On 10×10×2 µm microstructured surface (ridges and grooves 10 µm in width, grooves 2 µm deep), contact from microtrichia and fl are similar to the contact on the smooth surface. (c) On 3×3×2 µm, the microtrichia made tip contact on the ridges, as well as in the grooves, seen in (d). However, fewer microtrichia make contact within the narrow grooves compared to the 10×10×2 µ m surface. (e) On 3×3×4 µm, microtrichia make close contact on the ridges, but inside the deep grooves there is no contact (f). Scale bars: 3 µm for all images.

3.5 Discussion

3.5.1 Blephariceridlarvae attach with extreme strength to diverse surfaces

Blephariceridlarvae possess some of the most powerful and complex suction organs among animals. The three species of blephariceridlarvae studied here (*H. lugubris*, *L. cordata*, and *L. cinerascens*) produced extreme shear forces on smooth surfaces ranging from 320 to 1,170 times their own body-weight. In terms of weight-specific attachment performance, the larvae far outperform all terrestrial insects measured with comparable methods (i.e., whole-body centrifuge experiments) (Federle et al., 2000; Grohmann, Blankenstein, Koops, & Gorb, 2014). For example, the weight-specific shear attachment of blephariceridlarvae was 3 to 11 times greater than that of stick insects measured in this study. To achieve this extreme shear attachment, blephariceridsuction organs must come in close surface contact by generating effective seals. Based on our *in vivo* visualisations of *H. lugubris* attaching to smooth glass underwater, the microtrichia make close contact with the surface, helping to both seal the organ and generate friction. This corroborates our previous findings on the suction disc contact behaviour with *L. cinerascens* and *L. cordata* (Chapter 2). Likewise, the soft adhesive pads of stick insects make close contact on smooth surfaces, and although the weight-specific attachment forces were not as high as in blephariceridlarvae, they can still withstand forces close to 100 times their body-weight.

When we measured attachment performances on micro-rough surfaces, however, there was a 16-fold decrease in stick insect attachment. In contrast, blephariceridlarval performance decreased to a much lesser extent (two-fold). This difference in the impact of micro-roughness on attachment performance can be attributed to the two fundamentally different mechanisms of attachment: on micro-rough surfaces, neither the soft adhesive pads nor the tarsal claws of stick insects function properly (Bullock & Federle, 2011). This is in part due to the reduced effective contact area (as the adhesive pads cannot mould sufficiently to the asperities), and also due to the reduced friction from tarsal claws (because the claws cannot interlock with the small asperities). On the other hand, blephariceridsuction organs are still able to seal on micro-rough surfaces and microtrichia can interact with the asperities, which likely explains why their performance was not impacted as severely as stick insects. In addition, blephariceridsuction organs may adhere better to micro-rough surfaces because when they are in partial contact, the gaps between the detached regions and the substrate are filled with water, whereas

detached regions of stick insect pads are filled with air. As water is effectively incompressible and approximately 50 times more viscous than air, the water-filled contact zone can provide a much stronger resistance against detachment even under conditions of partial contact as on micro-rough substrates.

While blephariceridlarvae outperformed stick insects on micro-rough surfaces, the opposite effect was found on coarse-rough surfaces: for stick insects, there was no difference in performance between coarse-rough and smooth surfaces, whereas blephariceridlarvae attachment decreased 11-fold. It is likely that both blephariceridsuction organs and stick insect adhesive pads are unable to cope with coarse-roughness. Stick insects, in contrast, can interlock their large pretarsal claws with these large asperities for strong attachment. Previous studies on dock beetles (*Gastrophysa viridula*) and stick insects *(C. morosus*) reported that both beetle and stick insect attachments on coarse-rough surfaces decrease significantly when the claws are removed (Bullock & Federle, 2011; Scholz et al., 2010). This is important because, although stick insects and dock beetles use two distinct adhesive pad systems (smooth versus hairy), the combination of the claws and the adhesive pads produces the same trend: both insects attach strongly to smooth and coarse-rough surfaces but poorly on micro-rough surfaces. In contrast, the suction-based attachments without claws in blephariceridlarvae do not follow this trend, which is a consequence of the markedly different mechanisms involved. A similar trend was reported by Liu *et al.* using *Blepharicera sp.*, where the larval attachment performance decreased with increasing surface roughness, although no quantitative information on attachment forces can be extracted from their study (Liu et al., 2020). (The study also used a centrifuge, but only reported rotation speed but not the insects' mass and position; it is also unclear whether the larvae were wetted prior to the tests.)

3.5.2 Ultrastructural components may help to stabilise the suction disc under high stress

Recent work with suction cup-like cupped microstructures has revealed their mechanisms of failure during underwater detachments: (1) under sustained tensile stress, the rim slides inwards and the rim diameter contracts by ~30%; (2) immediately prior to detachment, sections of the rim buckle inwards, leading to adhesive failure (Yue Wang, Kang, Arzt, Federle, & Hensel, 2019). Similar failure modes were also reported for macroscopic

suction cups (Ditsche & Summers, 2019). The cupped microstructures had smooth contact surfaces that adhered strongly to smooth glass surfaces underwater, reaching peak adhesive stresses of ~1.3 MPa. Two structural features of the blephariceridsuction organs could represent adaptations that counter the aforementioned failure mechanisms seen in microscopic suction cups. First, microtrichia could interlock with surface asperities and minimise inward sliding. This has been reported for remora fish which have spinules within their suction organ that point posteriorly to passively engage with asperities during high-drag conditions (Beckert et al., 2015; Fulcher & Motta, 2006); similarly, blephariceridmicrotrichia are naturally angled (~40° relative to the horizontal) and point towards the centre of the suction disc (Chapter 2). Hence, inward sliding would passively promote additional interlocking of the microtrichia tips with the surface. Second, the internal radial beams can provide structural support to reduce inward sliding and buckling of the rim. Similar to how the flexible membrane of an umbrella is stiffened by radial spokes, these stiff cuticular radial beams can stabilise the suction disc when the organ is under high tensile stress. Bones within the clingfish suction organ may also prevent inward sliding (Ditsche & Summers, 2019). While we have yet to visualise blephariceridsuction organs failure under extreme forces, their powerful attachments suggest that they possess mechanisms to counter the common modes of suction cup failure. We propose that this is achieved through the microtrichia and the ultrastructural morphology of the suction disc.

3.5.3 Blephariceridsuction organs are unique among insects and highly specialised for fast-flow conditions

We have demonstrated that blephariceridsuction organs can attach with extreme strength to both smooth and rough surfaces. Despite the potential strength of each attachment, the larvae are surprisingly mobile in their natural habitat (Federle & Labonte, 2019; Frutiger, 1998). Both attachment force and mobility are required for blephariceridlarvae to survive in their challenging habitats, which include raging alpine torrents and near the base of waterfalls. As far as we know, blephariceridsuction organs are the only examples of piston-driven suction organs in the insect kingdom. The other well-known example of suction organs in insects are the circular setae of male diving beetles (Dytiscidae), although the two systems have markedly different morphologies. The key differences between dytiscid and blephariceridsuction organs are: (1) the ventral surfaces of circular setae are comparatively smooth; (2) circular setae lack a muscle-driven central piston; (3)

there are no known mechanisms for rapid detachment (Chen et al., 2014; Karlsson Green et al., 2013; Nachtigall, 1974). As male dytiscid beetles use their suction organs to attach to the smooth sections of the female's pronotum and elytra, their attachment works best on smooth surfaces and their performance declines dramatically on rough surfaces (Karlsson Green et al., 2013). Researchers have suggested that male and female dytiscid beetles are engaged in an evolutionary arms race driven by sexual conflict, as female cuticular surfaces are modified to hinder male attachment with suction discs (Bergsten, Y, & Nilsson, 2001; Karlsson Green et al., 2013). Interestingly, it appears that male beetles did not evolve friction-enhancing structures on their circular setae to facilitate adhesion to rougher regions of the female cuticle. In contrast, blephariceridsuction discs are covered in a dense array of microtrichia that likely enhance grip on rough surfaces in high-drag conditions. This difference in morphology may be due to a number of reasons; for example, male diving beetles may not need to attach to rough elytra if their setae can generate sufficient attachment forces on smooth cuticle alone. Alternatively, beetle seta could simply be limited in the structures that can be developed, especially because the blephariceridorgan is highly complex and multicellular.

A more comparable suction-based attachment system can be found in the remora fish. Remora use suction pads, which are highly modified dorsal fin spines, to attach to sharks, whales, and manta rays (Beckert et al., 2015; Fulcher & Motta, 2006). They attach well to both smooth surfaces and to rough sharkskin, resisting 11.2 ± 1.0 N and 17.4 ± 4.8 N (mean ± SD) of posterior shear force, respectively (Fulcher & Motta, 2006). Recent studies on the functional morphology of remora suction pads have greatly expanded our understanding on the mechanisms underlying their impressive performance (Beckert et al., 2015; Gamel, Garner, & Flammang, 2019; Yueping Wang et al., 2017). A remora suction pad comprises a soft fleshy outer rim and rows of lamellae topped with spine-like bony protrusions called spinules. The pitch of the lamellae is muscle-controlled to facilitate spinule contact with the host skin. When engaged, the tips of these stiff spinules interlock with surface asperities and increase friction, thereby increasing shear resistance. Moreover, as mentioned previously, the angled posterior-facing lamellae and spinules promote passive engagement when subjected to shear forces from a swimming host (Beckert et al., 2015; Fulcher & Motta, 2006). We believe that the remora suction pad is analogous to the blephariceridsuction organ as both animals have to cope with high shear forces (fast-swimming hosts and torrential rivers for the remora and blephariceridlarvae,

respectively). Functionally, the spinules from remora increase shear resistance, allowing the animal to attach strongly to rough sharkskin surfaces. In blephariceridsuction organs, we have shown that microtrichia makes tip contact not only on smooth but also on microstructured surfaces. This indicates that the suction organ moulds to surface roughness and microtrichia contact the valleys of these asperities. To avoid buckling and to function effectively, interlocking structures like spinules and claws need to be stiff and strong (Dai et al., 2002; Yueping Wang et al., 2017). Our results strongly suggest that microtrichia are stiff structures based on the following reasons: (1) they are solid cuticular projections, and dense cuticle can reach high elastic moduli (Parle, Dirks, & Taylor, 2017); (2) we only observed tip contact on various surfaces, and even when the disc was pressed again the ridges in microstructured surfaces, we consistently observed only tip contact; (3) the larvae have better grip on soft polymer substrates, where indicates that the microtrichia are stiff and can penetrate the polymer. Hence, the stiff microtrichia interact with rough surfaces and could function in a similar way to remora spinules. We plan to investigate this further by measuring the friction coefficient of microtrichia against surfaces with varying levels of roughness.

3.5.4 Effect of biofilm layer on suction attachments to natural rock surfaces

Since blephariceridlarvae attach to rocks underwater and feed on epilithic algae, their suction organs will in most cases contact biofilm; however, the details of this interaction are unknown (Frutiger & Buergisser, 2002). It is possible that the stiff microtrichia pierce the biofilm layer, as hypothesised previously (Nachtigall, 1974; Rietschel, 1961). As we do not know the thickness of the biofilm growing in a typical habitat for blephariceridlarvae, additional information is needed to understand whether microtrichia directly contact the surface in their natural habitat or if they remain embedded in the biofilm matrix. Although there is one estimate of freshwater biofilm thickness in the literature (~200 µm), the biofilm was cultivated in the laboratory and the height of biofilm will vary drastically in the wild due to differences in flowrate, surface profile, temperature, and species composition (Ditsche, Michels, et al., 2014; Ditsche, Wainwright, et al., 2014). Nevertheless, because blephariceridmicrotrichia are stiff cuticular structures and biofilm is soft (~200 kPa for freshwater biofilm (Ditsche, Michels, et al., 2014)), the microtrichia likely pierce the biofilm layer. In support of this, our findings on blephariceridsuction attachment to smooth soft polymer and hard glass substrates show that larvae were significantly less prone to sliding on the softer substrate. This may be due to the friction

forces generated from the stiff microtrichia engaging with the soft substrate, which suggests that a relatively soft biofilm layer on hard rock surfaces could be beneficial for larval attachment. Friction-enhancing pads with posterior-facing hairs and spines can be found on many species of fishes and mayfly larvae that inhabit fast-flowing waterways (Ditsche-Kuru, Koop, & Gorb, 2010; Lujan & Conway, 2015). Researchers found that a higher proportion of mayfly larvae can withstand fast flow-rates on smooth hard (epoxy) substrates when biofilm is present; hence, mayfly larvae perform better on surfaces with biofilm than without (Ditsche, Michels, et al., 2014). Moreover, the setae and spine-like acanthae on the ventral surfaces of mayfly larvae can generate friction forces on clean rough substrates (Ditsche-Kuru et al., 2010). The dense array of microtrichia on blephariceridsuction discs may function similarly on biofilm-covered rough surfaces.

3.6 Conclusion

Blephariceridlarvae use their suction organs to generate extreme attachment to diverse surfaces. We found that suction organ morphology is conserved between *Hapalothrix* and *Liponeura* larvae, featuring a suction disc that contacts the substrate, dense arrays of microtrichia on the disc surface, muscles to control the piston, and the V-notch detachment system. In addition, we characterised internal radial beam structures that could help to stabilise the suction disc when subjected to high stress. On smooth surfaces, blephariceridlarvae withstood shear forces equivalent to 320 - 1,120 times body weight, depending on the species. *H. lugubris* performed the best out of the tested species, reaching weight-specific shear attachments up to 1,970 and estimated shear stresses of 48.6 - 144.2 kPa. Although their attachment decreased with increasing surface roughness, blephariceridsuction organs performed better than smooth adhesive pads on micro-rough surfaces. We confirmed that blephariceridsuction organs can form a seal and mould to surface asperities, and that microtrichia can come into close contact between the asperities. The microtrichia are stiff spine-like structures that may increase friction forces by interlocking with asperities and penetrating soft substrates.

4 MOLECULAR INSIGHTS INTO THE POWERFUL MUCUS-BASED ADHESION OF LIMPETS (*PATELLA VULGATA* L.)

4.1 Summary

Limpets (*Patella vulgata* L.) are renowned for their powerful attachments to rocks on wave-swept seashores. Unlike adult barnacles and mussels, limpets do not adhere permanently; instead, they repeatedly transition between long-term adhesion and locomotive adhesion depending on the tide. Recent studies on the adhesive secretions (bio-adhesives) of marine invertebrates have expanded our knowledge on the composition and function of temporary and permanent bio-adhesives. In comparison, our understanding of the limpets' transitory adhesion remains limited. In this study, we demonstrate that suction is not the primary attachment mechanism in *P. vulgata*; rather, they secrete specialised pedal mucus for glue-like adhesion. Through combined transcriptomics and proteomics, we identified 171 protein sequences from the pedal mucus. Several of these proteins contain conserved domains found in temporary bio-adhesives from sea stars, sea urchins, marine flatworms, and sea anemones. Many of these proteins share homology with fibrous gel-forming glycoproteins, including fibrillin, hemolectin, and SCO-spondin. Moreover, proteins with potential protein and glycan degrading domains could have an immune defence role or assist degrading adhesive mucus to facilitate the transition from stationary to locomotive states. We also discovered glycosylation patterns unique to the pedal mucus, indicating that specific sugars may be involved in transitory adhesion. Our findings elucidate the mechanisms underlying *P. vulgata* adhesion and provide opportunities for future studies on bio-adhesives that form strong attachments and resist degradation until necessary for locomotion.

4.2 Introduction

Limpets (the Patellogastropoda) are an ancient and diverse group of marine gastropods. The earliest fossil records date back to the Middle Ordovician (ca. 450 million years ago), and extant species can be found on seashores around the world (Nakano & Ozawa, 2007). The common limpet, *Patella vulgata* L. (Patellidae), is widespread in Europe and is found

in the upper intertidal zone, a challenging habitat with strong forces from tidal waves and currents, as well as prolonged exposure to air and predators (Denny, 1988; Grenon & Walker, 1981; Hahn & Denny, 1989) . Limpets have characteristic conical shells and attach to the surface using their muscular pedal sole. The limpet's powerful attachment is well-established, with recorded tenacity values (normal peak attachment force divided by contact area) typically ranging between 0.1 – 0.2 MPa (Branch & Marsh, 1978; Denny et al., 1985; Grenon & Walker, 1981; A. M. Smith, 1991b), reaching 0.7 to 1.1 MPa in some reports (Branch & Marsh, 1978; Coleman et al., 2004). Such impressive attachments help them resist strong tidal waves and thwart predatory attacks (Denny, 2000; Hahn & Denny, 1989) (Figure 4.1). However, unlike adult mussels and barnacles that rely on filter-feeding and permanently adhere to surfaces in the intertidal zone, limpets are active grazers of biofilm and detritus (Burgos-Rubio et al., 2015); hence, they can travel considerable distances while feeding (up to 1.5 m (Branch & Marsh, 1978)). They must, therefore, alternate between powerful attachments during stationary periods at low tides and locomotory adhesion at high tides (A. M. Smith, 1992). We refer to this sub-type of transitory adhesion as tidal transitory adhesion.

Despite over a century of research, the mechanisms responsible for the patellid limpets' strong attachment remain unresolved (Grenon & Walker, 1981). So far, proposed ideas include: suction (A. M. Smith, 1991b, 1992; A. M. Smith et al., 1993) (lowering of pressure beneath the attachment organ by muscle contraction), clamping (muscles forcing shells against the substrate to provide additional friction) (Coleman et al., 2004; Ellem, Furst, & Zimmerman, 2002), viscous adhesion (resulting from the flow resistance of viscous secretions beneath the pedal sole) (Grenon & Walker, 1981), and glue-like adhesion (via secretions that form chemical interactions to link the pedal sole with the surface) (Grenon & Walker, 1980; A. M. Smith, 1992; A. M. Smith et al., 1999). Following a series of studies ruling out suction in *Patella* (Branch & Marsh, 1978; Grenon & Walker, 1980, 1981), suction as a potential mechanism of attachment was re-introduced in a distantly related family of limpets, Lottidae (A. M. Smith, 1991b; A. M. Smith et al., 1993). The authors found a relationship between tenacity and ambient pressure, and also measured pressures directly beneath the pedal sole. Consequently, Smith proposed that limpets alternate between actively creating suction for adhesive locomotion at high tide and glue-like adhesion using adhesive mucus for powerful long-term attachment at low tide (A. M. Smith, 1991b, 1992; A. M. Smith et al., 1993). Such relationships have not

been investigated in *Patella*. Furthermore, as Patellidae separated from Lottidae around 191 million years ago (Nakano & Ozawa, 2007), it is unclear if this dual mechanism of suction and glue-like mucus is also used by *P. vulgata*.

Figure 4.1. Limpets (*Patella vulgata*) have evolved powerful attachments to withstand crashing tidal waves and predatory attacks. Here, one of the authors lifted a heavy rock by hooking onto a single limpet.

If limpets do secrete a specialised pedal mucus for adhesion, a detailed biochemical characterisation could offer insights into how the molecular components interact to function as a bio-adhesive. Limpet pedal mucus, independent of the species, is largely comprised of water, around 90-95% wet weight, with the rest being proteins, carbohydrates, and inorganic material (Davies, Jones, & Hawkins, 1990; Grenon & Walker, 1980; A. M. Smith et al., 1999). Pedal mucus is highly resistant to solubilisation (Grenon & Walker, 1980; A. M. Smith et al., 1999), although addition of protein and sugar-degrading enzymes results in a complete breakdown of the mucus (Grenon & Walker, 1980). Two different types of pedal mucus were identified from *Lottia limatula*: a solid plaque ("adhesive mucus") that was inconsistently left attached to the substrate when stationary limpets were forcibly detached, and more viscous pedal mucus from active limpets ("non-adhesive mucus") (A. M. Smith, 1992; A. M. Smith et al., 1999). The biochemistry of the adhesive and non-adhesive mucus differed in two ways: first, there was around a two-fold increase in protein and carbohydrate content from non-adhesive to adhesive pedal mucus (A. M. Smith et al., 1999). Second, of the nine protein bands isolated from *L. limatula* pedal mucus, one protein (118 kDa) was present only in

the adhesive samples, while a 68 kDa protein was associated with the non-adhesive mucus. The study concluded that *L. limatula* can control the properties of the mucus and transition from a non-adhesive to an adhesive type by modulating both the level and type of proteins secreted.

Although studies have examined the physical and biochemical properties of *P. vulgata* pedal mucus (Grenon & Walker, 1978, 1980), none identified the different types of mucus as seen in *L. limatula*. Nine glands have been characterised from *P. vulgata* pedal sole, five of which can secrete pedal mucus into the contact zone (space between the pedal sole and the attachment surface) (Grenon & Walker, 1978). Histochemical tests indicated that proteins and sugars are stored within these glands, possibly as glycoproteins in some of them (Grenon & Walker, 1980). Although putative locomotory or adhesive functions were assigned to the glands, these designations were not experimentally validated. Eight proteins ranging from 23 to 195 kDa were extracted from one type of *P. vulgata* pedal mucus that is likely similar to "non-adhesive" mucus from *L. limatula* based on sampling method (Grenon & Walker, 1980). This pedal mucus is a viscoelastic material, exhibiting fluid and solid-like behaviour, and is likely a cross-linked gel (Grenon & Walker, 1980; A. M. Smith, 2016b). It is not soluble in water and requires strong reducing agents or harsh alkaline conditions for solubilisation, and proteolytic or glycosidic enzymes for full degradation (Grenon & Walker, 1980).

While these earlier efforts offer initial biochemical descriptions of the limpet pedal mucus, our knowledge of its molecular components and their function remains limited compared to our understanding of other marine bio-adhesive secretions. Advances in sequencing technology and bioinformatics have allowed researchers to assemble and analyse transcriptomes and proteomes in order to characterise the molecules and their interactions that govern bio-adhesive systems. Consequently, our understanding of marine bio-adhesives has drastically expanded over the last three decades (example publications, among many others, include (Hennebert, Maldonado, et al., 2015; Lengerer & Ladurner, 2018; A. M. Smith, 2016a; Waite & Tanzer, 1981)). However, the bulk of our knowledge stems from biological systems that use either temporary adhesion (e.g., sea stars, sea urchins, barnacle larvae, and flatworms) or permanent adhesion (e.g., mussels, adult barnacles, and macro-algae) (Hennebert, Maldonado, et al., 2015). Tidal transitory adhesion, as seen in limpets, requires different functionalities; limpets need to attach

weakly during locomotion, but also form strong attachments for long periods of time. Another crucial difference that makes limpet adhesion special and worth investigating, is that the long-term attachment is reversible or degradable for locomotion. At the same time, limpet adhesive mucus needs to withstand unwanted microbial degradation during stationary periods and potentially lower the risk of infection. A detailed molecular characterisation of limpet pedal mucus, therefore, can help us understand how strong resistant biomaterials are synthesised and function as bio-adhesives.

In this study, we used a range of appropriate molecular biology approaches to investigate tidal transitory adhesion in *Patella vulgata*, including transcriptomics, proteomics, lectin-based assays, and *in situ* hybridisation. We isolated and identified 171 candidate adhesive protein sequences from different types of pedal mucus. We also localised specific sugar residues to pedal glands and secretions. Fourteen candidate protein sequences were individually annotated with conserved protein domains, many of which are also present in published temporary adhesives from marine invertebrates. To elucidate the role of active suction in *P. vulgata* and to complement our molecular investigation, we performed sub-pedal pressure recordings while limpets were freely locomoting, under stimulated predatory attack, and during manual detachment via normal pull-offs. We conclude that *P. vulgata* limpets secrete pedal mucus that has similar molecular constituents to temporary bio-adhesives but with several clear distinctions. Furthermore, we found no evidence of large reductions in sub-pedal pressure, suggesting that suction is not the principal mechanism underlying the limpet's powerful attachment.

4.3 Materials and methods

4.3.1 Animal collection and maintenance

Limpets (*Patella vulgata*) were collected on five occasions from Sheringham, England. Individuals with shell widths of around 20 to 35 mm were removed from exposed rock surfaces during low tide using the following approach to minimise damage to the pedal sole: a flat tool (e.g., flathead screw-driver) was placed at a shallow angle to the horizontal and slowly chiselled into the shell margin until the limpet was cleanly dislodged. The pedal soles of all individuals were visually inspected for damage before being brought to the laboratory. Limpets were kept in a marine aquarium tank lined with polyvinyl chloride acetate (PVCA) sheets for easy detachments, and a pump was scheduled on a timer to simulate tidal waves. Fit individuals (based on their resistance to dislodgement and

clamping response) were detached without damaging their pedal soles for all the experiments.

4.3.2 In vivo pressure measurements

Pressure recordings were conducted *in vivo* to investigate the range of pressure differences generated beneath limpet pedal soles. Healthy individuals were placed on a custom-built underwater set-up consisting of a horizontal platform made from clear acrylic with four adjustable walls to constrain the path of the moving limpet (see Supplementary Figure 1). A small circular hole (0.5 mm radius) was laser-cut in the horizontal acrylic platform and connected to a pressure sensor (PX26-30DV, OMEGA Engineering, UK; see Supplementary Materials for details on calibration) via flexible tubing. For recording pressures beneath the pedal sole during locomotion, a limpet was first detached from the main tank, its pedal sole gently cleaned with lab tissue to remove existing mucus, then placed on the platform so that it had to locomote anteriorly and over the pressure sensor. In a second set of experiments, a predatory attack was simulated using a method adapted from (Coleman et al., 2004) to elicit a clamping response: a stainless steel ball bearing (10 mm radius; 32.3 g weight) was accelerated down a 6 cm path at 45° incline by gravity to fall on the shell of the limpet. Lastly, limpets were allowed to locomote over the pressure sensor, tapped on the shell to elicit clamping, then manually detached with a vertical pull. The voltage output from the pressure transducer was recorded using a USB DAQ (NI-6001, National Instruments, USA) and a MATLAB script (MATLAB version R2017b, The MathWorks Inc., MA, USA). Analysis of the recordings was conducted in MATLAB.

4.3.3 Adhesive mucus sampling for biochemical characterisation

Previous studies used different techniques to sample pedal mucus: Grenon and Walker detached *P. vulgata*, wiped the sole clean, and left them upturned for 30 minutes before collecting the secreted mucus (Grenon & Walker, 1978). The samples were pooled from multiple individuals for biochemical characterisation. Smith, on the other hand, differentiated between adhesive (“A”) and non-adhesive (“NA”) mucus: adhesive mucus was sampled by detaching *L. limatula* that had settled onto glass walls of an aquarium tank, whereupon roughly a third of the limpets left behind a solid “glue” that remained firmly adhered on the glass, while non-adhesive mucus was sampled by placing several

individuals in a plastic bag and making them move around without attaching firmly for 4 – 8 hours (A. M. Smith et al., 1999). Mucus samples from multiple *L. limatula* were then pooled for biochemical characterisation.

For our studies, we developed a specialised sampling technique to collect three different types of *P. vulgata* pedal mucus while minimising contamination and damage to the individual (Figure 4.2). Limpets were allowed to settle onto thin sheets of PVCA (around 200 μm thick) in an aquarium tank with circulating artificial saltwater (ASW, made per manufacturer instructions; Instant Ocean, Aquarium Systems, VA, USA) at the Biology of Marine Organisms and Biomimetics Unit, University of Mons, Belgium. Immediately before sampling, the plastic sheets with limpets were removed from the tank, cleaned of excess debris, and positions of each settled limpet were marked using a permanent marker. The limpets were then carefully detached from the thin PVCA sheet by peeling (Figure 4.2a) – this minimised both damage to the soft pedal sole and possible contamination from other mucus types. Since our collection method was similar to that used to sample barnacle cement ("primary cement" is secreted naturally for attachment, while "secondary cement" is secreted only during re-attachment (Liang et al., 2019)), we have adapted their terminology to define our three types of pedal mucus. The thin mucus layer found on the PVCA sheet, similar to the "adhesive" mucus from Smith, was defined as the "interfacial primary adhesive mucus" (IPAM; Figure 4.2b), while the mucus layer remaining on the pedal sole was termed "bulk primary adhesive mucus" (BPAM). IPAM were collected by scraping them off the plastic sheets using sterilised glass squares with different extraction buffers (see below for buffer descriptions). BPAM was collected directly from the pedal soles of upturned limpets by making the thin mucus film swell with a small volume of filtered ASW (Instant Ocean, per manufacturer instructions), then removing the swollen mucus using sterilised forceps. The third mucus type was isolated using a previously described method (Grenon & Walker, 1980) with some modifications : after the BPAM was collected, the pedal sole was thoroughly cleaned with ASW and lab tissue paper, then the limpet was left upturned in a humid container to stimulate fresh mucus production. After at least 30 minutes, a small volume of newly secreted mucus, called "secondary adhesive mucus" (SAM) was collected (Figure 4.2c). It should be noted that as SAM was collected in air, the composition may vary if sampled from individuals left in an aqueous environment. Samples from individual limpets were kept separate and kept frozen at -20°C until further analysis.

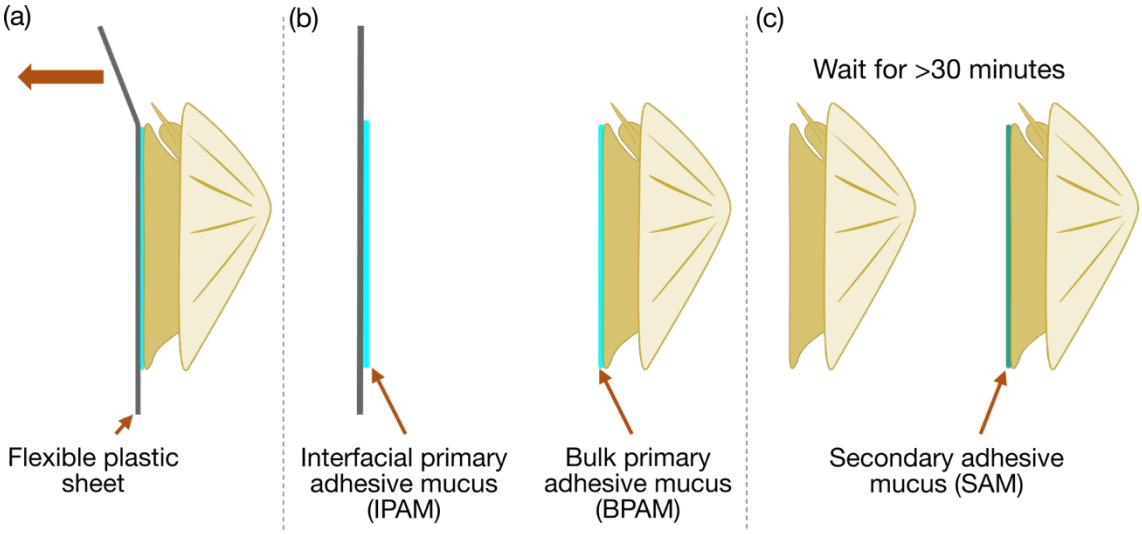

Figure 4.2. Three types of pedal mucus were sampled from individual *P. vulgata* limpets. (a) Limpets were allowed to settle onto thin PVCA films; (b) Interfacial primary adhesive mucus (IPAM) was collected by peeling a thin PVCA film from a settled limpet and scraping the thin layer on the PVCA, while bulk primary adhesive mucus (BPAM) was sampled from the limpet pedal sole; (c) Secondary adhesive mucus (SAM) was sampled by gently detaching a limpet, wiping the pedal sole clean, leaving it upturned for at least 30 min, then gently collecting the SAM from the pedal sole.

4.3.4 Protein extraction and gel electrophoresis with various staining methods

The three different mucus types (IPAM, BPAM, SAM) were solubilised and extracted for gel electrophoresis using the protocol described previously with minor modifications (Hennebert et al., 2014). The extraction buffer, made with 1.5 M Tris-HCl buffer at pH 7.8, 5 M urea, 2% (weight/volume) SDS, and 0.5 M dithiothreitol (DTT), was added to the samples and transferred to a glass pestle tissue homogeniser and manually ground for up to 5 min to thoroughly disrupt the mucus. The homogenised samples were then incubated at 60°C with agitation for 1 hour, followed by 5 min of cooling down to room temperature (RT). Sulfhydryl groups were carbamidomethylated with iodoacetamide used in a 2.5-fold excess (w/w) to DTT in the dark at RT for 20 min. An equal quantity of β-mercaptoethanol was added to stop the reaction, and the sample was centrifuged at 13,000 RPM for 15 min at 4°C. The supernatant containing solubilised proteins was transferred to Eppendorf tubes and stored in -20°C for future use.

For gel electrophoresis, Laemmli sample buffer (Bio-Rad) was added to the protein extracts with 5% (v/v) β-mercaptoethanol, heated for 2 minutes at 90°C, then centrifuged for 5 min at 16,000 *g*. 10% sodium dodecyl sulphate (SDS)–polyacrylamide gels were used and subsequently stained with Coomassie Blue (to visualise proteins), Periodic Acid Schiff (PAS; to visualise carbohydrates), or Stains-All (colour depends on protein properties; blue for acidic proteins or Ca^{2+}-binding proteins (K. P. Campbell, Maclennantll, & Jorgensen, 1983), purple for proteoglycans, pink for less acidic proteins (Goldberg & Warner, 1997)).

4.3.5 Peptide sequencing using mass spectrometry

Mass spectrometry was performed as previously described (Hennebert, Leroy, Wattiez, & Ladurner, 2015) with minor modifications. Proteins from whole extracts of IPAM, BPAM, and SAM were precipitated using cold acetone (repeated until DTT scent was not detectable), then subjected to trypsin digest at 37°C overnight (1 µg of trypsin per 50 µg of extracted protein; modified porcine trypsin, sequencing grade from Promega). Tryptic peptides were analysed by reverse-phase HPLC-ESI-MS/MS using an Eksigent NanoLC 400 2D Ultra Plus HPLC system connected to a TripleTOF 6000 quadrupole time-of-flight mass spectrometer (AB Sciex, Concord, ON, Canada). After injection, peptide mixtures were transferred to a AB Sciex column (3C18-CL 75µm x 15 cm) and eluted at

a flow rate of 300 nL/min. MS data was acquired using the TripleTOF 6000 mass spectrometer fitted with a Nanospray III source (AB Sciex) using a pulled quartz tip as the emitter (New Objectives, MA, USA).

4.3.6 RNA isolation and transcriptome generation

Total RNA was isolated from an individual *P. vulgata* limpet by the following method: first, the pedal sole was carefully excised from surrounding tissue on ice and divided into longitudinal sections. Next, each section was immediately frozen in liquid nitrogen, added to TRIzol (Life Technologies, Carlsbad, CA), then homogenised using a hand-held mechanical tissue homogeniser. After going through the recommended protocol using TRIzol reagent, quality of the isolated RNA was initially checked using spectrophotometry, at which point a second clean-up was conducted using RNeasy Mini-kit (Qiagen, CA, USA) to digest genomic DNA and to further purify the RNA. Subsequent sequencing, data processing, and transcriptome assembly were performed at the Beijing Genomic Institute, China (BGI). Integrity of the isolated RNA was assessed by gel electrophoresis and via Agilent Bioanalyser prior to sequencing (RNA integrity number: 6). Illumina HiSeqXTen platform was used to generate 150 bp paired-end reads, and the raw reads were filtered to remove adaptors and low-quality reads (see Supplementary Materials for more details). Cleaned reads were used for *de novo* assembly of the transcriptome with *Trinity* software v2.0.6 (Grabherr et al., 2011) and assembled into Unigenes with *Tgicl* v2.0.6 (Pertea et al., 2003). Fragments per kilobase of transcript per million mapped reads (FPKM) values were calculated by first mapping clean reads to Unigenes with *bowtie2* (Langmead & Salzberg, 2012) (v2.2.5, sensitive mode; see Supplementary Materials for full software settings), then *RSEM* (B. Li & Dewey, 2011) (v1.2.12, default parameters) was used to quantify expression levels. To assess transcriptome assembly and annotation completeness, we conducted an analysis based on the Benchmarking Universal Single-Copy Orthologs (BUSCO) using *BUSCO* v3.0.2 (Simão, Waterhouse, Ioannidis, Kriventseva, & Zdobnov, 2015) for metazoa_odb9 and eukaryote_odb9 datasets. Based on the metazoan dataset, the assembled transcriptome was estimated to be 91.5% complete with 894 complete BUSCOs, 4.4% (43) fragmented BUSCOs and 4.1% (41) missing BUSCOs from a total of 978 BUSCO groups searched. Similar values were obtained with the eukaryota dataset. Note that these BUSCO numbers are in line with those from the *Lottia gigantea* reference genome (Simão et al., 2015).

Raw sequencing reads and the assembled transcriptome has been deposited to the NCBI BioProject database under accession number PRJNA613775.

4.3.7 Searching for peptides against the transcriptome

The assembled transcriptome was translated into the six open reading frames (ORF) on a Galaxy Project server (https://usegalaxy.org (Afgan et al., 2018)). MS/MS data were searched for protein candidates against all ORFs using the software ProteinPilot 5.0 (AB Sciex). Carbamidomethyl cysteine was set as the fixed modification and trypsin as the digestive enzyme. For all samples, candidates with false discovery rates (FDR) above 0.01 were excluded from further analyses. Only sequences that appeared in all three individuals were compiled to form a single set of candidate proteins for IPAM, BPAM, and SAM. Additionally, these three lists were combined, and duplicates removed to create a total candidate protein list obtained from aligned transcriptome and proteome data. Homology against known proteins was assessed using NCBI Basic Local Alignment Search Tool for protein (blastp) against UniProtKB / SwissProt databases (www.uniprot.org (The UniProt Consortium, 2017)) set to the default parameters. Conserved protein domains were searched on InterPro (v75.0) (Mitchell et al., 2019). Clustal Omega (www.ebi.ac.uk/Tools/msa/clustalo) (Goujon et al., 2010) and Jalview Version 2 (v2.10.4b1) (Waterhouse, Procter, Martin, Clamp, & Barton, 2009) were used for multiple sequence alignments to check for conserved protein domains. The following suite of prediction algorithms were used to characterise the candidate proteins: DeepLoc 1.0 was used for localisation predictions(Almagro Armenteros, Sønderby, Sønderby, Nielsen, & Winther, 2017); NetCGlyc 1.0, NetNGlyc , and NetOGlyc 4.0 for C-, N-, and O-glycosylation predictions (Gupta & Brunak, 2002; Julenius, 2007; Steentoft et al., 2013); NetPhos 3.1 for phosphorylation predictions (Blom, Gammeltoft, & Brunak, 1999); and SulfoSite for predicting tyrosine sulphation sites (Chang et al., 2009).

4.3.8 Expression analysis of candidates using *in situ* hybridisation

From the combined list of candidate proteins, a subset was selected for further analysis using *in situ* hybridisation (ISH) based on the following criteria: first, we limited our selection to proteins that were ranked highly by ProteinPilot to ensure we were targeting proteins that were present in adhesive mucus. Second, we included candidates with conserved protein domains that were commonly associated with marine bio-adhesives

(e.g., vWFD, EGF, lectins). Finally, we sought to sample proteins across the different types of mucus with the goal of identifying candidates associated with specific types of mucus (IPAM, BPAM, and SAM). ISH probes were generated based on a modified protocol from (Lengerer et al., 2019) and is described in full in the Supplementary Materials. In summary, cDNA was generated from isolated total RNA (same limpet individual as the one sent for transcriptome sequencing) using Transcriptor First Strand cDNA Synthesis Kit (Roche). Gene-specific primers were designed with Primer 3 (http://primer3.ut.ee, v4.1.0) and used to synthesise template DNA for the production of digoxigenin-labelled (DIG) anti-sense RNA probes (see Supplementary Materials for list of primers used). Limpet tissues were fixed in 4% paraformaldehyde (PFA) in PBS, embedded in paraffin wax, then sectioned into 14 µm sections using a Microm HM 340 E microtome. Probes were added to tissue sections and developed using NBT/BCIP system (Roche) at 37°C. Sections were mounted and imaged with a Zeiss Axio Scope.A1 microscope.

4.3.9 Lectin staining to identify specific sugar residues within limpet pedal sole

Lectin staining was used to provide additional insight into the identity and locality of specific sugar residues within the limpet adhesive organ (see (Lengerer, Bonneel, et al., 2018) for additional information on lectin-based staining method to investigate adhesive organs). Nine biotinylated lectins (see Table 4.1; Vector Laboratories, USA) were applied to 5 µm paraffin sections of *P. vulgata* pedal sole and visualised using Texas Red conjugated Streptavidin. For the negative control, a section was prepared alongside the rest, but no lectin stains were added. A few sections were also stained with alcian blue at pH 2.5 and counterstained with phloxine to facilitate the interpretation of the lectin stains by providing an overview of the pedal sole morphology and glands. Sample images were taken at the following regions to aid in comparison between different staining patterns: marginal groove, anterior (immediately posterior to the marginal groove), middle, and posterior end of the foot. All images were taken with a Zeiss Axio Scope.A1 microscope. Qualitative assessment of lectin stain intensity was conducted based on images taken with the same exposure settings. Images for figures were post-processed in FIJI to enhance clarity (Schindelin et al., 2012).

4.4 Results

4.4.1 General observations on *Patella vulgata* attachment and *in vivo* pressure recordings

During the course of this study, we recorded four key observations about limpet attachments that provided novel insights into their adhesion: first, when stationary limpets were detached (by peeling from plastic sheets) and immediately placed onto a smooth flat surface (glass or plastic), their adhesion was insufficient to hold their own weight when turned upside-down, i.e., their re-attachment was not immediate. Once the limpets had time to locomote away from being returned to a surface (around 1 – 2 minutes), they consistently left behind a gel-like layer on the surface (likely similar to the BPAM collected for proteomics; see Supplementary Video 1). Such samples resisted degradation in the saltwater tank for several weeks. Second, stationary limpets that were well-attached remained so even when a length of wire was pushed through from one margin of the pedal sole to the other (Supplementary Video 2). Third, limpets crawled up the vertical wall of a basket made up of plastic fishing mesh placed in the aquarium and settled slightly above the waterline with strong adhesion (Supplementary Figure 2). Lastly, limpets that died while firmly adhered to plastic sheets remained well-attached, and the surface could be peeled away from them in a similar way to living limpets. Each of these observations suggested a mechanism of attachment that is not reliant on muscle-actuated suction, which is typically dynamic (fast attachments-detachments) (Federle & Labonte, 2019), detaches from a disruption of the rim, fails to seal on meshes or porous substrates, and is often not functional upon death of the animal.

To further investigate the contribution of reduced pressures beneath limpet pedal soles, pressure was measured beneath living limpets attached to a clean smooth acrylic surface. Plots from a representative experiment with three different conditions (free locomotion, simulated attack, and normal pull-off) are shown in Figure 4.3. When limpets were freely locomoting, we recorded both positive and negative pressures (relative to ambient pressure) beneath the pedal sole, ranging from -0.79 to 1.0 kPa (n = 20 measurements from 8 limpets). The average (± standard deviation, SD) minimum and maximum recorded pressures per limpet were -0.42 ± 0.23 kPa and 0.32 ± 0.33 kPa, respectively (n = 8). No discernible difference in pressures was observed when limpets were left to attach to the surface for 10 minutes or longer. When limpets were disturbed with a simulated predatory attack, we saw a distinct reduction in pressure (-2.3 ± 1.5 kPa, average ± SD; n

= 6 limpets). These pressure reductions decayed exponentially over time, taking 3.7 ± 3.0 seconds (average ± SD; n = 8 measurements from 5 limpets) to reach 60% of the minimum pressure. The most negative pressure value (-5.7 kPa) was recorded when an attached limpet was manually pulled off perpendicularly from the surface (see Supplementary Materials for additional information). The average pressure value for all manual detachments was -1.5 ± 1.9 kPa (± SD, n = 4 limpets).

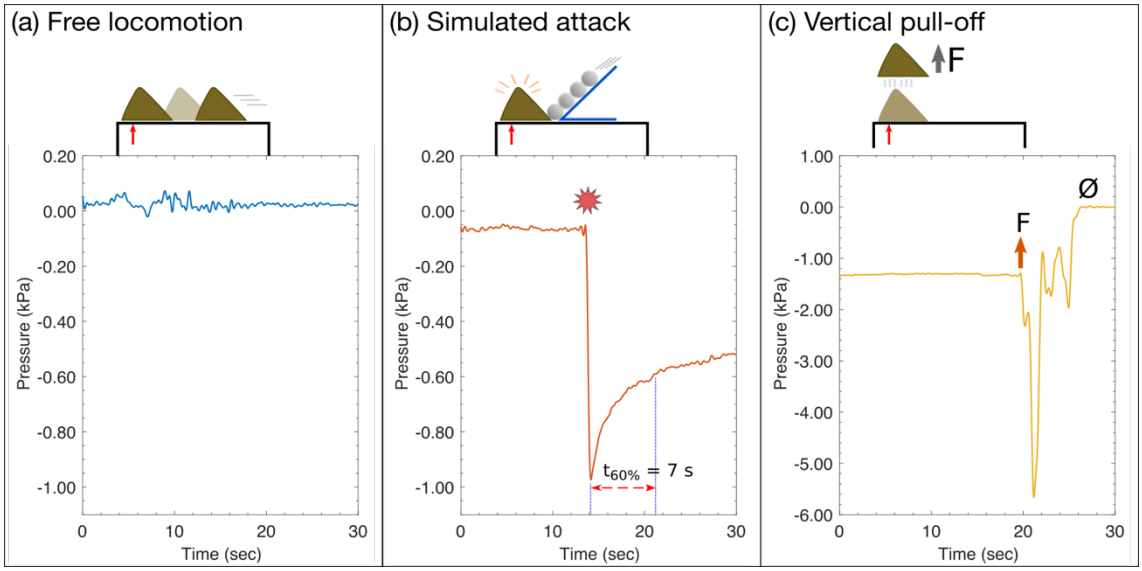

Figure 4.3. Representative *in vivo* sub-pedal pressure values from *P. vulgata* with schematics showing the different trial conditions. (a) Free locomotion: small pressure values (around -0.02 to +0.07 kPa) were observed when the limpet was undisturbed and locomoting over the sensor. (b) Simulated attack: when a ball bearing was used to simulate a predation event, the pressure was lower, at around -1.0 kPa. This negative peak decayed slowly, taking around 7 s to reach approximately 60% of the minimum pressure. (c) Normal pull off: when the limpet was allowed to settle over the sensor and then manually detached perpendicularly (arrow marks beginning of detachment), a sharp negative peak was recorded that reached -5.7 kPa, which returned to zero when the limpet detached (marked Ø). All tests were conducted under water.

4.4.2 Overview of the molecular components of *Patella vulgata* pedal mucus

As a result of our revised mucus collection method (Figure 4.2), we successfully isolated three types of limpet pedal mucus (IPAM, BPAM, and SAM). We observed a number of qualitative differences between the types of mucus: first, IPAM was a thin layer left on the surface when the limpet was detached that sometimes felt like a raised solid patch. The thin layer of IPAM became visible with crystal violet staining. BPAM, on the other hand, was visible as an opaque swollen layer on top of the pedal sole and could at times

be removed as an intact sheet of mucus. Lastly, the small quantities of SAM produced on the pedal sole easily broke apart during collection and did not form sheets like BPAM.

From the three types of pedal mucus collected from *P. vulgata,* we used gel electrophoresis to visualise multiple protein bands (Supplementary Figure 3). In total, at least 11 distinct protein bands were identified with Coomassie Blue staining, with molecular weight estimates ranging from 40 kDa to 190 kDa, and a few protein bands larger than 250 kDa. Unlike previous studies where mucus samples were pooled from many individual limpets, sufficient amounts of protein were collected to compare secreted proteins between individuals, although no discernible differences were observed. The most prominent protein bands across all three adhesive mucus types were 45, 55, 130, and 160 kDa, and a protein band outside the top range of the ladder (referred to as ">250 kDa"). While proteins from the three mucus types were similar in size, one smeared band around 60 kDa was associated with the IPAM samples (Supplementary Figure 3a). Periodic acid-Schiff (PAS) staining confirmed the presence of glycosylated proteins of ~60 kDa in size (Supplementary Figure 3b). PAS staining also revealed large glycosylated protein-based complexes that were not fully disrupted and failed to migrate into the gel. Stains-all cationic dye provided further insights into the differences between the types of mucus (Supplementary Figure 3c). We observed blue-stained protein bands (indicative of proteins that are highly acidic, negatively charged, and/or bind Ca^{2+}) at around ~110 kDa in both BPAM and IPAM, although the band stained more strongly in the latter. There was also a strong blue staining at the top of the gel that overlapped with the positive PAS staining, supporting the presence of large protein-sugar complexes that failed to enter the gel. Meanwhile, purple-stained bands (proteoglycans) at ~55 kDa and >250 kDa and a bright pink band (weakly acidic proteins) of ~160 kDa were associated with BPAM only. Once again, there was a smeared band ~60 kDa from all IPAM samples, and this band stained pink to purple.

Lectin assays provided additional information on the nature of the sugar residues present in limpet pedal mucus (Figure 4.4). Six of the nine tested lectins labelled specific glands and secreted mucus; four specifically targeted glands near the pedal sole and not the side-walls (Table 4.1). We discovered that *Lens culinaris* agglutinin (LCA), which recognises α-Mannose and/or α-Fucose linked to *N*-acetylchitobiose sugar residues, specifically stained glands within the pedal sole and not the side-wall. LCA revealed an anterior-

posterior gradient of stained glands, where the anterior of the foot featured the highest density of staining, followed by the posterior end of the foot, while the middle section was stained least intensely (Figure 4.4a). We observed oval glands within the pedal sole epithelium, while flask-shaped subepithelial glands were found in a zone of high glandular density extending from the epithelium to approximately 150 μm into the body (dorsally). In contrast to the strong and dense staining from LCA, the rest of the lectin stains localised to more specific glands within the foot, the pedal sole, or the side-wall. *Maackia amurensis* lectin II (MAL II) stains highlighted distinct granular contents within pedal sole glands, and succinylated wheat germ agglutinin (sWGA) stained granular gland contents distributed throughout the foot tissue as well as in pedal sole glands. Wheat germ agglutinin (WGA), unlike sWGA, did not stain pedal sole glands. Both WGA and sWGA strongly stained the epithelium. Notably, sWGA and LCA captured several glands in the midst of secreting mucus to the outside. We observed a dorsoventral gradient of glands with different sugar residues: while LCA, sWGA, and *Ulex europaeus* agglutinin 1 (UEA I) stained glands both close to the epithelium and deeper (dorsally) into the tissue, *Ricinus communis* agglutinin I (RCA I) and MAL II localised to specific glands further away from the epithelium. MAL II-stained glands particularly deep in the limpet foot (~60 to 150 μm away from the epithelium), with granular contents secreted through long necks to the outside.

4.4.3 Identification of putative limpet adhesive proteins from transcriptomics and proteomics

A *de novo* transcriptome was obtained from the *Patella vulgata* pedal sole (Supplementary Table 1). Functional annotation was conducted using seven databases (NR, NT, GO, KOG, KEGG, SwissProt and InterPro), which yielded 37,261 annotations overall (see Supplementary Table 2 for numbers from each database). This transcriptome was used as a reference to map peptide sequences of IPAM, BPAM, and SAM protein extracts from pedal mucus (n = 3 individuals). With this approach, 171 candidate sequences for limpet adhesive proteins were identified: 27% of them (46 sequences) were found in all three mucus types (to classify as being present in a type of mucus, a candidate sequence had to be found in all three individuals), while 22% (37 sequences) were present only in BPAM, 13% (23 sequences) in SAM, and 9% (15 sequences) only in IPAM. Note that, due to our selection criteria (where a candidate protein had to be present in all three limpet individuals in order to be attributed to BPAM, SAM, or IPAM), some proteins

may not have been assigned to a particular type of adhesive mucus. Nevertheless, this categorisation helped to form initial ideas about the potential functions of each isolated protein.

Table 4.1. List of lectin-based stains used to investigate sugar residues present in the limpet pedal sole.

Lectin	**Acronym**	**Target sugars**	**Staining intensity**	**Pedal sole**	**Side-wall**
Lens culinaris agglutinin	LCA	α-Man, α-Fuc linked to *N*-acetylchitobiose	+++	Glands	No
Ulex europaeus agglutinin I	UEA I	α-Fuc	+	Epithelium, Glands	No
Wheat germ agglutinin	WGA	GlcNAc (dimers or trimers preferred), chitobiose Sialic acid	++	Epithelium, Glands (also throughout the foot)	Epithelium
Succinylated wheat germ agglutinin	sWGA	GlcNAc (without sialic acid)	+++	Glands	Epithelium
Ricinus communis agglutinin I	RCA I	Gal, GalNAc	+	Glands	No
Maackia amurensis lectin II	MAL II	(α-2,3)-sialic acid	+	Glands	No
Soybean agglutinin	SBA	α- or β-GalNAc, Gal	+	Non-glandular structures throughout the foot	No
Concanavaline A	ConA	α-Man	+++	NA*	NA
Jacalin	Jacalin	Galβ-(1-->3)-GalNAc	-	No	No
None	Negative control	NA	-	-	-

Note |*NA: not applicable due to unspecific staining | -: no staining observed

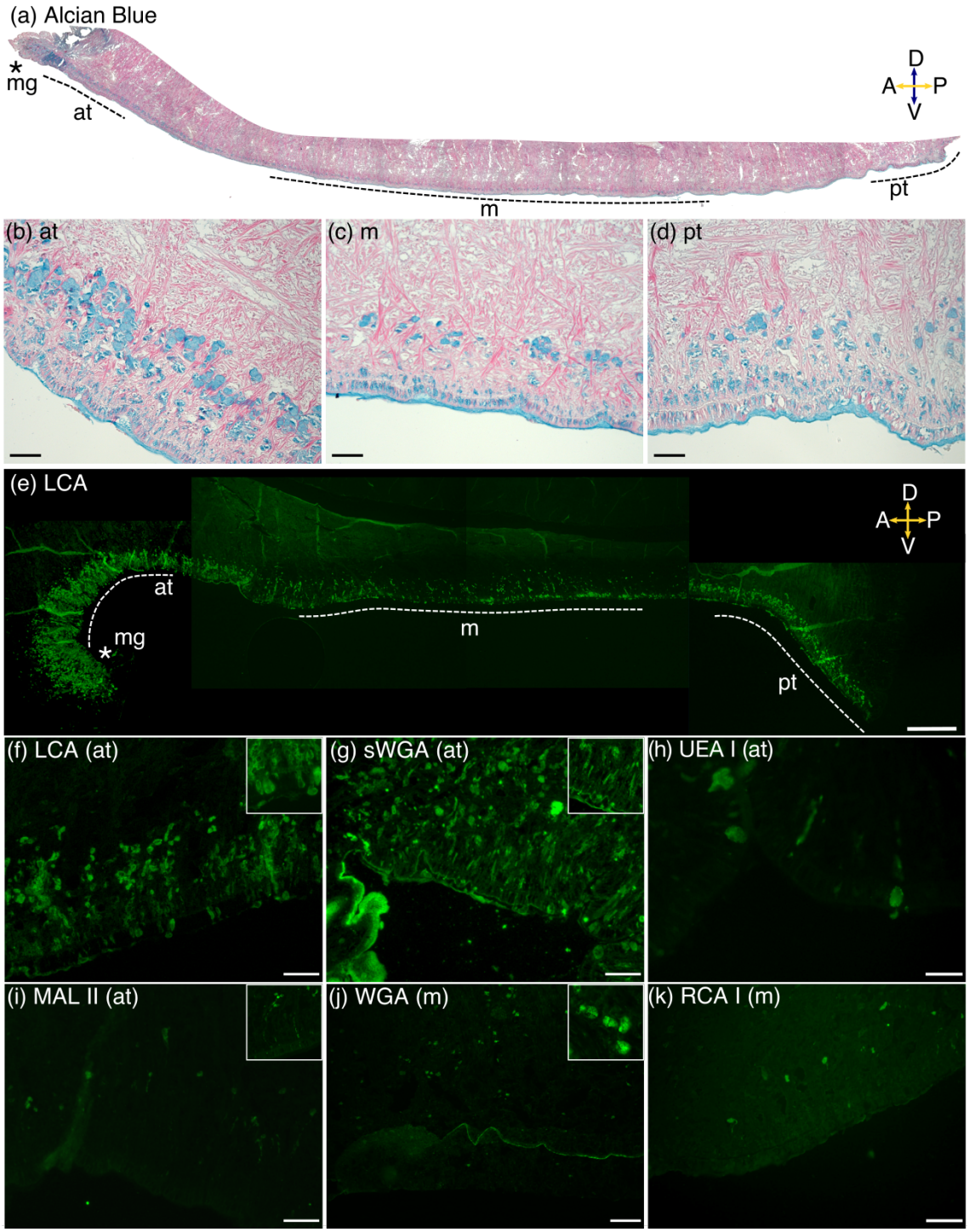

Figure 4.4. Overview of *P. vulgata* foot tissue and the chemistry of glandular secretions. **(a-d) Alcian blue** (pH 2.5) highlights glands in blue (carboxylate and sulphate moieties) and phloxine stains muscles in red. Note: Regions used for higher-magnification images **b-d** are labelled as marginal groove (mg), anterior (at), middle (m), and posterior (pt). Scale bars: 100 µm in **b-d**. Compass labels: A, anterior; P, posterior; D, dorsal; V, ventral. **(e-k)** Lectin stains highlight the different sugar residues present within specific glands. **(e) LCA**: stitched image showing the entire foot. Glands contain α-Man and/or α-Fuc linked to *N*-acetylchitobiose sugar residues. Side-wall glands are not stained. Dotted line marks the epithelium, and imaged regions are labelled as in **a**. Scale bar 400 µm. **(f) LCA (at)**: Stained glands are found within the epithelium and up to ~300 µm into the foot. Scale bar 100 µm. Stained mucus and gland secretions are visible (inset, 150 µm box). **(g) sWGA (at)**: *Continued overleaf.*

Secretions containing GlcNAc but not sialic acid are highlighted throughout the tissue. Scale bar 100 μm. Granules are secreted from long necks (inset, 200 μm box). **(h) UEA I (at)**: Specific glands contain α-Fuc. Scale bar 20 μm. **(i) MAL II (at):** Infrequent glands deep in the tissue (~100-150 μm) contain (α-2,3)-sialic acid. Scale bar 100 μm. Granules are secreted from long necks (inset, 370 μm box). **(j) WGA (m)**: Glands with GlcNAc are present throughout the foot tissue. Note the epithelium is strongly stained. Glands ~30 μm in size are full of granules (inset, 150 μm box). **(k) RCA I (m)**: Similar to MAL II but with GalNAc or galactose. Scale bar 50 μm. See text and Table 4.1 for additional information on the lectins used and their ligands.

Fourteen sequences (*P-vulgata_1* to *14*; see Figure 4.5) were chosen for a more detailed analysis with manual annotation of conserved protein domains and *in situ* hybridisation. Six of the fourteen sequences were found in all three pedal mucus types (*P-vulgata_1* to *6*); one was found in IPAM and BPAM only (*P-vulgata_7*); one from IPAM and SAM (*P-vulgata_11*); four from only IPAM (*P-vulgata_8 to 10*, *P-vulgata_12*), and one from each of the SAM and BPAM samples (*P-vulgata_13* and *P-vulgata_14*, respectively).

The following characteristics of the fourteen sequences are summarised in Table 4.2: the type of mucus it was isolated from (IPAM, BPAM, SAM), fragment per kilobase million (FPKM), sequence length in amino acids, presence of start and stop codons, cysteine content, homologs found in *Lottia gigantea* genome, signal peptide, predicted subcellular localisation, homologous proteins of interest based on NCBI blastp, conserved protein domains based on InterPro, predicted glycosylation (N, C, or O-linked), predicted phosphorylation, and predicted sulphation. The cysteine content ranged from 3.9% to 15.1%, with the exception of one protein that had a low content of 0.6% (*P-vulgata_5*). The most common protein domains included von Willebrand factor type D (vWFD), epidermal growth factors (EGF), Kazal-type serine protease inhibitors (KSPI), and scavenger receptor cysteine-rich (SRCR). All proteins were predicted to have post-translational modifications (PTMs), with at least one type of glycosylation and numerous phosphorylation sites. While half of the proteins were predicted to have sulphated tyrosine, this PTM was not detected in *P. vulgata* (neither on foot sections nor on mucus trails) using an anti-sulphotyrosine antibody (Hennebert, Gregorowicz, & Flammang, 2018).

BLAST analysis of the limpet proteins highlighted homology to a number of characterised proteins. Most notably, three proteins (*P-vulgata_1*, *2*, and 4) had the same group of homologous proteins: fibrillin, zonadhesin, alpha-tectorin, and fragment

crystallisable region of immunoglobin G (IgGFc)-binding protein. These proteins can participate in ligand-binding, adhesion, oligomerisation, or fibril formation: for example, zonadhesin is a multi-domain protein believed to facilitate the binding of sperm to the egg zona pellucida (Lea et al., 2001), while fibrillin is a large Ca^{2+}-dependent glycoprotein that forms microfibrils in the extracellular matrix (Handford, 2000). Moreover, both *P-vulgata_2* and *4* had sequence similarities to known adhesive proteins: adhesive protein 1 from *Minona ileanae* (QEP99777.1) (Pjeta et al., 2019) and sea star footprint protein 1 (Sfp-1) from *Asterias rubens* (AHN92641.1) (Hennebert et al., 2014), respectively. It is worth mentioning that *P-vulgata_4* featured two positively charged repeats at the C-terminus (amino acid sequence RRSRRNRNKARRSRRNRN) that did not align with any of the homologous proteins.

Two proteins – *P-vulgata_3* and *6* – were similar to SCO-spondin, a large secreted glycoprotein from the thrombospondin family involved in neural development with binding sites for sugars, proteins, and lipids (S Gobron et al., 1996; Vera et al., 2015). *P-vulgata_3* in particular was highly homologous to SCO-spondin, with homology to NCBI reference sequences for SCO-spondin from multiple unrelated species (e.g., 84% QC and 30.70% ID to SCO-spondin from *Gallus gallus*, NP_001006351.2; see Supplementary Figure 4.4a). Interestingly, *P-vulgata_3* was highly similar to a specific portion of SCO-spondin (Figure 4.6). The implications of this homology are discussed in the following section. While *P-vulgata_3* featured nearly all of the conserved domains of SCO-spondin (vWFD, TIL, C8, LDLrA), *P-vulgata_6* had just the repeating TSP-1-like domains in common. As a result of these repeating domains, however, *P-vulgata_6* aligned with a small portion of adhesion protein 2 from *Macrostomum lignano* (QAX24810.1) (Wunderer et al., 2019).

P-vulgata_5 was homologous to the settlement-inducing protein complex (SIPC) from barnacles (*Megabalanus coccopoma*; 91% QC, 27.70% ID; BAM28692.1), both of which contain alpha-2 macroglobulin domains. This protein's homology to SIPC is discussed in the subsequent section.

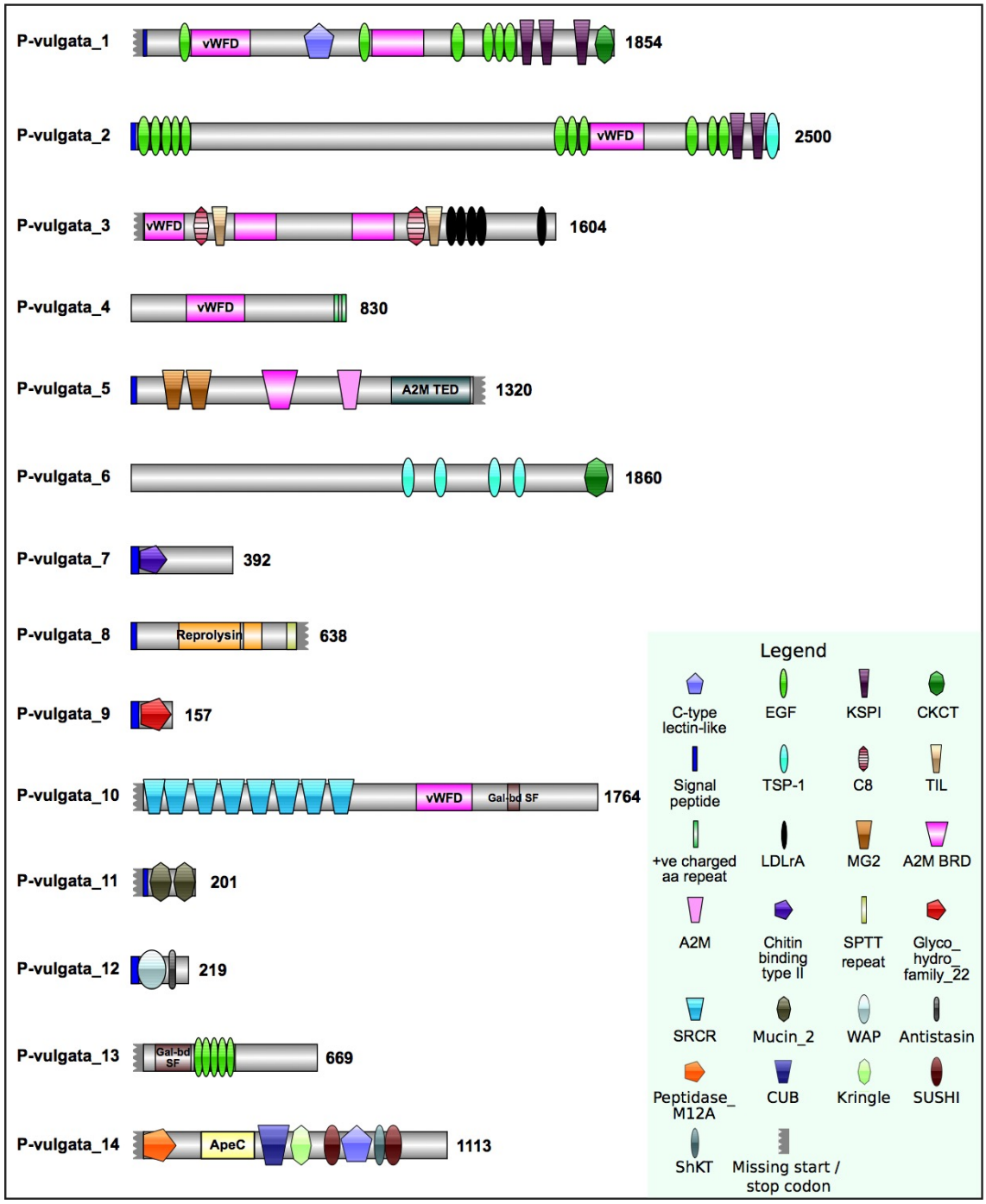

Figure 4.5. Conserved protein domains present in a subset of limpet pedal mucus proteins. Amino acid lengths are shown after the N-terminal of each sequence. See legend for details.

P-vulgata_8 featured one type of domain, reprolysin, which is a metallopeptidase (also called adamalysin M12B peptidase). Clustal alignment with reprolysin consensus sequence cd04267 from NCBI Conserved Domain Database (Marchler-Bauer et al., 2017) highlighted similarities between the proteins but, importantly, the conserved catalytic HEXXH motif was absent in in *P-vulgata_8* (Supplementary Figure 4b). In addition, unlike other adamalysin peptidases, *P-vulgata_8* featured nine tandem Ser-Pro-Thr-Thr repeats starting from residue position 598. This was likely incomplete as the stop codon was missing and the sequence terminated after the first Serine of the next repeat, i.e., S / PTT. Enrichment of Ser, Pro, and Thr residues began upstream of the SPTT repeat region (amino acid 550 to 638) and accounted for 73 of the last 89 residues (82%) of the sequence.

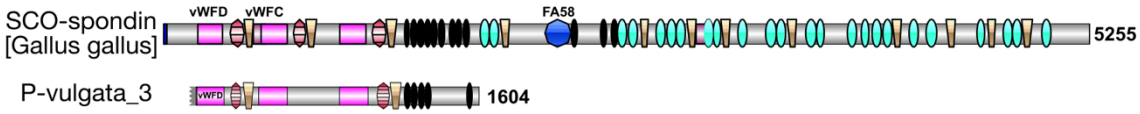

Figure 4.6. Comparison between *P-vulgata_3* and SCO-spondin from *Gallus gallus*. *P-vulgata_3* shares many conserved domains with the first one-third of SCO-spondin sequence.

P-vulgata_9 contained a predicted enzymatic domain, glycoside hydrolase family 22 (Glyco_hydro_family_22). This sequence was similar to a C-type lysozyme from *Haliotis discus hannai*, a species of abalone (92% QC, 48.99% ID; ADR70995.1), as well as with an NCBI reference sequence for lysozyme C from *Canus lupus familiaris* (88% QC, 38.03% ID; NP_001300804.1). The conserved catalytic Glu residue found in lysozymes was present in *P-vulgata_9*.

Due to the tandem SRCR repeats, *P-vulgata_10* aligned with an NCBI reference sequence for the deleted in malignant brain tumors 1 protein isoform c precursor from *Homo sapiens* (48% QC, 46.37% ID; NP_060049.2). Other notable homologs included SRCR-rich proteins from sea stars (*Asterias rubens*, QAA95957.1), sea urchins (*Strongylocentrotus purpuratus*, NP_999762.1), and sea anemones (*Exaiptasia pallida*, Aipgene2358 (Davey, Rodrigues, Clarke, & Aldred, 2019)).

No reliable homologs outside of hypothetical proteins were identified for *P-vulgata_12, 13,* and *14.* However, it is worth noting that the ShKT domain prediction in *P-vulgata_14*

was unexpected as it was first described as a potent ion channel toxin in sea anemones (Castañeda et al., 1995). Multi-sequence Clustal alignment of *P-vulgata_14* with four roundworm mucin proteins homologous to ShkT (Tc-MUC-1 to 4) (Loukas et al., 2000) confirmed the presence of the conserved cysteine residues (Supplementary Figure 4c). However, the catalytic dyad Lys-25/Tyr-26 found in ShKT was absent in *P_vulgata-14* and Tc-MUC-1 to 4.

4.4.4 Expression of putative limpet adhesive proteins

From the list of 171 candidate sequences isolated from the three mucus types, sixteen were selected for *in situ* hybridisation to determine their expression site within the limpet. These sixteen sequences were selected based on their relative ranking, domain similarity to published adhesive proteins, and presence in a specific mucus type (Supplementary Table 3). Specific expression patterns were obtained for *P-vulgata_1, P-vulgata_3, P-vulgata_4, P-vulgata_7,* and *P-vulgata_11* (Figure 4.7). As some of our samples had unspecific background staining, we only analysed those that produced distinct expression patterns (see Figure 4.7a, which shows the distinct specific and unspecific regions). A more detailed account of the background staining is provided in Supplementary Materials (Supplementary Figure 5). From the five samples with distinct expression sites, *P-vulgata_1, P-vulgata*_3, and P-*vulgata_4* stained a band of glands between ~30 to ~110 µm away from the epidermis, while *P-vulgata_7* localised to glands within the epidermis. These expression patterns confirm that the corresponding proteins were produced and secreted from glands specific to the pedal sole. *P-vulgata_11* specifically stained glands in the side-wall, which might indicate a contamination of the samples with side wall secretions.

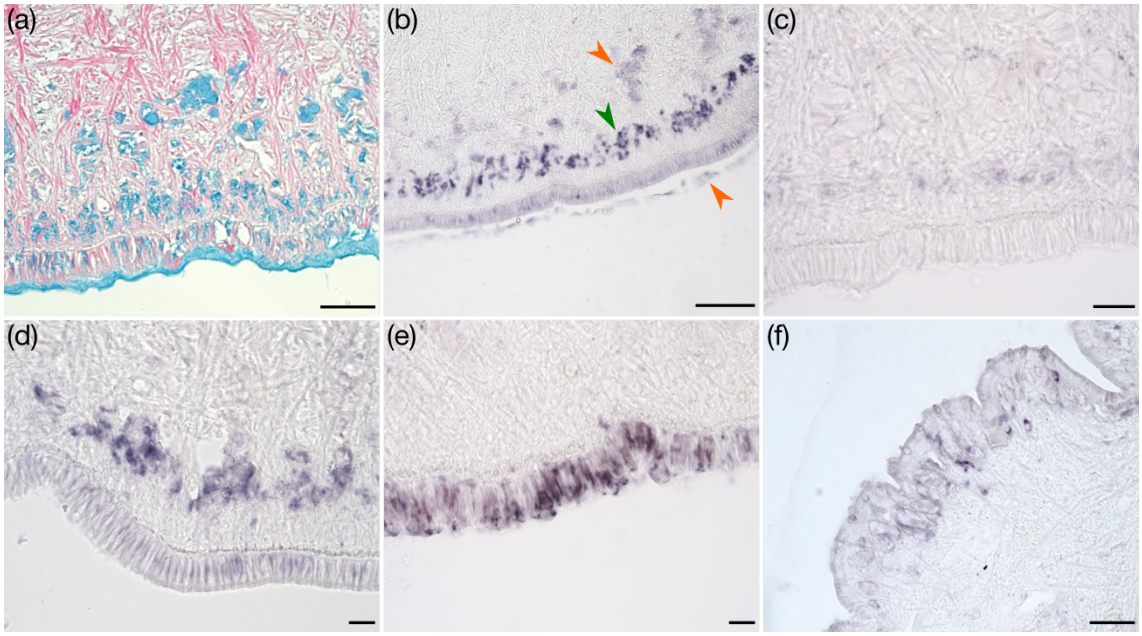

Figure 4.7. *In situ* hybridisation (ISH) of five protein sequences confirms the presence and locality of the target mRNA within *P. vulgata* foot**. (a)** Alcian blue stain highlights the glands present in the foot and provides context for the ISH stains. Scale bar 100 µm. Probes for *P-vulgata_1* **(b)**, *P-vulgata_3* **(c)**, and *P-vulgata_4* **(d)** localised to a specific band of glands ~30 to 110 µm away from the epithelium. Scale bars 100 µm, 20 µm, 20 µm, respectively. Note that in **b**, the weak staining around 150 µm away from the epithelium and in the mucus is unspecific background staining (orange arrowheads) that is distinct from the specific expression sites at ~100 µm away from the epithelium (green arrowheads). **(e)** *P-vulgata_7* stained the pedal sole epithelium. Scale bar 20 µm. **(f)** *P-vulgata_11* localised at the side-wall epithelium. Scale bar 50 µm.

Table 4.2. Summary of putative adhesive proteins and their characteristics. See Figure 4.5 and text for details.

Sequence ID	Found in which mucus types?	FPKM	Length (amino acids)	Start / Stop codon	Cysteine content (% of length)	Signal Peptide	Predicted localisation	Conserved protein domains (InterPro)	Homologous proteins of interest (BLASTp)	Predicted glycosylation	Predicted phosphorylation	Predicted sulphation
P-vulgata_1	All	737	1,854	N / Y	7.6%	Y	Secreted	vWFD x2, C-type lectin-like, EGF x6, cystine-knot C-terminal, KSPI x3	Fibrillin, zonadhesin, alpha-tectorin, IgGFc-binding protein	N, C, O	Numerous	1
P-vulgata_2	All	28	2,500	Y / N	7.8%	Y	Cell membrane	vWFD, EGF x11, KSPI x2, TSP1 x1	Fibrillin, zonadhesin, alpha-tectorin, IgGFc-binding protein, **adhesive protein 1 [Minona ileanae]**	N, C, O	Numerous	5
P-vulgata_3	All	2*	1,604	N / N	8.6%	N	Cell membrane	C8 domain x2, vWFD x3, TIL x2, LDL receptor class A binding repeats x5	SCO-spondin, hemolectin/hemocytin, mucin	N, O	Numerous	0
P-vulgata_4	All	17	830	Y / N	5.7%	N	Secreted	vWFD	Zonadhesin, alpha-tectorin, IgGFc-binding protein, **Sfp-1 [Asterias rubens]**	O	Numerous	0
P-vulgata_5	All	334	1,320	Y / N	0.6%	Y	Secreted	M2-like, A2M BRD, A2M, A2M TED	CD109-antigen-like, **SIPC [Megabalanus coccopoma]**	N, O	Numerous	0
P-vulgata_6	All	1,147	1,860	Y / Y	5.9%	N	Cell membrane	TSP1 x4, cystine-knot C-terminal	SCO-spondin, hemicentin, **adhesion protein 2 [Macrostomum lignano]**	N, C, O	Numerous	2
P-vulgata_7	IPAM & BPAM	21,122	392	Y / Y	5.9%	Y	Secreted	Chitin binding type II	BSMP14	N,O	Numerous	0
P-vulgata_8	IPAM	180	638	Y / N	3.9%	Y	Secreted	Reprolysin	ADAM family mig-17	N, O	Numerous	0
P-vulgata_9	IPAM	2,607	157	Y / Y	5.7%	Y	Secreted	Glyco_hydro family 22	C-type lysozyme	N, O	Numerous	0
P-vulgata_10	IPAM	9	1,764	N / Y	5.2%	N	Cell membrane	SRCR x8, vWFD, Galactose-binding domain superfamily	Deleted in malignant brain tumors-1, scavenger receptor cysteine-rich protein type 12 precursor	N, C, O	Numerous	4
P-vulgata_11	IPAM & SAM	4	201	N / Y	6.0%	Y	Secreted	Mucin x2	oikosin-like, mucin, cartilage intermediate layer-like	O	Numerous	1
P-vulgata_12	IPAM	399	219	Y / Y	15.1%	Y	Secreted	WAP, Antistasin-like	NA	N, O	Numerous	0
P-vulgata_13	SAM	162	669	N / Y	9.7%	N	Secreted	Galactose-binding domain superfamily, EGF x5	NA	N, O	Numerous	4
P-vulgata_14	BPAM	65	1,113	N / Y	4.9%	N	Secreted	Peptidase_M12A, ApeC, CUB, Kringle, SUSHI x2, C-type lectin-like, ShKT	NA	N, C, O	Numerous	1

*The sum of the FPKMs of two nearly identical contigs for P-vulgata_3 are shown.

4.5 Discussion

4.5.1 The role of sub-pedal pressure differences in limpet attachments

Numerous studies have sought to understand the principles behind the limpet's powerful attachment by ascribing it to suction (A. M. Smith, 1991b, 1992; A. M. Smith et al., 1993), clamping (Ellem et al., 2002), or glue-like secretions (Grenon & Walker, 1980; A. M. Smith, 1992; A. M. Smith et al., 1999). Smith reported a significant reduction in sub-pedal pressures when limpets (either *Tectura scutum* or *Lottia gigantea*) were placed on an acrylic surface and slid across the pressure gauge (approximately -20 kPa, relative to ambient), and an even larger reduction when irritated to illicit a clamping response (close to -50 kPa) (A. M. Smith, 1991b). Our sub-pedal pressure differential measurements using *Patella vulgata* revealed much smaller values, with the average minimum pressure during free locomotion of -0.42 ± 0.23 kPa. Even with a simulated predatory attack inducing a clamping response, our values (-2.3 ± 1.5 kPa) were smaller than those reported by Smith. Our locomotion pressures are in good agreement with previous sub-pedal pressure measurements from locomoting *P. vulgata* (reported as 6 cm of water, which is around 0.6 kPa) (H. D. Jones & Trueman, 1970). When a predatory attack was simulated, the limpet clamped its shell against the surface, resulting in a rapid decrease in sub-pedal pressure, followed by a less negative pressure as the limpet relaxed slightly but did not quickly return to ambient (taking around 3.7 seconds to reach 60% of the peak minimum value). This response is similar to the clamping behaviour of *Cellana tramoserica* reported by Ellem *et al.,* where initial irritation (single tap to the limpet shell or the experimental set-up) caused a clamping force of 2 - 5 N that decayed in 1 - 2 seconds to pre-stressed levels, while continued irritation (continuous tapping) resulted in a much higher force of 25 N that decayed slowly over 5 minutes (Ellem et al., 2002). While we measured the sub-pedal pressures and not the forces, we observed a similar sustained decay in response to a simulated predatory attack. Hence, when our sub-pedal pressure findings are considered in combination with our observations on limpet attachment (i.e., adhering strongly with a disrupted seal or climbing on a mesh but not being able to re-attach quickly), it is likely that *P. vulgata* does not actively generate suction for attachment. Rather, it is likely that, at least in this limpet species, the most critical element for adhesion is creating a strong yet reversible connection between the pedal sole and the surface that is independent of sub-pedal pressures. Consequently, when the limpet clamps down, the sole is able to sustain the reaction force even when a seal is absent. If a continuous seal is present or if influx is sufficiently low, then clamping will

result in a pressure reduction that may further contribute to the overall attachment; however, our pressure recordings and behavioural observations indicate that low sub-pedal pressures are not required for attachments in *P. vulgata*.

4.5.2 Generating adhesion through chemical interactions: how limpet pedal mucus may function as a bio-adhesive

Several studies have previously investigated the chemical constituents of limpet pedal mucus using histochemistry and gel electrophoresis (Grenon & Walker, 1978, 1980; Hennebert et al., 2018; A. M. Smith et al., 1999). Our results from lectin-binding assays and transcriptome-assisted proteomics have revealed novel insights into the biochemical properties of *P. vulgata* pedal mucus.

Lectin staining of *P. vulgata* revealed a highly complex glandular system within the foot. We found LCA to be a good candidate for a comprehensive labelling of pedal sole glands. This suggests that LCA's target sugar residues (α-Man and α-Fuc linked to *N*-acetylchitobiose) are specific to the pedal sole mucus and not to secretions from other parts of the body. Furthermore, we observed a dorsoventral gradient of lectin staining, where the longest subepithelial glands (whose cell bodies are located ~60 to 150 μm dorsally from the pedal sole epithelium) are labelled with RCA I and MAL II (*N*-acetylgalactosamine or sialic acid, respectively). The density of these glands was also lower than that of the shorter ones expressing other residues, such as mannose, fucose, chitobiose, sialic acid, or *N*-acetylglucosamine, which were found closer to the epithelium. At the other end of the spectrum, some glands were present within the epithelium, containing fucose, *N*-acetylglucosamine, chitobiose, or sialic acid residues. A dorsoventral gradient may be important for the timing of secretions: glands close to the surface would require less time to secrete than those deep inside the foot, where the secretion needs to be pushed out through long thin necks. Spatial distribution of glands may also be important for the digital mucus glands of tree frogs, where clusters of ventral and dorsal glands within the attachment organ, the toe pad, have distinct morphologies and locations that may be related to their functions (Langowski et al., 2019). The tubular ventral glands, which supplies mucus to the surface of the adhesive toe pad, are situated deep within the organ and have long thin necks to the ventral surface, similar to the glands found in limpets. An alternative explanation for the dorsoventral gradient may be related to the volume of the glands: one way to increase the gland volume is to lengthen it with

a long neck. Indeed, tubular glands are significantly larger than dorsal glands in tree frogs, and this is also likely the case for limpets. Our findings, which highlight the usefulness of lectins in clarifying limpet gland morphology and chemistry, also emphasise the need for future work on understanding the function of these glands and associated sugar chemistries.

From our transcriptome-assisted proteomics study of limpet pedal mucus, 171 sequences were identified from the limpet pedal mucus, of which fourteen were selected and manually characterised. To facilitate discussion about their putative functions, these proteins have been assigned to three broad functional categories based on their domain composition: (1) proteins likely to be involved in oligomerisation, ligand binding (proteins, sugars, metals), and peptide stabilisation (disulphide bridges); (2) enzymes or inhibitors, and (3) proteins with elements of both. It is worth mentioning that the transcriptome was based on the sequencing data from the pedal sole of a single limpet specimen. Since adhesive proteins are often large and repetitive (Hennebert et al., 2014; Wunderer et al., 2019), they tend to be inadequately assembled with short-read transcriptomics (Lengerer, Wunderer, et al., 2018; Pjeta et al., 2020). We sought to increase mapped transcript lengths by reducing the complexity of the input RNA and minimising transcript variation caused by pooling samples from multiple individuals. Although our analysis showed that the transcriptome is of good quality, we want to highlight that due to the limited sample size, some transcripts and transcript variations may not be represented in this dataset.

Proteins *P-vulgata_4, 6, 7, 10, 11, and 13* fall into the first category, sharing amongst them domains associated with multi-protein complex formation (vWFD, EGF, SRCR, and TSP-1) and protein-carbohydrate binding (C-type lectin-like, galactose binding-like domain superfamily, and chitin-binding type II). The ability to bind to other proteins and carbohydrates (either free-existing or attached to glycosylated proteins) is an important requirement for the cohesion of gastropod mucus and underwater adhesives, which are often cross-linked and are difficult to dissolve without potent denaturing agents (Grenon & Walker, 1980; Hennebert, Wattiez, Waite, & Flammang, 2012; Kamino et al., 2000; Lachnit, Buhmann, Klemm, Kröger, & Poulsen, 2019; A. M. Smith, 2006; Wilks, Rabice, Garbacz, Harro, & Smith, 2015). Furthermore, these proteins had elevated cysteine residue contents of 5% to 9.7%, much higher than the average for eukaryotes (1-2%),

although this may decrease when the full length of some of the proteins are sequenced. Nevertheless, as all limpet mucus samples were challenging to dissolve even in harsh extraction buffers and high heat, disulphide bridges (either intra- or intermolecular bonds) are probably present in limpet adhesive mucus. Besides cohesion, ligand interactions are also important for adhesion to surfaces, and the carbohydrate-binding domains may promote interactions with surface-adsorbed or biofilm-based sugars (A. M. Smith, Papaleo, Reid, & Bliss, 2017).

Proteins *P-vulgata_5, 8, 9, 12,* and *14* belong to the second category, with each sequence having at least one enzymatic (sugar-cleaving glycoside hydrolase and metallopeptidase) or inhibitory domain (WAP, antistasin, macroglobulin, and ShkT). *P-vulgata_8*, while sharing some conserved residues with other members of the adamalysin metallopeptidases, lacks the canonical catalytic HEXXH motif. It is unclear, therefore, if *P-vulgata_8* has any enzymatic function. This protein warrants further investigation, however, as it was found only in IPAM. Similarly, *P-vulgata_9* was also found in IPAM and is a secreted protein with a glycoside hydrolase domain that cleaves sugar bonds within carbohydrates or linked to a glycoprotein. Unlike *P-vulgata_8*, this protein did include the catalytic residue, and may be involved in active degradation of pedal mucus to transition from stationary to locomotive states. Alternatively, since *P-vulgata_9* is homologous to lysozymes, it may have a defensive function, similar to cp-16k, a lysozyme-like protein found in barnacle cement (Kamino, 2016). Follow-up studies on the activity of *P-vulgata_8* and *9* are necessary to understand their respective roles in limpet IPAM.

P-vulgata_12 and *14*, on the other hand, are more likely to serve a defensive role. *P-vulgata_12* contains a WAP domain, which is often found in proteins with antiproteinase and antimicrobial activities (Amparyup, Donpudsa, & Tassanakajon, 2008; V. J. Smith, Fernandes, Kemp, & Hauton, 2008), as well as an antistasin-like domain, a serine protease inhibitor (InterPro accession number IPR004094). Both domains contain multiple intramolecular disulphide bridges, which may afford stability in harsh physical conditions (Mason, McIlroy, & Shain, 2004). *P-vulgata_12*, therefore, may be a highly stable protease inhibitor present in IPAM to protect the protein and sugar rich pedal mucus against foreign degradation. *P-vulgata_14*, on the other hand, is notable as it contains numerous domains for recognising, binding, and degrading sugars and peptides. One of

its domains, Peptidase_M12A, is a zinc-dependent metallopeptidase, while Kringle, CUB, and SUSHI domains are involved in recognition processes and regulating proteolytic functions. Apextrin-like (ApeC) and C-type lectin-like domains are both involved in innate immune responses of invertebrates by binding to bacterial peptidoglycans (Gerdol & Venier, 2015; G. Huang et al., 2014; Zelensky & Gready, 2005), although it should be noted that C-type lectin-like domains can interact with other types of ligands, such as proteins, lipids, and inorganic compounds (Zelensky & Gready, 2005). One unexpected domain prediction is the ShKT, which is a potent potassium ion channel inhibitor originally characterised from the sea anemone *Stichodactyla helianthus*. Loukas *et al.* found homologous regions (referred by its alternative name, six-cysteine repeat, SXC) from four proteins (Tc-MUC-1 to 4) encoding for secreted mucins in the parasitic nematode *Toxocara canis* with no toxin-like function (Loukas et al., 2000). Our analysis of *P-vulgata_14*, Tc-MUC-1 to 4, and ShKT confirmed sequence homology to the ShKT domain; however, like Tc-MUC-1 to 4, *P-vulgata_14* lacks the functional dyad found in the ShKT toxins and is unlikely to function as a potent ion channel inhibitor. Instead, the domain could be involved in forming stable disulphide bridges that occurs in the native structure of the ShKT. The abundant target recognition and regulation-related domains suggest that *P-vulgata_14* acts as an antibacterial agent within the pedal mucus. Interestingly, since this protein was found only in the BPAM samples, possible roles of *P-vulgata_14* are to: (1) prevent microbial degradation of the secreted mucus, which has to remain functional over prolonged periods of time (e.g., during high tide, when the limpet typically stops foraging and remains stationary within the safety of its home scar), and (2) to minimise risk of infection. However, many aspects of this protein need to be further investigated to verify its purported function, such as its target specificity, stability, and how it interacts with the gel network.

P-vulgata_1, 2, and *3* belong to the third category, with numerous domains for diverse ligand-binding in combination with protease inhibitor domains. These proteins represent some of the longest, most well-represented, and complex sequences from the annotated set. Each protein contains at least four different domains and can potentially interact with proteins (through Ca^{2+}-binding EGF, TSP-1, vWFD), glycans (C-type lectin-like domain), or lipids (through lipoproteins binding to LDLrA). These domains suggest that these proteins can bind to diverse ligands that are soluble and/or adsorbed to the surface, as well as undergoing homo- or hetero-oligomerisation (for example, vWFD, lectins, and

cystine knot, C-terminal domains can self-oligomerise (Mayadas & Wagner, 1992; Meiniel & Meiniel, 2007; Zelensky & Gready, 2005)). Such functional domains could promote the formation of large networks with protein-protein and protein-glycan cross-links, which is essential for cohesive strength and is a mechanism to interact directly with surfaces or surface-adsorbed molecules (A. M. Smith et al., 2017). This hypothesis is supported by the type of homologous proteins identified through blastp analysis: *P-vulgata_1*, *2,* as well as *4*, shares homology with fibrillin, zonadhesin, alpha-tectorin, and IgGFc-binding protein. Incidentally, the similarities between these proteins have been reported previously in a study on the evolution of gel-forming mucin proteins (Lang, Hansson, & Samuelsson, 2007). These proteins form microfibrils (fibrillin; (Handford, 2000; Sherratt et al., 2003)), bind to glycoproteins (zonadhesin; (Hellberg, Dennis, Arbour-Reily, Aagaard, & Swanson, 2012)), recruit collagen fibrils to microvillar membrane surfaces (tectorin, (Kim et al., 2019)), and form gels (IgGFc-binding protein, (Harada et al., 1997)).

Similarly, *P-vulgata_3* is highly homologous with the consensus sequence for SCO-spondin, albeit only to roughly one-third of the total length. Similar to fibrillin, SCO-spondin is a large secreted glycoprotein present in the central nervous system and can be found either in a soluble state or aggregated into Reissner's fibre (Meiniel & Meiniel, 2007; Vera et al., 2015). The homologous segment contains vWFD, C8, TIL, and LDLrA domains, while the remainder features numerous copies of TSP-1, SCO-spondin region repeats (SCOR), TIL, and a CTCK (Meiniel & Meiniel, 2007). Interestingly, the TSP-1-rich segment from SCO-spondin that is absent in *P-vulgata_3* is specifically implicated in promoting neuronal development (Stéphane Gobron et al., 2000; Sakka et al., 2014), which appears to be a superfluous function for adhesive proteins. Furthermore, *in situ* hybridisation localised *P-vulgata_3* expression to the pedal sole, ruling out contamination as a possible source of SCO-spondin-like peptides. It is worth highlighting that the expression level of *P-vulgata_3* was low (based on FPKM; Table 4.2); however, it is often difficult to make conclusions on protein abundance based solely on the transcript expression levels, especially when the FPKM is derived from a single transcriptome. Additional investigation using techniques like exponentially modified protein abundance index (emPAI) is necessary to understand the relative abundance of *P-vulgata_3* and other adhesive proteins. Nevertheless, *P-vulgata_3* may represent a re-purposing of a highly conserved protein involved in neuronal development to an adhesive one through

the loss of the TSP-1 and SCOR repeats. Alternatively, the TSP-1 motifs in SCO-spondin sequences have been increasingly duplicated through evolution, as evident in the lengthening observed in SCO-spondin-like proteins from Echinodermata to Vertebrata (Meiniel et al., 2008). Ancestral SCO-spondin, therefore, may have served a conserved role in adhesion, then gradually lengthened to facilitate an increasingly important function in neuronal development. Indeed, the domains that were conserved, including vWFD, C8, TIL, and LDLrA, are adhesive-like by themselves and can participate in protein-protein interactions; for example, both C8 and TIL domains can form interdimer disulphide bridges with vWFD (Y. F. Zhou et al., 2012).

Unlike the other annotated limpet adhesive proteins, *P-vulgata_3* is unique in having five highly conserved LDLrA repeats that can bind to multiple targets other than lipoproteins, including glycoproteins like TSP-1 and reelin (Vera et al., 2015). Lipids are believed to be an important component of barnacle larvae and mussel permanent adhesives (Gohad et al., 2014; He et al., 2018). In barnacle larvae, lipidaceous granules (likely in the form of lipoproteins or lipopolysaccharides) are secreted as a primer to potentially displace water from the contact surface and to provide a protective and stabilising environment for the subsequent proteinaceous secretion (Gohad et al., 2014). Similarly, limpet pedal mucus likely contains lipidic moieties (Kang, *in prep*), which suggests an intriguing parallel between permanent and tidal transitory adhesives that has yet to be verified in temporary adhesive systems (but see (Flammang, Michel, Cauwenberge, Alexandre, & Jangoux, 1998; Wunderer et al., 2019)). However, more work is needed to understand the role of *P-vulgata_3*, including its relative abundance within the different types of adhesive mucus. Although its transcript expression level was low (Table 4.2), it is difficult to draw conclusions about protein abundance based solely on the transcript expression levels, especially when the FPKM is derived from a single transcriptome. Follow-up studies using techniques like exponentially modified protein abundance index (emPAI) can provide quantitative information on the abundance of *P-vulgata_3* and other adhesive proteins.

4.5.3 Comparing adhesive proteins from marine invertebrates

Limpets exhibit tidal transitory adhesion, where they transition from high-strength, semi-sessile attachment to locomotory attachment. While it is currently not feasible to tease

apart all the nuances of what makes a protein suitable for temporary, transitory, or permanent adhesion, our results offer some useful initial insights: (1) both transitory and temporary adhesive proteins in general appear to be large multidomain sequences, often with duplicated domains thought to facilitate protein-ligand interactions; (2) both transitory and temporary bio-adhesives contain numerous glycosylated proteins; (3) both transitory and temporary adhesives likely do not contain 3,4-dihydroxyphenyl-*L*-alanine (Dopa) (Kang, unpublished), and this modified amino acid is more often associated with permanent adhesives from mussels, sandcastle worms, and adult ascidians (S. Li, Huang, Chen, Li, & Zhan, 2019; Stewart et al., 2011).

While none of the annotated limpet adhesive proteins share homology with known permanent adhesive proteins, *P-vulgata_5* aligned well (QC 91%, ID 27.70%) with a glycoprotein secreted by barnacle larvae for temporary adhesion, called the barnacle settlement-inducing protein complex (SIPC; NCBI Accession BAM28692.1). SIPC can adsorb to surfaces and is part of larval footprints (Dreanno et al., 2006; Petrone, 2013). This further supports the proposed adhesive function of *P-vulgata_5* and is another example of the similarity between limpet adhesives proteins and temporary adhesives. Indeed, proteins *P-vulgata_2*, *4*, and *6* shares homology with known temporary adhesive proteins from flatworms (QEP99777.1 (Pjeta et al., 2019) and QAX24810.1 (Wunderer et al., 2019)) and sea stars (AHN92641.1; (Hennebert et al., 2014)). All these proteins also share similarities with the aforementioned group of proteins (fibrillin, zonadhesin, alpha-tectorin, IgGFc-binding protein). Moreover, a study examining the role of sulphated biopolymers in marine bio-adhesives also highlighted the similarities between transitory and temporary adhesive secretions, where such moieties may serve a cohesive function in the adhesive material of limpets and sea stars but not in tubeworms or sea cucumbers (Hennebert et al., 2018). Moreover, a review of adhesive secretions from marine invertebrates demonstrated that, based on comparisons between the amino acid compositions of whole adhesives, there are similarities between secretions from all species using non-permanent adhesion (i.e., temporary and transitory) (Flammang, 2006).

Another animal that uses a similar type of transitory adhesion is the sea anemone (Actiniaria). Sea anemones commonly occupy a similar ecological niche as limpets, and they can alternate between stationary and locomotive states (Ottaway, 1979). One species, *Epiactis prolifera*, is capable of an average daily movement of 0.18 pedal disc diameter

(Cowles, 1977). While the exact mechanism of pedal movement remains unclear, it seems likely that a combination of retrograde pedal waves and punctuated step-like movements is involved (Cowles, 1977). A recent transcriptomic study of the glass anemone *Exaiptasia pallida* has identified numerous upregulated genes in the pedal disc that may be important in bio-adhesion (Davey et al., 2019). Enriched domains include protease inhibitors and metallopeptidases, analogous to the limpet adhesive proteins that may serve a role in defence or to transition the mucus from adhesive to locomotive, and protein-ligand binding domains, similar to both the limpet and temporary adhesives. Interestingly, the most abundantly expressed sequence in the pedal disc, Aipgene2358, shared homology with *P-vulgata_10*, mainly from the tandem repeats of scavenger receptor cysteine-rich (SRCR) domains. Further studies are needed to ascertain the functional role of SRCR repeats in adhesive secretions, since SRCR participates in a wide range of activities, including ligand binding to lipoproteins and selected polyanions (Bowdish & Gordon, 2009; Yap, Whelan, Bowdish, & Golding, 2015), immune responses in marine invertebrates (Gerdol & Venier, 2015), and are also present in spider silk glands (Chaw, Correa-Garhwal, Clarke, Ayoub, & Hayashi, 2015). It should be noted, however, that although both limpets and sea anemones may participate in a similar type of adhesion and share related protein domains, there are no striking analogies that clearly differentiate transitory adhesive proteins from temporary adhesive ones.

4.6 Conclusion

The common limpet, *Patella vulgata*, has intrigued researchers for over a century with their impressive attachment strength. While previous studies have proposed both suction and glue-like attachment as mechanisms underlying limpet adhesion, we found only slight pressure differences generated beneath the pedal sole of *P. vulgata* during both undisturbed locomotion and simulated predatory attacks. Based on the pressure recordings and behavioural observations, we conclude that limpet pedal mucus is a bio-adhesive that provides a strong bond to the attachment surface. Our detailed analysis of the limpet pedal mucus has revealed novel insights into the molecular components of limpet bio-adhesive: (1) lectin staining assays confirmed the presence of several glycans specific to pedal sole glands and highlighted secretory granules; (2) transcriptome-guided proteomics identified 171 adhesive protein candidates present in three types of limpet pedal mucus; (3) *in situ* hybridisation localised the expression of a selection of these

proteins, four of which were present only at the pedal sole. Our annotation of pedal mucus protein sequences identified numerous domains often found in known temporary adhesives, along with multiple predicted sites for glycosylation. Furthermore, these proteins are capable of protein-ligand interactions and are likely to oligomerise and cross-link to form a strong bio-adhesive. We also identified two protein architectures that have not been previously described in marine adhesive secretions: first is an SCO-spondin-like protein *P-vulgata_3*, which can potentially form fibres and raises interesting questions about the re-purposing of a highly conserved protein during evolution; second is a potentially potent defensive protein *P-vulgata_14*, with multiple domains for recognition and degradation of proteins and glycans. Although we have yet to identify key molecular differences between temporary and tidal transitory adhesives, our study is the first in-depth molecular characterisation of a model organism for tidal transitory adhesion and provides a foundation for future work characterising its components in more detail.

5 HOW A STICKY FLUID FACILITATES PREY RETENTION IN A CARNIVOROUS PITCHER PLANT (*NEPENTHES RAFFLESIANA*)

5.1 Summary

Pitcher plants (*Nepenthes* genus) live in nutrient-poor soils and produce characteristic traps to capture and extract additional nutrients from animal prey. Previous research has found that the digestive fluid secreted by *N. rafflesiana* is a sticky viscoelastic fluid that is much more effective at retaining insects than water, even after significant dilution. Although the physical properties of the fluid are important for its retentive function, how the fluid interacts with the insect's cuticular surface and the detailed impact of its sticky nature on struggling insects are unclear. In this study, we have investigated the mechanisms responsible for the higher prey retention rate of *N. rafflesiana* pitcher fluid. By measuring the peak attractive force exerted on insect body-parts moving in and out of test fluids, we show that significantly more work is required to withdraw from pitcher fluid than water. Moreover, both the maximum force and energy required for pull-out increased as a result of repeated contact with the pitcher fluid. We found that it is easier for insects to enter pitcher fluid than water and, accordingly, the surface tension of *N. rafflesiana* pitcher fluid (60.2 mN/m) was significantly lower than that of water (72.3 mN/m). By analysing the pitcher fluid wetting behaviour, we demonstrate that it strongly resists dewetting from all tested surfaces, leaving behind residual films that facilitate subsequent re-wetting. This inhibition of dewetting may represent one of the most important consequences of the viscoelastic nature of the pitcher fluid and enhance its biological role in prey retention.

5.2 Introduction

Pitcher plants are striking examples of plants that have turned carnivorous to survive in nutrient-poor soils. Through their characteristic pitfall traps made from highly modified leaves – a design that has evolved independently at least six times across the kingdom – these plants lure, retain, and finally digest prey (Givnish, 2015; Thorogood et al., 2018). The prey, which include mostly ants but also flying insects, are normally capable of

climbing up vertical surfaces or flying away from danger, yet they struggle to escape from pitfall traps due to a combination of remarkable structural adaptations. Examples of pitcher traits and their proposed functions from various pitcher plant species include: (1) a highly wettable peristome that causes insects to slip on a stable water-film and fall into the pitcher (Bauer, Scharmann, Skepper, & Federle, 2012; Bohn & Federle, 2004); (2) wax crystals covering the inner pitcher wall surfaces in some species that produce fine-scale roughness and break off easily to contaminate insect tarsi, both of which negatively impact insect adhesion (Gaume et al., 2004; E. V. Gorb et al., 2005); (3) dense fields of large downward-pointing hairs that physically impede the escape of insects and also facilitate aquaplaning (Bauer et al., 2012; Jaffe, Michelangeli, Gonzalez, Miras, & Christine Ruiz, 1992); (4) directional microstructures that make it easier for insects to slip into the pitcher and hence prevent escape (E. V. Gorb & Gorb, 2011).

Although the structural adaptations of pitfall traps facilitate the capture and retention of nonflying prey that need to scale the inner wall to escape, they are less suitable for retaining flying insects. Indeed, video recordings of flies falling into containers of water show that they are able to recover and fly away without contacting the sides, which suggests that a watery fluid may not be effective in catching flying insects (Gaume & Forterre, 2007). Pitcher plants, however, catch a wide range of flying and nonflying insects, indicating that another mechanism exists to further enhance their capture rate (Adam, 1997; Cresswell, 1991; Moran, 1996). Since insects that fall into the traps land on the digestive fluid, it is possible that the fluid itself can help to maintain the prey. Such a mechanism would further benefit the plant by prohibiting the escape of nonflying insects as well, which can sometimes overcome the aforementioned structural adaptations and climb out (Bohn & Federle, 2004). Indeed, several studies have shown that insect retention rates in digestive fluids are drastically higher than in plain water: in several species of *Nepenthes* (Nepenthaceae) pitcher plants, including *N. rafflesiana*, *N. hemsleyana,* and *N. gracilis*, significantly more flies and ants were retained in isolated digestive fluid than in water (Bauer et al., 2011; Bazile et al., 2015; Gaume & Forterre, 2007). Fluid from young *N. rafflesiana* plants were the most effective, retaining 100% of the tested flies and around 90 to 100% of the ants, while less than 20% of the flies and none of the ants were retained in water (Bazile et al., 2015). Similar findings were reported with several pitcher plant members of the Sarraceniaceae family, which independently evolved pitfall traps to catch prey. Experiments using digestive fluid from

Sarracenia flava, *S. sledgei* (syn. *S. alata*), *S. drummondii* (syn. *S. leucophylla*), and *Darlingtonia carlifornica,* demonstrated that ants sank more rapidly in digestive fluid than in water (Armitage, 2016; Jaffe et al., 1992; F. M. Jones & Hepburn, 1927). It is important to note that insects rescued from pitcher fluid after retention trials managed to regain mobility and survived, indicating that the high retention rates are unlikely caused by noxious compounds released into the fluid. These findings support the idea of the dual functionality of the 'digestive' fluid, where it serves to both retain and digest insect prey. Thus, to recognise the retentive function of digestive fluid, we henceforth refer to the fluid as pitcher fluid (PF).

Despite the evidence for the retentive role of PF, we have yet to fully understand its underlying mechanisms. Researchers have so far focused on two PF properties to explain how it may function: viscoelasticity and surface tension. Many *Nepenthes* species produce PFs that form long sticky filaments when rapidly extended, which is characteristic of non-Newtonian viscoelastic fluids containing high molecular weight polymers (Bonhomme et al., 2011; Erni, Varagnat, Clasen, Crest, & McKinley, 2011; Gaume & Forterre, 2007). Gaume & Forterre investigated the viscoelastic properties of *N. rafflesiana* PF and suggested that its high apparent extensional viscosity and long relaxation times make it more difficult for a struggling insect to swim in and extract itself from the fluid (Gaume & Forterre, 2007). Although these findings offer insights into the rheological properties of the fluid, they do not help us understand how the fluid interacts with the insect, and why insects ultimately fail to escape. Furthermore, it is not clear how rheological parameters such as extensional viscosity and relaxation time influence the biological system: what forces do insects have to produce, and how much energy does it cost them to extract themselves from pitcher fluid compared to water?

Another property of pitcher fluid that has been explored in previous work is the fluid's surface tension (ST). A number of studies have reported that insects sink more readily in PF than in water (Armitage, 2016; Bazile et al., 2015; Di Giusto, Grosbois, Fargeas, Marshall, & Gaume, 2008; Jaffe et al., 1992; F. M. Jones & Hepburn, 1927; Lloyd, 1942). In Sarraceniaceae, ants sank rapidly in *Heliamphora sp.* fluid yet floated on rainwater (Jaffe et al., 1992), and in *D. californica*, 100% of the tested ants were retained while none broke the surface of pure water (Armitage, 2016). Additionally, an oiled needle repeatedly floated on water despite vigorous perturbation, while it readily sank in *S. flava*

PF (F. M. Jones & Hepburn, 1927). Quantitative ST measurements support these observations: fluids from open pitchers of *S. flava* and *D. californica* both produced ST values lower than water (66 mN/m and 47.9 mN/m, respectively) (Armitage, 2016; F. M. Jones & Hepburn, 1927). These findings confirm that ST is reduced in Sarraceniaceae PF, producing an air-fluid interface that is easier to penetrate than water. This fluid property can help explain the 'sinking ants' phenomenon: an insect falling into PF will mostly land on the fluid surface, but is then increasingly wetted through its struggles to escape, and become submerged (Armitage, 2016; Bauer et al., 2011). Armitage demonstrated that the bacterial community from *D. californica* PF plays a role in reducing the surface tension, although it is unclear if the plants secrete additional surface-active compounds (Armitage, 2016). Nevertheless, these studies clearly illustrate the importance of reduced ST for effective prey capture and retention in Sarraceniaceae PF.

Meanwhile, our understanding of the role of ST in *Nepenthes* remains controversial. On one hand, there are several reports of ants readily sinking in *Nepenthes* PF: in *N. hemsleyana*, up to 80% of tested ants were completely submerged, compared to 10% in water (Bauer et al., 2011). Similar observations have been reported elsewhere (Lloyd, 1942). On the other hand, surface tension measurements to date show that fluids from two *Nepenthes* species have similar ST to water (72 mN/m for *N. rafflesiana* (Bauer et al., 2011; Gaume & Forterre, 2007), 73 mN/m for *N. hemsleyana* (Bauer et al., 2011); 72 mN/m for water (Bauer et al., 2011; Gaume & Forterre, 2007)). Hence, based on these contradictory findings, it is difficult to conclude if ST is responsible for sinking prey and whether it influences insect retention in *Nepenthes* PF.

Here, we investigate the effect of sticky PF on insect prey retention, with a focus on adhesion of the fluid to insect cuticle. Using *N. rafflesiana* PF as our study system, we first quantify the forces exerted on an ant gaster as it is wetted and then retracted from the sticky fluid, thereby simulating an insect's attempt to escape. Next, we re-assess the role of surface tension in prey retention through two distinct approaches. Lastly, we study the wetting and dewetting behaviour of PF on different surfaces and highlight a novel function of the viscoelastic nature of the fluid and a new mechanism of prey retention. Based on our study, we illustrate the diversity of interactions between the fluid and the insect cuticle that becomes evident under dynamic testing conditions.

5.3 Materials and methods

5.3.1 Pitcher plant fluid samples

PF was collected from unopened pitchers that were close to opening from *Nepenthes rafflesiana* plants from Brunei, northern Borneo (4°34' N, 114°25' E; collection site with degraded kerangas forest on white sandy soil) and from greenhouse cultivars at the University of Bristol (courtesy of Dr. Ulrike Bauer, University of Bristol; plants sourced from Brunei, Malesiana Tropicals nursery, and Kew Gardens). Each pitcher was either cut open with a clean razor blade and its contents poured into a sterile plastic collection vial (field collections), or its lid was opened, and the fluid removed using a clean pipette (greenhouse collections). The fluids were kept frozen at -20°C until use. Prior to experiments, individual vials were thawed to room temperature, and a small aliquot was stored in a 4°C refrigerator while the stock was re-frozen. PF was stored at 4°C for the duration of the experiments with no growth of contaminants or visible changes to the fluid consistency.

5.3.2 Observations of insect prey in pitcher plant fluid

Ants from a colony of laboratory-maintained *Atta cephalotes* were used to observe the behaviour of live insect prey in *N. rafflesiana* PF. Note that *A. cephalotes* ants were used as a model prey system for all experiments in the study. Prey behaviour was assessed using methods similar to previous studies (Bauer et al., 2011; Bazile et al., 2015; Gaume & Forterre, 2007) with slight modifications: each ant was placed inside a slippery plastic container (coated with fluon) and positioned 5 cm above the fluid surface (an aquarium was constructed from microscope slides with dimensions 7.6×2.5×2.5 cm). The container was then slowly tipped so that the ant slid down the wall and into the fluid without manipulation or coerced acceleration. This method aimed to mimic ants naturally slipping on the peristome surface and free-falling into the pitcher. After each drop, the ant's behaviour was observed for 5 minutes and categorised using a similar metric to (Bazile et al., 2015): 'escaped,' if it removed all 6 legs out of the fluid; 'prostrate,' if it stopped moving within 5 minutes but did not sink, see next definition; 'sank,' if all of its body was completely submerged below the fluid surface; 'swimming,' if it remained active for 5 minutes with its legs making swimming motions but without all of its body submerged below the surface; 'floating/walking,' if its legs did not break the fluid meniscus and tried

to walk on the surface. Worker ants were tested in sticky pitcher fluid and in pure reverse osmosis water (RO water; n = 10 ants tested for each fluid).

5.3.3 Force measurements on ant gasters

A. cephalotes ants were used to measure the range of forces experienced by insects when interacting with pitcher fluid. Instead of using whole ants, which would introduce many uncontrollable variables regarding surface topography, orientation, and shape, we opted to use the gasters of similarly sized worker ants as a model cuticle surface (average weight ± SD: 7.6 ± 1.3 mg). We did not use the tarsus as preliminary trials had shown that it was too flexible and bent unpredictably. The gasters were prepared using the following approach: worker ants were collected from a large laboratory colony, euthanised by freezing, and weighed. From each ant, the gaster was cut at the petiole, and the tip of a micro-dissection insect pin (diameter 0.10 mm) inserted through the cut end. A small droplet of high viscosity super-glue (Loctite 454, Henkel AG & Co. KGaA, Düsseldorf, Germany) was applied at the junction to immobilise the gaster and left to cure for at least 1 hour. Special care was taken to avoid applying excess amount of super-glue to prevent accidental contamination of the cuticle surface. Each mounted gaster was inspected for contamination or damage prior to use.

A custom fibre-optic force transducer was set up as previously described with minor modifications (Supplementary Figure 1) (Labonte & Federle, 2015). A piece of reflective metal foil was glued onto a thin metal beam, which was then mounted on the Z-motor stage of a 3D motor system (M-126PD, Physik Instrumente, Karlsruhe, Germany). The tip of a fibre optic sensor (DMS-D12, Philtec, Inc., MD, USA) was gently lowered towards the reflective foil until the output was in the linear regime of the signal-to-distance curve. On the underside at the end of the metal beam, an insect pin bent into an L-shape was super-glued to the metal beam to provide a convenient attachment point for specimens mounted on insect pins. This force transducer was calibrated with objects pre-weighed using a high precision microgram balance (MC5 Microbalance, Sartorius GmbH, Goettingen, Germany) to obtain a signal-to-force relationship. A signal-to-displacement calibration was obtained by moving the metal beam in specific increments using the Z-motor stage. All movements of the 3D motor system and constant force feedback protocols were controlled using a custom LabVIEW programme (National Instruments, TX, USA). Triggers encoded by the LabVIEW programme were used to

capture synchronised video of the movements at 20 fps with a CMOS USB camera (DMK 23UP1300, The Imaging Source Europe GmbH, Bremen, Germany).

A fluid chamber was designed to hold small volumes of test fluids while providing a clear window for video recording (Supplementary Figure 1). A 3D model of an aquarium with two contiguous chambers (each 13.7×9.1×8 mm in width × depth × height) was designed in Fusion 360 (Autodesk, Inc., CA, USA) and printed using a resin 3D printer (Zortrax Inkspire, Zortrax S.A., Olsztyn, Poland). The two contiguous chambers facilitated testing the same gaster specimen on two different fluid samples without additional mounting steps. The 3D print was post-cured under UV light for 15 to 20 minutes, washed in high-grade pure ethanol (VWR International, Lutterworth, UK) overnight, and rinsed afterwards with RO water. Silicone-based dental impression wax (Elite HD+, Zhermack SpA, Italy) was used to attach clean coverslips to the chambers to allow filming through the fluid during the trials. Prior to each trial, the chamber was rinsed once with ethanol and once with RO water. Around 600 µL of RO water or pitcher fluid were transferred into each of the chambers using a micropipette. To attach the insect sample to the fibre-optic force transducer, the prepared insect pin (with ant gaster attached) was first bent with forceps to orient the gaster so that its dorsal side would first contact the fluid. This reduced the likelihood of the stinger and abdominal glands interfering with the measurements (e.g., sharp edge can easily pierce the meniscus, and dried glandular secretions can be hydrophilic). The insect pin was then attached to the L-shaped pin on the force transducer using a small amount of dental impression wax. Immediately prior to a trial, the gaster was manually lowered to be just above the liquid-air interface using a micromanipulator on the Z-motor stage. In order to reduce evaporation and contamination, the top of the second chamber was covered with a glass coverslip until further use.

Once the gaster was mounted and the fluids were pipetted into the wells, the motor movement programme executed the following protocol: 1. Lower into the fluid to reach a (feedback-controlled) preload of 50 µN; 2. Stay in preload for 4 s; 3. Move up (away from the fluid) by 10.5 mm at 3 mm/s; 4. Wait for 60 s with additional drying from a small fan; 5. Return to starting position (above fluid); 6. Repeat steps 1-3 twice to produce dips 1, 2, and 3. This movement protocol was designed to simulate repeated escape attempts by a fallen insect. All the trials were video recorded as described above. The

trials were paired so that each gaster was first tested in water (total of three dips), dried for at least 3 min, then tested again in pitcher fluid. We conducted control experiments with water in both wells to ensure that using the same gaster in a paired test did not affect its properties: there was no significant difference in peak force between the first and second water tests (paired *t*-tests for dips 1, 2, 3: $t_5 = -0.499$, $t_5 = -0.752$, $t_5 = -0.728$, all $p>0.05$; n = 6 gasters).

From each gaster trial, we calculated the work of retraction by calculating the area under the force-time curve from two time-points: the first time-point was defined as when the first positive force was recorded. The second time-point depended on the test liquid: for water, this was defined as when the gaster-liquid bridge abruptly collapsed (based on the synchronised video recordings). For PF, if the force-trace returned to zero before the next motor movement, the time-point immediately preceding this was used; if the force-trace remained above zero, then the time at which the next motor movement began was used as the end-point. The peak attractive force was defined as the maximum force recorded during the upward Z-motor movement. A total of six samples of sticky *N. rafflesiana* pitcher fluid was selected to measure the peak attractive force and work of retraction needed to dip ant gasters in and out of the fluid.

5.3.4 Statistical analyses

Restricted maximum-likelihood linear mixed-effects modelling was used to analyse the relationship between the dependent variables (work of retraction and peak attraction force; the former was natural log-transformed) and the independent variables (test liquid, with water and PF as levels, and dips). Test liquid, dips, and the interaction between the two were used as fixed effect terms. Individual ant gasters and pitcher fluid samples were used as random intercepts to account for the nested design and repeated sampling (each ant gaster tested first in water then in PF; six gasters tested per PF sample). Data from each dip were separated and analysed with the same parameters. *t*-tests were conducted via Satterthwaite's degree of freedom method per *lmerTest* package (Kuznetsova, Brockhoff, & Christensen, 2017). All tests were conducted in R v3.6.2 (run in RStudio v 1.2.5033) using R packages *lme4* v1.1-21 and *lmerTest* v3.1-1 (Bates, Mächler, Bolker, & Walker, 2015; Kuznetsova et al., 2017; R Core Team, 2019; RStudio Team, 2019).

5.3.5 Force measurements using antennae as model insect cuticle

Ant antennae are densely covered in hairs and preliminary tests confirmed that they strongly resisted wetting, and when submerged in water, a layer of air remained trapped between the hairs. As such, antennae of *A. cephalotes* ants were used to investigate if PF managed to wet highly hydrophobic surfaces. Soldier ants were selected for their large antennae. The ants were sacrificed and weighed, then each antenna was cut at the end of the first segment (scape). The cut end of the antenna was attached to an insect pin with a small droplet of high viscosity super-glue (careful inspection showed that the glue did not spread on the antenna). Both antennae from each individual ant were mounted using the same technique to produce comparable samples. Extreme care was taken to avoid touching the last few segments of the antenna, and each sample was visually inspected for contamination or damage prior to use. Since freshly prepared antennae were highly flexible and produced inconsistent results during pilot trials, all samples were stiffened by drying them in a desiccator for 2 to 3 hours prior to use.

For each trial, one insect pin-mounted antenna was attached to the fibre-optic force transducer with dental impression wax, then positioned while the wax was still wet so that the last segment pointed downwards to be the first to contact the fluid surface. One of the two antennae from an individual ant (referred to as sample A) was used to determine the loading force at which the antenna tip ruptured the RO water meniscus. The following Z-motor movement protocol was used to simulate an insect body-part falling onto the fluid interface and staying in contact for a period of time: 1. Slowly lower sample into the water until desired preload force; 2. Maintain at preload using force-feedback for 60 s; 3. Return to the starting position. If the water meniscus did not break, then the loading force was increased by one 5 μN increment and the trial repeated (tested force range was 30 to 50 μN). The maximum preload was defined as the force which was one increment smaller than the force needed to rupture the meniscus. Control experiments showed an antenna could be tested 4-5 times at its maximum preload on water without a change in response (n = 3 antennae), confirming that antennae were not wetted despite multiple dips in water. Nevertheless, to demonstrate that the antenna had not been wetted by water during the trials, every sample was tested twice at the same maximum loading force. If the antenna did not break the meniscus in both repetitions after 60 s, the trial was recorded as ‘meniscus held.’

Once the maximum loading force was determined, the antenna sample was replaced with the second antenna from the same individual (sample B), then the trial was repeated in PF. We hypothesised that, due to random variation between the first and second antenna for the maximum sustainable preload force, we conservatively expect 50% of the tested antennae to break through and sink into the fluid. In cases where the antenna broke the meniscus before the full duration of the trial (60 s), the sample was recorded as 'meniscus broke.' Six pairs of antennae were tested in each pair of RO water and PF (n = 3 different PFs).

5.3.6 Measuring the surface tension of pitcher fluid

Pendant drop tensiometry can be a highly accurate method of measuring surface tension with small volumes of test fluid if some precautions are taken to reduce experimental error (Berry, Neeson, Dagastine, Chan, & Tabor, 2015). The technique is based on analysing the static shape of a drop that results from a balance of its weight and surface tension force. This balance is represented by a dimensionless parameter called the Bond number:

$$Bo = \rho g R_0^2 / \gamma$$

where R_0 is the radius of curvature at the apex of the droplet. Berry *et al.* introduced a second dimensionless parameter, called the Worthington number:

$$Wo = \frac{V_d}{V_{max}}$$

where V_d is droplet volume and V_{max} is the theoretical maximum volume that can be formed by the needle (Berry et al., 2015). When Wo is greater than 0.6 the experimental error is below 1%; hence it serves as a useful criterion for minimising error. For our experiments, we used a similar approach to Berry *et al.* with slight modifications: ~50 µL of PF was withdrawn into a 1.0 mL syringe fitted with a blunt-ended needle (0.8 mm inner diameter). The syringe was then mounted on a high-precision syringe pump (AL-1000, World Precision Instruments, Florida, USA) to dispense the fluid at a constant flowrate of 7 µL/min. Droplets were grown to their maximum possible sizes and their formation was filmed using a CMOS USB camera at 3 fps (Basler acA1300-200um, Basler AG, Ahrensburg, Germany). A total of 10 sticky PF samples from *N. rafflesiana* were tested. In addition, fluid samples from another *Nepenthes* species (*N. inermis*) were included in the measurements as they were also sticky, and a healthy cultivar was accessible at the Cambridge University Botanical Gardens (n = 2 freshly opened pitchers).

Between 5 to 7 drops with Wo greater than 0.6 were selected for each sample and analysed using OpenDrop (http://opencolloids.com). All experiments were conducted at 25°C in ambient humidity. The analysed dataset is provided in Supplementary Table 1.

We checked if the surface tension of distilled water measured by our pendant drop method was in good agreement with the reference value of 71.99 mN/m at 25°C (Vargaftik, Volkov, & Voljak, 1983). To confirm if surface tension values of non-Newtonian fluids were in line with values from literature obtained with the Du Noüy ring method (B. B. Lee, Chan, Ravindra, & Khan, 2012; Nedjhioui, Moulai-Mostefa, Canselier, & Bensmaili, 2009), we measured the ST of dilute solutions of commercial xanthan gum (Sigma-Aldrich; molecular weight: ~$2x10^6$ Da; concentrations: 0.1, 0.2, 0.5% w/v in distilled water).

5.3.7 Visualising pitcher fluid dewetting behaviour on various substrates

A number of gasters and antennae tested with water and PF were subsequently imaged with scanning electron microscopy (SEM; n = 22 antennae, n = 20 gasters). Gasters prepared in the same way but not tested in any of the fluids served as controls. Specimens, kept in a desiccator after being used for the force measurements, were removed from the insect pins and mounted on aluminium SEM stubs using carbon tape. The samples were coated in 15 nm of iridium and imaged with a field emission SEM (Verios 460, Thermo Fisher Scientific, MA, USA).

To investigate how PF interacts with different surfaces, we recorded the dewetting of PF from three surfaces in comparison to water: clean glass coverslip (hydrophilic), clean smooth low-density polyethylene (PE, hydrophobic), and *A. cephalotes* gaster cuticle (freshly prepared as described above). We used interference reflection microscopy (IRM; as reported previously in (Federle et al., 2006; Yue Wang et al., 2019; Chapter 2&3) to visualise the formation and evolution of films throughout the dewetting process. More specifically, a small volume of test fluid (~5 µL) was first deposited on the glass surface using a micropipette. A clean pulled microcapillary tube connected to a microinjector (CellTram Air, Eppendorf, Hamburg, Germany) was brought into contact with the droplet, and the microinjector was used to slowly withdraw the fluid. Videos of the dewetting process were recorded at 25 fps with a CMOS USB camera (DMK 23UP1300),

and monochromatic green light was used for illumination (wavelength = 546 nm). Each fluid (n = 2 different PF samples, and RO water) was tested three times per substrate (glass, PE, and insect cuticle).

5.4 Results

5.4.1 Ant retention rates and behaviour in pitcher fluid compared with water

Our retention trials, where ants were dropped into *N. rafflesiana* PF and compared to water, revealed a striking difference in outcome (Figure 5.1a & b; Supplementary Video 1). While none of the ants dropped in water sank and 30% floated/walked on the water surface without breaking the meniscus, all the ants dropped in PF were wetted upon landing and none managed to float/walk on the PF meniscus (Figure 5.1c). Moreover, 20% of the ants sank into PF within 5 minutes. Ultimately, none of the ants managed to escape from PF, as opposed to 30% in water. Similar observations and results have been previously reported for *N. rafflesiana* and *N. hemsleyana* using different species of ants (Bauer et al., 2011).

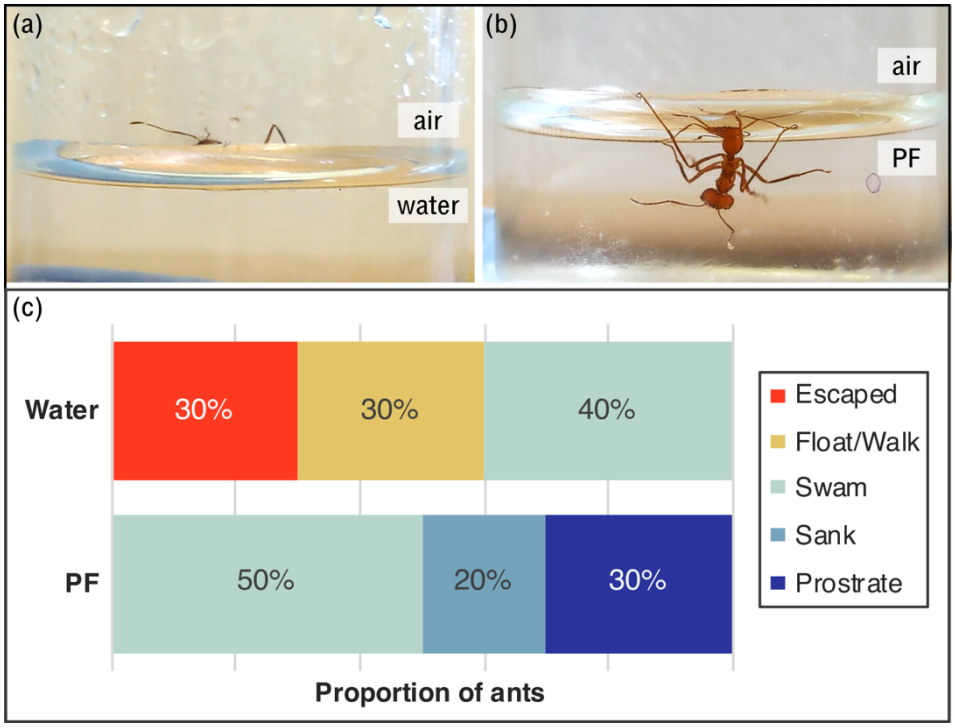

Figure 5.1. Ant retention tests in water and *Nepenthes rafflesiana* pitcher fluid (PF). (a) During retention tests in water, ants (*Atta cephalotes*) sometimes floated and failed to break the water meniscus. (b) When dropped into *N. rafflesiana* PF, ants readily broke through the pitcher fluid meniscus. Here, the test subject was submerged and failed to right itself. (c) The behaviour of the test ants was recorded for 5 minutes. While 30% of the ants escaped from water, none escaped from pitcher fluid. Additionally, 20% of the ants sank into pitcher fluid, which was not observed with water; instead, 30% floated and walked on the water meniscus.

5.4.2 Force and energy required to retract ant cuticle from pitcher fluid in simulated escapes

Using ant gasters mounted on a force transducer, we simulated the movements of an insect attempting to escape from PF or water and measured the resulting forces (see Figure 5.2 for a representative force-time plot). As evidenced by the jump into contact when the gaster approached the water surface (Figure 5.2a, asterisk), all tested gasters were wetted from the first dip. Although insect cuticle is covered by a waxy layer, it is known that cuticle wettability depends on the species, specific body-part, and surface roughness (from hairs) (Beament, 1961; Holdgate, 1955; Pal, 1950). In our trials, *A. cephalotes* gasters reached the desired preload of 50 µN with a partial immersion (Figure 5.2a, time-point t = 18.2 s). Upon retraction, a water bridge between the water meniscus and the gaster formed then rapidly collapsed, resulting in a sharp attractive force peak (Figure 5. 2a & b; t = 21.1 s). A small water droplet remained on the gaster immediately after the meniscus collapse, but it often evaporated before the next dip. SEM images of samples

tested in water showed no signs of contamination or residues after the trials (more details below).

When gasters were preloaded and retracted from PF, however, the peak attractive force was marginally larger than in water (Figure 5.2a). Moreover, upon retraction from PF, we observed filament formation between the cuticle and the fluid surface (Figure 5.2c). The adhesive effect of the filament, which essentially pulled the gaster back into the fluid, was visible on the force-trace as a slower and prolonged decay of the peak force (Figure 5.2c; t = 21.8 s). We also observed PF droplets on the gaster that, unlike water droplets, did not fully evaporate dewet after the same period.

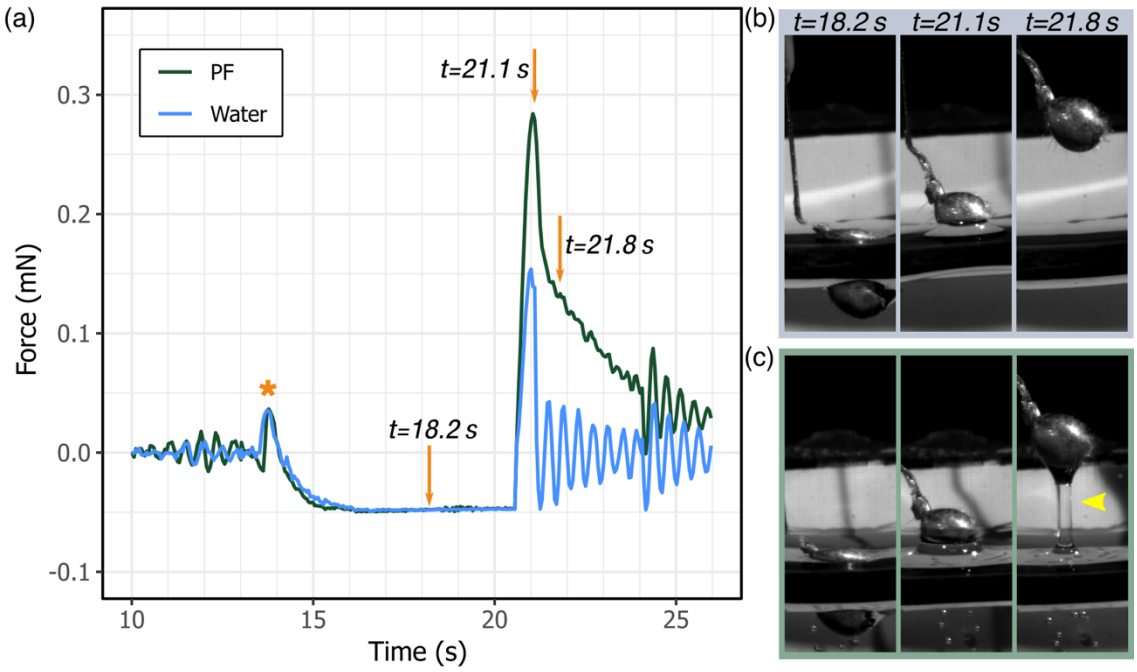

Figure 5.2. A representative force-time plot from force measurement trials of ant gasters dipped into water compared to *N. rafflesiana* PF. (a) The gaster was lowered into the test liquid with 50 µN preload force, maintained for 4 s, then retracted upwards. Note the small adhesive force that resulted from the gaster jumping into contact (marked *). (b) Images from time points as marked on the force plot. At t = 18.2 s, the abdomen in preload was visible. Upon withdrawal from water, a water bridge between the abdomen and the fluid rapidly collapsed, creating a sharp attractive force peak (t = 21.1 s). (c) In contrast, when the gaster was withdrawn from pitcher fluid, a fluid filament formed (yellow arrow), resulting in a higher peak attractive force and a slower and prolonged decay of the attractive force.

Comparisons between the peak attractive forces from all water and PF trials indicated a trend for a greater attractive force in the latter, but this was not statistically significant (Figure 5.3a; *t*-test based on the aforementioned linear mixed effects model, $t_{5.1} = 1.857$,

$p = 0.12$). In contrast, the work required during the simulated escape movement in PF was 2.9 times greater than in water (*t*-test, $t_{5.0} = 5.590$, $p < 0.01$), caused by the sustained adhesive force from the PF filament.

When we analysed the effect of dips on the peak attractive force, we found that within each dip, the peak attractive force for PF was marginally but significantly higher than water only by the third dip (Figure 5.3b; *t*-test, $t_{2.0} = 4.305$, $p < 0.05$). Across the dips overall, we found a significant interaction between the dips and the peak attractive force, where the effect of dips on peak attractive forces significantly depended on the test fluid (*t*-test, $t_{178} = 3.455$, $p < 0.001$). Subsequently, when water and PF were analysed separately, we confirmed that dips had no significant effect on the peak attractive force in water (*t*-test, $t_{74} = -0.55$, $p = 0.584$), while it had a clear impact on PF (*t*-test, $t_{74} = 5.243$, $p < 0.001$). Thus, peak attractive force did not change from multiple dips in water, whereas there was an increase in PF.

In contrast to the peak attractive force, the work of retraction needed to withdraw gasters from PF was consistently higher than in water within all three dips (Figure 5.3c; *t*-test, Dip1: $t_{2.59} = 7.071$, $p < 0.01$; Dip2: $t_{3.09} = 7.334$, $p < 0.01$; Dip3: $t_{3.55} = 6.904$, $p < 0.01$). The overall findings for the effect of dips on the work of retraction were similar to those stated above for the peak attractive force. Implications of these results are highlighted in the Discussion.

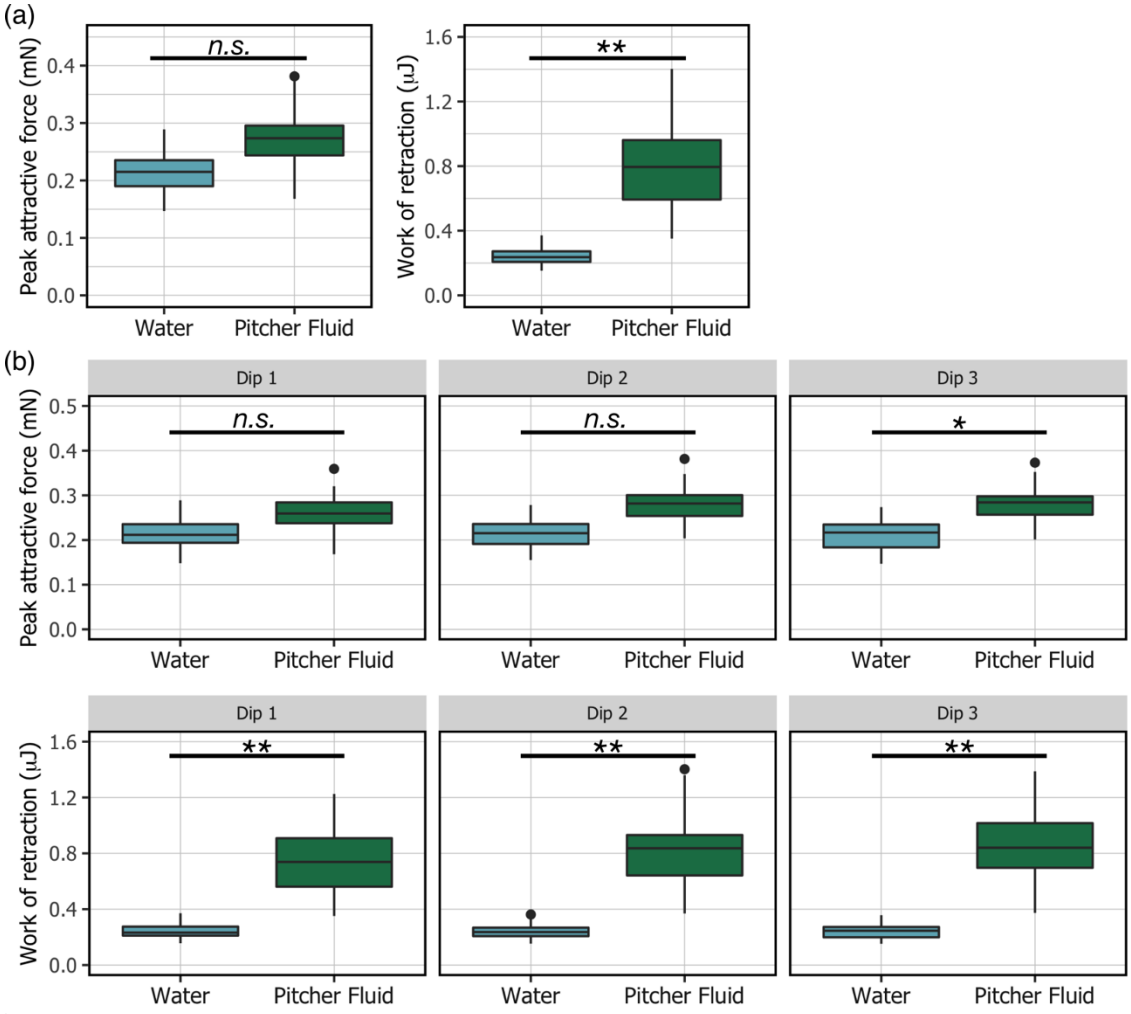

Figure 5.3. Effect of *N. rafflesiana* PF on the peak attractive force and work of retraction for an ant gaster. (a) Overall, the peak attractive force acting on the ant gaster during retraction was marginally higher in PF than in water but not significantly (n.s., $p = 0.12$). The work of retraction, however, was 2.9 times greater in PF than water (**$p < 0.01$). (b) When separated into the individual dips, PF exerted a significantly higher peak attractive force on ant gaster than water only by Dip 3 (*$p < 0.05$). (c) In contrast, PF consistently demanded higher work to retract within each dip compared to water (**$p < 0.01$). All statistical analyses were based on *t*-tests on linear mixed effects models (see text for details).

5.4.3 Loading the liquid-air interface to test if pitcher fluid meniscus breaks more readily than water

From our experiments using antennae to probe the liquid-air interface, we first identified the maximum preload force that the water meniscus could sustain (sample A, n = 16 antennae; Figure 5.4a). All of these samples failed to break the water-air interface to advance into the fluid during the entire 60 s preload (Figure 5.4b-d). Video recordings showed that while the very tip of the antenna broke through the meniscus, the water contact line was arrested at or before the widest point of the antenna and held for 60 seconds. For antennae (sample B) dipped in PF, however, the outcome was drastically different: 15 of the 16 antennae (93%) broke through the meniscus and continued to advance within 60 s (Figure 5.4b-PF & c-PF). Even using the most conservative assumption that 50% of the antennae break the meniscus by chance, this result is highly significant (binomial test; $p < 0.001$). Furthermore, of the 15 antennae that broke through the meniscus, four formed thin filaments upon withdrawal from the pitcher fluid (Figure 5.4e-PF).

To confirm that our findings were not affected by variation from switching sample A to B (e.g., mounting orientation), we tested the same antenna first in water then in PF without any manipulations (n = 12). None of the tested antennae broke through the water meniscus, even after two to five repeats; in contrast, 92% (11 antennae) broke through the PF meniscus. Again, even when the most conservative assumption was used (50% of the antennae break the meniscus by chance), this result is highly significant (binomial test; $p < 0.01$).

5.4.4 Surface tension of *Nepenthes* pitcher fluid and water

Surface tension measurements using pendant drop tensiometry fluid further substantiated our finding that surface tension is reduced in sticky *N. rafflesiana* PF (Figure 5.5). The surface tension value for water did not differ significantly from the reference value, which confirmed the validity of our method (72.3 ± 0.6 mN/m, mean ± SD; n = 10 droplets; one-sample *t*-test, $t_9 = 1.44$, $p = 0.18$). On the other hand, the surface tension of *N. rafflesiana* PF was significantly lower than that of water (60.2 ± 5.2 mN/m, mean of means ± SD of means; n = 10; one-sample *t*-test against reference value for water, $t_9 = -7.13$, $p < 0.001$). Preliminary tests from *N. inermis* PF produced a surface tension value of 34.6 ± 2.3 mN/m (n= 2). Commercial xanthan gum surface tension values were (mean ± SD): 66.8 ± 0.1

mN/m, 60.1 ± 0.5 mN/m, and 53.6 ± 0.7 mN/m, for concentrations 0.1, 0.2, and 0.5% w/v, respectively. These values generally agreed with literature values and followed the same trend, where an increase in xanthan gum concentration led to a decrease in surface tension (B. B. Lee et al., 2012; Nedjhioui et al., 2009).

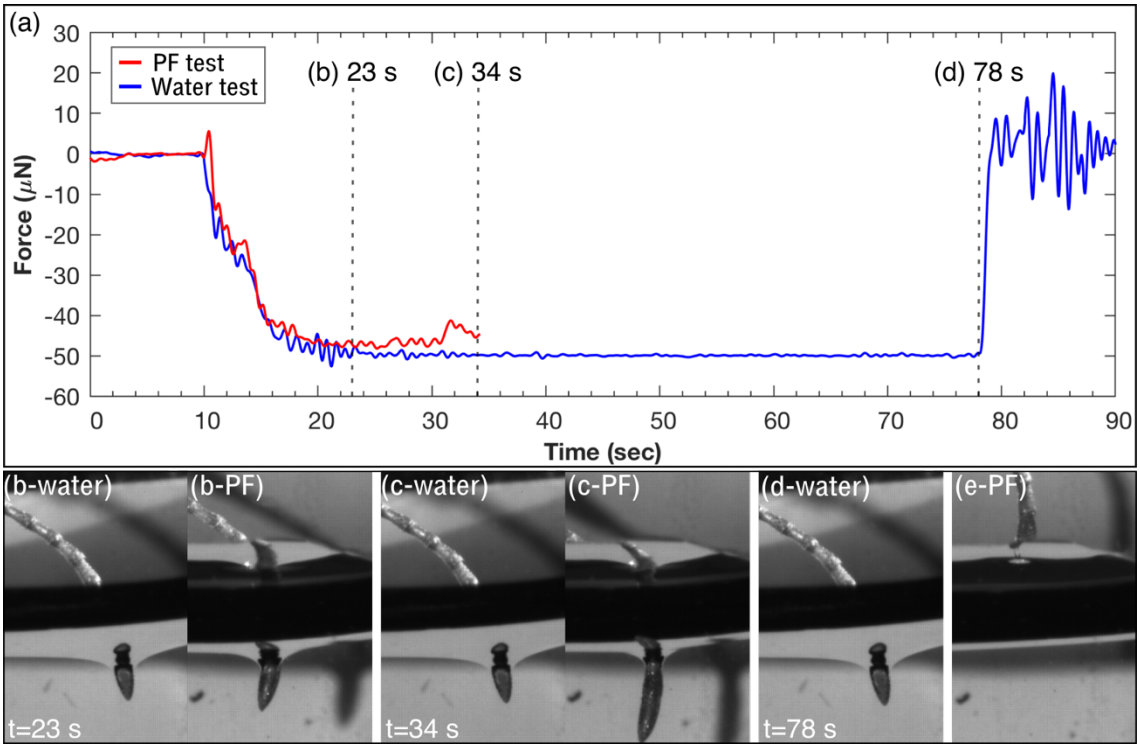

Figure 5.4. Using ant antennae to probe the surface tension of water versus pitcher fluid. (a) The ant antenna did not break through the water meniscus at the designated preload force (50 μN in this example) for the entire duration of the trial. The other antenna from the same ant tested in pitcher fluid failed to reach the designated preload as it readily broke through the meniscus and the movement was terminated. (b & c) Image sequences highlight the difference between the water and pitcher fluid trials. From 23 s to 34 s, the water-test antenna held steady at 50 μN preload, while the pitcher fluid antenna was pushed deeper into the fluid as it failed to reach the preload. (d) Over the full duration of the trial, the water meniscus remained steady. (e) Upon withdrawal of the antenna from the pitcher fluid, a thin fluid filament was observed.

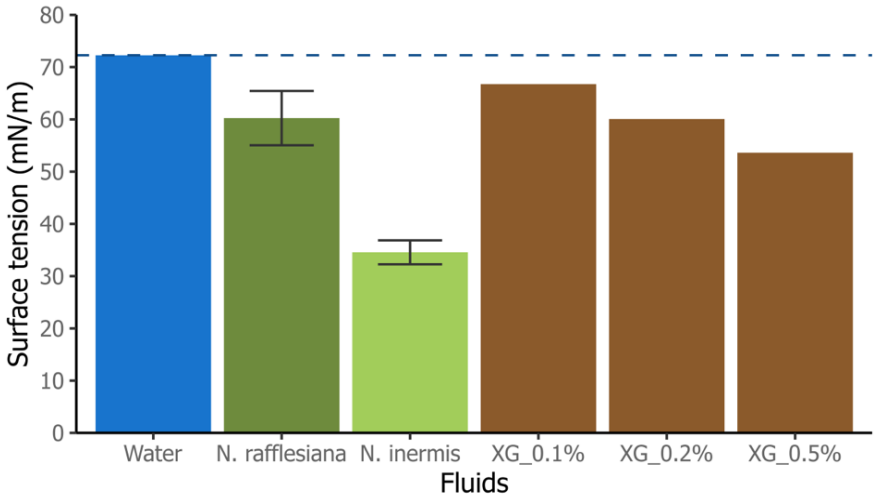

Figure 5.5. Surface tension values of *Nepenthes rafflesiana* and *N. inermis* PF compared to known fluids as measured by pendant drop tensiometry. Good agreement between measured surface tension of water and reference value at 25°C validated the method (72.3 ± 0.6 mN/m and 71.99 ± 0.36 mN/m, respectively). *N. rafflesiana* pitcher fluid surface tension values were significantly lower than reference value of water (*t*-test, t_9= -7.13, $p < 0.001$). *N. inermis* pitcher fluid produced the lowest surface tension value out of all tested fluids. Error bars shown only for *N. rafflesiana* and *N. inermis* (± standard deviation; see main text for water and xanthan gum values). Increasing concentrations of commercial xanthan gum (XG; w/v) led to a decrease in surface tension, a trend reported in other studies.

5.4.5 Conspicuous residues are present on insect cuticle after contact with pitcher fluid

After force measurement tests in water, gasters were free of any visible residues (Figure 5.6a-i & ii) and closely resembled control samples that were prepared using the same method but not tested. In stark contrast, after tests in PF, gaster cuticle and hairs were clearly coated with PF (Figure 5.6b-d). We observed films on significant areas of the gaster (smooth texture in some areas, porous in others; Figure 5.6b-i & ii). Dried fluid bridges between the hair and the gaster cuticle were also visible (Figure 5.6c). Polygonal crystals were sometimes present on the smooth cuticular surface. We also observed PF 'gripping' individual hairs to form solid filaments spanning between the main film and the hairs (Figure 5.6d). Note that these samples were not flash-frozen and freeze-dried but rather dried in a desiccator over several days, hence the filaments were stable structures.

SEM images of tested ant antennae highlighted the extreme density of cuticular hairs on the antennae, which likely inhibited wetting of the underlying smooth cuticle. We observed that antennae tested in water were mostly free of filaments (Figure 5.6e-i & ii), although dirt-like particles were present at the tip of some specimens (n= 4 out of 7 antennae). The majority of the antennae tested in PF looked similar to those tested in water, but several had filaments spanning between the hairs at the tip of the antennae (Figure 5.6 e-iii; n= 4 out of 15 antennae). No other residues or contaminants were found on the remaining antennal segments, and overall the antennae were cleaner than gasters after tests in PF.

5.4.6 Dewetting is slowed down or prevented in pitcher fluid

Water dewetted from the clean glass surface without leaving behind any residues or films (Figure 5.7a-i to iii; Supplementary Video 2). In stark contrast, PF on glass did not show any dewetting: the initial perimeter of the droplet did not contract, and continued withdrawal led to an increasingly thin film (Figure 5.7b-i to iii; Supplementary Video 3). Eventually, the film started to dry close to the microcapillary tube, and then at the outer fluid perimeter. This resulted in the formation of very thin layers and smaller filaments on the surface (see asterisk in Figure 5.7b-iii), although it is possible that the PF dewetted in between these regions. When the microcapillary was removed and the fluid began to evaporate, branched hygroscopic crystals formed that visibly absorbed the humidity from our breaths when we blew on the glass surface (Supplementary Video 3).

On hydrophobic PE surfaces, water also dewetted completely from the surface (Figure 5.7c-i to iii). On the other hand, PF formed thin layers and residues on PE surfaces (Figure 5.7d-i to iii). Furthermore, we observed fractal-like patterns comprised of thin solid filaments extending from the edge of the initial rim towards the centre (Figure 5.7d-iii). Once again, both crystals and thin residues were left behind on the PE surface upon evaporation; hence, both glass and PE surfaces were covered with PF after contact.

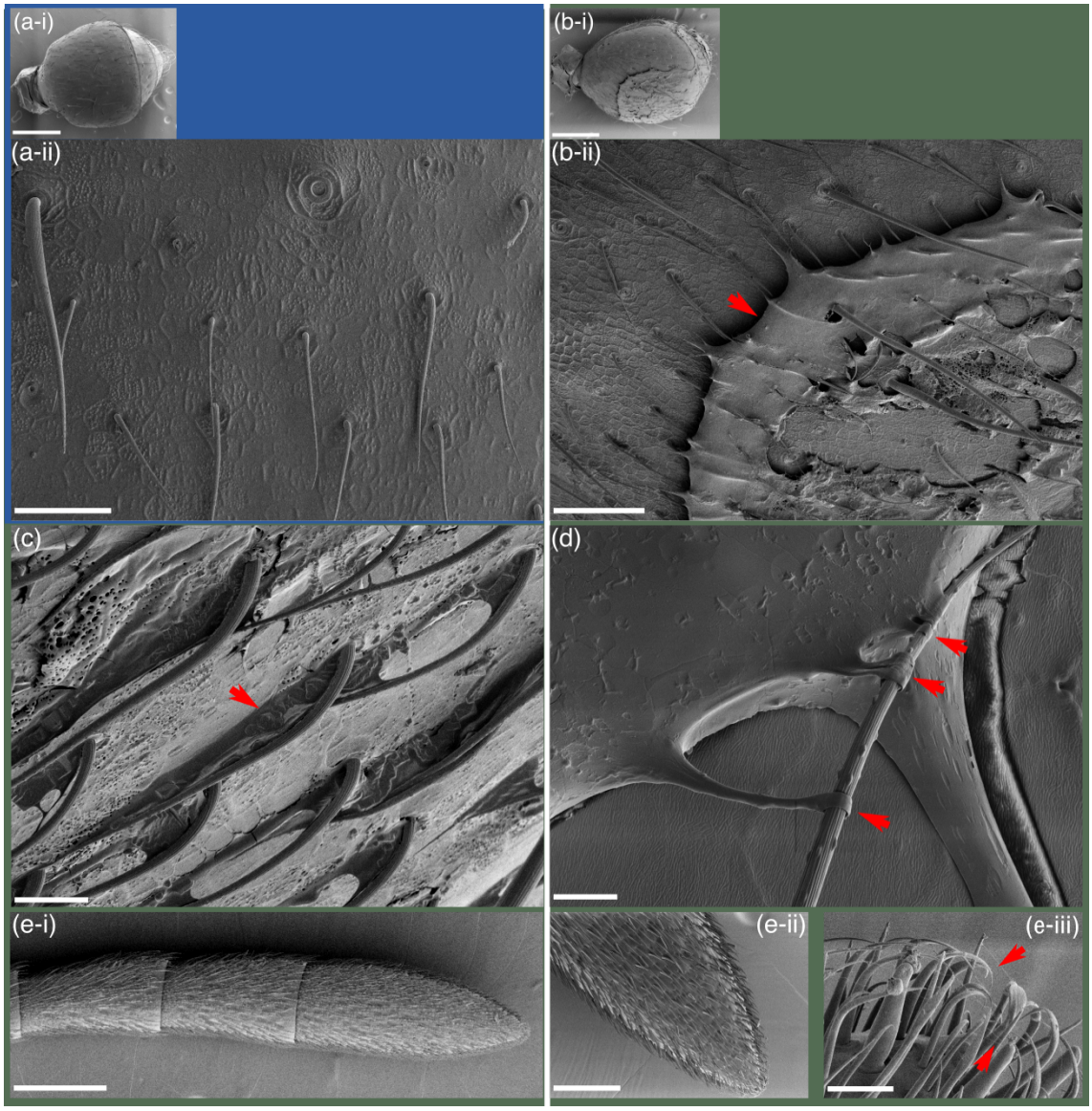

Figure 5.6. Scanning electron microscopy (SEM) images of ant gasters after testing in water (blue frame) and *N. rafflesiana* PF (green frame). (a-i & ii): Gasters tested in water had no visible contaminants or residues on their cuticular surfaces. Scale bars 500 µm and 50 µm, respectively. (b-i & ii) Large areas of the gasters tested in pitcher fluid were covered by solid films of dried pitcher fluid (marked by red arrow), coating both hairs and the cuticular surface. Scale bars 500 µm and 50 µm, respectively. (c) Dried pitcher fluid bridges between hairs and the cuticular surface (see red arrow). Scale bar 20 µm. (d) Filaments 'gripping' a single hair (each filament marked by a red arrow). Scale bar 5 µm. (e-i) Last three segments of an ant antenna. The entire antenna is densely covered in sensory hairs. (e-ii) Antennae were generally less contaminated with pitcher fluid residues than abdomens. (e-iii) Closer inspection of the antenna tip revealed pitcher fluid filaments between the hair tips (but not the cuticle between the hairs; see red arrow). Scale bars 250 µm, 100 µm, and 10 µm, respectively.

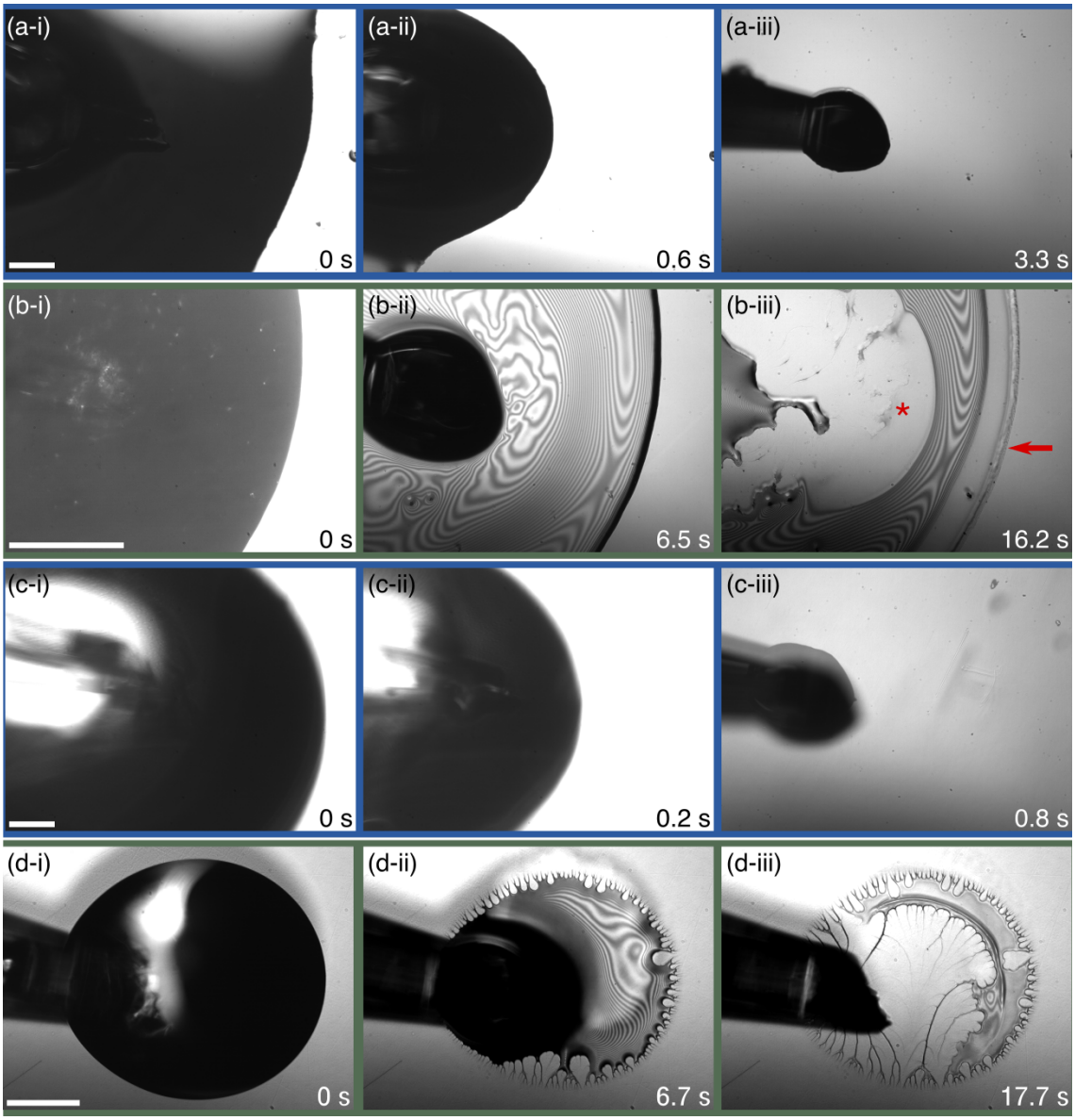

Figure 5.7. Dynamic dewetting behaviour of *N. rafflesiana* PF (green background) and water (blue background) on different surfaces visualised via interference reflection microscopy. (a-i, ii, iii) Water droplet retracted from clean glass (hydrophilic) surface. The droplet dewetted cleanly without leaving any residues within 3.3 seconds (s). (b-i, ii, iii) In contrast, PF resisted dewetting from glass, as evidenced by the formation of a thin layer (interference fringes visible in ii). Even after 16.2 s, there were residues on the surface, and the initial outermost rim had not contracted (marked by red arrow). Very thin films were left behind (marked by *). (c-i, ii, iii) On polyethylene (PE) hydrophobic surface, water droplets again dewetted completely. (d-i, ii, iii) PF, on the other hand, behaved similarly as on glass, where a thin layer was formed as more liquid was withdrawn. Moreover, the initial droplet rim did not retract; instead, solid fractal-like filaments were deposited. By 17.7 s, the surface remained partly coated by dried pitcher fluid films. All scale bars 200 µm.

On insect cuticle, small droplets of water readily dewetted and evaporated from both the smooth cuticle and underneath large hairs (Supplementary Video 4). PF, however, behaved differently on cuticular surfaces: although the strong reflectivity of the cuticle obscured any interference patterns during the withdrawal, PF again failed to fully dewet from the cuticle, leaving residues on some areas of the cuticle, similar to those on glass and PE surfaces (Supplementary Figure 2). The residues resembled the patterns seen in SEM images of gasters after force measurement tests in PF (Figure 5.6b-i). Moreover, we observed filaments forming between the receding PF and hairs on the gaster, which could give rise to the aforementioned hair-gripping structures (Figure 5.6d).

5.5 Discussion

Carnivorous plants have evolved a myriad of adaptations and mechanisms to prey on insects, ranging from trigger hair-activated leaves of Venus fly-traps, sticky 'glue' secretions of sundew plants, and pitfall traps of pitcher plants. Although there are several structural mechanisms of insect capture and retention in pitcher plants, it is increasingly evident that the digestive fluid itself can mechanically contribute to the capture and retention of insect prey. In the case of *N. rafflesiana* pitcher plants, one of several *Nepenthes* species that produces sticky PF, previous researchers have proposed two mechanisms responsible for the higher prey retention rate of the fluid compared to water. First, an insect that falls into the fluid will struggle and move rapidly to its own detriment: the non-Newtonian fluid responds elastically to fast shear-rates, which likely inhibits movements and hampers escape (Gaume & Forterre, 2007). Second, as the insect retracts its wetted limbs from the fluid during its struggles, filaments are formed that resist being stretched, which is a consequence of the fluid's high extensional viscosity (Gaume & Forterre, 2007). For both of these mechanisms to work, we need to assume that the fallen insect is wetted by the fluid. Insect cuticle, however, is covered by a waxy coating (Jackson & Baker, 1970), making them generally difficult to wet with water (although exceptions exist, see (Holdgate, 1955)). Moreover, while the surface tension of water is high, small insects like ants and flies have low mass, which means they will not easily break through the meniscus to become submerged in the first place. Our investigation of the interactions between PF and insect cuticle has revealed novel insights into the mechanisms underlying the adhesive and retentive property of sticky PF, which are discussed in the sections below.

5.5.1 Lower surface tension of pitcher fluid facilitates sinking of insect prey

From dropping ants into PF to mimic natural capture events, we found that ants only sank in PF but not in water. Additionally, ants floated and 'walked' on the water surface, which did not occur in PF. This suggests that ants break through the PF-air interface more easily than the water-air interface, which supports previous reports of insects sinking in *Nepenthes* PF (Bauer et al., 2011; Lloyd, 1942). Using an antenna, a highly non-wettable region of the ants' cuticle, we confirmed that the PF interface cannot sustain the same force as water. We found that at the maximum preload force, the water contact line was arrested and the meniscus held to prevent the antenna from sinking in deeper. In PF, however, at the same force, the meniscus consistently failed to arrest the contact line, and the antenna was pushed further into the fluid as the force transducer set-up tried to obtain the preload force. This result can be explained by a lower surface tension of PF compared to water. The ability of an object to float on a fluid-air interface depends on the fluid's surface tension and the object's geometry and surface wettability (Bush & Hu, 2006; Vella, 2015). If we consider a simple case of a long thin cylinder floating on a liquid-air interface, its weight must be balanced by surface tension forces:

$$F_w = 2\gamma L sin\theta$$

where γ is surface tension, θ is the slope of the water surface close to the cylinder, and L is the length of the cylinder. In our study, since the object geometry and surface wettability were kept approximately constant, the inability of the PF meniscus to withstand the same force must arise from a reduced surface tension. Indeed, our surface tension measurements confirmed that sticky PF from both *N. rafflesiana* and *N. inermis* have lower surface tension than water. Thus, our dual approach (probing the interface with a sensitive force measurement set-up and measuring surface tension with pendant drop tensiometry) provides new evidence that reduced surface tension is important for prey capture and retention in *Nepenthes* PF, a mechanism long suspected but unsubstantiated prior to our study (Lloyd, 1942).

We acknowledge, however, that our measured surface tension values differ from previously reported values from the same species (*N. rafflesiana*), and we offer some possible explanations below. One study used the capillary rise method, which relies on the height of the test fluid in a thin capillary tube to derive the surface tension. Using this technique, Bauer *et al.* conducted field measurements with fluid from unopened pitchers and 10 µL microcapillary tubes (Bauer et al., 2011). Given the small volume of the

capillary and the high accuracy of the method under ideal conditions, it is unlikely that a ~15% change in surface tension (and thus the height) would have been missed. Instead, the discrepancy between our values may result either from experimental conditions or biological variation.

Another study also used the pendant drop technique with pitcher fluid from opening *N. rafflesiana* pitchers and found no significant difference to water (Gaume & Forterre, 2007). One possible explanation is experimental error from how the droplets were dispensed: according to the study methods, a Pasteur pipette was used to form the droplets, implying that droplets were dispensed manually. Vibrations from manual injections could cause the droplet to pinch off prior to the maximum droplet size, a known source of error in pendant drop tensiometry (Berry et al., 2015). Furthermore, at large pipette diameters and low Bond numbers (e.g., when the deviation from sphericity is small, as seen in fluids with surface tension similar to water), there can be significant variation in the measured surface tension values, ranging from ~60 to ~95 mN/m for water (Berry et al., 2015). To address this source of error, Berry *et al.* introduced the Worthington number Wo, a dimensionless parameter that is a function of the relative precision of the pendant drop set-up (Berry et al., 2015). The study found that Wo greater than 0.6 corresponded to a standard error of less than 1%; thus, we ensured that the Wo value for each of our droplet measurements was greater than 0.6 (Supplementary Table 1). Despite the large sample size and low variation in surface tension values from the aforementioned study, the Bond numbers were not reported (Gaume & Forterre, 2007). (Note that the Worthingon number had not been introduced at time of publication and is thus not included in the justification.) Since it is challenging to handle viscoelastic PF for pendant drop measurements, we believe that it is important to conduct each measurement at sufficient Bond or Worthington numbers to minimise sources of error. It is worth highlighting that, using our pendant drop method, we found that a different *Nepenthes* species (*N. inermis*) had an even more reduced surface tension, at 34.6 mN/m. This is much lower than the surface tension of *N. rafflesiana*, as well as any of the previously reported measurements from Sarraceniaceae pitcher plant fluid (Armitage, 2016; Jaffe et al., 1992; F. M. Jones & Hepburn, 1927; Lloyd, 1942). These findings provide further support that a reduced surface tension may be a natural property of PF in at least some *Nepenthes* species. Future experiments could investigate the distribution and function of this fluid property among Nepenthaceae and Sarraceniaceae.

Only a few studies have attempted to identify the surface-active molecules responsible for the reduced surface tension in PF. Initial tests with several members of Sarraceniaceae failed to detect saponins (F. M. Jones & Hepburn, 1927), a type of organic surfactant found in various plants (Oleszek & Hamed, 2010; Ruyssen & Loos, 1947). Recently, Armitage successfully reproduced both the ant retention rate and the surface tension value of *D. californica* PF by inoculating sterile growth media with bacteria from *D. californica* PF (Armitage, 2016). This finding suggests that the bacterial community inhabiting *D. californica* PF, in addition to facilitating nutrient absorption by breaking down organic matter (Armitage, 2017), may also help to lower surface tension and improve prey retention. Although it is unclear whether the surface tension reduction is simply a by-product of the bacterial community or if the bacteria actively secrete surfactants, the effect clearly benefits both the host and the microbial community by improving the prey retention rate.

Meanwhile, nothing is currently known about the molecules responsible for the reduced surface tension of *Nepenthes* PF. Although we did not explore the role of bacteria in surface tension, future work is encouraged to assess the interplay between bacteria, surface tension, and retention rates in *Nepenthes* PF. However, it is worth pointing out that, due to the special physiochemical properties of *N. rafflesiana* fluid, neither bacteria nor specific surfactants may be necessary to lower the surface tension. Interestingly, previous researchers failed to detect bacteria from unopened pitcher fluid of several *Nepenthes* species, which suggests bacteria may not significantly influenced the surface tension of our samples. In addition, *N. rafflesiana* PF is known to be acidic (Bauer, Willmes, & Federle, 2009; Bazile et al., 2015), and solutions of organic acids have lower surface tension than water (Álvarez, Vázquez, Sánchez-Vilas, Sanjurjo, & Navaza, 1997; Lord, Hayes, Demond, & Salehzadeh, 1997). For example, a 1.6% w/w solution of acetic acid has a surface tension of 61.72 mN/m at 25°C (Álvarez et al., 1997). The acidic nature of *N. rafflesiana* pitcher fluid may be sufficient for decreasing the surface tension. Furthermore, it is hypothesised that large (high molecular weight) polysaccharides are present in *N. rafflesiana* pitcher fluid (Adlassnig et al., 2010; Gaume & Forterre, 2007). This could be an important factor since dilute solutions of large polysaccharides can also lower the surface tension: guar gum, for example, has a surface tension of ~50 mN/m (0.8% w/v) (Garti & Reichman, 1994), and xanthan gum of 42.3 mN/m (1% wt)

(Prud'Homme & Long, 1983). In dilute solutions of mamaku gum, a large polysaccharide with a chemical structure similar to the polysaccharide component of *Drosera* mucilage (Gowda, Reuter, & Schauer, 1982; Rost & Schauer, 1977), the surface tension ranged from 33.5 to 44.6 mN/m depending on the concentration (Jaishankar, Wee, Matia-Merino, Goh, & McKinley, 2015; Wee, Matia-Merino, Carnachan, Sims, & Goh, 2014). The combination of low pH and large polysaccharides can act in synergy to further reduce the surface tension: for xanthan gum, surface tension decreases from 67.09 mN/m to 63.96 mN/m at pH 5 and 2.5, respectively (Brunchi, Bercea, Morariu, & Dascalu, 2016). Since *N. rafflesiana* PF reaches pH values as low as 2 (Bauer et al., 2009) and likely contains acidic polysaccharides related to those found in mamaku gum and *Drosera* mucilage (see Chapter 6), these parameters could be important mechanisms through which the plant controls the surface tension. Future work can investigate this further by varying the concentration of PF polysaccharides or the pH and measuring the effect on surface tension.

5.5.2 Pitcher fluid adheres strongly to insect cuticle

Insect cuticular surface wettability is influenced by the waxy outer layer as well as surface patterning, often in the form of dense arrays of hairs and/or cuticle microstructures (Holdgate, 1955; Hu, Watson, Cribb, & Watson, 2011). Thus, the good wetting of ant gasters during our water trials is likely a result of its relatively smooth surface. A similar argument was proposed to explain why water alone retained certain species of ants and flies but not others: those with more wettable cuticular surfaces may be readily wetted and thus have higher likelihood of sinking (Bazile et al., 2015). In our trials, when *A. cephalotes* gasters were tested in water, we observed an initial jump into contact, followed by an overall repulsive force when lowered deeper into the liquid, and a sharp adhesion peak when retracted. The transient adhesive peak occurred just before the rapid collapse of the meniscus; hence, if a trapped ant is able to find a surface to adhere to and overcome this peak through a short yet forceful burst of movement, it could escape from water. To combat this, pitfall traps have structural adaptations on their inner walls to prevent the insects from gaining a sufficient foot-hold (e.g., slippery inner walls, downward-facing hairs). The situation is different with winged insects, however, since they can fly away and consequently their retention rate in pure water is low (Bazile et al., 2015). In such cases, sticky PF offers a clear advantage over water: while the peak attractive force is

only weakly higher than water, the displacement and hence the work of retraction is significantly larger. This is likely due to two factors: (1) the filament between the fluid and the gaster acts to pull the latter back; (2) a droplet remains adhered to the gaster and resists dewetting, adding weight and also facilitating re-wetting of the cuticle (more details below). Thus, insects have to sustain higher forces for longer durations to escape from PF compared to water. For nonflying prey like ants, the adhesion of PF to their cuticle can prevent the ants from escaping: during our retention trials, none of the ants managed to escape, and several were unable to pull themselves out of the fluid despite having a sufficient foothold on the glass wall (*personal observations*). Similarly, for a winged insect, any wetted body part will act like tethers to the fluid and further inhibit escape. Moreover, the reduced surface tension causes insects to sink more readily in PF, leading to larger areas of the cuticle to be wetted and increasing the overall effort needed for escape. Hence, these two PF properties can act in synergy to facilitate prey retention.

5.5.3 Pitcher fluid strongly resists dewetting and is extremely difficult to remove

Perhaps the most striking PF behaviour was its strong resistance to dewet from both hydrophilic and hydrophobic surfaces. When a droplet of PF was withdrawn from a glass surface, the initial contact line failed to move inward and instead the fluid formed a thin layer as it was actively withdrawn. PF also slowed down or prevented dewetting on hydrophobic surfaces, where it formed long fractal-like filaments branching out towards the initial rim. As a result, PF did not completely dewet on any of the tested surfaces, and large areas of the contact zone were left covered in PF. In contrast, water consistently dewetted on both hydrophilic and hydrophobic surfaces. The ability to strongly slow down or prevent dewetting is a mechanism typical of yield stress fluids. The yield stress prevents the contact angle from reaching its equilibrium value, and it therefore strongly increases contact angle hysteresis, i.e. the difference between advancing and receding contact angle (Barral et al., 2010; Boujlel & Coussot, 2013; Géraud et al., 2014; Jørgensen, Le Merrer, Delanoë-Ayari, & Barentin, 2015). This resistance to dewetting can enhance prey retention as follows: when an insect lands on the PF and struggles, parts of its body will become wetted. Through its struggles, the insect will raise its limbs or wings above the fluid surface (upstroke) then back down into the fluid (downstroke). According to our dewetting experiments, if the fluid was water, its limbs will tend to dewet from the surface during the upstroke, and upon the downstroke, water will need to

re-wet the surface, resulting in no overall advancement on the contact line. With PF, however, the upstroke will not dewet the fluid from the limb, and upon the downstroke, the fluid will readily interact with itself through the film or filament residues, thus facilitating the extension of the fluid contact line. In other words, the ant will be trapped in a positive feedback loop, similar to a ratchet motion, thereby constantly dragging itself into the fluid. Such a mechanism can work in combination with the reduced surface tension and may explain the sinking phenomena in PF but not in water. SEM images of tested gasters clearly show cuticular surfaces coated in PF residues, which is in stark contrast to the clean water-tested gasters. Analogous findings have been reported in carnivorous sundew plants (*Drosera* genus), which secrete droplets of sticky viscoelastic mucilage from stalked glands to ensnare their prey. This mucilage readily spreads on lepidopteran wings and leaf surfaces that are both highly non-wettable (Kokubun, 2017), and produces static contact angles lower than water on hydrophobic surfaces (47° compared to 83°) (Y. Huang, Wang, Sun, Agrawal, & Zhang, 2015). This implies that it is more energetically favourable for *Drosera* mucilage than for water to interact with hydrophobic surfaces, which is analogous to our findings with the sticky *N. rafflesiana* pitcher fluid.

5.6 Conclusion

Pitcher plants rely on multiple mechanisms to capture and retain insect prey. Aside from the well-studied structural mechanisms, the pitcher fluid within the trap serves both a digestive and a mechanical function for prey capture and retention. We investigated how the sticky pitcher fluid from *Nepenthes rafflesiana* adheres to insect cuticle and facilitates prey retention. Our findings show that the surface tension of pitcher fluid is significantly lower than water. This partly explains our observations of insects being wetted and sinking more readily in the pitcher fluid. Force measurements of insect cuticle dipped into and out of pitcher fluid demonstrated that significantly greater work is required to retract from PF than from water. This was due to the formation of filaments between the cuticle and the PF that produced an adhesive force back towards the fluid. Image analysis of the tested cuticular surfaces revealed that PF remained in contact with the cuticle. Pitcher fluid resisted dewetting on insect cuticle as well as hydrophobic and hydrophilic test surfaces, and left residues that could facilitate subsequent re-wetting of the cuticle. We propose that prey retention is based on a combination of two mechanisms: (1) When an

insect falls into the pitcher and lands on the pitcher fluid, it readily breaks through the meniscus; (2) Once wetted, it takes much more effort to escape due to the formation of filaments that pull the prey back into the fluid, along with the fluid's resistance to dewetting. Repeated attempts to escape only leads to further wetting of the cuticle, eventually ending with the prey being trapped by complete submersion or exhaustion.

6 PITCHER PLANTS (GENUS *NEPENTHES*) HAVE CO-OPTED THE WIDE-SPREAD POLYSACCHARIDE GLUCURONO-MANNAN TO PRODUCE STICKY INSECT CAPTURE FLUID

6.1 Summary

Pitcher plants (genus *Nepenthes*) are carnivorous plants that capture and digest prey to acquire additional nutrients. In *N. rafflesiana*, the fluid secreted into the pitfall traps is a sticky material that facilitates prey capture. While the physical properties of this fluid are crucial for catching prey, the molecules that give rise to these properties are unknown. Here, we identified the principal biopolymer in *N. rafflesiana* fluid to be an acidic polysaccharide with a glucurono-mannan backbone and arabinose and galactose substitutions. The same architecture was also present in *N. pervillei*, the most basal species of the genus, suggesting the use of glucurono-mannan within the genus is an ancestral trait. Polysaccharides with the same backbone structure have been previously isolated from the sticky capture mucilage of *Drosera*, a related group of carnivorous plants, as well as in mucilaginous exudates from diverse taxa across the plant kingdom. Our findings suggest that glucurono-mannan may be particularly suitable for producing mucilaginous exudates, and in carnivorous plants the polysaccharide may have been optimised to create highly sticky fluids to catch insects.

6.2 Introduction

Plants secrete sticky exudates as a means of manipulating their immediate surroundings to their benefit. Plant mucilage, a subset of exudates that is viscoelastic and often comprised of polysaccharides, fulfil a range of functions including defence, wound protection, water and salt regulation, microbiota growth promotion, and adhesion (Adlassnig et al., 2010; Galloway, Knox, & Krause, 2020). In several genera of carnivorous plants, secretions have been co-opted to serve a highly specific function: to adhere to prey. These carnivorous plants, including members of *Drosera*, *Drosophyllum, Triphyophyllum, Pinguicula, Byblis,* and *Philcoxia* genera, create adhesive traps by releasing sticky secretions that facilitate prey capture (Adlassnig et al., 2010; Płachno &

Muravnik, 2018). Despite the important functional role of these secretions, little is known about the molecules that give rise to their specialised physical properties. Histochemistry and monosaccharide analysis have shown that the mucilaginous glandular secretions from *Drosera*, *Drosophyllum, Triphyophyllum,* and *Pinguicula* are comprised of acidic polysaccharides (Adlassnig et al., 2010; Schnepf, 1963; Vintéjoux & Shoar-Ghafari, 2000). Information on the chemical composition of these secretions is scarce with the exception of *Drosera* (also known as the sundew plant). In *Drosera*, capture mucilage released from stalked glands on its modified leaves readily spreads on and adheres to insect cuticle and other hydrophobic surface (Y. Huang et al., 2015; Kokubun, 2017). Consequently, escape is impaired by the viscoelastic properties of the mucilage, which stiffens upon stretching and resists filament breakup, thereby restricting movement and preventing the prey from freeing itself (Erni et al., 2011). Such physical properties are afforded by the chemical composition of *Drosera* mucilage, which comprises of a single type of acidic polysaccharide (Rost & Schauer, 1977). This large linear polysaccharide (>2 x 10^6 Daltons, Da) has an inner core structure with alternating repeats of glucuronic acid and mannose monosaccharides called glucurono-mannan (GlcA-Man) (Aspinall, Puvanesarajah, Reuter, & Schauer, 1984; Gowda et al., 1982; Gowda, Reuter, & Schauer, 1983). Although the mucilage is a dilute solution of the polysaccharide (~4%), it has a high zero-shear viscosity of ~100 Pa s (approximately 10^5 greater than water) and exhibits a steep increase in extensional viscosity under large strain deformation (Erni et al., 2011). Chemical analysis of mucilage from two *Drosera* species showed the polysaccharide structures were nearly identical, suggesting that GlcA-Man usage is conserved in this group (Gowda et al., 1982).

In contrast, *Roridula*, a protocarnivorous plant with sticky traps that relies on a mutualistic hemipteran to digest the prey and provide nutrients in the form of excrements, does not appear to use polysaccharides to create its capture fluid. Instead, the secretion is similar to tree resin, and contains a mixture of mainly triterpenoids and relatively small polymers (<2 to ~7 kDa) that resemble ethylene–vinyl acetate copolymers (Frenzke et al., 2016; Simoneit, Medeiros, & Wollenweber, 2008). Hence, although the capture fluid from *Roridula* fulfils the same function as *Drosera* sticky mucilage and exhibits similar physical properties, its chemical composition appears to be completely different.

While the aforementioned plants are well-known examples of adhesive traps in carnivorous plants, several species of *Nepenthes* pitcher plants also secrete sticky fluids into their pitfall traps to help catch insects (Bonhomme et al., 2011; Moran, Gray, Clarke, & Chin, 2013). This trait is thought to be present in approximately 10% of all described *Nepenthes* species, ranging from the most basal species of the genus, *N. pervillei*, to the distinctive *N. inermis* with highly modified pitchers that may act more like adhesive traps than pitfall traps, and the well-studied *N. rafflesiana*, which produces several millilitres of sticky fluid in its pitchers (Di Giusto et al., 2008; Płachno & Muravnik, 2018). Although pitcher fluid is important for prey digestion, when the fluid is also sticky it drastically increases prey retention rates (Bazile et al., 2015; Gaume & Forterre, 2007). Similar to the *Drosera* capture mucilage, the viscoelastic properties of sticky pitcher fluids are crucial for its retentive function (Gaume & Forterre, 2007; Chapter 5). Since *Nepenthes* is distantly related to *Drosera*, previous researchers have postulated that the sticky fluid may also comprise of polysaccharides (Adlassnig et al., 2010; Bonhomme et al., 2011; Gaume & Forterre, 2007), but there has yet to be a detailed chemical characterisation of the fluid.

In this study, our main objective was to isolate and characterise the chemical constituents responsible for the sticky viscoelastic property of *N. rafflesiana* pitcher fluid. Protocols were developed and optimised to remove the side-group sugars in order to obtain oligomers of the hydrolysed backbone. Gel electrophoresis, liquid chromatography, and mass spectrometry were used to characterise the released oligomers. In addition, we also investigated *N. pervillei* since it is the most basal species of the genus and also secretes sticky pitcher fluids. Finally, implications of our findings and the potential applications of the isolated backbone oligomers are discussed. By characterising the chemical composition of sticky pitcher fluids, we provide a strong link between its chemistry, biological function, and ecology.

6.3 Abbreviations

Fuc: L-Fucose, Ara: L-Arabinose, Gal: D-Galactose, Xyl: D-Xylose, Man: D-Mannose, GalA: D-galacturonic acid, GlcA: D-glucuronic acid, GlcA-Man: glucurono-mannan, NR-RPE*: Nepenthes rafflesiana* raw polysaccharide extract, NP-RPE: *N. pervillei* raw polysaccharide extract, EtOH: ethanol, PACE: Polysaccharide Analysis using

Carbohydrate gel Electrophoresis, HPAEC-PAD: High-Performance Anion Exchange Chromatography with pulsed amperometric detection, MALDI-TOF-MS: Matrix-assisted laser desorption/ionization time-of-flight mass spectrometry.

6.4 Methods

6.4.1 Sample collection and storage

Samples of sticky pitcher fluid from *Nepenthes rafflesiana* were collected from unopened traps of greenhouse plants kept at the University of Bristol, UK. Samples were frozen in 15 mL Falcon tubes at -20°C until use. *N. pervillei* pitcher fluid was sampled from one unopened and one freshly opened trap in the field on Mahé Island, the Seychelles by Dr. Ulrike Bauer (n= 2 different pitchers). One fluid sample taken from a freshly opened *N. pervillei* pitcher was precipitated with pure ethanol in the field. *N. pervillei* samples were frozen after collection, kept at ambient temperature during transport to the UK, and stored in a -20°C freezer until further use. Note that, as it was not feasible to keep the samples in freezing temperatures for the entire journey from the field to the laboratory freezer, it is possible that *N. pervillei* samples thawed and then re-froze at various points.

6.4.2 Ethanol extraction of raw polysaccharide from pitcher fluid

Raw polysaccharide was extracted from *N. rafflesiana* via the following steps: Frozen *N. rafflesiana* fluid was thawed at room temperature, and a sample volume was transferred using a micro-pipette into a pre-weighed 15 mL Falcon tube. (Due to the high viscosity of pitcher fluid, this volume was an approximation, and the raw polysaccharide concentration was calculated using sample weights.) To the 15 mL Falcon tube, 0.8 M ammonium formate was added (0.1x of the sample volume) and mixed by shaking. Next, 5x sample volume of cold ethanol (4°C, 100%) was added one volume-equivalent at a time, with vigorous shaking after each addition. The ethanol-fluid mixture was left on an orbital shaker in a 4°C room for 15 minutes. Afterwards, the 15 mL Falcon tube was centrifuged at 3700 RPM, and the supernatant was decanted to retain a white gel-like pellet at the bottom. This pellet, referred to as *N. rafflesiana* raw polysaccharide extract (NR-RPE), was air-dried inside the Falcon tube with the top covered by perforated parafilm for at 1-2 days in the 4°C room. Since preliminary tests showed no difference between air dried and SpeedVac dried samples, subsequent NR-RPE samples were

SpeedVac dried and their dry weights were used for calculating the yield (weight by weight %). Three different *N. rafflesiana* pitcher fluid samples were prepared. The same method was used to isolate RPE from the two liquid *N. pervillei* pitcher fluid samples. The ethanol insoluble residues from these two samples, along with the third prepared in the field, were dried in a SpeedVac and referred as NP-RPE. The dried NR-RPE and NP-RPE samples were kept frozen at -20°C until further use.

6.4.3 Time-course acid hydrolysis and analysis of monomers and oligosaccharides

RPE samples were hydrolysed using 2M trifluoroacetic acid (TFA) at 120°C. Based on the previous studies on *Drosera* capture mucilage (Aspinall et al., 1984; Gowda et al., 1982, 1983; Rost & Schauer, 1977) and our own preliminary tests, we decided that an extended acid hydrolysis with sampling at multiple time points was the most appropriate approach to investigate the pitcher fluid polysaccharides. Two samples were taken at each time point, one for Polysaccharide Analysis using Carbohydrate gel Electrophoresis (PACE), and another for monomer analysis via High-Performance Anion Exchange Chromatography with pulsed amperometric detection (HPAEC-PAD). Samples were dried using SpeedVac and frozen at -20°C if not used immediately. PACE samples were prepared as described elsewhere (Goubet, Jackson, Deery, & Dupree, 2002; Pidatala, Mahboubi, & Mortimer, 2017). In brief, dried samples were derivatised with a labelling buffer containing 8-amino- naphthalene-1,3,6-trisulfonic acid (ANTS) at 37°C overnight, then dried in a SpeedVac. The labelled samples were re-suspended in 3M urea and used for PACE or kept in -20°C. The time-course acid hydrolysis protocol was optimised for PACE and subsequently used to purify the raw extracts (for *N. rafflesiana*, referred to as acid hydrolysis purified product, or NR-AHPP; for *N. pervillei,* NP-AHPP). Time-course acid hydrolysis and associated purification steps are summarised in Figure 6.1. Based on the PACE results, samples were selected for further characterisation using mass spectrometry (see below). Monosaccharide sugar analysis of NR-AHPP and NP-AHPP using HPAEC-PAD was conducted as described previously (Tryfona et al., 2012) and summarised here: unlabelled dried samples were re-suspended in Milli-Q water and run on a Dionex ICS-3000 (Thermo Fisher Scientific, Waltham, USA) equipped with a CarboPac PA20 column, a PA20 guard column and a borate trap. Neutral sugars were separated using the following protocol: the column was equilibrated with 12 mM KOH prior to injection from 0 to 5 min; post-injection, the eluant concentration was decreased

using a linear gradient to 1 mM from 5 to 20 min, followed by wash step (100 mM for 5 min). 100 mN KOH was added post-column to increase PAD sensitivity. To separate the acidic sugars, ammonium concentration was increased from 20 to 200 mM in 100 mM NaOH over 10 min then maintained for a further 10 min. A mixture of standard monosaccharides, with 25 mM of neutral sugars (L-Fucose, L-Arabinose, D-Galactose, D-Xylose, and D-Mannose) and acidic sugars (D-galacturonic acid and D-glucuronic acid) were run alongside the samples for peak detection.

6.4.4 Anion exchange column chromatography of NR-RPE

Anion exchange column chromatography was used to determine whether NR-RPE contained a single type of acidic polysaccharide as seen in *Drosera* (Rost & Schauer, 1977). A solution of ~1 mg/mL NR-RPE was prepared by dissolving 4.1 mg of NR-RPE in 4 mL of 1 mM sodium borate buffer at pH 8.5 (sample required approximately 24h shaking in a Thermomix at room temperature). The column (11 mL volume) was loaded using DEAE-Cellulose DE52 resin swollen in Milli-Q water (resin volume 5 mL). The column was washed with 10 mL of loading buffer (same sodium borate buffer as above) at a flow-rate of ~1 mL/min using a peristaltic pump. 1 mL of the prepared NR-RPE sample solution was diluted 5-fold using the same buffer and loaded into the column. After washing with 5 mL loading buffer, the sample was eluted in 2 mL fractions using a linear gradient of NaCl (0 to 1 M) in 0.25 M steps. The total sugar content was monitored using phenol-sulfuric acid colorimetric method with absorbance at 480 nm wavelength. The eluted samples were freeze-dried, re-suspended in Milli-Q water, and hydrolysed for 3h under with 2M TFA at 120°C. Samples were taken at 1, 2, and 3h time intervals for PACE and HPAEC-PAD. Since only trace amounts of sugars were found in the 1h samples based on HPAEC-PAD, these samples were not analysed with PACE.

6.4.5 Mass spectrometry

Matrix-assisted laser desorption/ionization time-of-flight mass spectrometry (MALDI-TOF-MS) was used to verify the backbone oligosaccharide sequence from NR-AHPP and NP-AHPP. One microlitre of each sample in Milli-Q water was mixed with an equal volume of 20 mg/mL 2,5-dihydroxybenzoic acid (DHB) in 50% methanol and spotted on a target plate (Bruker). The spotted samples were then dried in a vacuum desiccator before being analysed by mass spectrometry on an UltrafleXtreme matrix-assisted laser

desorption ionization time-of-flight (MALDI-TOF) instrument (Bruker Scientific Instruments, Billerica, USA). Data were collected using a 2-kHz smartbeam-II laser and acquired on negative ion reflector mode (mass range 500 - 3000 Da). FlexControl and FlexAnalysis softwares were used for data acquisition and analysis. On average, about 10,000 shots were used to obtain sufficient signal to noise ratio.

6.5 Results

6.5.1 Isolation and characterisation of polysaccharide from *N. rafflesiana* pitcher fluid

The yield for NR-RPE after ethanol extraction from sticky viscoelastic pitcher fluid was 0.6 ± 0.1% (weight by weight; mean ± standard deviation, SD; n = 3 fluid samples). A gel-like precipitate formed upon addition of ethanol, and its viscoelastic behaviour was completely eradicated. However, re-dissolving the precipitate in ammonium acetate buffer partially recovered the viscoelastic property (buffer concentration 50 mM, pH 6; n = 2 *N. rafflesiana* fluid samples tested).

In the initial trial to hydrolyse the extracted polysaccharide, a NR-RPE sample was first subjected to an eight-hour acid hydrolysis, with samples taken at time-points 0, 0.5, 1, 2, 4, 6, and 8 hours for PACE (see acid hydrolysis protocol version 1 in Figure 6.1). PACE analysis has previously been used to analyse the structure of plant polysaccharides; in particular, it can reveal characteristic patterns of oligosaccharides present in the polysaccharide, and band intensities are correlated with the quantity of the released sugars (Goubet et al., 2002; Tryfona & Stephens, 2010). Hence, we characterised the NR-RPE hydrolysis samples using PACE and found monosaccharides that co-migrated with standards for a pentose sugar Ara, hexose sugars Man and/or Gal (overlapping migration), and a hexuronic acid GlcA (Figure 6.2a; see Supplementary Figure 1 for gel image with standards). Both Ara and Man/Gal were readily hydrolysed from the raw polysaccharide after 0.5-hour of acid hydrolysis. In contrast, GlcA was released only after 4h and increased in amount over the rest of the hydrolysis. From 2h onwards, oligosaccharides with varying number of repeating units were faintly visible as a ladder (Figure 6.2a & b). However, further analysis from version 1 samples was hindered by overlapping ladders, smearing within the lanes from unresolved sugars, and oversaturation from the Ara and Man/Gal monomers.

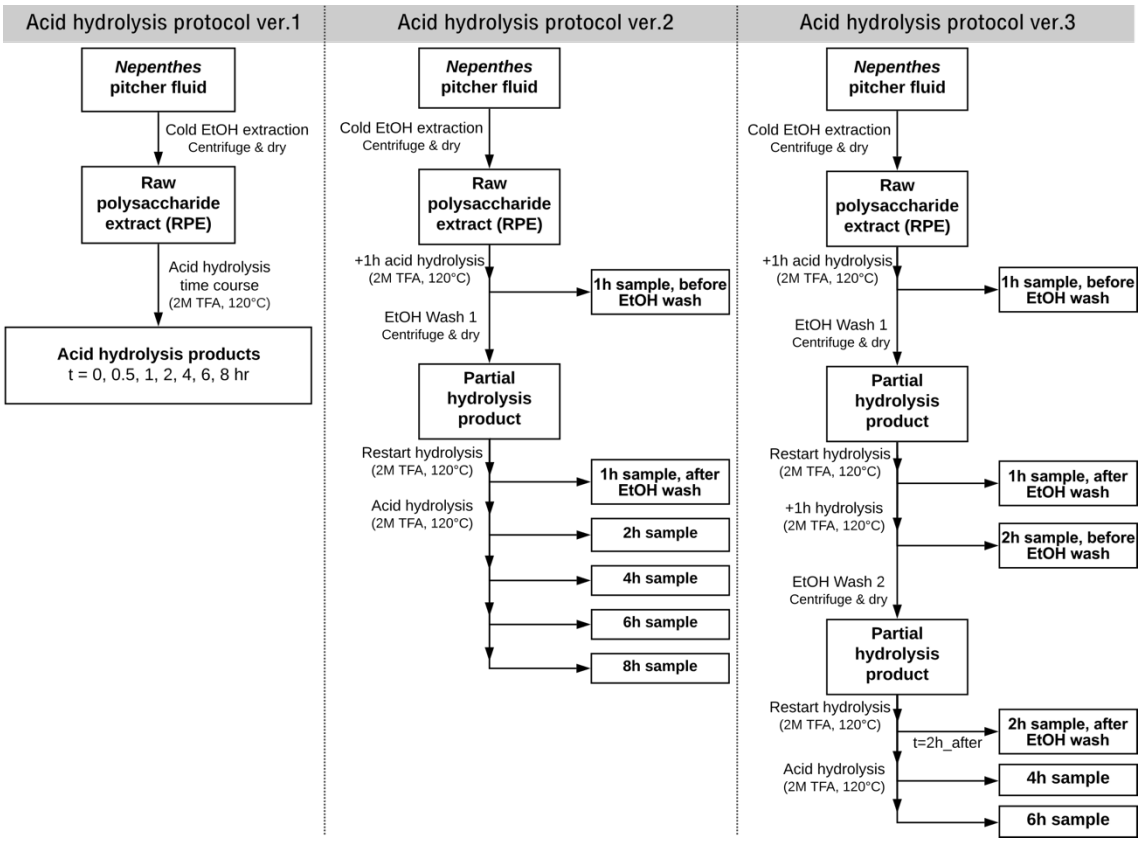

Figure 6.1: Protocol development to obtain GlcA-Man oligomers from raw *Nepenthes rafflesiana* pitcher fluid via partial acid hydrolysis and ethanol washes. Version 1 (ver.1) involved eight-hour acid hydrolysis with sampling at various points as outlined in the scheme. Ethanol (EtOH) washes were introduced in ver.2 (+1 wash) and ver.3 (+2 washes) to remove more acid labile sugar units from the sample, thus leaving a more purified sample containing fragments of the raw polysaccharide without side-group sugars. See Figure 6.2 for corresponding Polysaccharide Analysis using Carbohydrate gel Electrophoresis (PACE) of ver.1 and ver.3 experiments.

Additional ethanol washes (see protocols version 2 and 3 in Figure 6.1) were introduced in an effort to remove the more acid-labile sugars and other impurities to facilitate the interpretation of the PACE gels. Prior to the first ethanol (EtOH) wash, PACE analysis of the samples produced similar results to version 1, with pentose and hexose sugars being hydrolysed after 1h hydrolysis (lane 1 in Figure 6.2b). Post EtOH wash, however, both the released monosaccharides and the unresolved sugars within the lanes were removed, revealing a faint but clear ladder (lane 1* in Figure 6.2b). The ladder became more pronounced after another hour of hydrolysis, whereupon the individual monomers were again released in large amounts (lane 2 in Figure 6.2b). Results from the second EtOH wash were similar to the first wash, where monomers were removed while the larger

oligosaccharide ladder was retained. After 4 hours of hydrolysis, these oligosaccharides began breaking down, as evidenced by the loss of the upper bands of the ladder and a subsequent increase in intensity and size of the shorter oligosaccharides. This also corresponded to increases in Man/Gal, Ara, and GlcA monomers, with the most prominent increase seen in Man/Gal. The release of GlcA with increasing hydrolysis time, along with the condensed spacing between each ladder compared to the ladder of a neutral sugar (Man), suggested that the repeating unit contained a hexuronic acid. To further characterise the oligosaccharide structure, the 2h sample after two ethanol washes (sample 2*) was analysed using MALDI-TOF-MS (Figure 6.2c). The resulting mass spectrum confirmed the presence of oligosaccharides with masses that differed by 338 Da, which matched the theoretical mass of a dimer of a hexuronic acid and a hexose sugar **(UH)**. The number of repeats from the most abundant peaks ranged from two to seven, see **$(UH)_2$** to **$(UH)_7$** in Figure 6.2c. A minor ladder corresponding to an odd number of hexose units (e.g., **$U(UH)_3$**) was also present.

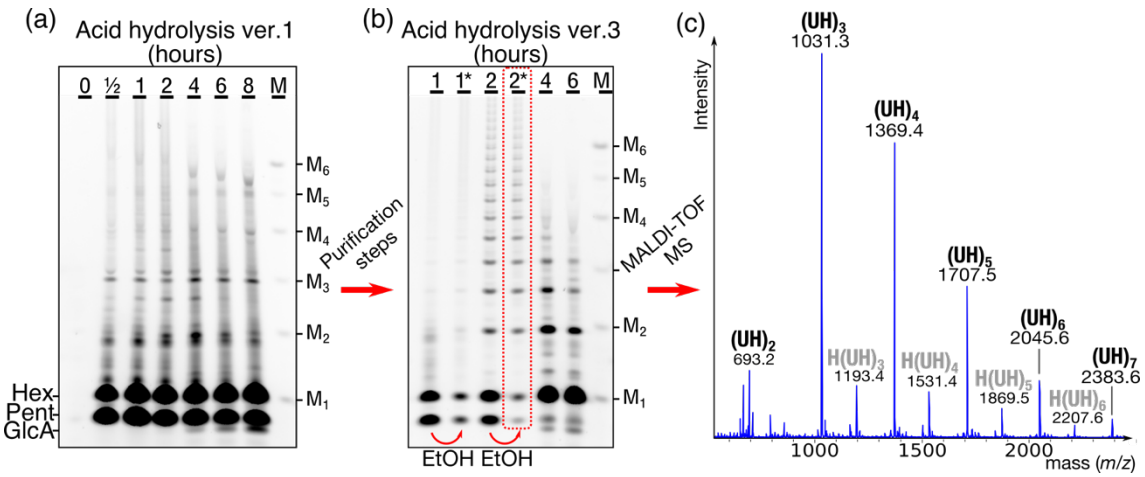

Figure 6.2: PACE and MALDI-TOF-MS analyses reveal the repetitive nature of the backbone of the purified *N. rafflesiana* pitcher fluid polysaccharide. (a) PACE of time-course samples from acid hydrolysis ver.1 (Figure 6.1) increasing in hydrolysis time from 0 to 8h. Mannose markers (M_1 to M_6) are shown on the right. Hydrolysed monomers co-migrated with standards for hexose sugars (Hex; either Man or Gal), a pentose sugar (Pent; Ara), and glucuronic acid (GlcA). Standards shown in Supplementary Figure 1. (b) In ver.3 samples, with additional EtOH washes (1* and 2* lanes, corresponding to 1h and 2h hydrolysis samples after EtOH wash), the amount of monomers decreased, and after 2 hours a clear ladder of oligosaccharides with different degrees of polymerisation (DP) became visible. (c) The 2* sample was analysed using MALDI-TOF-MS, where the mass differences between the main peaks (black labels) matched the theoretical mass of a dimer unit comprised of a hexuronic acid and a hexose sugar (**UH**; 338 Da after loss of free reducing end). Up to 7 repeats of **$(UH)_n$** were detected. Note the minor mass peaks (grey labels) corresponded to the major peaks minus a hexuronic acid.

Further insights from HPAEC-PAD helped to identify the monomers of the pitcher fluid polysaccharide, as well as the constituents of the **UH** dimer. Within the first hour of hydrolysis, Ara and Gal monomers were released while Man and GlcA were not detected (Figure 6.3a). After 8h hydrolysis, the amount of Ara and Gal remained largely unchanged, while Man and GlcA were now detectable. Moreover, an unknown peak appeared next to GlcA that did not match any of the tested standard monomers. Since it eluted in the region of acidic monomers and increased in abundance with longer hydrolysis, it was likely to be the hexuronic acid – hexose dimer unit, although this was not investigated in detail. Change in the proportion of the monomers over time supported the idea that Ara and Gal are released within an hour of acid hydrolysis, while the unknown/dimer sugar took 2 hours to appear in significant amounts (Figure 6.3b). Both Man and GlcA were detected after 4 hours, although greater proportion of GlcA were released. Between 6 and 8h, the relative amounts of unknown/dimer decreased, suggesting the dimer was being cleaved into monomers. In contrast, the relative amounts of Man and GlcA continuously increased from 4 to 8 h. The same trend was observed in trials with additional EtOH washes (version 2 & 3) and supported the results from PACE, where the EtOH wash helped to remove sugars that were released within the first two hours (mostly Ara and Gal; see Supplementary Figure 2).

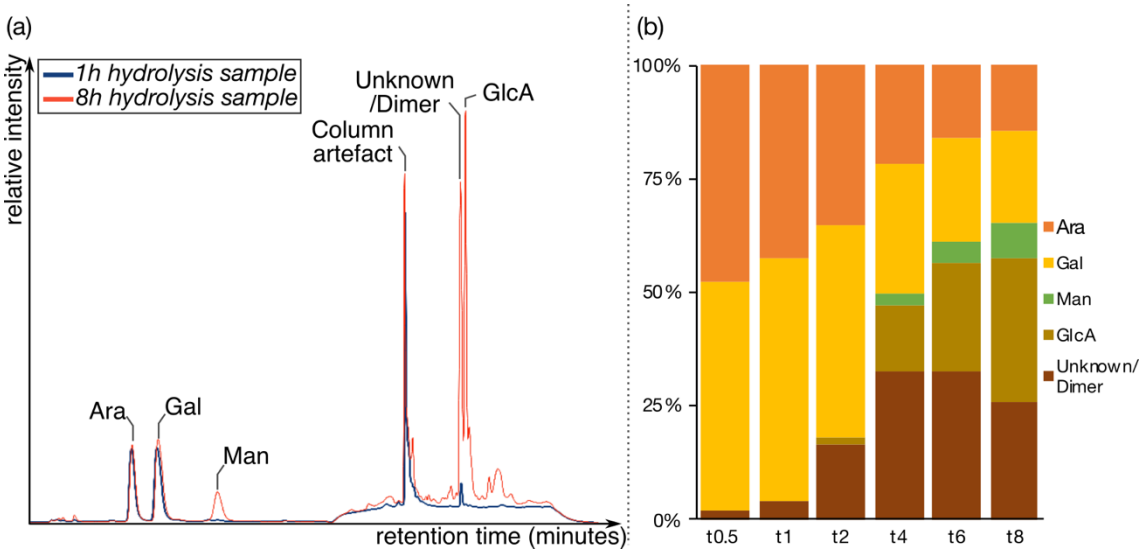

Figure 6.3: Monosaccharide identification through extended acid hydrolysis. (a) High-Performance Anion Exchange Chromatography with pulsed amperometric detection (HPAEC-PAD) retention spectrum of *N. rafflesiana* hydrolysis samples (from ver.1) featured four peaks that matched standards for Ara, Gal, Man, and GlcA, along with a large unknown peak close to GlcA that could be a dimer containing GlcA (Unknown/Dimer). Note that a column artefact peak appeared consistently in all the samples. Between the 1h and 8h hydrolysis samples, the amount of Ara and Gal remained largely unchanged, while Man, GlcA, and Unknown/Dimer peaks increased dramatically. See Supplementary Figure 2 for spectrum with standards. (b) Ratios of monosaccharides present in each time point according to HPAEC-PAD analysis (t; hours). Note the decrease in relative amounts of Ara and Gal with longer hydrolysis while Unknown/Dimer, GlcA, and Man increased.

Collectively, these findings showed that Ara and Gal monomers were present as side-group substitutions that were first to be cleaved during acid hydrolysis. After at least two hours of hydrolysis and with ethanol washes, the inner core of the polysaccharide was obtained, made up of repeats of a GlcA-Man dimer. Thus, using acid hydrolysis protocol version 3 we produced a mixture of GlcA-Man oligomers that make up the backbone of the pitcher fluid polysaccharide.

To further support our finding that *N. rafflesiana* pitcher fluid is a glucurono-mannan, we tested whether raw pitcher fluid contained other polysaccharides. Anion exchange column chromatography of NR-RPE and subsequent colorimetric tests showed that polysaccharides only eluted over a salt gradient ranging from 0.25 to 1.0 M, with the peak centred around 0.5 M (Supplementary Figure 3a). Partial acid hydrolysis and PACE analysis confirmed this distribution, where the most intense signals were present in 0.5 and 0.75 M NaCl fractions (Supplementary Figure 3b). Furthermore, not only was the same oligomeric ladder present across the 0.25 to 1.0 M elution samples, this ladder also

appeared to be identical to the one obtained from acid hydrolysis protocol version 3 as shown above (Figure 6.2c). This was corroborated by MALDI-TOF-MS, where the most abundant oligosaccharide peaks were again separated by repetitive units corresponding to a GlcA-Man dimer (338 Da; Supplementary Figure 3c). These results strongly suggested that raw pitcher fluid from *N. rafflesiana* was comprised of a single type of acidic polysaccharide with a backbone of repeating GlcA-Man dimers.

6.5.2 Isolation and characterisation of polysaccharide from *N. pervillei* pitcher fluid

The methods used to characterise the polysaccharide from *N. rafflesiana* pitcher fluid were applied to investigate *N. pervillei*. It should be noted that raw *N. pervillei* fluid was drastically less sticky and appeared more dilute than *N. rafflesiana* fluid. This was supported by the low yield of NP-RPE after ethanol extraction: 0.023 ± 0.003% (mean ± SD; n = 2 fluid samples). In addition, instead of a gel-like precipitate as seen with NR-RPE, only small white filaments formed when ethanol was added to *N. pervillei* fluid. Furthermore, while an extended acid hydrolysis was required to produce a clear oligosaccharide ladder with NR-RPE, 1h hydrolysis was sufficient to produce a ladder from NP-RPE (Figure 6.4a). Nevertheless, the ladders between the two species were identical, as supported by both PACE and MALDI-TOF-MS analyses (Figure 6.4a & b). The major mass peaks belonged to oligosaccharides comprised of **UH** dimers, where the degree of polymerisation ranged from 2 to 6. A minor ladder corresponding to oligosaccharides with an odd number of hexose sugars $\mathbf{H(UH)_n}$ was also identified. In addition, there was a third ladder of oligosaccharides with mass differences of 220 Da (Figure 6.4b). Since this mass difference did not match the theoretical mass of a **UH** dimer nor any intact sugar dimer and may arise from unresolved oligosaccharide fragments, its identity was not pursued further. Monosaccharide analysis of the *N. pervillei* and *N. rafflesiana* hydrolysis samples using HPAEC-PAD confirmed their compositions were identical, consisting of Ara, Gal, Man, GlcA, and an unknown/dimer (Figure 6.4c). Hence, the results from PACE, HPAEC-PAD, and MALTI-TOF-MS revealed that both *N. pervillei* and *N. rafflesiana* secrete a polysaccharide with GlcA-Man backbone and Ara and Gal side-groups.

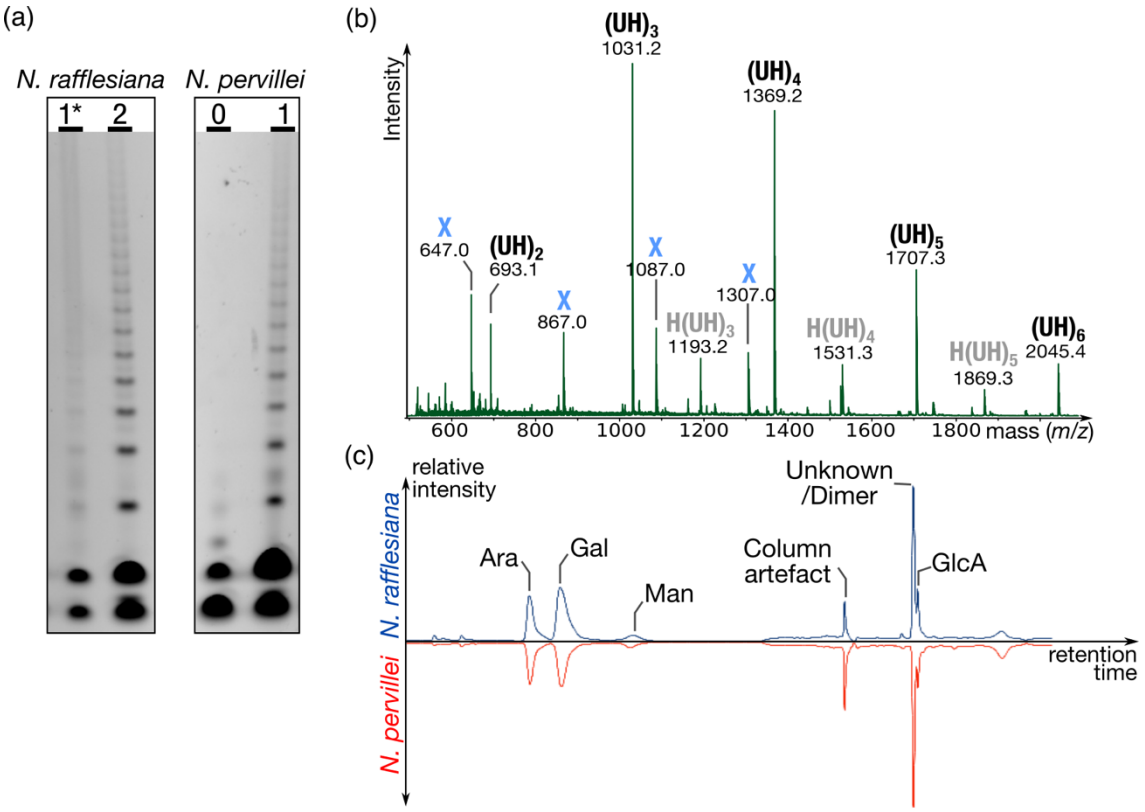

Figure 6.4: Polysaccharides isolated from *N. pervillei* and *N. rafflesiana* pitcher fluid have the same backbone structure. (a) PACE analysis of partial acid hydrolysis samples confirmed that the same pattern of oligosaccharides is present in both species. Labels for *N. rafflesiana* samples: 1*=1h hydrolysis followed by EtOH wash (same as in Figure 6.2); 2=2h hydrolysis. For *N. pervillei*: 0=before hydrolysis; 1=1h hydrolysis. Complete gel shown in Supplementary Figure 1. (b) Analysis of *N. pervillei* 2h hydrolysis sample using MALDI-TOF-MS revealed oligosaccharides with increasing DP of the **UH** dimer (black text). Two minor ladders were also present: one ladder with the same **UH** pattern but with an odd number of hexose (grey text), and another unidentified ladder with mass differences of 220 Da (labelled X). (c) Monosaccharide composition analysis using HPAEC-PAD showed that 4h hydrolysis samples from the two species contained identical sugars: Ara, Gal, Man, GlcA, and Unknown/Dimer.

6.6 Discussion

We have shown that sticky pitcher fluid from *N. rafflesiana* is made up of a single type of acidic polysaccharide with Ara, Gal, Man, and GlcA monosaccharides. When subjected to partial acid hydrolysis, Ara and Gal were readily lost from the polysaccharide, and additional hydrolysis produced a mixture of oligosaccharides sharing the same repetitive backbone consisting of GlcA-Man dimers. This finding, where acid-resistant GlcA-Man dimers are sequentially released from the backbone only after extended hydrolysis, is consistent with observations that the GlcA glycosidic linkages are relatively acid resistant, and it has been reported in the majority of the studies that have

characterised GlcA-Man from plant exudate (Table 6.1). For example, GlcA-Man, (GlcA-Man)$_2$, and larger repeats were released in partial hydrolysis of polysaccharide extracts from *Drosera*, *Actinidia, Encephalartos, Nicotiana*, *Ceiba*, and *Ornithogalum* (Di Fabio, Dutton, & Moyna, 1982; Gowda et al., 1982; Mabusela & Stephen, 1990; Mori & Kato, 1981; Redgwell, 1983; Vogt & Stephen, 1993). All of these polysaccharides consisted of the same backbone structure: **→4)-β-GlcA-(1→2)- α-Man-(1→**. Hence, in *N. rafflesiana* pitcher fluid, the acidic polysaccharide has a GlcA-Man backbone and substituted by Ara and Gal, although the linkages have yet to be fully characterised. Since the same backbone was identified in *N. pervillei*, the most basal species within *Nepenthes* (Murphy et al., 2020), the co-option of GlcA-Man synthesis for sticky pitcher fluid may be an ancestral trait.

6.6.1 Glucurono-mannan in sticky carnivorous plant secretions

We observed that removing polysaccharides from *Nepenthes* pitcher fluid via ethanol extraction caused a complete loss of its viscoelastic properties, which could then be partially recovered by re-dissolving the extract. These observations demonstrate that polysaccharides are the biopolymers responsible for this trait. These polysaccharides, containing a GlcA-Man backbone, influence the physical properties of the pitcher fluid, which in turn facilitate the insect-retaining function of the fluid.

Remarkably, the same relationship can be found in *Drosera*, a related genus of carnivorous plants within Caryophyllales with sticky flypaper traps. The principal biopolymer within their sticky capture mucilage is an acidic polysaccharide with the same GlcA-Man backbone as pitcher fluid polysaccharide (Aspinall et al., 1984; Gowda et al., 1982, 1983; Rost & Schauer, 1977). So far, GlcA-Man polysaccharides characterised from two *Drosera* species have nearly identical chemical structures, which suggests that the use of this polysaccharide for prey capture is also conserved within *Drosera* (Gowda et al., 1982). Like pitcher fluid, the physical properties of *Drosera* mucilage are fundamental to its biological function: first, the mucilage readily spreads on both natural and synthetic hydrophobic surfaces (Y. Huang et al., 2015; Kokubun, 2017), thereby increasing surface contact and adhesion; second, it has a high extensional viscosity and forms filaments upon stretching which resist breakup (Erni et al., 2011). In combination, these mechanisms likely impair the struggling movements of insects. Similar mechanisms of action have been reported for sticky pitcher fluid from *N. rafflesiana* (see Chapter 5).

In *Drosera* mucilage, the GlcA-Man polysaccharide is a large biopolymer of at least 2 x 10^6 Da and is present in relatively low concentrations but much higher than in pitcher plant fluid (4% aqueous solution) (Rost & Schauer, 1977). The polysaccharide is lightly substituted yet has a high molecular weight; thus, it is likely a long-chained biopolymer, which is a key parameter for the formation of stable filaments upon stretching (Clasen, Eggers, Fontelos, Li, & McKinley, 2006; Tirtaatmadja, McKinley, & Cooper-White, 2006). Similarly, pitcher fluid polysaccharide is also likely to be long-chained given its ability to form long filaments of liquid (Collett et al., 2015; Gaume & Forterre, 2007). A noteworthy difference between *Drosera* mucilage and pitcher fluid, however, is that GlcA-Man is present in the latter in much lower concentrations (~0.5% w/w). Despite its dilute nature, sticky pitcher fluid is highly effective at retaining insect prey (Bauer et al., 2011; Gaume & Forterre, 2007). This ability to produce adhesive secretions using small amounts of polysaccharide may be an adaptive strategy: not only is the resource cost of carnivory reduced, it may also protect the fluid from losing efficiency when diluted by rainfall. Indeed, researchers have demonstrated that *N. rafflesiana* pitcher fluid can maintain high retention rates even after a 50-fold dilution (Gaume & Forterre, 2007).

Why these two carnivorous plant genera use GlcA-Man for their sticky capture fluid and not any other polysaccharide is an interesting albeit challenging question to answer. One idea is that the carboxylic group on the GlcA monomer can be useful in manipulating the bulk material properties of the secretion (Goh, Matia-Merino, & Wee, 2015; Nep et al., 2016; Yuguchi, Urakawa, & Kajiwara, 1997). In the deprotonated form, the carboxylate groups can promote strong intermolecular interactions via electrostatic bonds with cations. Such interactions drive the gelation of other uronic acid-containing polysaccharides when cations are added, for example, gellan, alginate, and pectin (Pawar & Edgar, 2012; Thakur, Singh, & Handa, 1997; Yuguchi et al., 1997). In the protonated form, GlcA can engage in hydrogen bonding to influence the bulk physical properties of the fluid, as seen in mamaku gum, which contain a similar GlcA-Man backbone but with methylesterified GlcA (Goh et al., 2015). In the low pH environment of *N. rafflesiana* pitcher fluid, where the pH is typically lower than 3.3, the p*Ka* of GlcA (Bauer et al., 2009; Kohn & Kovác, 1978), GlcA is likely to remain protonated. This will result in overall weaker interactions than in *Drosera*, where the higher pH of 5 facilitates electrostatic interactions between deprotonated GlcA and cations. The availability of

stronger interactions, in combination with the higher concentration of polysaccharides in *Drosera* compared to *N. rafflesiana,* could account for the drastically higher zero shear viscosity in *Drosera* (two to three orders of magnitude greater than *N. rafflesiana* pitcher fluid) (Erni et al., 2011; Gaume & Forterre, 2007). This high shear viscosity, along with other relevant physical properties, may have evolved in *Drosera* to facilitate insect capture with extremely limited volumes of sticky mucilage that strongly adheres to insect cuticle (Erni et al., 2011). In contrast, while pitcher fluid is more dilute and may have weaker intermolecular interactions than *Drosera* mucilage, the insect is submerged in a much larger volume which promotes more interactions with the cuticle. Furthermore, the reduced surface tension of pitcher fluids encourages the sinking of insect prey, which is a mechanism that cannot be utilised by *Drosera* (Chapter 5). Hence, although similar GlcA-Man polysaccharides are utilised in two different carnivorous plant genera to catch prey, each genus has tailored its secretion to address specific functional requirements.

Another reason why the GlcA-Man and not another type of polysaccharide is used by carnivorous plants may be related to its chemical stability. The GlcA-Man glycosidic bond is highly resistant to acidic hydrolysis, and all the aforementioned studies used harsh conditions (prolonged treatments with concentrated acid at high temperatures) to degrade the backbone (see references in Table 6.1). The pH of pitcher fluid from *N. rafflesiana* is acidic, typically ranging below 3 (Bauer et al., 2009). Such acidic conditions may be necessary for both optimal proteolytic enzyme activity and for cultivating acidophilic microbes to facilitate prey digestion while restricting the growth of other microorganisms (Bauer et al., 2009; Gilbert, Bittleston, Tong, & Pierce, 2020). Inside the acidic and partially exposed environment of the *N. rafflesiana* pitfall trap, the secreted polysaccharide needs to resist degradation and remain functional for a couple of weeks to maximise prey capture (Bauer et al., 2009). It should be noted that pitcher fluid stickiness does decrease over time, which suggests that there are enzymes either from the plant or from microbes that can act on the polysaccharide. However, it is unclear if the loss of the side-groups alone can cause this, or if the GlcA-Man backbone itself needs to be cleaved. Interestingly, *Drosera* mucilage, despite being less acidic and completely exposed to the environment and dead insect prey, does not appear lose its stickiness after several weeks once secreted onto the stalked glands (*personal observations*). The stable GlcA-Man bond, therefore, could be well-suited to make up the backbone of these biopolymers that are essential for prey capture in carnivorous plants. Future work could explore this further

by investigating the molecular weight distribution of GlcA-Man under field conditions over time.

6.6.2 Developing tools to study GlcA-Man in other plant mucilage and exudates

A survey of prior work on GlcA-Man has revealed that this backbone architecture is far more wide-spread than previously realised (Stephen, Eagles, Mabusela, Vogt, & Lawson, 1991), having been identified from at least 28 species spread across ten plant orders (Table 6.1 & Figure 6.5). There is a large variety in the structure of polysaccharides with this backbone: some are sparsely branched (e.g., *Drosera*, *Nicotiana*, *Ornithogalum, Dicerocaryum, Vochysia*; see Table 6.1 for full list), while others are complex, where the GlcA-Man core is buried deep within extensive side-group branching (e.g., *Ceiba*, *Anogeissus, Encephalartos*, *Hakea*, *Cyathea*). What is common between all these isolates, however, is the source of the polysaccharide: GlcA-Man is consistently isolated from plant exudate, often mucilage or gum. Therefore, while we originally thought that GlcA-Man was unique to the sticky fluid of carnivorous plants, it seems that these plants have instead co-opted a conserved polysaccharide biosynthetic pathway which predates seed plants (Figure 6.5). Despite their wide-spread occurrence, almost nothing is known about the origin of GlcA-Man polysaccharides: how are they synthesised, transported, secreted and digested? Why is GlcA-Man so often associated with plant exudates? To pursue these fundamental questions, molecular tools are needed to localise and track GlcA-Man. Such tools could be carbohydrate-binding modules (CBM) or antibodies, both of which have been used to for *in situ* visualisation of specific sugar residues within plant cell walls, Golgi bodies, and seed coat mucilage (G.T., McCartney, & Knox, 2001; Knox, 2008; Vicré, Jauneau, Knox, & Driouich, 1998). A ready supply of purified GlcA-Man is needed to develop such molecular probes; based on our findings, we propose that sticky pitcher fluid is a suitable source for GlcA-Man oligomers. Once these tools are available, it can help reveal novel insights into the biosynthesis and function of GlcA-Man not just in sticky prey capture mucilage but in plant exudates overall.

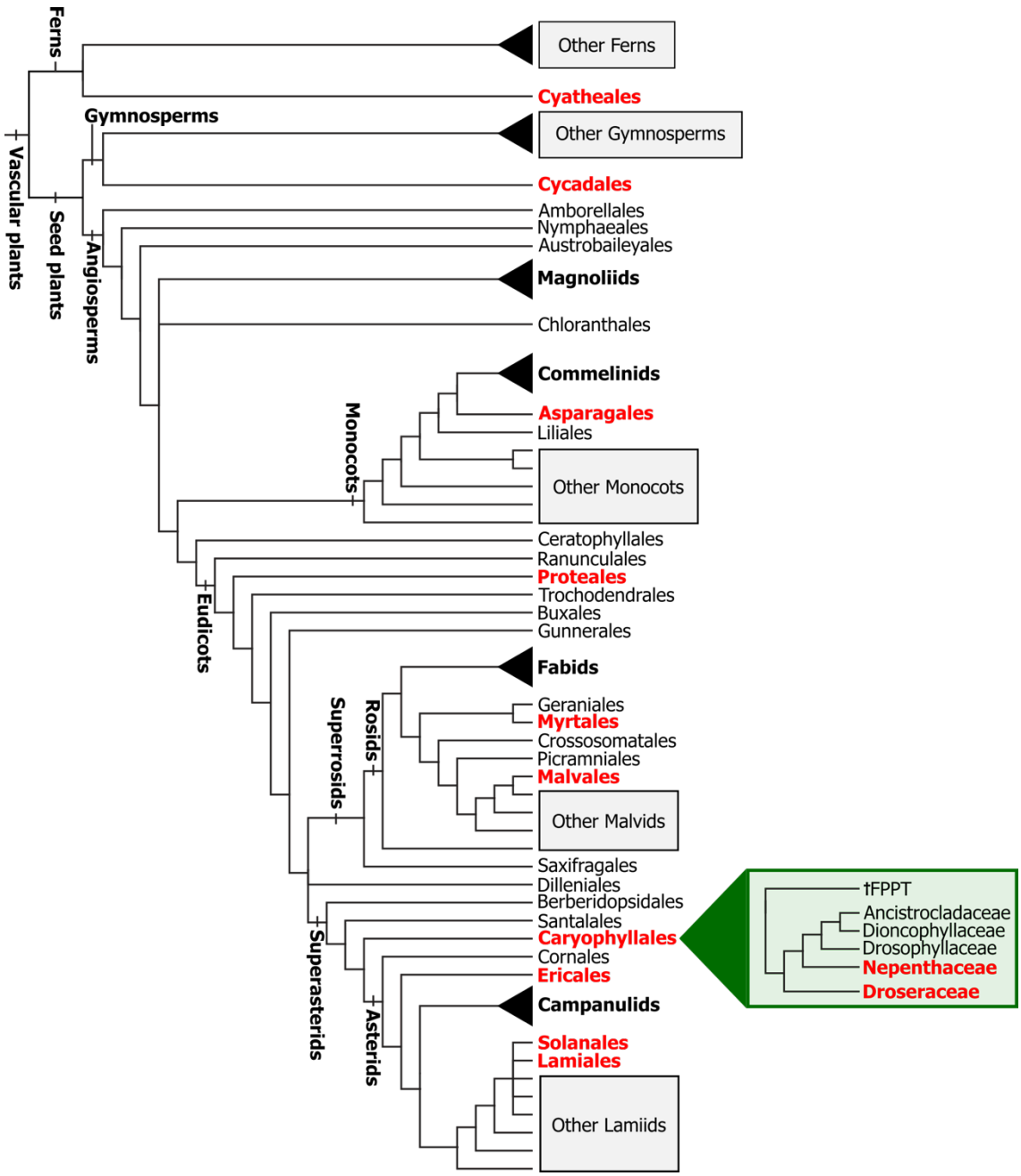

Figure 6.5: Overview of vascular plant phylogeny with an emphasis on plant orders from which polysaccharides with glucurono-mannan backbones have been characterised (bold red text). The Caryophyllales, which include the carnivorous plant families Nepenthaceae and Droseraceae, are shown in detail (green box). †FPPT: Frankeniaceae, Polygonaceae, Plumbaginaceae, Tamaricaceae. Note: the tree is meant to be a schematic representation of the wide-spread occurrence of glucurono-mannan. Thus, branch lengths do not reflect relatedness or metrics of time, and terminals were collapsed for simplification. Phylogeny based on (Heubl, Bringmann, & Meimberg, 2006; Renner & Specht, 2011; Wickett et al., 2014; Chase et al., 2016).

Table 6.1. Studies that have isolated and characterised acidic polysaccharides with glucurono-mannan (GlcA-Man) backbone architecture.

Source plant (common name; order)	Source material	Proposed function in plant or human applications (see References)	Estimated polysaccharide structural complexity✣	Side-group monosaccharides	References
Cyathea medullaris ‡ (Cyatheales)	Stem pith mucilage	Ethnobotanical use in New Zealand (e.g., as food and medicine by indigenous Māori)	Complex	Xyl, Gal, Rha, GlcA, Fuc (trace), Glc (trace)	(Wee, Matia-Merino, Carnachan, Sims, & Goh, 2014)
Encephalartos longifolius & *E. friderici-guilielmi* (Cycadales)	Gum exudate from bark and cone	NA	Complex	Gal, Rha, 3MeRha, Ara, GlcA	(Stephen & de Bruyn, 1967; Vogt & Stephen, 1993b, 1993a)
Ceratozamia spinosa (Cycadales)	Mucilage	NA	Complex	Ara, Rha, 3MeRha, Xyl, Man, GlcA	(Barone et al., 1994)
Ornithogalum thyrsoides (chincherinchee; Asparagales)	Water-soluble mucilage from leaves	NA	Simple	Ara	(Mabusela & Stephen, 1990; Stephen et al., 1991)
Agave amica^ (previously *Polianthes tuberosa*); (tuberose; Asparagales)	Extracellular polysaccharide (ECP; calli from flowers)	NA	Simple	Ara, Gal	(Honda, Inaoka, Takei, Sugimura, & Otsuji, 1996)
Hakea sericea & *H. gibbosa* (Proteales)	Gum exudate (hard nodules on stems)	NA	Complex	Ara, Gal, Xyl	(Eagles, Stephen, & Churms, 1993; Stephen et al., 1991)
Anogeissus leiocarpus & *A. latifolia* (Myrtales)	Gum exudate (Note: *A. latifolia* source of gum ghatti)	Not provided (but gums typically protect or help heal wounds)	Complex	Ara, Gal, Rha, Xyl, GlcA	(G. O. Aspinall, Auret, & Hirst, 1958a, 1958b; G. O. Aspinall, Bhavanandan, & Christensen, 1965; G. O. Aspinall, Carlyle, McNab, & Rudowski, 1969; G. O. Aspinall, Hirst, & Wickstrøm, 1955; G. O. Aspinall & Christensen, 1965; Gerald Oliver Aspinall & Puvanesarajah, 1983)

Vochysia lehmannii, V. tucanorum, V. thyrsoidea (Myrtales)	Gum exudate	Typical function of gums (see above)	Complex	Ara, Gal, Xyl	(R. Wagner et al., 2004; Ricardo Wagner et al., 2007, 2008)
Ceiba speciosa (previously *Chorisia speciosa*); (silk floss tree; Malvales)	Gum exudate	Typical function of gums (see above)	Complex	Ara, Rha, Gal, GlcA, Xyl (trace)	(Di Fabio et al., 1982)
Drosera capensis & D. binata (sundew plant; Caryophyllales)	Mucilage secreted from glandular trichomes	Sticky for insect capture & retention	Simple	Ara, Xyl, Gal, sulphate ester (trace)	(Gowda et al., 1982, 1983; Rost & Schauer, 1977)
Nepenthes rafflesiana & N. pervillei (pitcher plant; Caryophyllales)	Digestive fluid in pitchers	Sticky for insect retention	Unknown	Ara, Gal	Current study
Actinidia deliciosa & eight other species (kiwifruit plant; Ericales)	Mucilage from parts of the plant and fruit, including stem, root, stem pith, leaf	Ethnobotanical use in China (e.g., road paving, wallpaper, inks, dyes)	Complex	Ara, Fuc, Gal	(Redgwell, 1983; Redgwell, O'Neill, Selvendran, & Parsley, 1986a, 1986b)
Nicotiana tabacum (tobacco plant; Solanales)	ECP	NA*	Simple	Ara, Gal	(Akiyama, Eda, Mori, & Kato, 1984; Kunio Kato, Watanabe, & Eda, 1977; Mori & Kato, 1981)
Sesamum radiatum (sesame plant; Lamiales)	From leaves; see below	Possible lubricant during leaf expansion; pharmaceutical application (e.g., pill formulation)	Simple	Xyl, Gal	(Nep et al., 2016)
Dicerocaryum zanguebaricum (Lamiales)	From leaves (has mucilaginous trichomes)	Ethnobotanical use (e.g., medicine and shampoo)	Simple	Xyl, Gal	(Barone et al., 1996)

Notes: ✢Polysaccharide structural complexity was estimated to be 'simple' if the GlcA-Man backbone was lightly substituted with single sugar units or short branches; 'complex' structures typically featured extensive branching and diverse composition of side-group monosaccharides. ‡In *Cyathea*, the GlcA in the backbone is methylesterified, 6-*O*-methyl GlcA. ^In *Agave*, ~35% of the GlcA in the backbone is methylesterified. *NA: not available from references.

6.7 Conclusion

Pitcher fluid secreted by *N. rafflesiana* consists of an acidic polysaccharide with a GlcA-Man backbone and arabinose and galactose side-groups. This result was validated with pitcher fluid from *N. pervillei*, which is the most basal species of *Nepenthes* pitcher plants, indicating that use of this polysaccharide may be an ancestral trait within the genus. The same GlcA-Man backbone has been previously reported in another genus of carnivorous plants, *Drosera*. In both *Drosera* and *Nepenthes*, the GlcA-Man polysaccharide is the principal biopolymer component of the sticky capture fluid, suggesting a close relationship between polysaccharide structure and function. Intriguingly, while the use of GlcA-Man is wide-spread within the plant kingdom, it appears to be strictly associated with mucilaginous and sticky materials. To understand the role of GlcA-Man in plants and its biosynthesis, a reliable supply of the backbone is required to develop molecular tools. We propose *N. rafflesiana* pitcher fluid as a suitable source for GlcA-Man, where a simple work-up is sufficient to obtain oligomers of the backbone. Hence, our work opens the door for future research on this common yet poorly understood plant polysaccharide.

7 CONCLUDING REMARKS

The ability to generate adhesion in wet environments has enabled animals to survive in challenging environments with crashing waves and raging torrents, and plants to capture insects to survive in poor-quality soil. In this thesis, I investigated the adaptations and mechanisms responsible for adhesion under wet conditions in three biological study systems: net-winged midge larvae, common limpets, and carnivorous pitcher plants. I present below a selection of my key findings that have advanced not only our understanding of each system but also our general knowledge of the mechanisms of adhesion in wet conditions.

In net-winged midge larvae (Diptera: Blephariceridae), I found that their highly specialised suction organs can generate powerful and controllable attachments underwater. In the three species that I studied (*Liponeura cordata, L. cinerascens, Hapalothrix lugubris*), the overall morphology of the suction organs was conserved, with each organ possessing the following functionally important components:

i. A suction disc with dense array of microtrichia
ii. Complex internal ultrastructure with cuticular radial beams, ring channels, and fan-fibres
iii. A dense cuticular cuff to prevent collapse of the suction chamber during attachments
iv. A V-notch system with dedicated apodemes and muscles for detachment
v. A central piston with large powerful muscles to generate the pressure difference.

The suction disc microtrichia were responsible for both sealing and interlocking with surface asperities to increase shear resistance. In *L. cordata*, the sealing rim consisted of specialised flat rim microtrichia, which were distinct from the sealing region in *L. cinerascens* and *H. lugubris*, where the rim was formed by short, upright, and densely packed microtrichia. The microtrichia are stiff and spine-like cuticular structures that only make tip contact with the substrate, and on uneven surfaces, the suction disc moulds to the asperities so that the microtrichia can interlock. This suggests that the spine-like microtrichia play an important role in blephariceride attachment to rough substrates, and

indeed I found that the larvae can resist high shear forces on micro-rough substrates and to a lesser extent on coarse-rough substrates. In contrast, peak shear forces from stick insects, which are a model system for climbing insects with smooth adhesive pads, decreased dramatically on micro-rough compared to smooth substrates as both their claws and smooth pads cannot function effectively. Moreover, the blephariceridlarvae were able to generate better grip on soft compared to hard substrates, which provides further support for the spine-like nature of the microtrichia. Friction-enhancing structures like the suction disc microtrichia have been reported in a number of unrelated animals that also use suction attachments in high-drag environments (e.g., fish that live in fast-flowing rivers and the remora fish), and is thus a good example of convergent evolution in suction organs.

Although powerful suction attachments are necessary for survival in torrential waterways, it is also important to have controllable adhesion for locomotion. I discovered that the V-notch is actively controlled by a system of apodemes and muscles that can open the suction disc to neutralise the pressure difference. The V-notch apodemes are long thin cuticular structures that originate at the flanks of the V-notch and attach to muscles deep within the body of the larva. Actuation of the V-notch muscles pulls open the V-notch and floods the suction chamber, and other muscles that attach to the suction organ which work to raise and re-position the disc for the next attachment.

Net-winged midge larvae, therefore, use their suction organs with specialised structures to attach to rough wet surfaces, relying on physical mechanisms (sealing, reducing internal pressure, increasing shear resistance) to do so. An important parameter that has be investigated in more detail in future studies is biofilm: how do friction-enhancing structures like the microtrichia interact with a natural biofilm layer? How does biofilm affect whole-animal attachment performance? With the blephariceridstudy system, it is possible to explore such questions for additional mechanistic insights into biological suction attachments.

In the patellid limpet *Patella vulgata*, I have shown that the small pressures generated beneath the limpet foot are insufficient to account for the high attachment strengths that have been widely reported by previous researchers. Instead, I found that *P. vulgata*

limpets secrete adhesive mucus for alternating between powerful adhesion at low and locomotion at high tide, referred to as tidal transitory adhesion. Histochemistry and lectin staining assays of the limpet foot produced new insights into the complex glandular system, highlighting the presence of sugars and charged chemical groups in the pedal mucus. Since several sugar residues were specific to the pedal sole glands and not the side-wall, it is possible that certain sugars are needed to form the pedal adhesive mucus. Some of these sugars are likely components of glycosylated proteins, although it is also possible that they are present as free oligosaccharides. Molecular characterisation of the pedal mucus identified numerous protein sequences with predicted domains capable of binding to sugars, proteins, metal ions, and lipidic molecules. Such domains can facilitate strong intra- and intermolecular interactions that are necessary for the secretion to be an effective adhesive in seawater. Interestingly, the majority of these protein domains are also present in adhesive proteins of other mobile marine invertebrates, including sea stars, sea urchins, marine flatworms, and sea anemones. With the exception of sea anemones, these marine animals utilise temporary adhesion and make relatively rapid attachments and detachments to the substrate. While both sea anemones and limpets have extended periods of being stationary, they are still able to locomote, and this may be reflected to an extent in the molecular composition of the bio-adhesive, which bears no semblance to the cement proteins of adult barnacles and mussels that mediate permanent adhesion.

While protein sequences allow us to make predictions about the types of interactions that are possible, functional studies (e.g., with recombinant proteins or RNA knockouts) are needed to verify the exact roles of limpet mucus proteins. By providing the first transcriptome and proteome of the patellid pedal sole and by identifying promising candidates for adhesive proteins, my work facilitates such follow-up studies. Moreover, it draws interest to tidal transitory adhesion, which has received considerably less attention than temporary and permanent adhesion and requires more investigation to fill in the gaps in our knowledge.

A rather different set of mechanisms are used within the pitfall traps of *Nepenthes* pitcher plants, which rely on sticky fluids to adhere to and retain insect prey in the wet environment. First, when ants fall into sticky pitcher fluid, they become readily wetted and at times end up fully submerged. I found that the surface tension of sticky pitcher fluid is significantly lower than that of water, which resulted in hydrophobic cuticle

breaking through the pitcher fluid meniscus more easily than water. Second, once pitcher fluid wets insect cuticle, the viscoelastic properties of the fluid inhibit dewetting, causing the cuticle to remain covered by pitcher fluid residue. These residues likely facilitate subsequent re-wetting, further wetting, and eventually sinking of the insect. Third, force measurements of ant gasters dipped in and out of pitcher fluid or water showed significantly greater work was needed to retract from the pitcher fluid. This was caused by the sticky fluid wetting the insect cuticle and forming a thick filament that effectively pulled the ant gaster back into the fluid. These three properties - reduced surface tension, resistance to dewetting, and filament-forming when stretched - make pitcher fluid a deadly adhesive for insect prey.

I then investigated the chemical components of pitcher fluids that give rise to their stickiness. When ethanol was added to *N. rafflesiana* pitcher fluid, I observed a complete loss of its sticky filament-forming property, which indicated that polysaccharides were responsible for the fluid's viscoelasticity. Indeed, chemical characterisation revealed that pitcher fluid is a dilute solution of a specific type of acidic polysaccharide called glucurono-mannan. I confirmed that this type of polysaccharide is also present in *N. pervillei*, which is the most basal species of *Nepenthes* pitcher plants. This strongly suggests that the use of glucurono-mannan is an ancestral trait, although it remains to be seen if the genes involved in its biosynthesis are inactive or absent in *Nepenthes* species without sticky pitcher fluids. Interestingly, this type of polysaccharide is also used by the sundews (*Drosera*), a related carnivorous plant genus, to produce extremely sticky capture mucilage. My in-depth review of the literature identified that these polysaccharides are actually widespread in diverse non-carnivorous plants, and their physiological roles are still currently unknown. To investigate the wide range of possible roles of glucurono-mannan in plants, additional molecular tools are needed to better understand their biosynthesis and distribution within plants. Hence, the protocols I developed to isolate, purify, and characterise glucurono-mannan oligosaccharides from pitcher fluid can be used to generate new tools for research into this understudied type of polysaccharide.

The breadth of the mechanisms covered in this thesis underscores the diversity in strategies that have evolved for adhesion in wet environments. This may be a reflection

of the immense variation in surface conditions that these plants and animals need to interact with to produce adhesion underwater. For each of my study systems, I have identified novel adaptations and mechanisms that facilitate adhesion to a range of surfaces underwater. Thus, my research contributes to the general understanding of biological adhesion and also lays the foundation for future studies to further our knowledge and appreciation of the natural world.

8 APPENDIX

8.1 Supplementary material for Chapter 2

8.1.1 Supplementary Figures

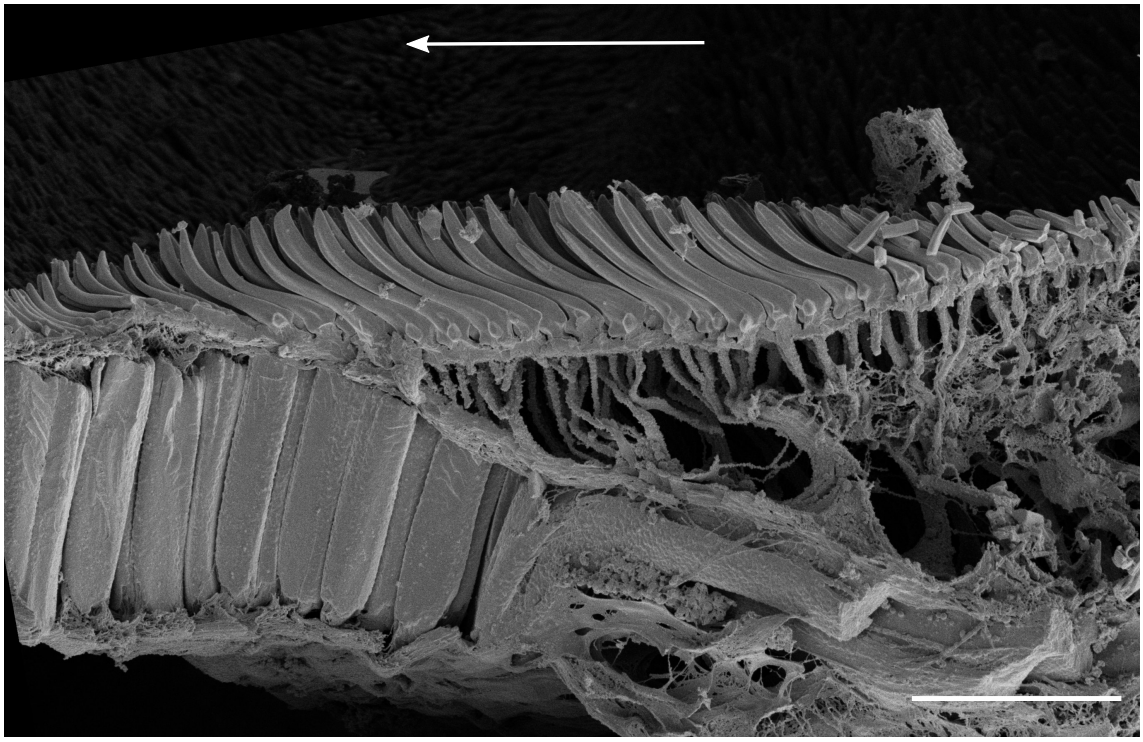

Supplementary Figure 1. Freeze-fracture SEM image of a *Liponeura cinerascens* suction disc showing spine-like microtrichia. The spine-like microtrichia are similar in shape to those found in *L. cordata* (see Fig. 2.5b). Arrow points towards the centre. Scale bar 5 µm.

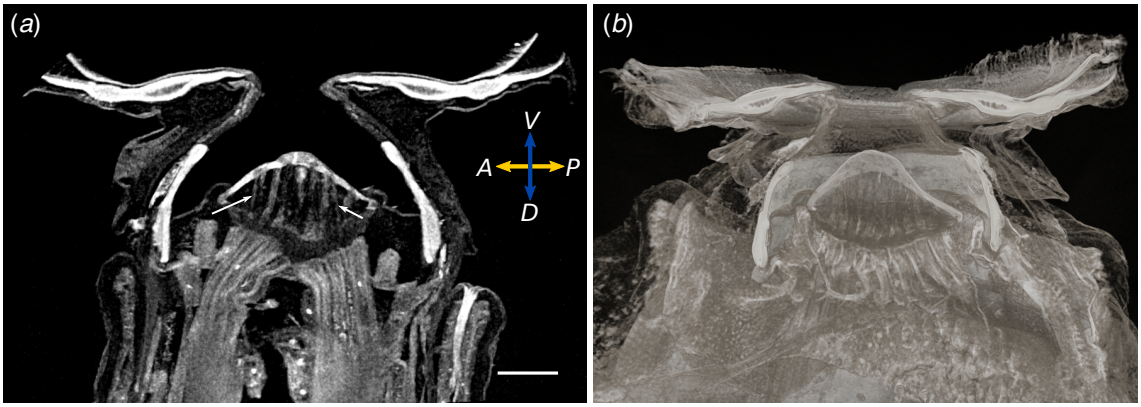

Supplementary Figure 2. Thread-like attachments between piston muscles and the piston cone. From *Liponeura cordata* micro-CT data. (a) Lateral view of piston cone shows a void volume where the thread-like attachments connect the ends of the muscles to the top of the piston cone. Arrows indicate thread-like attachments. A: anterior, P: posterior, L: left, R: right. Scale bar 50 µm. (b) 3D rendering highlighting the thin fibrous nature of the thread-like attachments.

8.1.2 Supplementary Videos

Supplementary Video 1 (SV1). Video of *Liponeura cinerascens* larva crawling on a rock in a torrential alpine river.

Supplementary Video 2 (SV2). Interference reflection microscopy (IRM) video recording of a live *Liponeura cordata* larva attaching to a surface. Scale bar 15 µm.

Supplementary Video 3 (SV3). Interference reflection microscopy (IRM) video recording of a live *Liponeura cinerascens* larva. A suction disc is in contact with the surface and pulsing of the suction disc microstructures are visible. Scale bar 20 µm.

Supplementary Video 4 (SV4). Interference reflection microscopy (IRM) video recording of a live *Liponeura cinerascens* larva attaching to a surface. When the piston is raised, the pressure inside the suction disc is lowered, and a larger portion of the disc is brought into contact. Scale bar 50 µm.

Supplementary Video 5 (SV5). Interference reflection microscopy (IRM) video recording of a live *Liponeura cinerascens* larva. The V-notch is opened from its flanks as a detachment mechanism for the suction organ. Scale bar 50 µm.

Supplementary Video 6 (SV6). Interference reflection microscopy (IRM) video recording of a live *Liponeura cinerascens* larva. The V-notch valves contract and get closer to the surface when the piston contracts and lowers the suction organ pressure. When the piston is relaxed, flickering of the valves indicate water flow. Scale bar 30 µm.

8.2 Supplementary material for Chapter 3

8.2.1 Detailed methods on substrate profilometry

White-light optical interferometry was used to measure the surface profile of the micro-rough surface (0.05 μm polishing film; Zygo NewView 200, Zygo Corporation, CT, USA). The micro-rough surface was first sputter-coated with 5 nm of iridium prior to scanning to improve the surface reflectivity, and then four random regions were imaged with both 20x and 50x objectives. The roughness average, i.e. the arithmetic mean of the deviation from the mean profile height (R_a), the root-mean-squared deviation from the mean profile height (R_q), and the peak-to-valley height difference (PV) were measured using MetroPro software (Zygo). Since values from 20x and 50x objectives were similar, only data from the 50x are shown in Table 3.1. The coarse-rough surface (30 μm polishing film) was characterised using Z-stack image focal-depth analysis (Sarmiento-Ponce et al., 2018). One hundred Z-stack images of the uncoated surface were taken using an Olympus BX51 optical microscope with a 20x objective and Leica LAS software (LAS Core v4.6.0). Height maps were calculated from the image stack using custom MATLAB script based on shape-from-focus technique and were used to obtain the R_a, R_q, and PV values.

Optical interferometry was again used to characterise the microstructured epoxy substrates (Table 3.1). Four to five regions from each uncoated substrate were imaged using the 50x objective, and only regions without artefacts were used in the final calculation. The average ± standard deviation of the R_a, R_q, and PV (from line plots) were used throughout the main text. For simplicity, when referring to the substrates in the main text, the depths of the grooves were reported to 1 significant figure (3 by 3 by 2 μm, 3 by 3 by 4 μm, and 10 by 10 by 2 μm, for widths of ridges, grooves, and ridge height).

8.2.2 Supplementary Figures

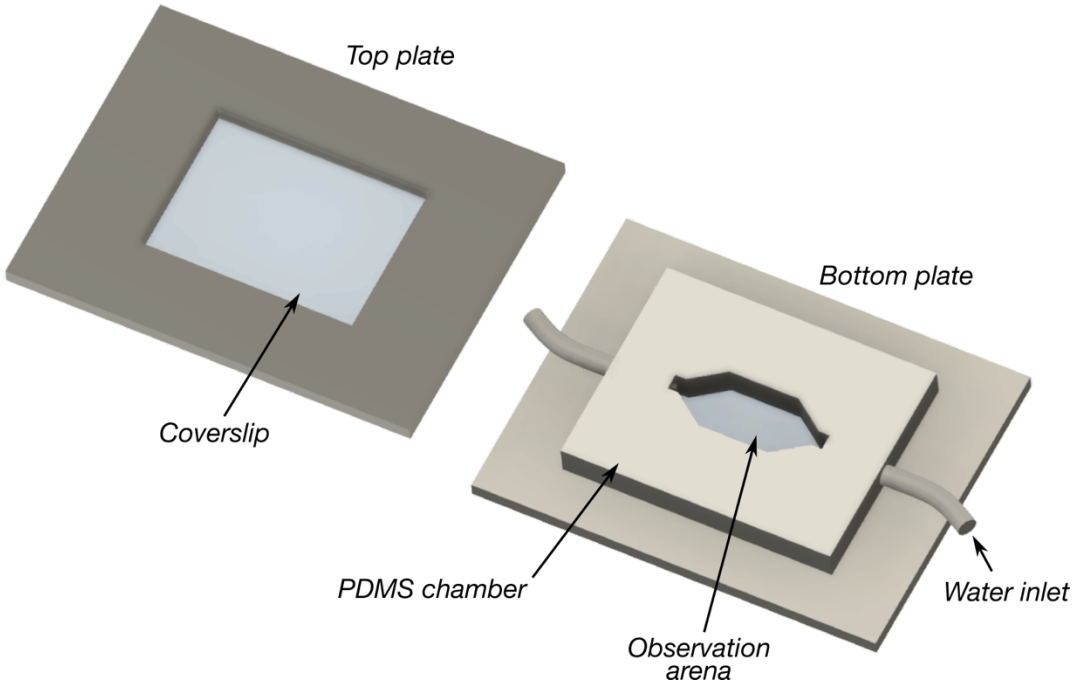

Supplementary Figure 1. Schematic of the flow-chamber used to observe blephariceridlarvae locomoting under fast-flow conditions. Two to five larvae were placed inside the observation arena, covered with the top plate, and imaged with an interference reflection microscopy. A water pump continuously circulated cooled water. Coverslip thickness: 0.16 - 0.19 mm.

8.2.3 Supplementary Videos

Supplementary Video 1. Opening of the V-notch is shown using *in vivo* interference reflection microscopy of a *Hapalothrix lugubris* larva. The larva was filmed in a custom-built flow-chamber. Note: video is slowed down 15x.

Supplementary Video 2. The V-notch opens when the larva detaches and re-attaches its suction organ. Note: video is slowed down 10x.

8.3 Supplementary material for Chapter 4

8.3.1 Supplementary Videos

Supplementary Video 1. When a *P. vulgata* limpet is detached then returned to a surface, it leaves behind a gel-like adhesive mucus (BPAM) that is resistant to degradation in saltwater.

Supplementary Video 2. Despite a clear disruption of the contact area, the limpet remained strongly attached.

8.3.2 Supplementary Figures & Tables

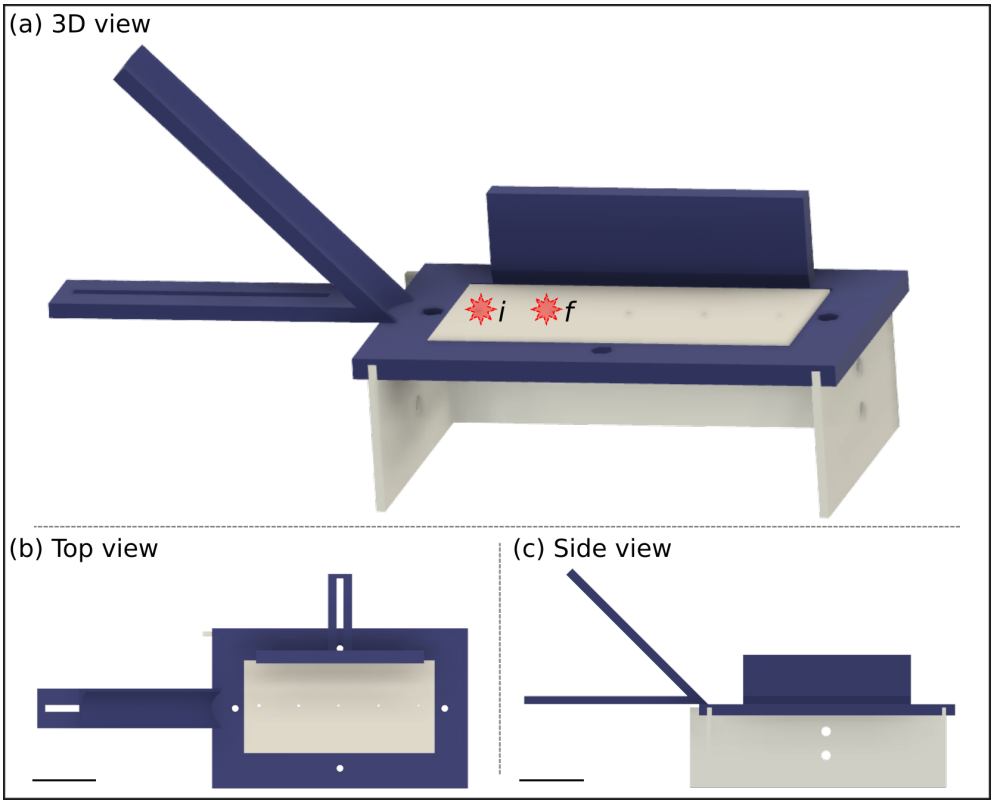

Supplementary Figure 1. Schematic of the *in vivo* pressure sensor rig made using 3D printed PLA components and laser-cut acrylic sheets. (a) 3D view, showing the 45° ramp used to accelerate the ball bearing. Red stars indicate initial *i* and final *f* position of limpets during free locomotion trials. (b) & (c) Top and side view of the set-up, respectively. Scale bar 40 mm.

Supplementary Figure 2. Example of a limpet that managed to crawl up and adhere to plastic mesh.

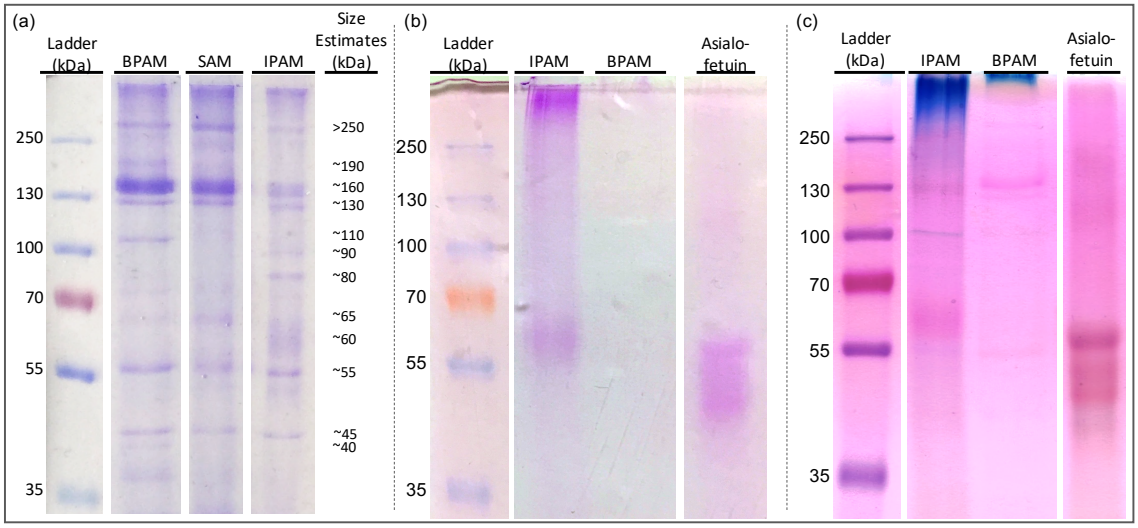

Supplementary Figure 3. SDS-PAGE gels of protein extracts from *P. vulgata* pedal sole mucus stained for additional information. BPAM: bulk primary adhesive mucus; SAM: secondary adhesive mucus; IPAM: interfacial primary adhesive mucus. (a) Coomassie Blue stain identified at least 11 prominent protein bands, ranging from ~40 to greater than 250 kDa. Note the approximate protein band sizes to the right of the gel image. (b) Smeared purple bands from PAS staining confirms that the presence of glycosylation for specific proteins within IPAM and not in BPAM. The strong smearing at the top of the gel indicates large complexes that failed to properly migrate into the gel. Asialo-fetuin from bovine serum used to as a reference glycoprotein to illustrate smearing pattern. (c) Multi-coloured bands from Stains-All highlight several differences between BPAM and IPAM (blue for highly acidic proteins and Ca^{2+}-binding proteins, purple for intact proteoglycans, and pink for weakly acidic proteins).

Supplementary Figure 4. Clustal alignments for SCO-spondin, Reprolysin, and Tc-MUC. (a). Multiple SCO-spondin precursors and *P-vulgata_3* alignment. *Continued overleaf.*

SCO-spondin *Gallus gallus* (truncated) and *P-vulgata_3* alignment showing SCOR regions

(b) Reprolysin CDD conserved sequences and *P-vulgata_8* alignment

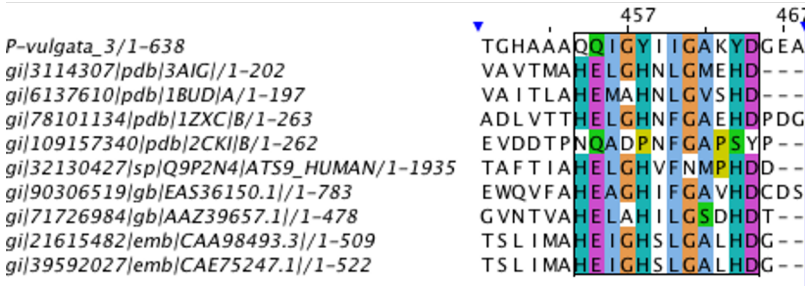

(c) Tc-MUC and *P-vulgata_14* alignment

Supplementary Table 1. Transcriptome sequencing and assembly results of mRNA isolated from limpet pedal sole.

Sequencing output	
Total raw reads (M)	256.35
Total clean reads (M)	220.91
Total clean bases (Gbp)	33.14
High quality reads	
Q20 (%)	97.74%
Q30 (%)	94.30%
De novo assembly result	
Transcript number	86,396
Total size (bp)	81,369,009
Transcript N50 length (bp)	1,860
Transcript mean length (bp)	941
GC percentage (%)	35.59%

Supplementary Table 2. Functional annotation across seven databases.

Values	Total	Nr	Nt	SwissProt	KEGG	KOG	InterPro	GO	Intersection	Overall
Number	86,396	32,756	12,014	22,852	24,514	21,018	24,900	17,754	4,510	37,261
Percentage	100%	37.91%	13.91%	26.45%	28.37%	24.33%	28.82%	20.55%	5.22%	43.13%

Supplementary Table 3. List of limpet protein sequences tested with ISH.

Trinity assigned ID	**Manuscript ID**
Unigene47813	P-vulgata_1
Unigene46021	P-vulgata_2
CL3399.Contig1	P-vulgata_3
CL6799.Contig2	P-vulgata_4
CL6346.Contig2	P-vulgata_6
CL4559.Contig2	NA*
Unigene2524	NA
Unigene11734	P-vulgata_7
Unigene35700	NA
CL3409.Contig2	NA
Unigene36817	P-vulgata_8
CL489.Contig2	NA
CL5700.Contig1	P-vulgata_10
Unigene11944	P-vulgata_11
CL1231.Contig2	P-vulgata_12
Unigene15438	P-vulgata_14

*: Not applicable (NA), where a manuscript ID was not generated for a given Trinity-assigned protein ID as it was not included in downstream manual annotation and ISH was unsuccessful.

Supplementary Table 4. List of primers used to synthesise ISH probes

Manuscript ID	Primer Sequence
FW_P-vulgata_1_T7	GGATCCTAATACGACTCACTATAGGTTCCACATCAACCTTGTTCACC
FW_P-vulgata_2	TTTACGAATGTACGGCATCACC
FW_P-vulgata_3	TGTGATGGAGCAAACTGTACCC
FW_P-vulgata_4	GAAAACGACCATGTTCCAATCC
FW_P-vulgata_6_T7	GGATCCTAATACGACTCACTATAGGGCTGGGTTTCTCATTAGGTTCG
FW_P-vulgata_7_T7	GGATCCTAATACGACTCACTATAGGTCCTGGTGATTTCAATGGTAGC
FW_P-vulgata_8	ATTCTATCGGCGCATATTACGG
FW_P-vulgata_10	CAAAAAGAACGTGTTCCAGTCG
FW_P-vulgata_11	CTGTTGTGGTTTACAACCATGC
FW_P-vulgata_12_T7	GGATCCTAATACGACTCACTATAGGCACCCACCACAGTAGTTAGAGACG
FW_P-vulgata_14_T7	GGATCCTAATACGACTCACTATAGGTTCCACTATGCGACACAAGAGC
FW_PV2524_T7	GGATCCTAATACGACTCACTATAGGTTTCGATCTAGGCAGAGAAATCC
FW_PV3409_T7	GGATCCTAATACGACTCACTATAGGTTCGAATTTTGCTCAACAGTGC
FW_PV35700_T7	GGATCCTAATACGACTCACTATAGGGGCCTCAAAACAGGTACATTGG
FW_PV4559	TTGTCTTGGAAGGAAACACAGC
FW_PV489	GGAGATATTGGTGCTGTTGACG
RV_P-vulgata_1	CAAAAGAAAAGGACGCAGATCC
RV_P-vulgata_2_T7	GGATCCTAATACGACTCACTATAGGCAATGCCACAGTTACAGTTCC
RV_P-vulgata_3_T7	GGATCCTAATACGACTCACTATAGGTGAAATCTTTTCCAGGGTTTGG
RV_P-vulgata_4_T7	GGATCCTAATACGACTCACTATAGGCAGGGTTTCCATCGAAGTTACC
RV_P-vulgata_6	TGCAAATGTGATATGCTCAACG
RV_P-vulgata_7	GATACGTGGTCCCAGAGAATCC
RV_P-vulgata_8_T7	GGATCCTAATACGACTCACTATAGGAAAGGTACAATGTGTGCGATCC
RV_P-vulgata_10_T7	GGATCCTAATACGACTCACTATAGGTAAACGTGTCTTGGATGGATGG
RV_P-vulgata_11_T7	GGATCCTAATACGACTCACTATAGGACTGGCCGTACTTGTCAAAAGG
RV_P-vulgata_12	AAATTACGTCGGAATGAATTAGCC
RV_P-vulgata_14	CCTTACGAAAAGGATGGATTCG
RV_PV2524	ACTAGCTCTGGTGGCTTACACG
RV_PV3409	GTAGAATGTACCGGCGAAGAGC
RV_PV35700	TACATCGAGTTGTCCCAACAGC
RV_PV4559_T7	GGATCCTAATACGACTCACTATAGGTTTCCAGGTCACCATCATAACG
RV_PV789_T7	GGATCCTAATACGACTCACTATAGGTCAATTTTATTCGGACGTGATCC

8.3.3 Additional information on sequence quality check, trimming, and assembly

Quality check and trimming

Raw reads were filtered to remove reads with adaptors, reads with >5% unknown bases, and low quality reads (defined by BGI as reads in which the proportion of bases with a quality score < 10 was greater than 20%).

Assembly settings

The full software setting for read alignment using bowtie2, v2.2.5 was as follows: Parameters: -q --phred64 --sensitive --dpad 0 --gbar 99999999 --mp 1,1 --np 1 --score-min L,0,-0.1 -I 1 -X 1000 --no-mixed --no-discordant -p 1 -k 200.

8.3.4 Detailed protocol of in situ hybridization (ISH)

RNA probe synthesis. Primers were designed with Primer3 (http://primer3.ut.ee, v4.1.0) and for antisense/sense probe production a T7/SP6 promoter region was added at the 5`end of the reverse/forward primers. cDNA was generated from isolated total RNA of the limpet tissue, (same limpet individual as the one sent for transcriptome sequencing) using Transcriptor First Strand cDNA Synthesis Kit (Roche). PCR reactions were performed with Q5® High-Fidelity DNA Polymerase (NEB) and their correct length verified on a 1 % agarose gel. The PCR products were purified with Wizard® SV Gel and PCR Clean-Up System (Promega). To synthesize single stranded digoxigenin-labelled RNA probes, T7/Sp6 polymerase (Promega) and DIG labelling mix (Roche) were used according to manufactures' protocols. DIG-labelled RNA probes were precipitated with isopropanol and bands length and intensity checked on a 1 % agarose gel. RNA probes were diluted in hybmix to an estimated concentration of 5ng/µl (based on gel images) and stored at -80°C until usage. Probes were used at a final concentration of approximately 0.2 ng/µl. We repeatedly observed unspecific background staining using sense probes, which should not be able to bind to any mRNA specifically (supplementary figure 4a). After extensive troubleshooting we realised that the precipitation with isopropanol was not sufficient to eliminate unbound DIG-labelled nucleotides, which were the source of this background staining. Please also see *background staining in the in situ hybridization experiments* addressing this issue.

Paraffin section *in situ* hybridization. For section *in situ* hybridization, Patella tissue was dissected and fixed in 4% PFA in PBS overnight. After several washes in PBS, the tissue was dehydrated in an ethanol series until 100% ethanol. Tissue pieces were treated with xylene for 8 and 5 min and immediately placed in 60°C preheated liquid paraffin wax. The tissue was moved to fresh preheated paraffin wax every hour for three times and left at 60°C overnight. Afterwards, the samples were moved to room temperature for the paraffin blocks to harden. The paraffin-embedded tissue was then cut into 14 µm thick sections using a Microm HM 340 E microtome. The sections were placed on Superfrost ultra plus® slides (Thermo scientific) and heated in an oven at 60 °C for 1 h and allowed to cool down for 15 min. After dewaxing in xylene and rehydration, sections were postfixed in 4% PFA in PBS for 20 min, washed several times in PBS and treated with 0.2 M HCl for 10 min. Following washes in PBS, sections were treated with Proteinase K (20 µg/ml) for 20 min. Sections were postfixed in 4 % PFA in PBS for 5 min, washed in PBS and placed in 0.1 M triethanolamine (pH 8) containing 0.5 % acetic anhydride for 20 min (exchanging the solution after 10 min). Afterwards sections were washed and gradually dehydrated with ethanol. To dry the sections, Chloroform was dropped on the sections and allowed to evaporate. Slides were placed in a humidity chamber and incubated with hybmix at 55 °C for 30 min. Sections were incubated with RNA probes diluted in hybmix (0.2 ng/µl) overnight at 55 °C. To avoid evaporation of the liquid, sections were covered with fresh parafilm pieces during this step. The following day the sections were incubated in 50 % formamide in 2x SSC at 62 °C (3 x 20 min). After washes with 1x SSC and PBS, sections were blocked in blocking reagent (Roche) for 1 h at 4 °C. Sections were incubated with Anti-digoxigenin-AP Fab fragments (Roche) 1:2000 in blocking reagent overnight at 4 °C. Following several washes, the signal was developed using the NBT/BCIP system (Roche) at 37 °C. Colour reaction was stopped with ethanol and sections washed several times with PBS. Sections were mounted in Mowiol® 4–88 (Roth, Germany), prepared according to the manufacturer's protocol and images were taken with a Zeiss Axioscope A1 microscope.

Background staining in the *in situ* hybridization experiments. For ISH negative control samples, we used DIG-labelled RNA sense probes that should not bind to any mRNA sequences. However, we repeatedly observed unspecific background staining in the negative controls in glands ~100-150 µm from the epithelium, in the epithelium and secreted mucus (Supplementary Figure 5a). No staining was observed when no ISH

probes were added to the samples (not shown). For interpretation of ISH results in this study, we only considered probes that consistently stained differently to the background in two to three repeated ISH experiments. Using *P-vulgata_3* as an example (Supplementary Figure 5c; modified version of Figure 3b), the positive stainings were distinct in intensity and locality compared to background stainings (Supplementary Figure 5a). Subsequent troubleshooting by B.L. in Mons, where all the ISH experiments were conducted, identified the probable cause as short DIG-labelled nucleotides that freely bound to unspecific regions of the tissue. When negative control probes were additionally purified through a Micro Bio-Spin® Chromatography Column (Biorad) and re-tested, the unspecific background staining issue was resolved (Supplementary Figure 5b). Unfortunately, data collection for the project had concluded several months prior to this clarification, and the lead author had already returned to Cambridge, UK, hence ISH could not be repeated again. Nevertheless, by carefully considering the differences between background and signal staining patterns and by upholding a high threshold for inclusion, we are confident that we have reported valid results for the five candidate probes (shown in Figure 4.7 of the main text).

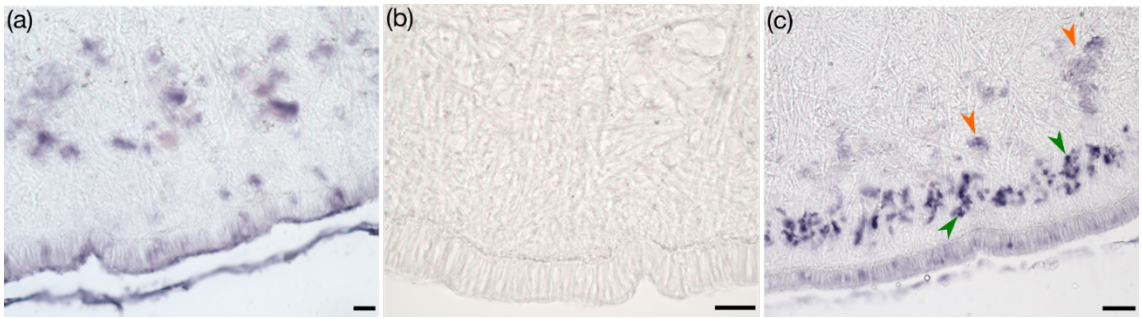

Supplementary Figure 5. Unspecific background staining due to DIG-labelled nucleotides present in the ISH probes. (a) Unspecific background stains in the negative control samples were diffuse and localised to ~100-150 µm from the epithelium. Scale bar 20 µm. (b) When negative control probes were additionally purified through microspin columns, background stains were eradicated. Scale bar 20 µm. (c) *P-vulgata_3* staining, showing the distinct staining pattern between the signal (green arrows) and the background (orange). Based on our prior experiences with ISH, the sharp intense stains indicated by the green arrows are indicative of positive stains. Additionally, the background and positive stains were segregated by location within the tissue. ISH probes that did not fit these criteria were not included in the analysis.

8.3.5 Additional information on PX26-30DV pressure sensor calibration

The pressure sensor was calibrated by connecting a syringe pump to an analogue pressure gauge (WIKA Instruments Ltd, UK), which in turn was connected to the sensor port. The

syringe pump was used to increase the pressure (relative to ambient) from 0 to +40 kPa in 10 kPa bar steps, and the same to decrease the pressure from 0 to -40 kPa. Sensor output voltage was then plotted against pressure, and a linear regression (intercept set to 0) was fit to obtain the relationship Pressure (kPa) = 8.6979 * Volts (V), with a Pearson's correlation r^2 = 0.9995 (see below). This linear model was used to analyse the in vivo sub-pedal pressures from *P. vulgata*.

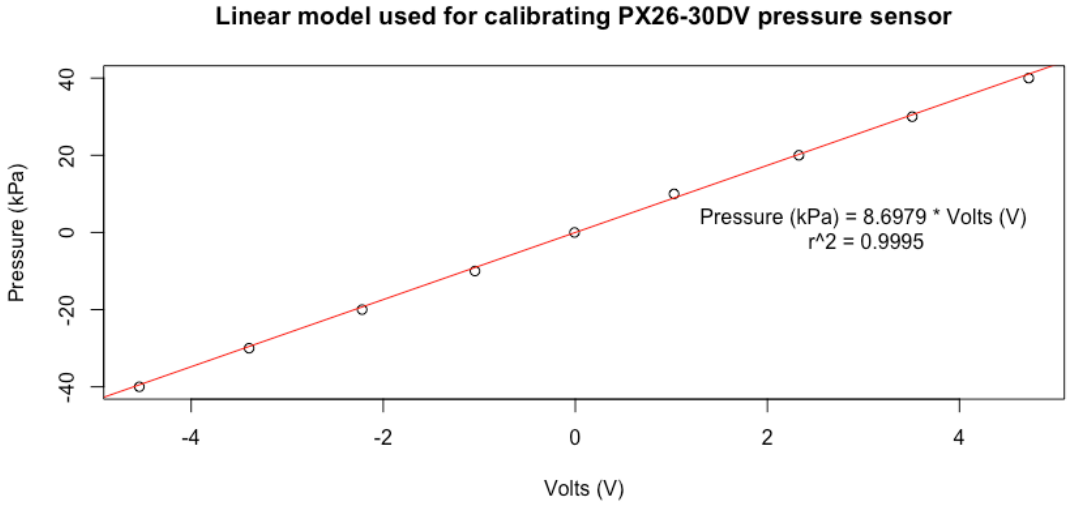

8.3.6 Additional information for manual vertical pull-off experiments

For the trial shown in Figure 3c, the limpet had been disturbed previously and had clamped down, corresponding to the slight negative pressure (around -1.4 kPa). The pull-off force was applied by gripping the limpet's shell with fingers and pulling upwards starting from ~20s until detachment at ~25s. Because of this method, we cannot state with confidence whether the applied detachment force was constant during the whole duration. For this particular trial, we observed an initial negative peak of around -2 kPa, followed by a second much larger peak of -5.7 kPa, and then the pressure returned to -2 kPa for ~3 s before full detachment. One possible explanation for this second dip is that as the limpet was being pulled, it attempted to clamp down, which would result in a decrease in sub-pedal pressure. Once it relaxed, the pressure returned to around -1.4 kPa, before being fully detached. We wrote in the Discussion that clamping can lead to a sub-pedal pressure reduction, although this still requires adhesion between the contact area and the surface, which we propose is provided by adhesive mucus.

8.4 Supplementary material for Chapter 5

8.4.1 Supplementary Figures & Tables

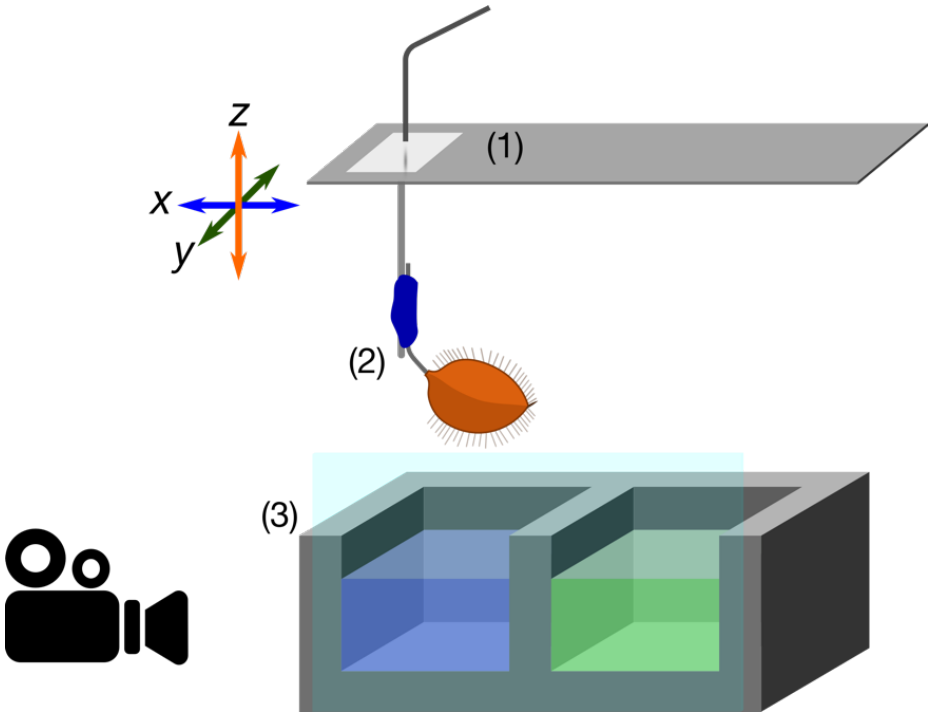

Supplementary Figure 1: Schematic of the fibre-optic force transducer set-used to quantify forces acting on ant gaster upon retraction from fluids. (1) A fibre optic sensor signal reflecting off the reflective metal foil glued on a thin metal beam was used as the translate displacement into forces. (2) Atta cephalotes gaster was mounted onto the force transducer with dental impression wax. The metal beam and the gaster could be moved in three dimensions through a motor stage. (3) A 3D printed aquarium with two contiguous wells, one for water (blue) and the other for pitcher fluid (green). After testing in water, the gaster was moved to pitcher fluid and tested without changing the experimental set-up. Video recordings were synchronised with the force transducer movements.

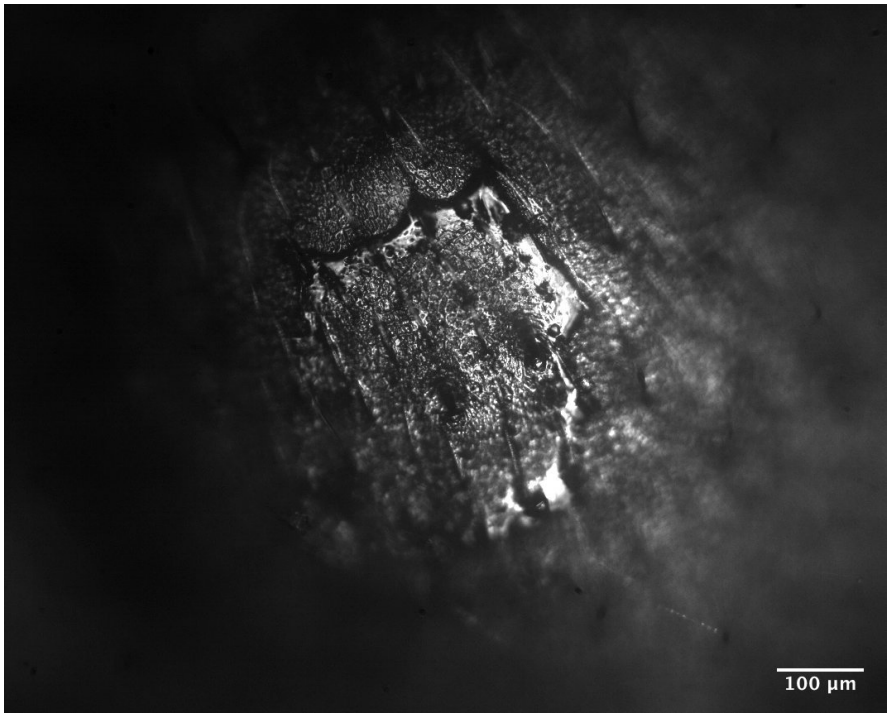

Supplementary Figure 2: Pitcher fluid does not easily dewet from inset cuticle, as seen in this light microscopy image of an ant gaster after a droplet of sticky pitcher fluid was placed on the surface and left to dry.

8.4.2 Supplementary Videos

Supplementary Video 1. Example video of an ant retention trial. Once an ant falls onto water, it fails to break the meniscus and floats, where it tries to walk on the water surface. In pitcher fluid, however, an ant readily breaks through the meniscus and sometimes sinks below the surface.

Supplementary Video 2. IRM video recording of water being withdrawn from a glass surface using a microcapillary tube.

Supplementary Video 3. IRM video recording of pitcher fluid being withdrawn from a glass surface using a microcapillary tube.

Supplementary Video 4. Video recording of water evaporating and dewetting from the cuticular surface of an ant gaster. Note that the cuticle is clean and free of residues, in contrast to Supplementary Figure 2.

Supplementary Table 1. Surface tension measurement values including Worthington numbers.

SAMPLE	BOND NUMBER	WORTHINGTON NUMBER	SURFACE TENSION	VOLUME (μL)
AP1	0.26	0.78	59.55	11.86
AP1	0.33	0.77	51.64	15.21
AP1	0.32	0.74	55.69	15.83
AP1	0.33	0.73	47.74	13.36
AP1	0.25	0.72	60.26	11.14
AP2	0.33	0.78	50.54	15.06
AP2	0.33	0.77	53.13	15.64
AP2	0.32	0.77	55.70	16.37
AP2	0.32	0.76	53.72	15.71
AP2	0.32	0.72	52.77	14.59
AP3	0.31	0.77	65.05	19.19
AP3	0.32	0.76	59.36	17.30
AP3	0.31	0.76	65.84	19.17
AP3	0.32	0.76	56.10	16.32
AP3	0.31	0.76	65.41	18.97
AP4	0.32	0.77	56.80	16.80
AP4	0.33	0.77	51.52	15.24
AP4	0.32	0.77	56.23	16.63
AP4	0.32	0.77	55.07	16.26
AP4	0.32	0.77	60.60	17.87
AP4-BRI	0.27	0.81	62.12	12.92
AP4-BRI	0.26	0.81	66.70	13.85
AP4-BRI	0.26	0.80	68.04	13.93
AP4-BRI	0.26	0.80	66.20	13.54
AP4-BRI	0.26	0.80	65.30	13.27
AP5	0.26	0.74	58.50	11.14
AP5	0.25	0.74	64.28	12.15
AP5	0.24	0.67	63.02	10.79
AP5	0.24	0.66	61.52	10.32
AP5	0.24	0.64	59.11	9.65
AP5-BRI	0.26	0.80	68.56	13.95
AP5-BRI	0.26	0.79	68.05	13.69
AP5-BRI	0.32	0.79	63.39	19.11
AP5-BRI	0.31	0.78	63.69	18.99
AP5-BRI	0.32	0.77	62.08	18.41
GP1-BRI	0.32	0.77	54.53	16.15
GP1-BRI	0.32	0.77	57.13	16.90
GP1-BRI	0.31	0.76	62.32	18.16
GP1-BRI	0.31	0.74	59.44	16.79
GP1-BRI	0.30	0.67	59.12	15.23
GP3-BRI	0.27	0.81	58.37	12.08
GP3-BRI	0.27	0.81	60.05	12.41
GP3-BRI	0.27	0.80	58.41	11.99
GP3-BRI	0.27	0.80	55.84	11.36
GP3-BRI	0.27	0.79	58.13	11.73
GP4-BRI	0.26	0.81	68.57	14.15
GP4-BRI	0.26	0.80	69.37	14.17
GP4-BRI	0.26	0.80	69.55	14.20
GP4-BRI	0.26	0.79	67.76	13.76

GP4-BRI	0.25	0.78	68.04	13.58
WATER	0.25	0.80	72.62	15.07
WATER	0.25	0.80	72.79	15.11
WATER	0.26	0.80	71.81	14.89
WATER	0.26	0.80	71.13	14.74
WATER	0.26	0.80	71.82	14.86
WATER	0.25	0.80	72.11	14.87
WATER	0.25	0.80	73.17	15.08
WATER	0.25	0.80	72.97	15.03
WATER	0.25	0.80	72.23	14.87
WATER	0.25	0.79	72.06	14.80
XG 0.5%	0.35	0.84	53.41	14.25
XG 0.5%	0.35	0.81	52.84	13.65
XG 0.5%	0.36	0.89	53.78	15.20
XG 0.5%	0.35	0.83	53.45	14.07
XG 0.5%	0.35	0.85	54.62	14.78
XG 0.2%	0.32	0.73	60.36	15.76
XG 0.2%	0.32	0.74	59.84	15.79
XG 0.2%	0.32	0.75	60.51	16.12
XG 0.2%	0.32	0.73	59.21	15.52
XG 0.2%	0.32	0.74	60.29	15.92
XG 0.1%	0.31	0.75	66.78	18.48
XG 0.1%	0.31	0.75	66.59	18.53
XG 0.1%	0.30	0.72	66.73	17.68
XG 0.1%	0.31	0.73	66.77	18.04
XG 0.1%	0.31	0.74	66.89	18.36

8.5 Supplementary material for Chapter 6

8.5.1 Supplementary Figures & Tables

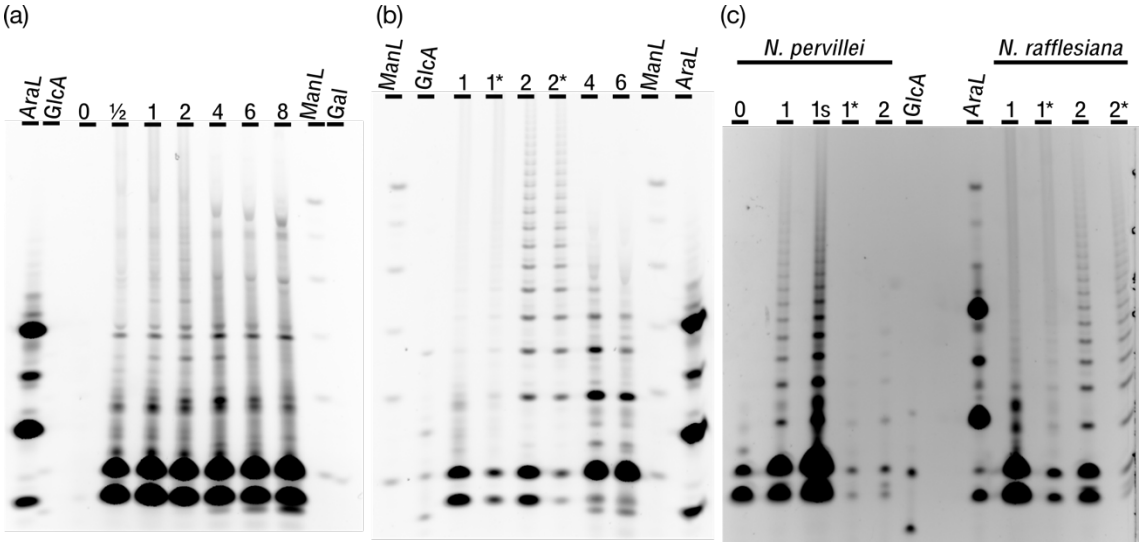

Supplementary Figure 1. PACE gels of *Nepenthes* pitcher fluid polysaccharide hydrolysis and standards. (a) PACE analysis of *N. rafflesiana* pitcher fluid raw polysaccharide extract via acid hydrolysis protocol version 1. Samples were taken at time-points from 0 to 8h per lane labels. Standards provided a putative identification of the released monomers, which were then verified using HPAEC-PAD. Standards: Ara ladder of 1 to 4 units (AraL); GlcA monomer (note: faint bands visible, of which the lower one is GlcA); Man ladder of 1 to 6 units (ManL); Gal monomer. As Man and Gal monomers migrated close to each other, the two could not be differentiated in *N. rafflesiana* hydrolysis samples. (b) Acid hydrolysis protocol version 3 with *N. rafflesiana*, which included two additional ethanol (EtOH) washes after 1 and 2h hydrolysis. Samples taken immediately after EtOH wash are marked with * (1* & 2*). Note that AraL sample was affected by being at the edge of the gel. (c) Comparison between *N. pervillei* and *N. rafflesiana* polysaccharide samples. 1s: supernatant from EtOH wash after 1h hydrolysis. 1* & 2*: same as in (b). Note the AraL contained oligosaccharides Ara_1 to Ara_4 and unresolved oligosaccharides.

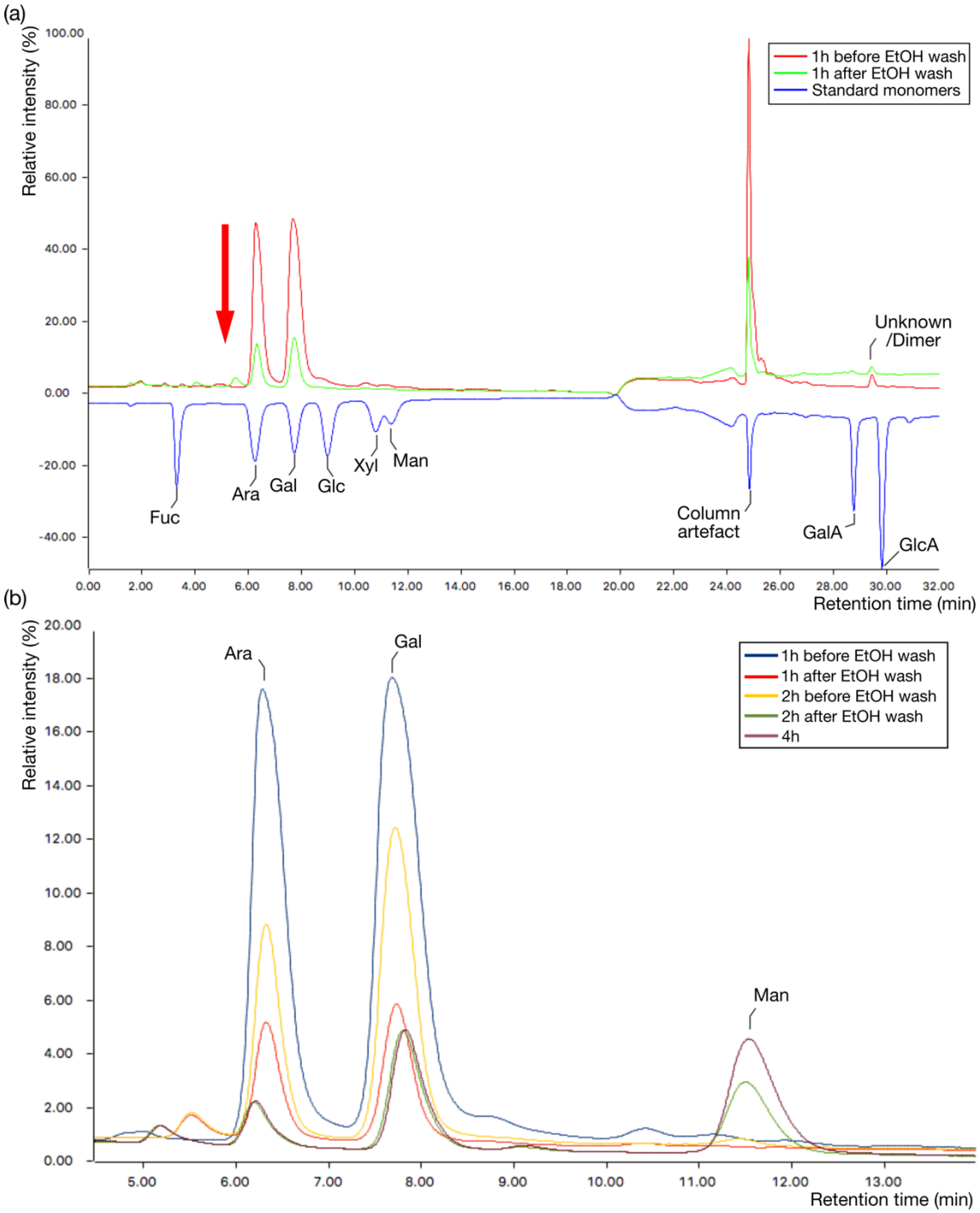

Supplementary Figure 2. Effect of additional EtOH wash on monomer composition during partial acid hydrolysis. (a) Ara and Gal were hydrolysed in the first hour of hydrolysis, along with a trace amount of unknown/dimer (red spectrum). Immediately after EtOH wash, there was a clear reduction in all the monomers in the sample. Standard monomers are shown as an inverted trace (blue). (b) Highest amounts of Ara and Gal were obtained within 1h of hydrolysis. After 2h of hydrolysis, additional Ara and Gal were released but not to the same extent as in the 1h hydrolysis. Upon second EtOH wash (yellow trace) and continued hydrolysis, there was no further increase in Ara and Gal (green and purple traces for 2 and 4h, respectively). In contrast, Man was not detected until after 2h, then increased with further hydrolysis. Note: 2h after EtOH wash and 4h spectra were shifted by 0.4 minutes to align with the other spectra after checking that the peaks matched the respective standards.

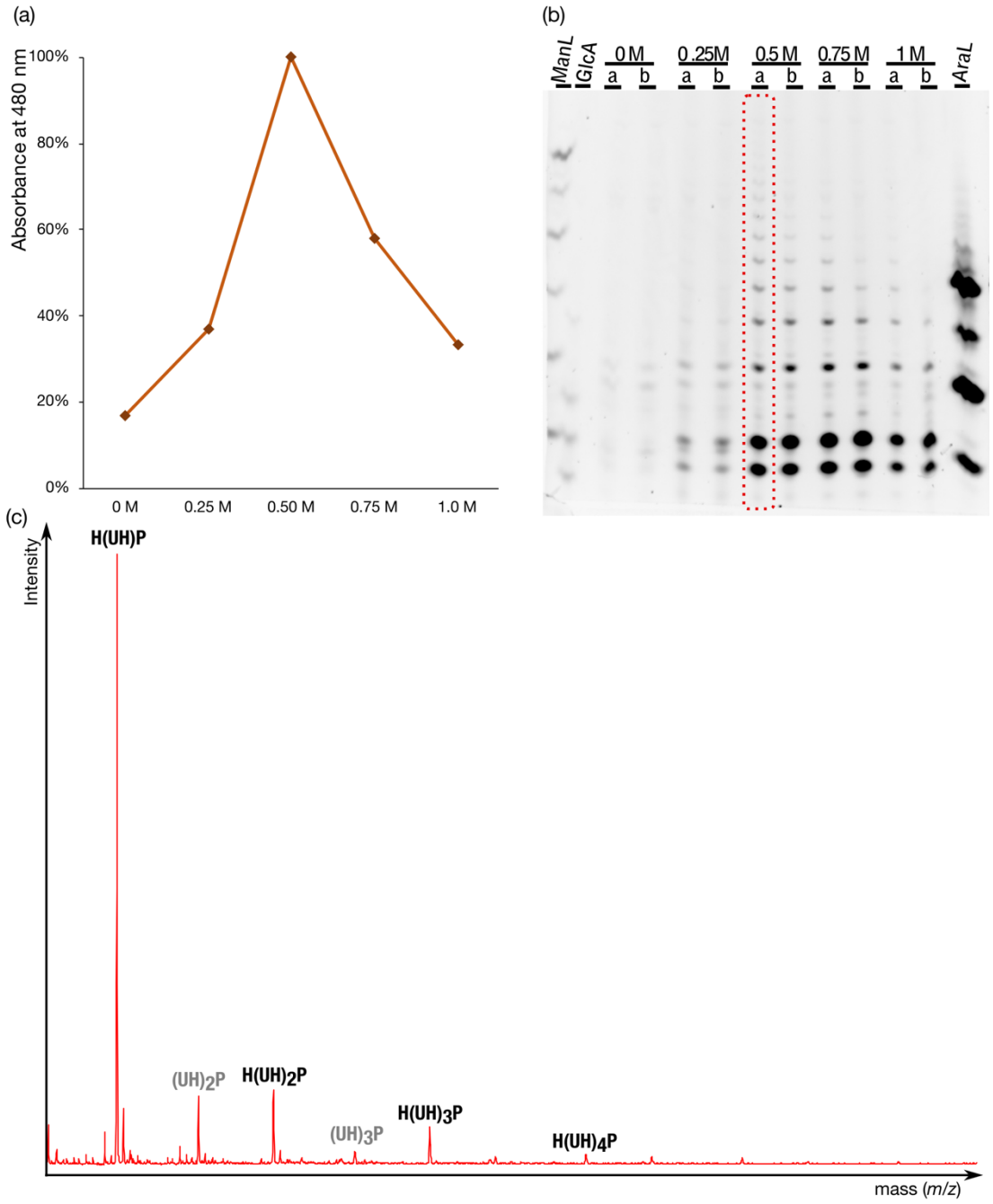

Supplementary Figure 3. Analyses on *N. rafflesiana* raw polysaccharide extract after DEAE-Cellulose column chromatography. (a) Relative sugar levels present in each column elution fraction ranging from 0 to 1.0 M of NaCl, measured using phenol-sulfuric colorimetry test (absorbance at 480 nm wavelength). There is a broad elution profile with a peak in the 0.5 M fraction. (b) PACE analysis of the column fractions after 2 and 3h acid hydrolysis supported the colorimetric test results, with the highest intensity and number of bands observed with the 0.5 M fraction. Note how the longer repeats either disappear or decrease in intensity going from 2 to 3h hydrolysis. These ladders were similar to those seen in Figure 6.2a & 6.4a. The 0.5 M fraction after 2h hydrolysis was selected for MALDI-TOF-MS (outlined in red). (c) MALDI-TOF-MS spectrum confirmed that the repeating unit was a hexuronic acid-hexose dimer **(UH)**, although the individual oligosaccharides also contained a single pentose mass. All the detected peaks corresponded to **(UH)** with an additional hexose and/or pentose, showing that the Ara and Gal side-groups were yet to be completely removed.

9 BIBLIOGRAPHY

Adam, J. H. (1997). Prey Spectra of Bornean Nepenthes Species (Nepenthaceae) in Relation to their Habitat. *Pertanika Journal of Tropical Agricultural Science*, *20*, 121–133.

Adlassnig, W., Lendl, T., Peroutka, M., & Lang, I. (2010). 2. Deadly Glue - Adhesive Traps of Carnivorous Plants. In J. von Byern & I. Grunwald (Eds.), *Biological Adhesive Systems* (pp. 15–25). Springer Vienna.

Afgan, E., Baker, D., Batut, É., Beek, M. van den, Bouvier, D., Čech, M., … Blankenberg, D. (2018). The Galaxy platform for accessible, reproducible and collaborative biomedical analyses: 2018 update. *Nucleic Acids Research*, *46*, W537–W544.

Aguayo, R., Lavilla, E. O., Vera Candioti, M. F., & Camacho, T. (2009). Living in fast-flowing water: Morphology of the gastromyzophorous tadpole of the bufonid Rhinella quechua (R. veraguensis Group). *Journal of Morphology*, *270*, 1431–1442.

Aiken, R. ., & Khan, A. (1992). The adhesive strength of the palettes of males of a boreal water beetle, Dytiscus alaskanus J. Balfour Browne (Coleoptera: Dytiscidae). *Canadian Journal of Zoology*, *70*, 1321–1324.

Almagro Armenteros, J. J., Sønderby, C. K., Sønderby, S. K., Nielsen, H., & Winther, O. (2017). DeepLoc: prediction of protein subcellular localization using deep learning. *Bioinformatics*, *33*, 3387–3395.

Álvarez, E., Vázquez, G., Sánchez-Vilas, M., Sanjurjo, B., & Navaza, J. M. (1997). Surface tension of organic acids + water binary mixtures from 20°C to 50°C. *Journal of Chemical and Engineering Data*, *42*, 957–960.

Amparyup, P., Donpudsa, S., & Tassanakajon, A. (2008). Shrimp single WAP domain (SWD)-containing protein exhibits proteinase inhibitory and antimicrobial activities. *Developmental and Comparative Immunology*, *32*, 1497–1509.

Arita, G. S. (1967). *A comparative study of the structure and function of the adhesive apparatus of the Cyclopteridae and Gobiesocidae*. The University of British Columbia.

Armitage, D. W. (2016). Bacteria facilitate prey retention by the pitcher plant Darlingtonia californica. *Biology Letters*, *12*, 2–5.

Armitage, D. W. (2017). Linking the development and functioning of a carnivorous

pitcher plant's microbial digestive community. *ISME Journal*, *11*, 2439–2451.

Aspinall, G. O., Puvanesarajah, V., Reuter, G., & Schauer, R. (1984). Selective cleavage of β-d-glucopyranosiduronic acid linkages in methylated polysaccharide acids from Drosera species. *Carbohydrate Research*, *131*, 53–60.

Autumn, K. (2006). Frictional adhesion: a new angle on gecko attachment. *Journal of Experimental Biology*, *209*, 3569–3579.

Autumn, K., Niewiarowski, P. H., & Puthoff, J. B. (2014). Gecko Adhesion as a Model System for Integrative Biology, Interdisciplinary Science, and Bioinspired Engineering. *Annual Review of Ecology, Evolution, and Systematics*, *45*, 445–470.

Autumn, K., Sitti, M., Liang, Y. a, Peattie, A. M., Hansen, W. R., Sponberg, S., … Full, R. J. (2002). Evidence for van der Waals adhesion in gecko setae. *Proceedings of the National Academy of Sciences of the United States of America*, *99*, 12252–12256.

Baik, S., Kim, D. W., Park, Y., Lee, T.-J., Ho Bhang, S., & Pang, C. (2017). A wet-tolerant adhesive patch inspired by protuberances in suction cups of octopi. *Nature*, *546*, 396–400.

Bandyopadhyay, P. R., Hrubes, J. D., & Leinhos, H. A. (2008). Biorobotic adhesion in water using suction cups. *Bioinspiration & Biomimetics*, *3*, 016003.

Barral, Q., Ovarlez, G., Chateau, X., Boujlel, J., Rabideau, B., & Coussot, P. (2010). Adhesion of yield stress fluids. *Soft Matter*, *6*, 1343–1351.

Bates, D., Mächler, M., Bolker, B., & Walker, S. (2015). Fitting Linear Mixed-Effects Models Using {lme4}. *Journal of Statistical Software*, *67*, 1–48.

Bauer, U., Grafe, T. U., & Federle, W. (2011). Evidence for alternative trapping strategies in two forms of the pitcher plant, Nepenthes rafflesiana. *Journal of Experimental Botany*, *62*, 3683–3692.

Bauer, U., Scharmann, M., Skepper, J., & Federle, W. (2012). "Insect aquaplaning" on a superhydrophilic hairy surface: how Heliamphora nutans Benth. pitcher plants capture prey. *Proceedings of the Royal Society B*, *280*, 20122569.

Bauer, U., Willmes, C., & Federle, W. (2009). Effect of pitcher age on trapping efficiency and natural prey capture in carnivorous Nepenthes rafflesiana plants. *Annals of Botany*, *103*, 1219–1226.

Bazile, V., Moguédec, G. Le, Marshall, D. J., & Gaume, L. (2015). Fluid physico-chemical properties influence capture and diet in Nepenthes pitcher plants. *Annals of Botany*, *115*, 705–716.

Beament, J. W. L. (1961). THE WATER RELATIONS OF INSECT CUTICLE. *Biological Reviews*, *36*, 281–320.

Beckert, M., Flammang, B. E., & Nadler, J. H. (2015). Remora fish suction pad attachment is enhanced by spinule friction. *Journal of Experimental Biology*, *218*, 3551–3558.

Bergsten, J., Y, A. T. O., & Nilsson, A. N. (2001). Intraspecific variation and intersexual correlation in secondary sexual characters of three diving beetles (Coleoptera : Dytiscidae). *Biological Journal of Linnean Society*, *73*, 221–232.

Berry, J. D., Neeson, M. J., Dagastine, R. R., Chan, D. Y. C., & Tabor, R. F. (2015). Measurement of surface and interfacial tension using pendant drop tensiometry. *Journal of Colloid and Interface Science*, *454*, 226–237.

Bing-Shan, H., Li-Wen, W., Zhuang, F., Yan-Zheng, Z., Hu, B., Wang, L.-W., … Zhao, Y. (2009). Bio-inspired miniature suction cups actuated by shape memory alloy. *International Journal of Advanced Robotic Systems*, *6*, 151–160.

Bischoff, W. (1928). Die Ökologie der paläarktischen Blepharoceridae. *Ergebnisse Und Fortschritte Der Zoologie*, *7*, 209–278.

Blom, N., Gammeltoft, S., & Brunak, S. (1999). Sequence and structure-based prediction of eukaryotic protein phosphorylation sites. *Journal of Molecular Biology*, *294*, 1351–1362.

Bohn, H. F., & Federle, W. (2004). Insect aquaplaning: Nepenthes pitcher plants capture prey with the peristome, a fully wettable water-lubricated anisotropic surface. *Proceedings of the National Academy of Sciences of the United States of America*, *101*, 14138–14143.

Bonhomme, V., Pelloux-Prayer, H., Jousselin, E., Forterre, Y., Labat, J. J., & Gaume, L. (2011). Slippery or sticky? Functional diversity in the trapping strategy of Nepenthes carnivorous plants. *New Phytologist*, *191*, 545–554.

Boujlel, J., & Coussot, P. (2013). Measuring the surface tension of yield stress fluids. *Soft Matter*, *9*, 5898–5908.

Bowdish, D. M. E., & Gordon, S. (2009). Conserved domains of the class A scavenger receptors: Evolution and function. *Immunological Reviews*, *227*, 19–31.

Branch, G. M., & Marsh, A. C. (1978). Tenacity and shell shape in six Patella species: Adaptive features. *Journal of Experimental Marine Biology and Ecology*, *34*, 111–130.

Brunchi, C.-E., Bercea, M., Morariu, S., & Dascalu, M. (2016). Some properties of

xanthan gum in aqueous solutions: effect of temperature and pH. *Journal of Polymer Research*, *23*, 123.

Bullock, J. M. R., & Federle, W. (2011). The effect of surface roughness on claw and adhesive hair performance in the dock beetle Gastrophysa viridula. *Insect Science*, *18*, 298–304.

Burgos-Rubio, V., De la Rosa, J., Altamirano, M., & Espinosa, F. (2015). The role of patellid limpets as omnivorous grazers: a new insight into intertidal ecology. *Marine Biology*, *162*, 2093–2106.

Bush, J. W. M., & Hu, D. L. (2006). Walking on Water: Biolocomotion at the Interface. *Annual Review of Fluid Mechanics*, *38*, 339–369.

Campbell, J. W. (1920). Notes on the Blepharoceridae (Diptera) of New Zealand. *N.Z. Inst. Trans. Proc.*, *53*, 258–288.

Campbell, K. P., Maclennantll, D. H., & Jorgensen, A. (1983). Staining of the Ca2+-binding Proteins, Calsequestrin, Calmodulin, Troponin C, and S-100, with the Cationic Carbocyanine Dye "Stains- all"*. *The Journal of Biological Chemistry*, *258*, 11267–11273.

Castañeda, O., Sotolongo, V., Amor, A. M., Stöcklin, R., Anderson, A. J., Harvey, A. L., … Karlsson, E. (1995). Characterization of a potassium channel toxin from the Caribbean sea anemone Stichodactyla helianthus. *Toxicon*, *33*, 603–613.

Cecilia, A., Rack, A., Douissard, P.-A., Martin, T., dos Santos Rolo, T., Vagovič, P., … Baumbach, T. (2011). LPE grown LSO:Tb scintillator films for high-resolution X-ray imaging applications at synchrotron light sources. *Nuclear Instruments and Methods in Physics Research Section A: Accelerators, Spectrometers, Detectors and Associated Equipment*, *648*, S321–S323.

Chang, W.-C., Lee, T.-Y., Shien, D.-M., Hsu, J. B.-K., Horng, J.-T., Hsu, P.-C., … Pan, R.-L. (2009). Incorporating support vector machine for identifying protein tyrosine sulfation sites. *Journal of Computational Chemistry*, *30*, 2526–2537.

Chaw, R. C., Correa-Garhwal, S. M., Clarke, T. H., Ayoub, N. a, & Hayashi, C. Y. (2015). Proteomic Evidence for Components of Spider Silk Synthesis from Black Widow Silk Glands and Fibers. *Journal of Proteome Research*, 150824105308000.

Chen, Y., Shih, M., Wu, M., Yang, E., & Chi, K. (2014). Underwater attachment using hairs: the functioning of spatula and sucker setae from male diving beetles. *Journal of The Royal Society Interface*, *11*, 20140273.

Clasen, C., Eggers, J., Fontelos, M. A., Li, J., & McKinley, G. H. (2006). The beads-on-string structure of viscoelastic threads. *Journal of Fluid Mechanics*, *556*, 283–308.

Cochard, H. (2006). Cavitation in trees. *Comptes Rendus Physique*, *7*, 1018–1026.

Coleman, R. A., Browne, M. A., & Theobalds, T. (2004). Aggregation as a defense: Limpet tenacity changes in response to simulated predator attack. *Ecology*, *85*, 1153–1159.

Collett, C., Ardron, A., Bauer, U., Chapman, G., Chaudan, E., Hallmark, B., … Wilson, D. (2015). A portable extensional rheometer for measuring the viscoelasticity of pitcher plant and other sticky liquids in the field. *Plant Methods*, *11*, 16.

Cowles, D. (1977). Locomotion by Epiactis prolifera (Coelenterata: Actiniaria). *Marine Biology*, *39*, 67–70.

Craig, D. A. (1966). *The biology of some New Zealand Blepharoceridae (Diptera : Nematocera)*.

Craig, D. A. (1969). A Taxonomic Revision of New Zealand Blepharoceridae and the Origin and Evolution of the Australasian Blepharoceridae (Diptera: Nematocera)*. *Trans. R. Soc. N.Z., Biol. Sciences*, *11*, 101–151.

Cresswell, J. E. (1991). Capture Rates and Composition of Insect Prey of the Pitcher Plant Sarracenia purpurea. *American Midland Naturalist*, *125*, 1–9.

Dai, Z., Gorb, S. N., & Schwarz, U. (2002). Friction of the beetle claw system. *Journal of Experimental Biology*, 2479–2488.

Davenport, J., & Thorsteinsson, V. (1990). Sucker action in the lumpsucker Cyclopterus lumpus L. *Sarsia*, *75*, 33–42.

Davey, P. A., Rodrigues, M., Clarke, J. L., & Aldred, N. (2019). Transcriptional characterisation of the Exaiptasia pallida pedal disc. *BMC Genomics*, *20*, 1–15.

Davies, M. S., Jones, H. D., & Hawkins, S. J. (1990). Seasonal variation in the composition of pedal mucus from Patella vulgata L. *Journal of Experimental Marine Biology and Ecology*, *144*, 101–112.

Denny, M. W. (1988). *Biology and the Mechanics of the Wave-Swept Environment*. Princeton, N.J. : Princeton University Press, [1988].

Denny, M. W. (2000). Limits to optimization: fluid dynamics, adhesive strength and the evolution of shape in limpet shells. *The Journal of Experimental Biology*, *203*, 2603–2622.

Denny, M. W., & Blanchette, C. A. (2000). Hydrodynamic effects on limpet survivorship. *The Journal of Experimental Biology*, *203*, 2623–2639.

Denny, M. W., Daniel, T. L., & Koehl, M. A. R. (1985). Mechanical Limits to Size in Wave-Swept Organisms. *Ecological Monographs*, *55*, 69–102.

Di Fabio, J. L., Dutton, G. G. S., & Moyna, P. (1982). The structure of Chorisia speciosa gum. *Carbohydrate Research*, *99*, 41–50.

Di Giusto, B., Grosbois, V., Fargeas, E., Marshall, D. J., & Gaume, L. (2008). Contribution of pitcher fragrance and fluid viscosity to high prey diversity in a Nepenthes carnivorous plant from Borneo. *Journal of Bioscience*, *33*, 121–136.

Dirks, J.-H., & Federle, W. (2011). Fluid-based adhesion in insects – principles and challenges. *Soft Matter*, *7*, 11047.

Dirks, J.-H., Li, M., Kabla, A., & Federle, W. (2012). In vivo dynamics of the internal fibrous structure in smooth adhesive pads of insects. *Acta Biomaterialia*, *8*, 2730–2736.

Ditsche-Kuru, P., Koop, J. H. E., & Gorb, S. N. (2010). Underwater attachment in current: the role of setose attachment structures on the gills of the mayfly larvae Epeorus assimilis (Ephemeroptera, Heptageniidae). *Journal of Experimental Biology*, *213*, 1950–1959.

Ditsche, P., Michels, J., Kovalev, A., Koop, J., & Gorb, S. (2014). More than just slippery : the impact of biofilm on the attachment of non-sessile freshwater mayfly larvae. *Journal of the Royal Society Interface*, *11*, 20130989.

Ditsche, P., & Summers, A. (2019). Learning from Northern clingfish (Gobiesox maeandricus): Bioinspired suction cups attach to rough surfaces. *Philosophical Transactions of the Royal Society B: Biological Sciences*, *374*, 1784.

Ditsche, P., & Summers, A. P. (2014). Aquatic versus terrestrial attachment: Water makes a difference. *Beilstein Journal of Nanotechnology*, *5*, 2424–2439.

Ditsche, P., Wainwright, D. K., & Summers, A. P. (2014). Attachment to challenging substrates - fouling, roughness and limits of adhesion in the northern clingfish (Gobiesox maeandricus). *Journal of Experimental Biology*, *217*, 2548–2554.

dos Santos Rolo, T., Ershov, A., van de Kamp, T., & Baumbach, T. (2014). In vivo X-ray cine-tomography for tracking morphological dynamics. *Proceedings of the National Academy of Sciences*, *111*, 3921–3926.

Dreanno, C., Matsumura, K., Dohmae, N., Takio, K., Hirota, H., Kirby, R. R., & Clare, A. S. (2006). An α2-macroglobulin-like protein is the cue to gregarious settlement of the barnacle Balanus amphitrite. *Proceedings of the National Academy of*

Sciences of the United States of America, *103*, 14396–14401.

Ellem, G. K., Furst, J. E., & Zimmerman, K. D. (2002). Shell clamping behaviour in the limpet Cellana tramoserica. *Journal of Experimental Biology*, *205*, 539–547.

Ellison, A., & Adamec, L. (2018). Carnivorous Plants. In A. Ellison & L. Adamec (Eds.), *Carnivorous Plants: Physiology, Ecology, and Evolution* (Vol. 1). Oxford: Oxford University Press.

Erni, P., Varagnat, M., Clasen, C., Crest, J., & McKinley, G. H. (2011). Microrheometry of sub-nanolitre biopolymer samples: non-Newtonian flow phenomena of carnivorous plant mucilage. *Soft Matter*, *7*, 10889.

Federle, W. (2006). Why are so many adhesive pads hairy? *Journal of Experimental Biology*, *209*, 2611–2621.

Federle, W., Barnes, W. J. P., Baumgartner, W., Drechsler, P., & Smith, J. M. (2006). Wet but not slippery: Boundary friction in tree frog adhesive toe pads. *J. R. Soc. Interface*, *3*, 689–697.

Federle, W., & Labonte, D. (2019). Dynamic biological adhesion: Mechanisms for controlling attachment during locomotion. *Philosophical Transactions of the Royal Society B: Biological Sciences*, Vol. 374, p. 20190199.

Federle, W., Riehle, M., Curtis, A. S. G., & Full, R. J. (2002). An Integrative Study of Insect Adhesion : Mechanics and Wet Adhesion of Pretarsal Pads in Ants. *Integrative and Comparative Biology*, *1106*, 1100–1106.

Federle, W., Rohrseitz, K., & Hölldobler, B. (2000). Attachment forces of ants measured with a centrifuge: Better “wax-runners” have a poorer attachment to a smooth surface. *Journal of Experimental Biology*, *203*, 505–512.

Flammang, P. (2006). Adhesive Secretions in Echinoderms: An Overview. In A. M. Smith & J. A. Callow (Eds.), *Biological Adhesives* (pp. 183–206). Berlin, Heidelberg: Springer Berlin Heidelberg.

Flammang, P., Michel, A., Cauwenberge, A. V, Alexandre, H., & Jangoux, M. (1998). A study of the temporary adhesion of the podia in the sea star Asterias rubens (Echinodermata, Asteroidea) through their footprints. *The Journal of Experimental Biology*, *201*, 2383–2395.

Frenzke, L., Lederer, A., Malanin, M., Eichhorn, K. J., Neinhuis, C., & Voigt, D. (2016). Plant pressure sensitive adhesives: similar chemical properties in distantly related plant lineages. *Planta*, *244*, 145–154.

Frutiger, A. (1998). Walking on suckers - new insights into the locomotory behavior of

larval net-winged midges (Diptera : Blephariceridae). *Journal of the North American Benthological Society*, *17*, 104–120.

Frutiger, A. (2002). The function of the suckers of larval net-winged midges (Diptera: Blephariceridae). *Freshwater Biology*, *47*, 293–302.

Frutiger, A., & Buergisser, G. M. (2002). Life history variability of a grazing stream insect (Liponeura cinerascens minor; Diptera: Blephariceridae). *Freshwater Biology*, *47*, 1618–1632.

Frutiger, A., & Gammeter, S. (1998). Faunistics and altitudinal distribution of net-winged midges (Diptera: Blephariceridae) in Switzerland and Liechtenstein. *Journal of the Swiss Entomological Society*, *71*, 115–124.

Frutiger, A., & Jolidon, C. (2000). Bestimmungsschlüssel für die Larven und Puppen der in der Schweiz, in Österreich und in Deutschland vorkommenden Netzflügelmücken (Diptera, Blephariceridae), mit Hinweisen zu ihrer Verbreitung und Phänologie. *Bull. Soc. Ent. Suisse*, *73*, 93–108.

Fukushima, K., Fang, X., Alvarez-Ponce, D., Cai, H., Carretero-Paulet, L., Chen, C., … Hasebe, M. (2017). Genome of the pitcher plant Cephalotus reveals genetic changes associated with carnivory. *Nature Ecology & Evolution*, *1*, 0059.

Fulcher, B. A., & Motta, P. J. (2006). Suction disk performance of echeneid fishes. *Canadian Journal of Zoology*, *84*, 42–50.

G.T., W., McCartney, L., & Knox, J. P. (2001). In-situ analysis of pectic polysaccharides in seed mucilage and at the root surface of Arabidopsis thaliana. *Planta*, *213*, 37–44.

Galloway, A. F., Knox, P., & Krause, K. (2020). Sticky mucilages and exudates of plants: putative microenvironmental design elements with biotechnological value. *New Phytologist*, *225*, 1461–1469.

Gamel, K. M., Garner, A. M., & Flammang, B. E. (2019). Bioinspired remora adhesive disc offers insight into evolution. *Bioinspiration and Biomimetics*, *14*, 056014.

Garti, N., & Reichman, D. (1994). Surface properties and emulsification activity of galactomannans. *Topics in Catalysis*, *8*, 155–173.

Gaume, L., & Forterre, Y. (2007). A viscoelastic deadly fluid in carnivorous pitcher plants. *PloS ONE*, *2*, e1185.

Gaume, L., Perret, P., Gorb, E. V., Gorb, S., Labat, J. J., & Rowe, N. (2004). How do plant waxes cause flies to slide? Experimental tests of wax-based trapping mechanisms in three pitfall carnivorous plants. *Arthropod Structure and*

Development, *33*, 103–111.

Géraud, B., Jørgensen, L., Petit, L., Delanoë-Ayari, H., Jop, P., & Barentin, C. (2014). Capillary rise of yield-stress fluids. *EPL (Europhysics Letters)*, *107*, 58002.

Gerdol, M., & Venier, P. (2015). An updated molecular basis for mussel immunity. *Fish and Shellfish Immunology*, *46*, 17–38.

Gil-Azevedo, L. H., & Santos, D. D. S. (2016). Family Blephariceridae. *Zootaxa*, *4122*, 182–186.

Gilbert, K. J., Bittleston, L. S., Tong, W., & Pierce, N. E. (2020). Tropical pitcher plants (Nepenthes) act as ecological filters by altering properties of their fluid microenvironments. *Scientific Reports*, *10*, 1–13.

Givnish, T. J. (2015). New evidence on the origin of carnivorous plants. *Proceedings of the National Academy of Sciences*, *112*, 10–11.

Gobron, S, Monnerie, H., Meiniel, R., Creveaux, I., Lehmann, W., Lamalle, D., … Meiniel, A. (1996). SCO-spondin: a new member of the thrombospondin family secreted by the subcommissural organ is a candidate in the modulation of neuronal aggregation. *Journal of Cell Science*, *109*, 1053–1061.

Gobron, Stéphane, Creveaux, I., Meiniel, R., Didier, R., Herbet, A., Bamdad, M., … Meiniel, A. (2000). Subcommissural organ/Reissner's fiber complex: Characterization of SCO-spondin, a glycoprotein with potent activity on neurite outgrowth. *Glia*, *32*, 177–191.

Goh, K. T. K., Matia-Merino, L., & Wee, S. M. M. (2015). The cation-controlled and hydrogen bond-mediated shear-thickening behaviour of a tree-fern isolated polysaccharide. *Carbohydrate Polymers*, *130*, 57–68.

Gohad, N. V., Aldred, N., Hartshorn, C. M., Lee, Y. J., Cicerone, M. T., Orihuela, B., … Mount, A. S. (2014). Synergistic roles for lipids and proteins in the permanent adhesive of barnacle larvae. *Nature Communications*, *5*, 1–9.

Goldberg, H. A., & Warner, K. J. (1997). The Staining of Acidic Proteins on Polyacrylamide Gels : Enhanced Sensitivity and Stability of "' Stains-All "' Staining in Combination with Silver Nitrate. *Analytical Biochemistry*, 227–233.

Gorb, S. N. (2002). Attachment Devices of Insect Cuticle. In *Attachment Devices of Insect Cuticle*. Dordrecht: Kluwer Academic Publishers.

Gorb, S. N., Gorb, E. V., & Kastner, V. (2001). Scale effects on the attachment pads and friction forces in syrphid flies (Diptera, Syrphidae). *The Journal of Experimental Biology*, *204*, 1421–1431.

Gorb, E. V., & Gorb, S. N. (2011). The effect of surface anisotropy in the slippery zone of Nepenthes alata pitchers on beetle attachment. *Beilstein Journal of Nanotechnology*, *2*, 302–310.

Gorb, E. V., Haas, K., Henrich, A., Enders, S., Barbakadze, N., & Gorb, S. (2005). Composite structure of the crystalline epicuticular wax layer of the slippery zone in the pitchers of the carnivorous plant Nepenthes alata and its effect on insect attachment. *Journal of Experimental Biology*, *208*, 4651–4662.

Goubet, F., Jackson, P., Deery, M. J., & Dupree, P. (2002). Polysaccharide Analysis Using Carbohydrate Gel Electrophoresis: A Method to Study Plant Cell Wall Polysaccharides and Polysaccharide Hydrolases. *Analytical Biochemistry*, *300*, 53–68.

Goujon, M., McWilliam, H., Li, W., Valentin, F., Squizzato, S., Paern, J., & Lopez, R. (2010). A new bioinformatics analysis tools framework at EMBL–EBI. *Nucleic Acids Research*, *38*, W695–W699.

Gowda, D. C., Reuter, G., & Schauer, R. (1982). Structural features of an acidic polysaccharide from the mucin of Drosera binata. *Phytochemistry*, *21*, 2297–2300.

Gowda, D. C., Reuter, G., & Schauer, R. (1983). Structural studies of an acidic polysaccharide from the mucin secreted by Drosera capensis. *Carbohydrate Research*, *113*, 113–124.

Grabherr, M. G., Haas, B. J., Yassour, M., Levin, J. Z., Thompson, D. A., Amit, I., … Regev, A. (2011). *Full-length transcriptome assembly from RNA-Seq data without a reference genome*. *29*. https://doi.org/10.1038/nbt.1883

Gradwell, N. (1972). Behaviors of the leech, Placobdella , and transducer recordings of suctorial pressures. *Canadian Journal of Zoology*, *50*, 1325–1332.

Grenon, J.-F., & Walker, G. (1978). The histology and histochemistry of the pedal glandular system of two limpets, Patella vulgata and Acmaea tessulata (Gastropoda: Prosobranchia). *Journal of the Marine Biological Association of the United Kingdom*, *58*, 803–816.

Grenon, J.-F., & Walker, G. (1980). Biochemical and rheological properties of the pedal mucus of the limpet, Patella vulgata L. *Comparative Biochemistry and Physiology*, *66B*, 451–458.

Grenon, J.-F., & Walker, G. (1981). The tenacity of the limpet, Patella vulgata L.: an experimental approach. *Journal of Experimental Marine Biology and Ecology*, *54*,

277–308.

Grohmann, C., Blankenstein, A., Koops, S., & Gorb, S. N. (2014). Attachment of Galerucella nymphaeae (Coleoptera, Chrysomelidae) to surfaces with different surface energy. *Journal of Experimental Biology*, *217*, 4213–4220.

Gronenberg, W., Paul, J., Just, S., & Hölldobler, B. (1997). Mandible muscle fibers in ants: Fast or powerful? *Cell and Tissue Research*, *289*, 347–361.

Gupta, R., & Brunak, S. (2002). Prediction of glycosylation across the human proteome and the correlation to protein function. *Pacific Symposium on Biocomputing*, 310–322. Lihue, Hawaii.

Hahn, T., & Denny, M. W. (1989). Tenacity-mediated selective pecdation by oystercatchers on intertidal limpets and its role in maintaining habitat partitioning by "Collisella" scabra and Lottia digitalis. *Marine Ecology Progress Series*, *53*, 1–10.

Handford, P. A. (2000). Fibrillin-1, a calcium binding protein of extracellular matrix. *Biochimica et Biophysica Acta - Molecular Cell Research*, *1498*, 84–90.

Harada, N., Iijima, S., Kobayashi, K., Yoshida, T., Brown, W. R., Hibi, T., … Morikawa, M. (1997). Human IgGFc binding protein (FcγBP) in colonic epithelial cells exhibits mucin-like structure. *Journal of Biological Chemistry*, *272*, 15232–15241.

Harrington, B. J., Hageage, G. J., & Abmm, D. (2003). Calcofluor White : A Review of its Uses and Applications in Clinical Mycology and Parasitology. *Laboratory Medicine*, *34*, 361–367.

He, Y., Sun, C., Jiang, F., Yang, B., Li, J., Zhong, C., … Ding, H. (2018). Lipids as integral components in mussel adhesion. *Soft Matter*, *14*, 7145–7154.

Hellberg, M. E., Dennis, A. B., Arbour-Reily, P., Aagaard, J. E., & Swanson, W. J. (2012). The tegula tango: A coevolutionary dance of interacting, positively selected sperm and egg proteins. *Evolution*, *66*, 1681–1694.

Hennebert, E., Flammang, P., Demeuldre, M., Hennebert, E., & Santos, R. (2016). Adhesive Secretions in Echinoderms: A Review. In A. M. Smith (Ed.), *Biological Adhesives* (pp. 193–222). Cham: Springer International Publishing.

Hennebert, E., Gregorowicz, E., & Flammang, P. (2018). Involvement of sulfated biopolymers in adhesive secretions produced by marine invertebrates. *Biology Open*, bio.037358.

Hennebert, E., Leroy, B., Wattiez, R., & Ladurner, P. (2015). An integrated transcriptomic and proteomic analysis of sea star epidermal secretions identifies

proteins involved in defense and adhesion. *Journal of Proteomics*, *128*, 83–91.

Hennebert, E., Maldonado, B., Ladurner, P., & Flammang, P. (2015). Experimental strategies for the identification and characterization of adhesive proteins in animals : a review. *Interface Focus*, *5*, 20140064.

Hennebert, E., Wattiez, R., Demeuldre, M., Ladurner, P., Hwang, D. S., Waite, J. H., & Flammang, P. (2014). Sea star tenacity mediated by a protein that fragments, then aggregates. *Proceedings of the National Academy of Sciences of the United States of America*, *111*, 6317–6322.

Hennebert, E., Wattiez, R., Waite, J. H., & Flammang, P. (2012). Characterization of the protein fraction of the temporary adhesive secreted by the tube feet of the sea star Asterias rubens. *Biofouling*, *28*, 289–303.

Hensel, R., Moh, K., & Arzt, E. (2018). Engineering Micropatterned Dry Adhesives: From Contact Theory to Handling Applications. *Advanced Functional Materials*, *28*, 1800865.

Hermann, H. R., Mullen, M. A., & Wallace, J. B. (1975). Suction discs of Blepharocera separata. *J. Georgia Entomol. Soc.*, *10*, 145–150.

Hofeneder, K. (1927). Über die Larven der Blepharoceriden und ihren merkwürdigen Anheftungsapparat. *Verhandlungen Der Zoologisch-Botanischen Gesellschaft in Wien*, *77*, 82–98.

Holdgate, M. (1955). The Wetting of Insect Cuticles by Water. *Journal of Experimental Biology*, *32*, 591–617.

Hora, S. L. (1930). Ecology, Bionomics and Evolution of the Torrential Fauna, with Special Reference to the Organs of Attachment. *Philosophical Transactions of the Royal Society of London B*, *218*, 171–282.

Hu, H. M. S., Watson, G. S., Cribb, B. W., & Watson, J. A. (2011). Non-wetting wings and legs of the cranefly aided by fine structures of the cuticle. *Journal of Experimental Biology*, *214*, 915–920.

Huang, G., Huang, S., Yan, X., Yang, P., Li, J., Xu, W., … Xu, A. (2014). Two apextrin-like proteins mediate extracellular and intracellular bacterial recognition in amphioxus. *Proceedings of the National Academy of Sciences of the United States of America*, *111*, 13469–13474.

Huang, Y., Wang, Y., Sun, L., Agrawal, R., & Zhang, M. (2015). Sundew adhesive: a naturally occurring hydrogel. *Journal of The Royal Society Interface*, *12*, 20150226–

20150226.

Huang, Yujian, Wang, Y., Tan, L., Sun, L., Petrosino, J., Cui, M. Z., … Zhang, M. (2016). Nanospherical arabinogalactan proteins are a key component of the high-strength adhesive secreted by English ivy. *Proceedings of the National Academy of Sciences of the United States of America*, *113*, E3193–E3202.

Jackson, L. L., & Baker, G. L. (1970). Cuticular Lipids of Insects. *Lipids*, *5*, 239–246.

Jaffe, K., Michelangeli, F., Gonzalez, J. M., Miras, B., & Christine Ruiz, M. (1992). Carnivory in pitcher plants of the genus Heliamphora (Sarraceniaceae). *New Phytologist*, *122*, 733–744.

Jaishankar, A., Wee, M., Matia-Merino, L., Goh, K. K. T., & McKinley, G. H. (2015). Probing hydrogen bond interactions in a shear thickening polysaccharide using nonlinear shear and extensional rheology. *Carbohydrate Polymers*, *123*, 136–145.

Jones, F. M., & Hepburn, J. S. (1927). Observations on the pitcher liquor of the Sarraceniaceae. *Trans. Wagner Free Inst. Sci.*, Vol. 11, pp. 35–48.

Jones, H. D., & Trueman, E. R. (1970). Locomotion of the Limpet, Patella Vulgata L . *Journal of Experimental Biology*, *52*, 201–216.

Jørgensen, L., Le Merrer, M., Delanoë-Ayari, H., & Barentin, C. (2015). Yield stress and elasticity influence on surface tension measurements. *Soft Matter*, *11*, 5111–5121.

Julenius, K. (2007). NetCGlyc 1.0: Prediction of mammalian C-mannosylation sites. *Glycobiology*, *17*, 868–876.

Kamino, K. (2008). Underwater adhesive of marine organisms as the vital link between biological science and material science. *Marine Biotechnology*, *10*, 111–121.

Kamino, K. (2016). Barnacle underwater attachment. In A. M. Smith (Ed.), *Biological Adhesives, Second Edition* (pp. 153–176). Cham: Springer International Publishing.

Kamino, K., Inoue, K., Maruyama, T., Takamatsu, N., Harayama, S., & Shizuri, Y. (2000). Barnacle cement proteins: Importance of disulfide bonds in their insolubility. *Journal of Biological Chemistry*, *275*, 27360–27365.

Kampowski, T., Eberhard, L., Gallenmüller, F., Speck, T., & Poppinga, S. (2016). Functional morphology of suction discs and attachment performance of the Mediterranean medicinal leech (Hirudo verbana Carena). *Journal of the Royal Society, Interface*, *13*, 20160096.

Karlsson Green, K., Kovalev, A., Svensson, E. I., & Gorb, S. N. S. N. (2013). Male clasping ability, female polymorphism and sexual conflict: fine-scale elytral morphology as a sexually antagonistic adaptation in female diving beetles. *J. R. Soc.*

Interface, *10*, 20130409.

Kellogg, V. L. (1900). Notes on the Life-history and Structure of Blepharocera capitata Loew. *Ent. News*, *11*, 305–318.

Kellogg, V. L. (1903). The Net-Winged Midges (Blepharoceridae) of North America. *Proceedings of the California Academy of Sciences*, *3*, 187–224.

Kier, W. M., & Smith, A. M. (1990). The morphology and mechanics of octopus suckers. *Biological Bulletin*, *178*, 126–136.

Kier, W. M., & Smith, A. M. (2002). The Structure and Adhesive Mechanism of Octopus Suckers. *Integrative and Comparative Biology*, *42*, 1146–1153.

Kim, D., Kim, J. A., Park, J., Niazi, A., Almishaal, A., & Park, S. (2019). The release of surface-anchored alpha-tectorin, an apical extracellular matrix protein, mediates tectorial membrane organization. *Science Advances*, *5*, 1–10.

Knox, J. P. (2008). Revealing the structural and functional diversity of plant cell walls. *Current Opinion in Plant Biology*, *11*, 308–313.

Kohn, R., & Kovác, P. (1978). Dissociation constants of D-galacturonic and D-glucuronic acid and their O-methyl derivatives. *Chem. Zvesti*, *32*, 478–485.

Kokubun, T. (2017). Occurrence of myo-inositol and alkyl-substituted polysaccharide in the prey-trapping mucilage of Drosera capensis. *The Science of Nature*, *104*, 83.

Komárek, J. (1914). Die Morphologie und Physiologie der Haftscheiben der Blepharoceridenlarven. *Sitzungsberichte Der Königlich Böhmischen Gesellschaft Der Wissenschaften II Classe*, 1–28.

Komárek, J., & Wimmer, A. (1922). The Larvae of the European Blepharoceridae (Diptera). *Annales de Biologie Lacustre*, 63–77.

Kuznetsova, A., Brockhoff, P. B., & Christensen, R. H. B. (2017). {lmerTest} Package: Tests in Linear Mixed Effects Models. *Journal of Statistical Software*, *82*, 1–26.

Labonte, D., & Federle, W. (2015). Rate-dependence of 'wet' biological adhesives and the function of the pad secretion in insects. *Soft Matter*, *11*, 8661–8673.

Labonte, D., Williams, J. A., & Federle, W. (2014). Surface contact and design of fibrillar "friction pads" in stick insects (Carausius morosus): mechanisms for large friction coefficients and negligible adhesion. *J. R. Soc. Interface*, *11*, 20140034.

Lachnit, M., Buhmann, M. T., Klemm, J., Kröger, N., & Poulsen, N. (2019). Identification of proteins in the adhesive trails of the diatom Amphora coffeaeformis. *Philosophical Transactions of the Royal Society B: Biological Sciences*, *374*,

20190196.

Lam, J. H. C., Ranganathan, N., Wigle, E. D., & Silver, M. D. (1970). Morphology of the Human Mitral Valve: I. Chordae Tendineae: A New Classification. *Circulation*, *41*, 449–458.

Lang, T., Hansson, G. C., & Samuelsson, T. (2007). Gel-forming mucins appeared early in metazoan evolution. *Proceedings of the National Academy of Sciences of the United States of America*, *104*, 16209–16214.

Langmead, B., & Salzberg, S. L. (2012). Fast gapped-read alignment with Bowtie 2. *Nature Methods*, *9*, 357–359.

Langowski, J. K. A., Singla, S., Nyarko, A., Schipper, H., Van Den Berg, F. T., Kaur, S., … Van Leeuwen, J. L. (2019). Comparative and functional analysis of the digital mucus glands and secretions of tree frogs. *Frontiers in Zoology*, *16*. https://doi.org/10.1186/s12983-019-0315-z

Lea, I. A., Sivashanmugam, P., Rand, M. G. O., Hill, C., Carolina, N., & Al, L. E. A. E. T. (2001). *Zonadhesin : Characterization , Localization , and Zona Pellucida Binding 1*. *1700*, 1691–1700.

Lee, B. B., Chan, E. S., Ravindra, P., & Khan, T. A. (2012). Surface tension of viscous biopolymer solutions measured using the du Nouy ring method and the drop weight methods. *Polymer Bulletin*, *69*, 471–489.

Lee, D. H., Kim, Y., Fearing, R. S., & Maboudian, R. (2011). Effect of fiber geometry on macroscale friction of ordered low-density polyethylene nanofiber arrays. *Langmuir*, *27*, 11008–11016.

Lengerer, B., Algrain, M., Lefevre, M., Delroisse, J., Hennebert, E., & Flammang, P. (2019). Interspecies comparison of sea star adhesive proteins. *Philosophical Transactions of the Royal Society B: Biological Sciences*, *374*, 20190195.

Lengerer, B., Bonneel, M., Lefevre, M., Hennebert, E., Leclère, P., Gosselin, E., … Flammang, P. (2018). The structural and chemical basis of temporary adhesion in the sea star Asterina gibbosa. *Beilstein Journal of Nanotechnology*, *9*, 2071–2086.

Lengerer, B., & Ladurner, P. (2018). Properties of temporary adhesion systems of marine and freshwater organisms. *The Journal of Experimental Biology*, *221*, jeb182717.

Lengerer, B., Wunderer, J., Pjeta, R., Carta, G., Kao, D., Aboobaker, A., … Ladurner, P. (2018). Organ specific gene expression in the regenerating tail of Macrostomum lignano. *Developmental Biology*, *433*, 448–460.

Li, B., & Dewey, C. N. (2011). RSEM: accurate transcript quantification from RNA-Seq

data with or without a reference genome. *BMC Bioinformatics*, *12*, 323.

Li, S., Huang, X., Chen, Y., Li, X., & Zhan, A. (2019). Identification and characterization of proteins involved in stolon adhesion in the highly invasive fouling ascidian Ciona robusta. *Biochemical and Biophysical Research Communications*, *510*, 91–96.

Liang, C., Strickland, J., Ye, Z., Wu, W., Hu, B., & Rittschof, D. (2019). Biochemistry of Barnacle Adhesion: An Updated Review. *Frontiers in Marine Science*, *6*, 1–20.

Limaye, A. (2012). Drishti: a volume exploration and presentation tool. In S. R. Stock (Ed.), *Proceedings of SPIE* (Vol. 8506, p. 85060X).

Lin, A. Y. M., Brunner, R., Chen, P. Y., Talke, F. E., & Meyers, M. A. (2009). Underwater adhesion of abalone: The role of van der Waals and capillary forces. *Acta Materialia*, *57*, 4178–4185.

Liu, G.-L., Chang, H.-K., Chuang, Y.-C., Lin, Y.-M., & Chen, P.-Y. (2020). Reversible Underwater Adhesion: The Unique C-shaped Suckers of Net-winged Midge Larvae (Blepharicera sp.). *Scientific Reports*, *10*, 9395.

Lloyd, F. E. (1942). *The Carnivorous Plants*. Waltham, Mass.,: Chronica Botanica Company.

Loew, H. (1844). Beschreibung einiger neuer Gattungen der europäischen Dipterenfauna. *Stettiner Entomologische Zeitung*, *5*, 114–130, 154–173, 165–168.

Lord, D. L., Hayes, K. F., Demond, A. H., & Salehzadeh, A. (1997). Influence of organic acid solution chemistry on subsurface transport properties. 1. Surface and interfacial tension. *Environmental Science and Technology*, *31*, 2045–2051.

Loukas, A., Hintz, M., Linder, D., Mullin, N. P., Parkinson, J., Tetteh, K. K. A., & Maizels, R. M. (2000). A family of secreted mucins from the parasitic nematode Toxocara canis bears diverse mucin domains but shares similar flanking six-cysteine repeat motifs. *Journal of Biological Chemistry*, *275*, 39600–39607.

Lujan, N. K., & Conway, K. W. (2015). Life in the Fast Lane: A Review of Rheophily in Freshwater Fishes. In R. Riesch, M. Tobler, & M. Plath (Eds.), *Extremophile Fishes: Ecology, Evolution, and Physiology of Teleosts in Extreme Environments* (pp. 107–136). Cham: Springer International Publishing.

Mabusela, W. T., & Stephen, A. M. (1990). An arabinoglucuronomannoglycan from the leaves of Ornithogalum thyrsoides. *Carbohydrate Research*, 332–335.

Maie, T., Schoenfuss, H. L., & Blob, R. W. (2012). Performance and scaling of a novel locomotor structure: adhesive capacity of climbing gobiid fishes. *Journal of*

Experimental Biology, *215*, 3925–3936.

Majidi, C. S., Groff, R. E., & Fearing, R. S. (2005). Attachment of fiber array adhesive through side contact. *Journal of Applied Physics*, *98*. https://doi.org/10.1063/1.2128697

Mannheims, B. J. (1935). Beiträge zur Biologie und Morphologie der Blepharoceriden (Dipt.). *Zoologische Forschungen*, 1–115.

Marchler-Bauer, A., Bo, Y., Han, L., He, J., Lanczycki, C. J., Lu, S., … Bryant, S. H. (2017). CDD/SPARCLE: Functional classification of proteins via subfamily domain architectures. *Nucleic Acids Research*, *45*, D200–D203.

Mason, T. A., McIlroy, P. J., & Shain, D. H. (2004). A cysteine-rich protein in the Theromyzon (Annelida: Hirudinea) cocoon membrane. *FEBS Letters*, *561*, 167–172.

Mayadas, T. N., & Wagner, D. D. (1992). Vicinal cysteines in the prosequence play a role in von Willebrand factor multimer assembly. *Proceedings of the National Academy of Sciences of the United States of America*, *89*, 3531–3535.

Meiniel, O., & Meiniel, A. (2007). The complex multidomain organization of SCO-spondin protein is highly conserved in mammals. *Brain Research Reviews*, *53*, 321–327.

Meiniel, O., Meiniel, R., Lalloué, F., Didier, R., Jauberteau, M. O., Meiniel, A., & Petit, D. (2008). The lengthening of a giant protein: When, how, and why? *Journal of Molecular Evolution*, *66*, 1–10.

Michels, J. (2010). Assessment of Congo red as a fluorescence marker for the exoskeleton of small crustaceans and the cuticle of polychaetes. *Journal of Microscopy*, *238*, 95–101.

Mitchell, A. L., Attwood, T. K., Babbitt, P. C., Blum, M., Bork, P., Bridge, A., … Finn, R. D. (2019). InterPro in 2019: Improving coverage, classification and access to protein sequence annotations. *Nucleic Acids Research*. https://doi.org/10.1093/nar/gky1100

Moran, J. A. (1996). Pitcher Dimorphism, Prey Composition and the Mechanisms of Prey Attraction in the Pitcher Plant Nepenthes Rafflesiana in Borneo. *The Journal of Ecology*, *84*, 515.

Moran, J. A., Gray, L. K., Clarke, C., & Chin, L. (2013). Capture mechanism in Palaeotropical pitcher plants (Nepenthaceae) is constrained by climate. *Annals of Botany*, *112*, 1279–1291.

Mori, M., & Kato, K. (1981). An arabinoglucuronomannan from suspension-cultured

cells of Nicotiana tabacum. *Carbohydrate Research*, *91*, 49–58.

Murphy, B., Forest, F., Barraclough, T., Rosindell, J., Bellot, S., Cowan, R., … Cheek, M. (2020). A phylogenomic analysis of Nepenthes (Nepenthaceae). *Molecular Phylogenetics and Evolution*, *144*, 106668.

Nachtigall, W. (1974). *Biological mechanisms of attachment: the comparative morphology and bioengineering of organs for linkage, suction, and adhesion*. Berlin, New York: Berlin, New York : Springer-Verlag.

Nakano, T., & Ozawa, T. (2007). Worldwide phylogeography of limpets of the order Patellogastropoda: Molecular, morphological and palaeontological evidence. *Journal of Molluscan Studies*, *73*, 79–99.

Nedjhioui, M., Moulai-Mostefa, N., Canselier, J. P., & Bensmaili, A. (2009). Investigation of combined effects of xanthan gum, sodium dodecyl sulphate, and salt on some physicochemical properties of their mixtures using a response surface method. *Journal of Dispersion Science and Technology*, *30*, 1333–1341.

Nep, E. I., Carnachan, S. M., Ngwuluka, N. C., Kontogiorgos, V., Morris, G. A., Sims, I. M., & Smith, A. M. (2016). Structural characterisation and rheological properties of a polysaccharide from sesame leaves (Sesamum radiatum Schumach. & Thonn.). *Carbohydrate Polymers*, *152*, 541–547.

Nixon, M., & Dilly, P. (1977). Sucker surfaces and prey capture. *Symp. Zool. Soc. Lond*, *38*, 447–511.

Oleszek, W., & Hamed, A. (2010). Saponin-Based Surfactants. In M. Kjellin & I. Johansson (Eds.), *Surfactants from Renewable Resources* (pp. 239–250). John Wiley & Sons, Ltd.

Osten Sacken, C. R. (1895). Contributions to the Study of the Liponeuridae Loew. (Blepharoceridae Loew, olim). *Berliner Entomologische Zeitschrift*, *40*, 148–169.

Ottaway, J. R. (1979). *Population ecology of the intertidal anemone Actinia tenebrosa Farquhar (Cnidaria: Anthozoa)*. University of Canterbury, New Zealand.

Pal, R. (1950). The Wetting of Insect Cuticle*. *Bulletin of Entomological Research*, *41*, 121–139.

Parle, E., Dirks, J.-H., & Taylor, D. (2017). Damage, repair and regeneration in insect cuticle: The story so far, and possibilities for the future. *Arthropod Structure and Development*, *46*, 49–55.

Pawar, S. N., & Edgar, K. J. (2012). Alginate derivatization: A review of chemistry,

properties and applications. *Biomaterials*, *33*, 3279–3305.

Persson, B. N. J. (2002). Adhesion between an elastic body and a randomly rough hard surface. *The European Physical Journal E*, *8*, 385–401.

Pertea, G., Huang, X., Liang, F., Antonescu, V., Sultana, R., Karamycheva, S., … Quackenbush, J. (2003). TIGR gene indices clustering tools (TGICL): A software system for fast clustering of large EST datasets. *Bioinformatics*, *19*, 651–652.

Petrone, L. (2013). Molecular surface chemistry in marine bioadhesion. *Advances in Colloid and Interface Science*, *195–196*, 1–18.

Pidatala, V. R., Mahboubi, A., & Mortimer, J. C. (2017). Structural Characterization of Mannan Cell Wall Polysaccharides in Plants Using PACE. *JoVE*, e56424.

Pjeta, R., Lindner, H., Kremser, L., Salvenmoser, W., Sobral, D., Ladurner, P., & Santos, R. (2020). Integrative transcriptome and proteome analysis of the tube foot and adhesive secretions of the sea urchin paracentrotus lividus. *International Journal of Molecular Sciences*, *21*. https://doi.org/10.3390/ijms21030946

Pjeta, R., Wunderer, J., Bertemes, P., Hofer, T., Salvenmoser, W., Lengerer, B., … Ladurner, P. (2019). Temporary adhesion of the proseriate flatworm Minona ileanae. *Philosophical Transactions of the Royal Society B: Biological Sciences*, *374*, 20190194.

Płachno, B. J., & Muravnik, L. E. (2018). Functional anatomy of carnivorous traps. In A. M. Ellison & L. Adamec (Eds.), *Carnivorous Plants: Physiology, Ecology, and Evolution* (pp. 167–179). Oxford University Press.

Pound, R. J., Miller, L. P., King, F. A., & Burnaford, J. L. (2020). Temperature affects susceptibility of intertidal limpets to bird predation. *The Journal of Experimental Biology*, *223*, jeb.213595.

Prezant, R. S. (1985). Molluscan mucins: a unifying thread. *American Malacological Bulletin*, *1*, 35–50.

Prud'Homme, R. K., & Long, R. E. (1983). Surface tensions of concentrated xanthan and polyacrylamide solutions with added surfactants. *Journal of Colloid And Interface Science*, *93*, 274–276.

R Core Team. (2019). *R: A Language and Environment for Statistical Computing*. Vienna, Austria.

Redgwell, R. J. (1983). Composition of Actinidia mucilage. *Phytochemistry*, *22*, 951–956.

Rietschel, P. (1961). Bau, Funktion und Entwicklung der Haftorgane der

Blepharoceridae. *Z. Morph. Ökol. Tiere*, *50*, 239–265.

Rost, K., & Schauer, R. (1977). Physical and chemical properties of the mucin secreted by Drosera capensis. *Phytochemistry*, *16*, 1365–1368.

RStudio Team. (2019). *RStudio: Integrated Development Environment for R*. Boston, MA.

Ruyssen, R., & Loos, R. (1947). Properties of saponins. Surface activity and degree of dispersion. *Journal of Colloid Science*, *2*, 429–451.

Sacks, M. S., Merryman, W. D., & Schmidt, D. E. (2009). On the biomechanics of heart valve function. *Journal of Biomechanics*, *42*, 1804–1824.

Sakka, L., Delétage, N., Lalloué, F., Duval, A., Chazal, J., Lemaire, J. J., … Gobron, S. (2014). SCO-spondin derived peptide NX210 induces neuroprotection in vitro and promotes fiber regrowth and functional recovery after spinal cord injury. *PLoS ONE*, *9*. https://doi.org/10.1371/journal.pone.0093179

Sareh, S., Althoefer, K., Li, M., Noh, Y., Tramacere, F., Sareh, P., … Kovac, M. (2017). Anchoring like octopus: biologically inspired soft artificial sucker. *J. R. Soc. Interface*, *14*.

Sarmiento-Ponce, E. J., Sutcliffe, M. P. F., & Hedwig, B. (2018). Substrate texture affects female cricket walking response to male calling song. *Royal Society Open Science*, *5*. https://doi.org/10.1098/rsos.172334

Schindelin, J., Arganda-Carreras, I., Frise, E., Kaynig, V., Longair, M., Pietzsch, T., … Cardona, A. (2012). Fiji: An open-source platform for biological-image analysis. *Nature Methods*, *9*, 676–682.

Schnepf, E. (1963). Zur Cytologie und Physiologie pflanzlicher Drüsen: 1. Teil. Über den Fangschleim der lnsektivoren. *Flora Oder Allgemeine Botanische Zeitung*, *153*, 1–22.

Scholz, I., Bückins, M., Dolge, L., Erlinghagen, T., Weth, A., Hischen, F., … Baumgartner, W. (2010). Slippery surfaces of pitcher plants: Nepenthes wax crystals minimize insect attachment via microscopic surface roughness. *Journal of Experimental Biology*, *213*, 1115–1125.

Sherratt, M. J., Baldock, C., Haston, J. L., Holmes, D. F., Jones, C. J. P., Shuttleworth, C. A., … Kielty, C. M. (2003). Fibrillin microfibrils are stiff reinforcing fibres in compliant tissues. *Journal of Molecular Biology*, *332*, 183–193.

Simão, F. A., Waterhouse, R. M., Ioannidis, P., Kriventseva, E. V., & Zdobnov, E. M.

(2015). BUSCO: Assessing genome assembly and annotation completeness with single-copy orthologs. *Bioinformatics*, *31*, 3210–3212.

Simoneit, B. R. T., Medeiros, P. M., & Wollenweber, E. (2008). Triterpenoids as major components of the insect-trapping glue of Roridula species. *Zeitschrift Fur Naturforschung C*, *63c*, 625–630.

Smith, A. M. (1991a). Negative Pressure Generated By Octopus Suckers: a Study of the Tensile Strength of Water in Nature. *Journal of Experimental Biology*, *157*, 257–271.

Smith, A. M. (1991b). The Role of Suction in the Adhesion of Limpets. *Journal of Experimental Biology*, *161*, 151–169.

Smith, A. M. (1992). Alternation between attachment mechanisms by limpets in the field. *Journal of Experimental Marine Biology and Ecology*, *1600*, 205–220.

Smith, A. M. (1996). Cephalopod sucker design and the physical limits to negative pressure. *The Journal of Experimental Biology*, *199*, 949–958.

Smith, A. M. (2006). The Biochemistry and Mechanics of Gastropod Adhesive Gels. In A. M. Smith & J. A. Callow (Eds.), *Biological Adhesives* (pp. 167–182). Berlin, Heidelberg: Springer Berlin Heidelberg.

Smith, A. M. (2016a). Biological Adhesives, second edition. In A. M. Smith (Ed.), *Biological Adhesives*. Springer International Publishing.

Smith, A. M. (2016b). The Biochemistry and Mechanics of Gastropod Adhesive Gels. In A. M. Smith (Ed.), *Biological Adhesives* (pp. 177–192). Springer, Cham.

Smith, A. M., Kier, W. M., & Johnsen, S. (1993). The Effect of Depth on the Attachment Force of Limpets. *Biological Bulletin*, *184*, 338–341.

Smith, A. M., Papaleo, C., Reid, C. W., & Bliss, J. M. (2017). RNA-Seq reveals a central role for lectin, C1q and von Willebrand factor A domains in the defensive glue of a terrestrial slug. *Biofouling*, *33*, 741–754.

Smith, A. M., Quick, T. J., & St. Peter, R. L. (1999). Differences in the composition of adhesive and non-adhesive mucus from the limpet Lottia limatula. *Biological Bulletin*, *196*, 34–44.

Smith, V. J., Fernandes, J. M. O., Kemp, G. D., & Hauton, C. (2008). Crustins: Enigmatic WAP domain-containing antibacterial proteins from crustaceans. *Developmental and Comparative Immunology*, *32*, 758–772.

Steentoft, C., Vakhrushev, S. Y., Joshi, H. J., Kong, Y., Vester-Christensen, M. B., Schjoldager, K. T.-B. G., … Clausen, H. (2013). Precision mapping of the human

O-GalNAc glycoproteome through SimpleCell technology. *The EMBO Journal*, *32*, 1478–1488.

Stephen, A. M., Eagles, P. F. K., Mabusela, W. T., Vogt, D. C., & Lawson, A. M. (1991). Mannoglucuronoglycans from plant sources. *Food Hydrocolloids*, *5*, 159–161.

Stewart, R. J., Ransom, T. C., & Hlady, V. (2011). Natural underwater adhesives. *Journal of Polymer Science, Part B: Polymer Physics*, *49*, 757–771.

Thakur, B. R., Singh, R. K., & Handa, A. K. (1997). Chemistry and Uses of Pectin - A Review. *Critical Reviews in Food Science and Nutrition*, *37*, 47–73.

The UniProt Consortium. (2017). UniProt: the universal protein knowledgebase. *Nucleic Acids Research*, *45*, D158–D169.

Thorogood, C. J., Bauer, U., & Hiscock, S. J. (2018). Convergent and divergent evolution in carnivorous pitcher plant traps. *New Phytologist*, *217*, 1035–1041.

Tirtaatmadja, V., McKinley, H. G., & Cooper-White, J. J. (2006). Drop formation and breakup of low viscosity elastic fluids: Effects of molecular weight and concentration. *Physics of Fluids*, *18*. https://doi.org/10.1063/1.2190469

Tonnoir, A. L. (1930). Notes on Indian Blepharocerid larvae and pupae with remarks on the morphology of Blepharocerid larvae and pupae in general. *Records of the Indian Museum, 32*, 161–124.

Tramacere, F., Beccai, L., Kuba, M., Gozzi, A., Bifone, A., & Mazzolai, B. (2013). The Morphology and Adhesion Mechanism of Octopus vulgaris Suckers. *PLoS ONE*, *8*. https://doi.org/10.1371/journal.pone.0065074

Tramacere, F., Follador, M., Pugno, N. M., & Mazzolai, B. (2015). Octopus-like suction cups: from natural to artificial solutions. *Bioinspiration & Biomimetics*, *10*, 035004.

Tramacere, F., Kovalev, A., Kleinteich, T., Gorb, S. N., & Mazzolai, B. (2013). Structure and mechanical properties of Octopus vulgaris suckers. *Journal of The Royal Society Interface*, *11*, 20130816–20130816.

Tryfona, T., Liang, H. C., Kotake, T., Tsumuraya, Y., Stephens, E., & Dupree, P. (2012). Structural characterization of Arabidopsis leaf arabinogalactan polysaccharides. *Plant Physiology*, *160*, 653–666.

Tryfona, T., & Stephens, E. (2010). Analysis of carbohydrates on proteins by offline normal-phase liquid chromatography MALDI-TOF/TOF-MS/MS. *Methods in Molecular Biology (Clifton, N.J.)*, *658*, 137–151.

Vargaftik, N. B., Volkov, B. N., & Voljak, L. D. (1983). International Tables of the

Surface Tension of Water. *Journal of Physical and Chemical Reference Data*, *12*, 817.

Vella, D. (2015). Floating Versus Sinking. *Annual Review of Fluid Mechanics*, *47*, 115–135.

Vera, A., Recabal, A., Saldivia, N., Stanic, K., Torrejon, M., Montecinos, H., & Caprile, T. (2015). Interaction between sco-spondin and low density lipoproteins from embryonic cerebrospinal fluid modulates their roles in early neurogenesis. *Frontiers in Neuroanatomy*, *9*, 1–12.

Vera Candioti, F., Haas, A., Altig, R., & Peixoto, O. (2017). Cranial anatomy of the amazing bromeliad tadpoles of Phyllodytes gyrinaethes (Hylidae: Lophyohylini), with comments about other gastromyzophorous larvae. *Zoomorphology*, *136*, 61–73.

Vicré, M., Jauneau, A., Knox, J. P., & Driouich, A. (1998). Immunolocalization of β-(1→4) and β-(1→6)-D-galactan epitopes in the cell wall and Golgi stacks of developing flax root tissues. *Protoplasma*, *203*, 26–34.

Vintéjoux, C., & Shoar-Ghafari, A. (2000). Cellules productrices de mucilages chez les plantes carnivores. *Acta Botanica Gallica*, *147*, 5–20.

Vogelgesang, M., Farago, T., Morgeneyer, T. F., Helfen, L., dos Santos Rolo, T., Myagotin, A., & Baumbach, T. (2016). Real-time image-content-based beamline control for smart 4D X-ray imaging. *Journal of Synchrotron Radiation*, *23*, 1254–1263.

Vogt, D. C., & Stephen, A. M. (1993). The gum exudate of Encephalartos longifolius Lehm. (female): further hydrolytic studies. *Carbohydrate Research*, *238*, 249–260.

Wainwright, D. K., Kleinteich, T., Kleinteich, A., Gorb, S. N., & Summers, A. P. (2013). Stick tight: suction adhesion on irregular surfaces in the northern clingfish. *Biology Letters*, *9*, 20130234.

Waite, J. H. (1987). Nature's underwater adhesive specialist. *International Journal of Adhesion and Adhesives*, *7*, 9–14.

Waite, J. H. (2002). Adhesion a la Moule. *Integrative and Comparative Biology*, *42*, 1172–1180.

Waite, J. H. (2017). Mussel adhesion – essential footwork. *The Journal of Experimental Biology*, *220*, 517–530.

Waite, J. H., & Tanzer, M. L. (1981). Polyphenolic Substance of Mytilus edulis: Novel Adhesive Containing L-Dopa and Hydroxyproline. *Science (New York, N.Y.)*, *212*,

1038–1040.

Wang, Yue, Kang, V., Arzt, E., Federle, W., & Hensel, R. (2019). Strong Wet and Dry Adhesion by Cupped Microstructures. *ACS Applied Materials & Interfaces*, *11*, 26483–26490.

Wang, Yueping, Yang, X., Chen, Y., Wainwright, D. K., Kenaley, C. P., Gong, Z., … Wen, L. (2017). A biorobotic adhesive disc for underwater hitchhiking inspired by the remora suckerfish. *Science Robotics*, *2*, 1–10.

Waterhouse, A. M., Procter, J. B., Martin, D. M. A., Clamp, M., & Barton, G. J. (2009). Jalview Version 2—a multiple sequence alignment editor and analysis workbench. *Bioinformatics*, *25*, 1189–1191.

Wee, M. S. M., Matia-Merino, L., Carnachan, S. M., Sims, I. M., & Goh, K. K. T. (2014). Structure of a shear-thickening polysaccharide extracted from the New Zealand black tree fern, Cyathea medullaris. *International Journal of Biological Macromolecules*, *70*, 86–91.

Wilks, A. M., Rabice, S. R., Garbacz, H. S., Harro, C. C., & Smith, A. M. (2015). Double-network gels and the toughness of terrestrial slug glue. *The Journal of Experimental Biology*, *218*, 3128–3137.

Wunderer, J., Lengerer, B., Pjeta, R., Bertemes, P., Kremser, L., Lindner, H., … Ladurner, P. (2019). A mechanism for temporary bioadhesion. *Proceedings of the National Academy of Sciences*, *116*, 201814230.

Yap, N. V. L., Whelan, F. J., Bowdish, D. M. E., & Golding, G. B. (2015). The evolution of the scavenger receptor cysteine-rich domain of the class A scavenger receptors. *Frontiers in Immunology*, *6*, 1–9.

Yuguchi, Y., Urakawa, H., & Kajiwara, K. (1997). Structural Characteristics of Crosslinking Domain in Gellan Gum Gel. *Macromol. Symp.*, *120*, 77–89.

Yule, A. B., & Walker, G. (1984). The adhesion of the barnacle, balanus balanoides, to slate surfaces. *Journal of the Marine Biological Association of the United Kingdom*, *64*, 147–156.

Zelensky, A. N., & Gready, J. E. (2005). The C-type lectin-like domain superfamily. *FEBS Journal*, *272*, 6179–6217.

Zhang, M., Liu, M., Prest, H., & Fischer, S. (2008). Nanoparticles secreted from ivy rootlets for surface climbing. *Nano Letters*, *8*, 1277–1280.

Zhou, Y. F., Eng, E. T., Zhu, J., Lu, C., Walz, T., & Springer, T. A. (2012). Sequence and

structure relationships within von Willebrand factor. *Blood*, *120*, 449–458.

Zhou, Y., Robinson, A., Steiner, U., & Federle, W. (2014). Insect adhesion on rough surfaces : analysis of adhesive contact of smooth and hairy pads on transparent microstructured substrates. *J. R. Soc. Interface*, *11*, 20140499.

Zwick, P. (1980). The Net-Winged Midges of Italy and Corsica (Diptera: Blephariceridae). *Aquatic Insects*, *2*, 33–61.

Zwick, P. (2004). Insecta: Diptera, Blephariceridae. In C. . Yule & H. . Yong (Eds.), *Freshwater Invertebrates of the Malaysian Region* (pp. 736–749). Academy of Sciences Malaysia.